

Mathematical Modelling and Simulation  
of  
Biogrout

PROEFSCHRIFT

ter verkrijging van de graad van doctor  
aan de Technische Universiteit Delft,  
op gezag van de Rector Magnificus prof.ir. K.C.A.M. Luyben,  
voorzitter van het College voor Promoties,  
in het openbaar te verdedigen op

dinsdag 12 januari 2016 om 10:00 uur

door

Wilhelmina Kornelia  
VAN WIJNGAARDEN-VAN ROSSUM

wiskundig ingenieur, Technische Universiteit Delft  
geboren te Cromstrijen

Dit proefschrift is goedgekeurd door de

promotor: prof.dr.ir. C. Vuik

copromotor: dr.ir. F.J. Vermolen

Samenstelling promotiecommissie:

Rector Magnificus

voorzitter

Prof.dr.ir. C. Vuik

Technische Universiteit Delft, promotor

Dr.ir. F.J. Vermolen

Technische Universiteit Delft, copromotor

*Onafhankelijke leden:*

Prof.dr. J. Bruining

Technische Universiteit Delft

Prof.dr. I.S. Pop

Technische Universiteit Eindhoven

Prof.dr. R.J. Schotting

Universiteit Utrecht

Prof.dr. P.L.J. Zitha

Technische Universiteit Delft

Prof.dr.ir. A.W. Heemink

Technische Universiteit Delft, reservelid

*Overig lid:*

Dr.ir. G.A.M. van Meurs

Deltares, The Netherlands

Mathematical Modelling and Simulation of BiogROUT.

Dissertation at Delft University of Technology.

Copyright © 2015 by W.K. van Wijngaarden-van Rossum



The work described in this thesis was financially supported by Deltares, the Delft Institute of Applied Mathematics (DIAM) of the Delft University of Technology and the Dutch Technology Foundation STW, which is part of the Netherlands Organisation for Scientific Research (NWO), and which is partly funded by Ministry of Economic Affairs, Agriculture and Innovation.

Cover picture: Wind erosion

ISBN 978-94-6295-418-2

Printed by: Proefschriftmaken.nl || Uitgeverij BOXPress

## Dankwoord

Dit boek is af. Natuurlijk is het niet perfect, maar toch: het is klaar. Aan jaren van promoveren is een einde gekomen. Tijd om stil te staan en terug te blikken. Tijd om te bedanken!

Allereerst wil ik mijn begeleiders Fred, Kees en Gerard bedanken:

Fred, we ontmoetten elkaar bij het derdejaarsvak 'Numerieke methoden II' en sindsdien was je mijn vaste begeleider. Eerst bij mijn bacheloreindwerk, toen bij mijn masterthesis en nu bij mijn promotieonderzoek, waar je ook mijn co-promotor bent. Ik kijk terug op een fijne samenwerking. Het was fijn om de inhoud van mijn promotiewerk regelmatig met iemand te kunnen delen, die me ook nog eens de goede richting opwees als ik ergens mee worstelde. Ik heb veel van je geleerd en heb je leren kennen als een mens met het hart op de goede plek. Bedankt!

Kees, met het tweedejaarsvak 'Numerieke methoden I' heb je de basis gelegd voor mijn numerieke wiskunde. Daarna was ook jij een vaste begeleider bij mijn bacheloreindwerk, masterthesis en promotiewerk. Je was heel betrokken, keek mee van een wat grotere afstand en stelde op het juiste moment de goede vragen. Bedankt!

Gerard, jij was contactpersoon voor het mastereindopdrachtvoorstel met de titel 'Warmte- en koudeopslag in de bodem' en zo kwam ik binnen bij GeoDelft (nu Deltares). Aan warmte- en koudeopslag heb ik niets gedaan, want je had een andere opdracht liggen: Het modelleren van Biogrout. Dat beviel zo goed, dat er een promotieonderzoek volgde. Jij was mijn begeleider bij de masterthesis en het promotieonderzoek en je stimuleerde me om model en praktijk te verbinden. Bedankt!

Leon, hoewel niet als officiële begeleider, heb jij ook in grote mate bijgedragen aan de totstandkoming van dit proefschrift. Jij bent gepromoveerd op het Biogrout-proces en hebt me veel proceskennis bijgebracht, die ik voor een gedeelte in een model heb kunnen verwerken en die me hielp om experimentele resultaten beter te begrijpen. Bedankt!

Commissieleden, bedankt dat jullie plaats wilden nemen in mijn commissie. Bedankt voor het lezen van mijn proefschrift en voor jullie inbreng.

Promoveren doe je niet in een zolderkamertje. Ik in ieder geval niet. Ik had de gelegenheid om bij Deltares te promoveren. Ik heb in vijf verschillende afdelingen

gezet en ben daarnaast vijf keer verhuisd. Op deze manier heb ik veel verschillende collega's leren kennen. En als promovenda had ik daarnaast ook nog collega's op de TU. Collega's: bedankt voor wie jullie waren, voor wat ik van jullie heb kunnen leren en voor de gezellige lunches! Thank you for being my colleagues and for the nice lunches!

Wie ben je zonder je ouders? Lieve ouders, bedankt! Bedankt voor jullie opvoeding, voor jullie vorming, voor het leggen van de basis voor lezen, schrijven en wiskunde, voor het leren trekker rijden en bomen snoeien, voor het oppassen en voor al het andere!

Vrienden, bedankt voor jullie vriendschap en ondersteuning. Bedankt ook voor jullie 'hoteldiensten' in de buurt van Delft.

Schoonouders, bedankt voor mijn geweldige man en voor de gezellige vakanties aan boord van jullie 'Tramp'.

Lucas, Natasha en Silas: jullie waren een geweldig mooie afwisseling op het promoveren! Bedankt voor jullie inspirerende ontdekkingszin.

Lieve Arend, deze promotie duurt al bijna ons hele huwelijk, maar gelukkig houdt het ene niet op als het andere stopt! Heel hartelijk bedankt voor jarenlange liefde en aanmoediging!

Hemelse Vader, U bent mijn Schepper en Redder. Dank U wel voor inspiratie en energie, voor Uw aanwezigheid in vreugdevolle dagen en in dagen van verdriet!

## Samenvatting

### Het Modelleren en Simuleren van Biogrout

Biogrout is een methode om zand en grind te verstevigen door de productie van calciumcarbonaat. Dit calciumcarbonaat wordt geproduceerd door gebruik te maken van micro-organismen die zich in de bodem bevinden of er in geïnjecteerd worden. De micro-organismen worden voorzien van ureum en calcium. Vervolgens catalyseren zij de hydrolyse van ureum, waarbij carbonaat wordt gevormd. In de aanwezigheid van calcium, precipiteert (slaat neer) de carbonaat als calciumcarbonaat. Ammonium is het ongewenste bijproduct van deze reactie. De calciumcarbonaatkristallen worden gevormd in de poriën en zij verbinden de korrels. Op deze manier wordt de sterkte van het materiaal verhoogd.

Biogrout kan toegepast worden op locaties waar grondverbetering gewenst is. In dat geval heeft men een betrouwbare voorspelling van het effect van de Biogroutbehandeling nodig. Daarvoor is een goed begrip van het proces nodig en is een goed wiskundig model onmisbaar. In dit proefschrift focussen we op het modelleren van het Biogroutproces.

We beginnen met een wiskundig model voor de hydrolyse-precipitatiereactie (Hoofdstuk 2 en 3). Vanwege de precipitatie (neerslag) van de vaste stof calciumcarbonaat neemt de porositeit af. Hierdoor neemt de doorlatendheid ook af. Door de precipitatiereactie verdwijnen er stoffen uit de oplossing, wat voor een afname van het vloeistofvolume zorgt. Aan de andere kant is er ook minder ruimte beschikbaar door de afnemende porositeit. Deze fenomenen zorgen voor een uitwaartse stroming vanuit de poriën. De stoffen ureum, calcium en ammonium zijn opgelost in de vloeistof. De concentraties worden gemodelleerd met een advectie-dispersie-reactievergelijking. De dichtheid van de vloeistof verandert door de tijd door de veranderende samenstelling, wat een dichtheidsgedreven component aan de stroming geeft. Er wordt aangenomen dat de vaste stof calciumcarbonaat niet getransporteerd wordt. Daarom bevat de differentiaalvergelijking voor calciumcarbonaat alleen een accumulatie- en reactieterm. De reactiesnelheid hangt af van de

hoeveelheid micro-organismen in de grond. In deze hoofdstukken wordt aangenomen dat de micro-organismen homogeen verdeeld zijn. De Eindige Elementen Methode (EEM) wordt gebruikt om de modelvergelijkingen op te lossen. Omdat hoge stroomsnelheden niet wenselijk zijn in het Biogrout proces vanwege uitspoeling van de micro-organismen, is advectie niet dominant. Daarom kan de Standaard Galerkin EEM worden gebruikt. De Euler Achterwaarts methode wordt gebruikt voor de tijdsdiscretisatie en Newton's methode wordt toegepast voor de niet-lineariteiten.

Hoofdstuk 4 beschrijft een model voor de plaatsing van micro-organismen en beschouwt drie soorten concentraties van micro-organismen: gesuspendeerde micro-organismen, (tijdelijk) geadsorbeerde micro-organismen en gefixeerde micro-organismen. Deze fixatie vindt plaats na contact tussen de fixatievloeistof en de micro-organismen.

De resulterende microbiële concentraties kunnen gebruikt worden als invoer voor de reactiesnelheid in het hydrolyse-precipitatiemodel. Dit wordt gedaan in hoofdstuk 5 door de modellen te combineren.

In hoofdstuk 6 worden verschillende differentiaalvergelijkingen voor de stroming vergeleken. Dit leidt tot een aanpassing van de differentiaalvergelijking voor de stroming die in de eerste hoofdstukken gebruikt wordt.

Vaak wordt er een hydrostatische druk gebruikt als randvoorwaarde. Hoofdstuk 7 legt uit hoe deze druk berekend kan worden in het geval van veranderende vloeistofdichtheden.

Vanwege de opgeloste stoffen is de vloeistof zwaarder dan water. Als zo'n zware vloeistof geïnjecteerd wordt kunnen er frontinstabiliteiten in de vorm van vingers ontstaan. In hoofdstuk 8 worden de frontinstabiliteiten opgewekt door een initiële variatie van de porositeit in de ruimte. Er wordt gekeken naar het effect van frontinstabiliteiten op het Biogrout proces.

In het laatste hoofdstuk worden verschillende experimentele resultaten vergeleken met de numerieke resultaten van simulaties met het model. Het blijkt dat het model de experimentele resultaten behoorlijk goed kan beschrijven.

# Modelling and Simulation of Biogrout

Biogrout is a method to reinforce sand and gravel by the production of calcium carbonate. This calcium carbonate is produced using micro-organisms that are either present in the subsoil or injected into it. The micro-organisms are supplied with urea and calcium. Subsequently, they catalyse the hydrolysis of urea, by which carbonate is formed. In the presence of calcium, the carbonate precipitates as calcium carbonate. Ammonium is the unwanted by-product of this reaction. The calcium carbonate crystals are formed in the pores and they connect the grains. In this way, the strength of the material is increased.

Biogrout can be applied on locations where soil improvement is desired. Upon doing so, one needs to have a reliable prediction of the effect of the Biogrout treatment. Therefore, a thorough understanding of the process is necessary and a sound mathematical model is dispensable. In this thesis we focus on the modelling of the Biogrout process.

We start with a mathematical model for the hydrolysis-precipitation reaction (Chapters 2 and 3). As a result of the precipitation of the solid calcium carbonate, the porosity decreases. Therefore, the permeability decreases as well. Due to the precipitation reaction, chemicals disappear from the solution causing a decrease in liquid volume. On the other hand, there is less void space available due to the decreasing porosity. These phenomena cause a net outflow out of the pores. The chemicals urea, calcium and ammonium are dissolved in the fluid. The concentrations are modelled with an advection-dispersion-reaction-equation. The density of the fluid evolves over time as a result of the altering composition, which gives a density-driven component to the flow. It is assumed that the solid calcium carbonate is not transported. Therefore, the differential equation for calcium carbonate only contains an accumulation and a reaction term. The reaction rate depends on the amount of micro-organisms present in the soil. In these chapters, it is assumed that the micro-organisms are homogeneously distributed. The Finite Element Method

(FEM) is used to solve the model equations. Since high flow rates are not desirable in the Biogrout process, since such a high flow rate will flush out the micro-organisms, advection is not dominating. Hence, the Standard Galerkin FEM can be used. The Backward Euler method is used for the time discretisation and Newton's method is applied to deal with the non-linearities.

Chapter 4 describes a model for the placement of micro-organisms and considers three concentrations of micro-organisms: suspended micro-organisms, (temporarily) adsorbed micro-organisms and fixated micro-organisms. This fixation takes place after contact between the fixation fluid and the micro-organisms.

The resulting microbial concentrations can be used as input for the reaction rate in the hydrolysis-precipitation model. This is done in Chapter 5 by combining the models.

In Chapter 6 several differential equations for the fluid are compared. This leads to an adaptation of the differential equation for the flow that is used in the first chapters.

Often, a hydrostatic pressure is used as a boundary condition. Chapter 7 explains how this pressure can be calculated in case of dynamically evolving fluid densities.

Due to the dissolved chemicals, the fluid is denser than water. If such a dense fluid is injected, front instabilities in the form of fingers might occur. In Chapter 8 the front instabilities are induced by an initial variation of the porosity in the spatial domain. The effect of front instabilities on the Biogrout process is considered.

In the last chapter, several experimental results are compared to the numerical results of simulations with the model. It appears that the model can describe the experimental results reasonably well.

# Contents

<b>Dankwoord</b>	<b>iii</b>
<b>Samenvatting</b>	<b>v</b>
<b>Summary</b>	<b>vii</b>
<b>1 Introduction</b>	<b>1</b>
1.1 Biogrout - a soil improvement method . . . . .	1
1.2 Biogrout - applications . . . . .	2
1.3 The chemistry and biology behind Biogrout . . . . .	3
1.4 Biogrout - the modelling . . . . .	4
1.5 Organisation of this thesis . . . . .	5
<b>2 Modelling Biogrout</b>	<b>7</b>
2.1 Introduction . . . . .	8
2.2 The mathematical model . . . . .	9
2.2.1 Derivation of the differential equations . . . . .	9
2.2.2 Exact solution for a special case . . . . .	14
2.3 Numerical method . . . . .	15
2.3.1 Aqueous species . . . . .	16
2.3.2 Pressure and flow . . . . .	17
2.3.3 Non aqueous species . . . . .	17
2.3.4 Scheme for solving the equations . . . . .	17
2.4 Results . . . . .	18
2.4.1 Configuration and boundary conditions (1D) . . . . .	18
2.4.2 Results (1D) . . . . .	19
2.4.3 Configuration and boundary conditions (2D) . . . . .	24
2.4.4 Results (2D) . . . . .	25
2.5 Conclusions and Discussion . . . . .	28

<b>3</b>	<b>Modelling Biogrout: extension to 3D</b>	<b>31</b>
3.1	Introduction . . . . .	32
3.2	The Mathematical Model . . . . .	32
3.3	Numerical Method . . . . .	35
3.4	Results . . . . .	36
3.5	Conclusions and Discussion . . . . .	38
<b>4</b>	<b>The placement of bacteria</b>	<b>39</b>
4.1	Introduction . . . . .	40
4.2	Mathematical model . . . . .	41
4.2.1	Derivation of the model equations . . . . .	41
4.2.2	Initial conditions and boundary conditions . . . . .	44
4.3	Analytical Solution and Numerical Methods . . . . .	44
4.3.1	Analytical solution . . . . .	45
4.3.2	Case study . . . . .	50
4.3.3	Numerical Methods . . . . .	51
4.4	Results . . . . .	51
4.5	Discussion and Conclusions . . . . .	56
<b>5</b>	<b>Bacterial placement and soil reinforcement</b>	<b>59</b>
5.1	Introduction . . . . .	60
5.2	Mathematical Model . . . . .	61
5.2.1	Model equations for the placement of the bacteria . . . . .	61
5.2.2	Model equations for calcium carbonate . . . . .	63
5.2.3	Boundary Conditions and Initial Conditions . . . . .	66
5.2.4	Analytical solution . . . . .	66
5.3	Numerical Methods . . . . .	71
5.4	Results . . . . .	72
5.4.1	Numerical results . . . . .	72
5.4.2	The current model versus a homogeneous distribution . . . . .	75
5.4.3	Analytical results . . . . .	76
5.4.4	Comparison of the numerical and analytical solutions . . . . .	77
5.5	Discussion and Conclusions . . . . .	80
<b>6</b>	<b>Various flow equations</b>	<b>83</b>
6.1	Introduction . . . . .	84
6.2	The Mathematical Model . . . . .	84
6.3	Strategy and Numerical Methods . . . . .	87
6.4	Results . . . . .	88
6.5	Discussion and Conclusions . . . . .	90
<b>7</b>	<b>Dealing with pressure boundary conditions</b>	<b>91</b>
7.1	Introduction . . . . .	92
7.2	Mathematical model . . . . .	93
7.2.1	Model equations . . . . .	93
7.2.2	Experimental set-up, initial and boundary conditions . . . . .	95
7.3	Numerical Methods . . . . .	97
7.4	Results . . . . .	100

---

7.4.1	Comparison of three methods . . . . .	100
7.4.2	The outflow boundary of the 100m <sup>3</sup> experiment . . . . .	104
7.4.3	Application: a 100m <sup>3</sup> experiment . . . . .	108
7.5	Discussion and Conclusions . . . . .	110
<b>8</b>	<b>Front instabilities in density driven flow</b>	<b>113</b>
8.1	Introduction . . . . .	114
8.2	Materials and Methods . . . . .	115
8.3	Case study set-up . . . . .	116
8.4	Mathematical Model . . . . .	118
8.4.1	Experiment . . . . .	118
8.4.2	Case study . . . . .	122
8.5	Numerical Methods . . . . .	124
8.6	Results . . . . .	126
8.6.1	Simulation with a homogeneous medium . . . . .	126
8.6.2	Simulation with an inhomogeneous porous medium . . . . .	127
8.6.3	Variation in substrate concentration . . . . .	132
8.6.4	Case study simulations . . . . .	132
8.7	Discussion and Conclusions . . . . .	138
<b>9</b>	<b>Comparison to experimental data</b>	<b>141</b>
9.1	Introduction . . . . .	142
9.2	Materials and Methods . . . . .	143
9.2.1	Column preparation . . . . .	143
9.2.2	Experiment . . . . .	143
9.3	Mathematical Model . . . . .	144
9.3.1	Model Equations . . . . .	144
9.3.2	Reaction rate . . . . .	147
9.3.3	Parameter values . . . . .	149
9.3.4	Initial and boundary equations . . . . .	149
9.4	Numerical Methods . . . . .	150
9.5	Results . . . . .	152
9.5.1	Experimental Results . . . . .	153
9.5.2	Numerical Results . . . . .	156
9.6	Conclusions and Discussion . . . . .	161
<b>10</b>	<b>General conclusions and Outlook</b>	<b>165</b>
<b>Appendices</b>		
<b>A</b>	<b>LIST OF SYMBOLS</b>	<b>167</b>
	<b>Curriculum vitae</b>	<b>181</b>
	<b>List of publications</b>	<b>182</b>



This introduction explains what Biogrout is, where it can be applied and how this process can be modelled. Furthermore, a literature review is given as well as the outline of the thesis.

## 1.1 Biogrout - a soil improvement method

Nowadays, there is a trend to consider the soil as a living ecosystem. This gives the possibility to look for innovative and sustainable solutions to geotechnical problems. It requires a multidisciplinary approach since, besides geotechnology and hydrology, both microbiology and geochemistry are involved. A review on biogeochemical processes and their geotechnical applications can be found in [24].

One such biogeochemical process is MICP: Microbially-induced calcium carbonate precipitation, [4, 5, 22, 59, 83, 97]. Certain micro-organisms can catalyse chemical reactions by which carbonate ions ( $\text{CO}_3^{2-}$ ) are formed. These ions precipitate in the presence of calcium ions ( $\text{Ca}^{2+}$ ) as calcium carbonate ( $\text{CaCO}_3$ ). Other names for this specific biogeochemical process are: Biocement ([96]), Biocementation ([14]) and Biogrout ([30, 83, 85]). In this thesis, the term Biogrout is used.

Urea ( $\text{CO}(\text{NH}_2)_2$ ) is one of the possible sources for the production of carbonate. A review on MICP based on urea hydrolysis can be found in [63]. The focus of this thesis is on (modelling and simulating) the urea-based MICP. The micro-organism used in the urea-based Biogrout is *Sporosarcina pasteurii*, previously known as *Bacillus pasteurii*.

Figure 1.1 shows a result of the treatment of glass beads with Biogrout. The spherical objects are the glass beads. The calcium carbonate crystals (the non spherical objects) are formed in the pore space and connect the grains. In this way, Biogrout improves granular soil by increasing the strength [87], such that the soil can sustain large constructions and if necessary earthquakes, [83]. Biogrout also

improves other soil properties, including permeability, stiffness, compressibility, and volumetric behaviour [23].

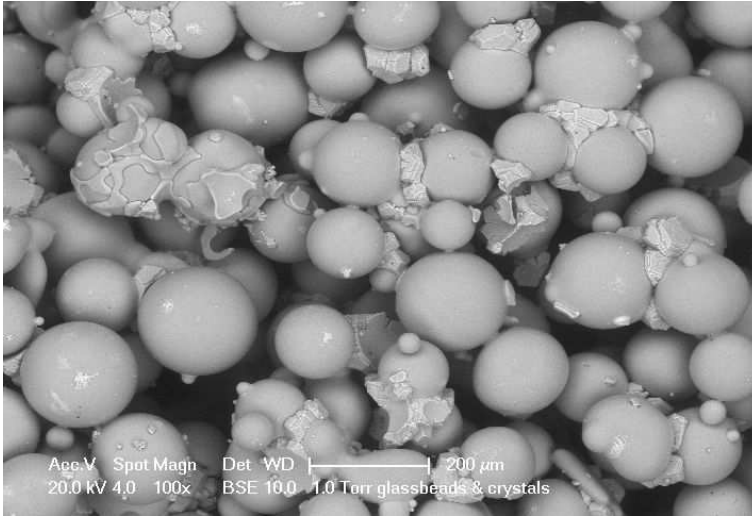


Figure 1.1: Biogrout increases the strength of granular soils since the calcium carbonate crystals (the non spherical objects) connect the grains. Here, Biogrout was applied in glass beads (spheres).

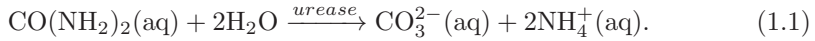
## 1.2 Biogrout - applications

Because of its soil improving properties, Biogrout has the following applications:

- piping prevention [9];
- prevention of liquefaction [23, 76];
- reduction of the impacts of earthquakes [84];
- bore hole stabilization [77];
- slope stabilization [23];
- stabilization of railroad tracks [83];
- reinforcement of dunes to decrease effects of wave erosion, and hence to protect delicate coastlines [96];
- erosion prevention by increasing the resistance to erosive forces of water flow [23];
- building settlement reduction and increase of the bearing capacity for foundations [23].

## 1.3 The chemistry and biology behind Biogrout

The Biogrout process consists of two important parts: the formation of carbonate (in this thesis by the hydrolysis of urea) and the precipitation of calcium carbonate. Hydrolysis of urea is an irreversible reaction in which urea reacts with water to form carbonate and ammonium ( $\text{NH}_4^+$ ):



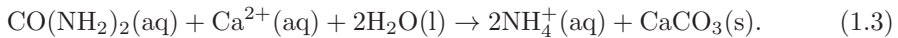
The hydrolysis reaction is catalysed by the *urease* enzyme in the *Sporosarcina pasteurii* micro-organisms.

When the micro-organisms produce a sufficient amount of carbonate in the presence of calcium, the solution becomes oversaturated and calcium carbonate will precipitate:



For a detailed explanation about the nucleation of calcium carbonate crystals, crystal growth and type of calcium carbonate crystals, see [83].

Combining reactions (1.1) and (1.2) gives the overall urea-based Biogrout reaction:



Since almost all the involved species in these equations form acid-base equilibria, several other species are involved in the Biogrout process. An extensive model is proposed in Chapter 2 of [83], which includes the acid-base equilibria. The equilibrium constants for the acid-base equilibria are given for a temperature of 25°C and a pressure of 1 bar and come from [62]. The extensive model is compared to a model based on the simplified reaction (1.3). The study in [83] shows that it is justified to work with the simplified equation (1.3), since the simplified model leads to the same concentrations of the main compounds as the model including all the equilibria. The concentrations of the other species seem negligible (less than 1% of the main compounds). Reaction (1.3) is considered to be irreversible, since the (nett) dissolution of calcium carbonate is assumed to be negligible in the Biogrout process. For more details about the Biogrout process, see [83, 96].

While applying Biogrout, first the micro-organisms are injected into the soil and transported by water flow to the location where strengthening is required. Several placement procedures are reported in [36]. Subsequently, urea and calcium chloride (dissolved in water) are injected into the soil, where the micro-organisms will catalyse the Biogrout reaction. The side-product of the reaction is ammonium, which should be extracted from the soil, since the concentrations are too high to leave it there. The density of the urea/calcium chloride solution is larger than the density of water. Besides that, the density changes as a result of reaction (1.3). Hence, when applying Biogrout, one should be aware of density driven flow effects. Furthermore, the solid calcium carbonate is formed in the pores, causing a decrease in porosity and permeability.

## 1.4 Biogrout - the modelling

In the applications, mentioned in Subsection 1.2, it is desirable, if not essential, to be able to give a good prediction of the result of the Biogrout treatment. Therefore, a thorough understanding of the process is crucially important as well as a good model to describe it. The following parameters play a major role in the Biogrout process and should be contained in the model:

- the microbial activity;
- the concentrations of urea, calcium, ammonium and calcium carbonate, which change due to dispersion, advection and reaction;
- flow through the porous medium, which is influenced by injection, extraction and changing density, porosity and permeability.
- porosity and permeability, which decrease as a result of the precipitation of the solid calcium carbonate;
- the density of the solution, which changes due to its altering composition and which is larger than the density of water, resulting into density driven flow effects;

Since the process is quite complex and since the parameters influence each other, a good model, combining these essential features, is indispensable, though a balance between simplicity and complexity should also be sought since very complicated models often require the use of many parameters that are hard or even impossible to obtain. Fitting procedures [6,98] will become expensive and even ill-posedness of the optimization problem with respect to experimentally measured results can occur if the number of (unknown) object parameters is large. The aim of the simulations in this thesis is the prediction of the calcium carbonate concentration. A relation with strength is given in [87].

This thesis focusses on reactive transport in fully saturated porous media, including the transport of micro-organisms. The effect of density driven flow on the Biogrout process is also considered. Reactive transport in porous media is a well-known issue in the literature, see for example [2, 11, 16, 44, 45, 49, 50, 52, 65–68, 79, 81]. Further, the transport of micro-organisms has been studied for decades, [32, 33, 38, 41, 55, 56, 64, 74, 82, 99]. In this thesis (Chapter 8), front instabilities or fingers are induced by generating an inhomogeneous porous media. The model equations, used to describe the Biogrout process, are used to investigate the effect of the formation of fingers on the Biogrout process. Density driven flow is studied more exhaustively in [15, 21, 25, 26, 29, 40, 42, 58, 70, 78].

In the literature, three other models are found that describe MICP: [6, 27, 31]. These references all describe Darcy scale (macro-scale) models.

The model in [6] includes the reaction of the hydrolysis of urea and the precipitation/dissolution of calcium carbonate. The porosity is assumed to be constant and the transport of bacteria is not considered. Flow column experiments were compared to 1D simulations. The two constants in the initial distribution function

for the amount of urease and the precipitation rate constant were fitted in order to find a good match to the experimental data.

In [27] a more complex model is proposed to investigate the use of MICP to set up subsurface hydraulic barriers to increase the storage security near boreholes of CO<sub>2</sub> storage sites. The formalism includes multiphase flow, transport, hydrolysis of urea, precipitation/dissolution of calcium carbonate, acid-base equilibria, growth and decay of micro-organisms and a decreasing porosity.

In [31] the transport of bacteria, urea hydrolysis and calcium carbonate precipitation are combined with the mechanical properties of the treated soil. Besides transport and reactions, it predicts porosity and permeability reduction, compressibility reduction and stiffness increase.

## 1.5 Organisation of this thesis

In **Chapter 2**, model equations are derived in order to describe the Biogrout process, assuming a reaction rate that is homogeneous in space. Several simulations are done with one and two-dimensional configurations. In **Chapter 3**, the extension to 3D is made. **Chapter 4** proposes a model for the placement of the micro-organisms and gives the analytical solution for a specific case. The placement model is combined with the soil reinforcement model in **Chapter 5**. Chapter 6 to Chapter 8 report the research on certain specific aspects: **Chapter 6** compares several flow equations. This comparison leads to an adaptation of the flow equation, that was used earlier. **Chapter 7** proposes a way to deal with hydrostatic pressure boundary conditions with an altering fluid density. **Chapter 8** focuses on front instabilities in density driven flow, comparing simulations with an experiment. **Chapter 9** compares the outcome of numerical simulations with a Biogrout experiment. Finally, some general conclusions and outlook can be found in **Chapter 10**. A list with the used symbols is given in **Appendix A**.



**Modelling Biogrout: a new ground improvement  
method based on microbial induced carbonate  
precipitation**

This chapter has been published as:

Van Wijngaarden, W.K., Vermolen, F.J., van Meurs, G.A.M., Vuik, C.: Modelling Biogrout: A New Ground Improvement Method Based on Microbial-Induced Carbonate Precipitation. *Transport in Porous Media* **87-2**, 397–420 (2011)

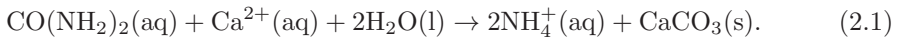
## Abstract

Biogrout is a new soil reinforcement method based on microbial induced carbonate precipitation. Bacteria are placed and reactants are flushed through the soil, resulting in calcium carbonate precipitation, causing an increase in strength and stiffness of the soil. Due to this precipitation, the porosity of the soil decreases. The decreasing porosity influences the permeability and therefore the flow. To analyse the Biogrout process, a model was created that describes the process. The model contains the concentrations of the dissolved species that are present in the biochemical reaction. These concentrations can be solved from a advection-dispersion-reaction equation with a variable porosity. Other model equations involve the bacteria, the solid calcium carbonate concentration, the (decreasing) porosity, the flow and the density of the fluid. The density of the fluid changes due to the biochemical reactions, which results in density driven flow. The partial differential equations are solved by the Standard Galerkin Finite Element Method. Simulations are done for some 1D and 2D configurations. A 1D configuration can be used to model a column experiment and a 2D configuration may correspond to a sheet or a cross section of a 3D configuration.

## 2.1 Introduction<sup>1</sup>

Biogrout is a new soil reinforcement method based on microbial induced carbonate precipitation (MICP), see, among others, [97] and [83].

The overall Biogrout reaction equation is given by:



Urea ( $\text{CO}(\text{NH}_2)_2$ ) is hydrolysed and if calcium ions ( $\text{Ca}^{2+}$ ) are present, ammonium ( $\text{NH}_4^+$ ) and calcium carbonate ( $\text{CaCO}_3$ ) are formed. The current model for Biogrout is inspired by the study of [100]. In Chapter 2 and 3 of aforementioned book, the Advection-Diffusion-Reaction differential equation in saturated porous media has been derived for a time independent porosity. In the Biogrout case, the porosity is time dependent. Hence, to get the right differential equation for the concentration of urea, ammonium and calcium, this derivation should be repeated for a time dependent porosity. Also the differential equation for the (non aqueous) calcium carbonate concentration should be derived. Of course, the flow should also be known. The flow can be calculated from a differential equation for it. Another possibility is to calculate the flow from a differential equation for the pressure, since the pressure is related to the flow by Darcy's Law, derived in Chapter 1 of [100]. Since the boundary conditions are often given in terms of pressure and the density of the fluid is not constant, it is better to calculate the flow from a differential equation for the pressure. Hence, a differential equation for the pressure should be derived. Because of the decreasing porosity, this is not really trivial. To use Darcy's Law, the intrinsic permeability should be known. For a relation between the intrinsic permeability and the porosity, [7] has been used. Further, for a relation between the density and the various concentrations, [95] has been used.

<sup>1</sup>Parts of the original introduction have been skipped in order to prevent too much repetition of the Introduction from Chapter 1.

In [101] is explained how differential equations can be solved with the Finite Element Method. The partial differential equations that are derived are (non-linear) hyperbolic differential equations. [53] provide a method to solve this kind of differential equations with Finite Elements. If the transport equations are advection dominated, instead of the SG (Standard Galerkin) method a SUPG (Streamline Upwind Petrov Galerkin) method can be used to get a stable solution, see for instance [28, 37, 51]. Also the DG (Discontinuous Galerkin) method can be applied, see [3, 18], preferably with slope limiters, see for instance [17] and [48]. In [13, 52] several numerical methods are applied to model reactive transport in porous media.

This chapter contains the following. Section 2.2 describes the model for the Biogrout process and gives an exact solution for a special case. The model is based on the overall Biogrout reaction equation (2.1). Furthermore, in Section 2.2 partial differential equations are derived to describe the concentration of all the species in this reaction equation. Due to the precipitation of calcium carbonate, the porosity decreases. A relation between the calcium carbonate concentration and the porosity is also given in Section 2.2, just like the derivation of the flow equations. Under particular conditions, an exact solution can be found. The derivation of this solution can be found in Subsection 2.2.2. Section 2.3 is devoted to the numerical methods that are used. Section 2.4 contains some computer simulations and in Section 2.5 some conclusions and discussion can be found.

## 2.2 The mathematical model

In Subsection 2.2.1, the differential equations that are needed to describe the Biogrout process are derived. In Subsection 2.2.2, an exact solution for the porosity and the calcium carbonate concentration is derived for a special case.

### 2.2.1 Derivation of the differential equations

In this section, a model is developed for the Biogrout process. The differential equations are derived for the concentrations of the various species, for the porosity and for the flow. These differential equations are derived under the assumptions that:

1. Only dissolved species react;
2. The reaction consists of sorption, an hydrolysis reaction and a precipitation reaction;
3. The equilibrium between the sorbed and the dissolved phase is reached instantaneously;
4. The biochemical reaction of the Biogrout process is governed by reaction (2.1) and is also assumed to take place instantaneously;
5. Calcium carbonate is not transported but it precipitates on the matrix of the porous medium;

6. The fluid is incompressible;
7. The hydrolysis of urea and the precipitation of calcium carbonate have no influence on the total volume of the fluid over the entire domain of computation;
8. The viscosity is constant.

### The differential equations for the aqueous species: urea, calcium chloride and ammonium chloride

First the differential equations for the aqueous species are derived. In [100], the Advection-Dispersion-Reaction equation for the transport of a solute species in porous media has been derived for a time independent porosity. Following this derivation, but now for a time dependent porosity and under assumption 2, the following differential equation is derived:

$$R\theta\frac{\partial C}{\partial t} = \nabla \cdot (\theta\mathbf{D} \cdot \nabla C) - \mathbf{q} \cdot \nabla C + q_s C_s - \left( \frac{\partial \theta}{\partial t} + \nabla \cdot \mathbf{q} \right) C + \theta m r_{hp}, \quad (2.2)$$

where the retardation factor is given by

$$R = 1 + \frac{\rho_b}{\theta} \frac{\partial \bar{C}}{\partial C}. \quad (2.3)$$

In these equations,  $C$  is the dissolved concentration of the species (per pore volume),  $\bar{C}$  is the sorbed concentration,  $\theta$  is the porosity,  $\mathbf{D}$  is the dispersion tensor,  $\mathbf{q}$  is the Darcy velocity,  $q_s$  is the volumetric flow rate, representing fluid sources (positive) and sinks (negative),  $C_s$  is the concentration of the source or sink,  $r_{hp}$  is the reaction rate of equation (2.1),  $m$  is some constant and  $\rho_b$  is the bulk dry density.

The term at the left-hand side of equation (2.2) represents the accumulation and contains the retardation factor  $R$ , which is a measure for the retarding effect of sorption. The first term at the right-hand side represents the effect of dispersion and diffusion, the second term models advection and the third term represents a source or a sink. The fourth term is a result of the chain rule, applied on the accumulation term and the advection term. The last term represents the rate of change in solute mass (or moles) of a particular species due to the reaction as given in equation 2.1.

In one dimension, the dispersion tensor is given by  $\mathbf{D} = \alpha_L |\mathbf{v}|$ . In more dimensions, the coefficients of the dispersion tensor  $\mathbf{D}$  are represented by  $D_{ij} = (\alpha_L - \alpha_T) \frac{v_i v_j}{|\mathbf{v}|} + \delta_{ij} \alpha_T \sum_i \frac{v_i^2}{|\mathbf{v}|}$ , see [100]. The quantity  $\alpha_L$  is the longitudinal dispersivity and  $\alpha_T$  is the transverse dispersivity. The values for the longitudinal and transverse dispersivity that are used in this chapter come from [34]. The quantity  $\delta_{ij}$  is the Kronecker delta that equals 1 if  $i = j$  and 0 otherwise. The factor  $\mathbf{v}$  is the pore water velocity and the relation with the Darcy velocity,  $\mathbf{q}$ , is given by:  $\mathbf{v} = \frac{\mathbf{q}}{\theta}$ . The quantity  $r_{hp} = r_{hp}(C^{urea}, C^{NH_4^+}, C^{Ca^{2+}}, C^{CaCO_3}, \theta, t)$  is the reaction rate of the reaction given in equation 2.1 (in mole per pore volume per unit of time) and is a possibly non-linear function of the concentrations, the porosity and time. The value of the constant  $m$  differs from species to species and follows from the relation between the reactants and products in reaction equation (2.1). The value of  $m$  for calcium carbonate is given by  $m = 1$ , since calcium carbonate is formed at

a rate  $r_{hp}$ . If one mole of calcium carbonate is formed, two moles of ammonium are formed and one mole of calcium and one mole of urea are consumed. Hence, in the differential equation for ammonium, the value  $m = 2$  is used and in the differential equation for calcium and urea, the value  $m = -1$  is used. This gives the following differential equations for urea, calcium chloride and ammonium chloride:

$$R^{urea}\theta\frac{\partial C^{urea}}{\partial t} = \nabla \cdot [\theta\mathbf{D} \cdot \nabla C^{urea}] - \mathbf{q} \cdot \nabla C^{urea} + q_s^{urea}C_s^{urea} + \theta r_{hp} - \left(\frac{\partial\theta}{\partial t} + \nabla \cdot \mathbf{q}\right)C^{urea}, \text{ with } R^{urea} = 1 + \frac{\rho_b}{\theta}\frac{\partial\bar{C}^{urea}}{\partial C^{urea}}, \quad (2.4)$$

$$R^{Ca^{2+}}\theta\frac{\partial C^{Ca^{2+}}}{\partial t} = \nabla \cdot [\theta\mathbf{D} \cdot \nabla C^{Ca^{2+}}] - \mathbf{q} \cdot \nabla C^{Ca^{2+}} + q_s^{Ca^{2+}}C_s^{Ca^{2+}} + \theta r_{hp} - \left(\frac{\partial\theta}{\partial t} + \nabla \cdot \mathbf{q}\right)C^{Ca^{2+}}, \text{ with } R^{Ca^{2+}} = 1 + \frac{\rho_b}{\theta}\frac{\partial\bar{C}^{Ca^{2+}}}{\partial C^{Ca^{2+}}}, \quad (2.5)$$

$$R^{NH_4^+}\theta\frac{\partial C^{NH_4^+}}{\partial t} = \nabla \cdot [\theta\mathbf{D} \cdot \nabla C^{NH_4^+}] - \mathbf{q} \cdot \nabla C^{NH_4^+} + q_s^{NH_4^+}C_s^{NH_4^+} + 2\theta r_{hp} - \left(\frac{\partial\theta}{\partial t} + \nabla \cdot \mathbf{q}\right)C^{NH_4^+}, \text{ with } R^{NH_4^+} = 1 + \frac{\rho_b}{\theta}\frac{\partial\bar{C}^{NH_4^+}}{\partial C^{NH_4^+}}. \quad (2.6)$$

### The differential equation for the non aqueous species: calcium carbonate

Next, a differential equation is derived for the concentration of the non aqueous calcium carbonate. Once calcium carbonate is generated, it immediately precipitates and attaches onto the matrix of the porous medium. Therefore, its concentration is defined in terms of weight per unit volume (and not per unit pore volume). Since it has been assumed that the calcium carbonate will not be transported, the concentration of calcium carbonate will only be changed by the biochemical reaction. Consider a small box. The number of calcium carbonate ions per pore volume that will be formed in this small box in time  $\Delta t$  is given by  $r_{hp}\Delta t$ . The number of *grams* of calcium carbonate ions per *total* volume within time period  $\Delta t$  is given by  $\Delta C^{CaCO_3} = m_{CaCO_3}\theta r_{hp}\Delta t$ , where  $m_{CaCO_3}$  is the molar mass of calcium carbonate. Dividing by  $\Delta t$  and taking the limit of  $\Delta t \rightarrow 0$  gives the following differential equation for the concentration of calcium carbonate:

$$\frac{\partial C^{CaCO_3}}{\partial t} = m_{CaCO_3}\theta r_{hp}. \quad (2.7)$$

### The differential equation for the porosity

Since the pore volume is being filled with calcium carbonate, the porosity (which is, by definition, the pore volume per total volume  $\left(\frac{V_{pore}}{V_{total}}\right)$ ) decreases. The change in porosity,  $\Delta\theta = -\frac{\Delta V_{pore}}{V_{total}} = -\frac{\Delta C^{CaCO_3}}{\rho_{CaCO_3}}$ , in which  $\rho_{CaCO_3}$  is the density of calcium

carbonate. If this change is considered per time  $\Delta t$ , subsequently taking the limit of  $\Delta t \rightarrow 0$ , the following differential equation is obtained for the porosity:

$$\frac{\partial \theta}{\partial t} = -\frac{1}{\rho_{CaCO_3}} \frac{\partial C^{CaCO_3}}{\partial t}. \quad (2.8)$$

Solving this differential equation gives:

$$\theta(t) = \theta(0) - \frac{C^{CaCO_3}(t) - C^{CaCO_3}(0)}{\rho_{CaCO_3}}. \quad (2.9)$$

Hence, if the concentration of calcium carbonate is known, subsequently the porosity can be calculated.

### The differential equations for the flow

It has been assumed that the fluid is incompressible and that the hydrolysis of urea and the precipitation of calcium carbonate have no influence on the total volume of the fluid over the entire domain of computation (assumption 6 and 7). These two assumptions imply that there is conservation of fluid volume. Due to the precipitation of calcium carbonate, the pore space decreases. Hence, the nett fluid flow through  $\Gamma_\epsilon$ , the boundary of any control volume  $\Omega_\epsilon$  in the computational domain  $\Omega$ , must equal the decrease in pore volume in  $\Omega_\epsilon$  per unit of time. Hence:

$$\int_{\Gamma_\epsilon} \mathbf{q} \cdot \mathbf{n} d\Gamma = - \int_{\Omega_\epsilon} \frac{\partial \theta}{\partial t} d\Omega. \quad (2.10)$$

Applying the divergence theorem of Gauss to the left-hand side of (2.10) gives

$$\int_{\Omega_\epsilon} \nabla \cdot \mathbf{q} d\Omega = - \int_{\Omega_\epsilon} \frac{\partial \theta}{\partial t} d\Omega. \quad (2.11)$$

Equation (2.11) holds for any  $\Omega_\epsilon \subseteq \Omega$  and hence

$$\nabla \cdot \mathbf{q} = -\frac{\partial \theta}{\partial t}. \quad (2.12)$$

Substituting (2.7) into (2.8) and substituting the result into (2.12), gives the following differential equation for the flow:

$$\nabla \cdot \mathbf{q} = \frac{m_{CaCO_3}}{\rho_{CaCO_3}} \theta r_{hp}. \quad (2.13)$$

In [100], Darcy's Law is given by:

$$\begin{aligned} q_x &= -\frac{k_x}{\mu} \frac{\partial p}{\partial x}, \\ q_y &= -\frac{k_y}{\mu} \frac{\partial p}{\partial y}, \\ q_z &= -\frac{k_z}{\mu} \left( \frac{\partial p}{\partial z} + \rho_l g \right). \end{aligned} \quad (2.14)$$

In Darcy's Law,  $p$  is the pressure,  $k$  is the intrinsic permeability in the various coordinate directions,  $\mu$  is the viscosity that is assumed to be constant in the Biogrowth case and  $\rho_l$  is the density of the solution.

Substituting (2.14) into (2.13), using (2.16), gives the following differential equation for the pressure:

$$-\nabla \cdot \left( \frac{k}{\mu} (\nabla p + \rho_l g \mathbf{e}_z) \right) = \frac{m_{CaCO_3} \theta r_{hp}}{\rho_{CaCO_3}}. \quad (2.15)$$

The resulting pressure is used to calculate the flow, using Darcy's Law (2.14).

### The intrinsic permeability and the density

To calculate the pressure and the flow, the intrinsic permeability and the density of the solution should be known.

The intrinsic permeability is determined, using the Kozeny-Carman relation: an empiric relation between the intrinsic permeability and the porosity that is commonly used in ground water flow modelling (see [7]):

$$k = k_x = k_y = k_z = \frac{(d_m)^2}{180} \frac{\theta^3}{(1 - \theta)^2}. \quad (2.16)$$

In this relation,  $d_m$  is the mean particle size of the subsurface medium. If the porosity is very low, it might be that the pores are not connected. Hence, the intrinsic permeability is zero. This phenomenon is not directly incorporated in the Kozeny-Carman relation, [61]. If the porosity is close to zero, the Kozeny-Carman relation behaves as a third order polynomial. and the permeability is almost zero, although not equal to zero. Since in the simulations of the Biogrowth process the porosity is higher than 0.12, the use of the Kozeny-Carman relation is maintained.

The density of the solution (at 20°C) will be calculated with the following experimental relation:

$$\rho_l = 1000 + 15.4996C^{urea} + 86.7338C^{Ca^{2+}} + 15.8991C^{NH_4^+}. \quad (2.17)$$

This relation has been found, using [95]. From the tables of the individual species, a linear relation between the concentration and the density increase has been found. By adding the contributions of the several species, relation (2.17) was found. Experimental validation showed that this relation is a good description of reality.

### The reaction rate

The reaction rate depends on many factors, like the number of bacteria, growth and storage conditions before use [96]. Conditions in the subsoil can also influence the reaction rate, like the temperature [4] and the pH [71, 96]. The concentrations of urea, ammonium chloride and calcium chloride might be too high for the bacteria. Encapsulation by calcium carbonate crystals can make a diffusion barrier around the bacteria [5]. Another point is that aerobic bacteria are injected into an anaerobic subsoil. Due to the lack of oxygen, the bacteria die. All these phenomena make it likely that the reaction rate decreases. This is also shown in experiments [97].

For the moment a linear decay has been assumed: in  $t_{max}$  seconds the reaction rate decreases from a maximal reaction rate,  $v_{max}$ , to zero. The quantity  $v_{max}$  is constant, since the distribution of bacteria is assumed to be homogeneous. Further, the reaction rate equals zero, if there is no urea present and is maximal if an abundant amount of urea is present. The following formula will be used for the reaction rate:

$$r_{hp} = \begin{cases} v_{max} \frac{C^{urea}}{K_{m,urea} + C^{urea}} \left(1 - \frac{t}{t_{max}}\right) & \text{if } 0 \leq t \leq t_{max} \\ 0 & \text{else} \end{cases} \quad (2.18)$$

In this equation, the saturation constant  $K_{m,urea}$  is small.

### General perspective and initial conditions

For the aqueous species (urea, calcium and ammonium), differential equations (2.4), (2.5) and (2.6) were derived. For the non aqueous species (calcium carbonate), differential equation (2.7) was derived. The porosity can be calculated with formula (2.9). For the pressure, differential equation (2.15) was derived. The flow can be calculated with Darcy's law, (2.14). The intrinsic permeability  $k$ , the density of the solution  $\rho_l$  and the reaction rate  $r_{hp}$  can be calculated with respectively formula (2.16), (2.17) and (2.18). The quantities  $q_s$ ,  $C_s$ ,  $\mathbf{D}$ ,  $m_{CaCO_3}$ ,  $\rho_{CaCO_3}$ ,  $d_m$ ,  $\mu$ ,  $g$ ,  $v_{max}$ ,  $t_{max}$ ,  $K_{m,urea}$  and  $\frac{\partial \bar{C}}{\partial C}$  are assumed to be known. Initially, the concentration of calcium carbonate, urea, calcium and ammonium are equal to zero. The boundary conditions for the pressure and the concentration of urea, calcium and ammonium are given in Section 2.4, since they differ from case to case. Having these boundary conditions, the equations have a unique solution. How this solution will be approximated, will be explained in Section 2.3. But first an exact solution will be derived for a special case.

### 2.2.2 Exact solution for a special case

In this subsection, a formula will be derived to calculate the calcium carbonate concentration as a function of time ( $0 \leq t \leq t_{max}$ ) for a constant urea (and calcium) concentration.

The rate function (2.18) on this time interval is substituted in the differential equation for the calcium carbonate concentration (2.7). The result is substituted into the differential equation for the porosity:

$$\frac{\partial \theta}{\partial t} = -\theta r_{hp} \frac{m_{CaCO_3}}{\rho_{CaCO_3}} = -\theta \frac{m_{CaCO_3}}{\rho_{CaCO_3}} v_{max} \frac{C^{urea}}{K_{m,urea} + C^{urea}} \left(1 - \frac{t}{t_{max}}\right). \quad (2.19)$$

Solving equation (2.19) by dividing by  $\theta$  and integrating from 0 to  $t$  gives the following function for the porosity as a function of time:

$$\theta(t) = \theta_0 \exp \left\{ -\frac{m_{CaCO_3}}{\rho_{CaCO_3}} v_{max} \frac{C^{urea}}{K_{m,urea} + C^{urea}} \left( t - \frac{t^2}{2t_{max}} \right) \right\}. \quad (2.20)$$

Substituting equation (2.20) and rate function (2.18) into the differential equation for calcium carbonate, (2.7), gives

$$\begin{aligned} \frac{\partial C^{CaCO_3}}{\partial t} = & m_{CaCO_3} \theta_0 \left\{ v_{max} \frac{C^{urea}}{K_{m,urea} + C^{urea}} \left( 1 - \frac{t}{t_{max}} \right) \right\} \cdot \\ & \cdot \exp \left\{ - \frac{m_{CaCO_3}}{\rho_{CaCO_3}} v_{max} \frac{C^{urea}}{K_{m,urea} + C^{urea}} \left( t - \frac{t^2}{2t_{max}} \right) \right\}. \end{aligned} \quad (2.21)$$

Solving equation (2.21) by integrating from 0 to t, gives the following solution:

$$\begin{aligned} C^{CaCO_3}(t) = & C^{CaCO_3}(0) + \rho_{CaCO_3} \theta_0 + \\ & - \rho_{CaCO_3} \theta_0 \exp \left\{ - \frac{m_{CaCO_3}}{\rho_{CaCO_3}} v_{max} \frac{C^{urea}}{K_{m,urea} + C^{urea}} \left( t - \frac{t^2}{2t_{max}} \right) \right\}. \end{aligned} \quad (2.22)$$

This formula can be used to calculate the development of the calcium carbonate concentration exactly (for  $0 \leq t \leq t_{max}$ ) at places with a constant urea (and calcium chloride) concentration. This is for example at the inflow boundary. In Figure 2.1 the calcium carbonate concentration has been plotted as a function of time. The values of the constants in equation (2.22), that has been chosen to plot this figure, can be found in Table 2.1.

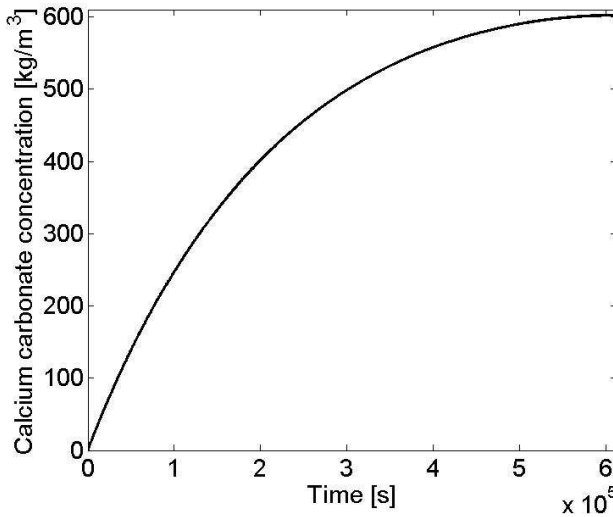


Figure 2.1: Plot of equation (2.22): the calcium carbonate concentration as a function of time for a constant urea and calcium concentration. The values of the constants in equation (2.22) can be found in Table 2.1.

## 2.3 Numerical method

In this section is explained which numerical methods are used to solve the equations in order to do simulations with the model.

### 2.3.1 Numerical method to solve the equations for the aqueous species

Currently, the Biogrout process is applied to sand. In that case, sorption of calcium, urea and ammonium plays an insignificant role. Hence, it can be assumed that the retardation factors for these species are equal to one. In the current model, there are no internal sources or sinks, hence  $q_s^{urea} = q_s^{Ca^{2+}} = q_s^{NH_4^+} = 0$ . Then, using equations (2.4), (2.5) and (2.6), combining them with equation (2.12), gives the following differential equations for the aqueous species:

$$\theta \frac{\partial C^{urea}}{\partial t} = \nabla \cdot [\theta \mathbf{D} \cdot \nabla C^{urea}] - \mathbf{q} \cdot \nabla C^{urea} - \theta r_{hp}, \quad (2.23)$$

$$\theta \frac{\partial C^{Ca^{2+}}}{\partial t} = \nabla \cdot [\theta \mathbf{D} \cdot \nabla C^{Ca^{2+}}] - \mathbf{q} \cdot \nabla C^{Ca^{2+}} - \theta r_{hp}, \quad (2.24)$$

$$\theta \frac{\partial C^{NH_4^+}}{\partial t} = \nabla \cdot [\theta \mathbf{D} \cdot \nabla C^{NH_4^+}] - \mathbf{q} \cdot \nabla C^{NH_4^+} + 2\theta r_{hp}. \quad (2.25)$$

These differential equations now become linear in the concentration, except for the differential equation for urea, since the reaction term, (2.18), is non-linear.

The differential equations for the pressure, the velocities and the concentrations of the aqueous species are solved by the Standard Galerkin Finite Element Method. First, the weak formulation is derived by multiplication by a test function  $\eta \in H^1(\Omega)$  and integration over the domain  $\Omega$ . For the time integration, an IMEX (implicit-explicit) scheme is used. That gives the following weak formulations for the urea concentration:

$$\begin{aligned} & \int_{\Omega} \theta^n \frac{(C^{urea})^{n+1} - (C^{urea})^n}{\Delta t} \eta d\Omega + \int_{\Omega} \left( \theta^n \mathbf{D}^n \cdot \nabla (C^{urea})^{n+1} \right) \cdot \nabla \eta d\Omega + \\ & - \oint_{\Gamma} \eta \left( \theta^n \mathbf{D}^n \nabla (C^{urea})^{n+1} \right) \cdot \mathbf{n} d\Gamma + \int_{\Omega} \mathbf{q}^{n+1} \cdot \nabla (C^{urea})^{n+1} \eta d\Omega = \\ & - \int_{\Omega} \theta^n r_{hp}^{n+1} \eta d\Omega, \end{aligned} \quad (2.26)$$

for all  $\eta \in H^1(\Omega)$ , which vanish at location of the boundary where  $C^{urea}$  is prescribed explicitly. Here only the equation for urea has been given since the other equations are dealt with analogously.

The Newton-Cotes quadrature rules have been used for the development of the element matrices and vectors. Line elements are used in 1D, whereas triangular elements are used in 2D. In both cases linear basis functions are used.

### 2.3.2 Numerical method to solve the equations for the pressure and the flow

For the pressure,  $p$ , the following weak formulation is derived:

$$\begin{aligned} \int_{\Omega} \frac{k^n}{\mu} (\nabla p^{n+1} + \rho_l^n g \mathbf{e}_z) \cdot \nabla \eta d\Omega - \oint_{\Gamma} \eta \frac{k^n}{\mu} (\nabla p^{n+1} + \rho_l^n g \mathbf{e}_z) \cdot \mathbf{n} d\Gamma = \\ = \int_{\Omega} \frac{m_{CaCO_3}}{\rho_{CaCO_3}} \theta^n r_{hp}^n \eta d\Omega, \end{aligned} \quad (2.27)$$

and for the flow the following:

$$\int_{\Omega} q_x^{n+1} \eta d\Omega = - \int_{\Omega} \frac{k^n}{\mu} \frac{\partial p^{n+1}}{\partial x} \eta d\Omega, \quad (2.28)$$

$$\int_{\Omega} q_y^{n+1} \eta d\Omega = - \int_{\Omega} \frac{k^n}{\mu} \frac{\partial p^{n+1}}{\partial y} \eta d\Omega, \quad (2.29)$$

$$\int_{\Omega} q_z^{n+1} \eta d\Omega = - \int_{\Omega} \frac{k^n}{\mu} \left( \frac{\partial p^{n+1}}{\partial z} + \rho_l^n g \right) \eta d\Omega. \quad (2.30)$$

Also for these equations, the Newton-Cotes quadrature rules have been used for the development of the element matrices and vectors. Line elements are used in 1D, whereas triangular elements are used in 2D. In both cases linear basis functions are used.

### 2.3.3 Non aqueous species

Since the differential equation for the concentration of calcium carbonate, (2.7), is an ordinary differential equation (in each grid point), it is not necessary to use the Finite Element Method. Using an IMEX-scheme for the time integration, the following equation can be used to calculate the calcium carbonate concentration on the next time step:

$$\frac{(C^{CaCO_3})^{n+1} - (C^{CaCO_3})^n}{\Delta t} = m_{CaCO_3} \theta^n r_{hp}^{n+1}. \quad (2.31)$$

### 2.3.4 Scheme for solving the equations

In order to do simulations with the model, the time span has been divided into equisized time steps. At each time step, equation (2.26) to (2.31) are solved. First the equation for the pressure, (2.27), is solved, using the intrinsic permeability, density, porosity and reaction rate from the previous time step. Subsequently, the velocities are calculated, using equation (2.28), (2.29) and/or (2.30). Again, the intrinsic permeability and the density from the previous time step are used. The differential equation for the urea concentration, (2.26), is solved implicitly, using the porosity from the previous time step. Newton's method is used, to cope with

the non-linearity in the reaction term. Due to the mass balance, in each differential equation for the concentration the same  $r_{hp}$  should be used. This  $r_{hp}$  follows from the differential equation for the urea concentration. The differential equations for the concentrations of calcium and ammonium are also solved using an implicit-explicit method, with the porosity from the previous time step. Subsequently the equation for the calcium carbonate concentration, (2.31), is solved, using the porosity from the previous time step and the reaction rate on the new one. Finally, the porosity ( $\theta$ ) and the intrinsic permeability ( $k$ ) are recalculated with (2.9) and (2.16), respectively. If necessary, also the boundary conditions and the density of the fluid ( $\rho_l$ ) are updated. The density of the fluid is calculated with the use of equation (2.17).

## 2.4 Results

In this section, the results of several simulations with the model are shown. In Subsection 2.4.2, some one-dimensional simulations are presented. The configuration and the boundary conditions are given in Subsection 2.4.1. Subsection 2.4.4 contains results from simulations with the two-dimensional model. The configuration and boundary conditions for the various 2D cases are given in Subsection 2.4.3.

Table 2.1 shows the values that are taken for the various constants. These values are used in both the 1D simulations and the 2D simulations, unless stated otherwise.

$m_{CaCO_3}$	$= 0.1001 \text{ kg mol}^{-1}$ ,	$\rho_{CaCO_3}$	$= 2710 \text{ kg m}^{-3}$ ,
$v_{max}$	$= 9.0 \cdot 10^{-2} \text{ mol m}^{-3}\text{s}^{-1}$ ,	$K_{m,urea}$	$= 10 \text{ mol m}^{-3}$ ,
$c_{in}$	$= 1.0 \cdot 10^3 \text{ mol m}^{-3}$ ,	$q_{in}$	$= 5.0 \cdot 10^{-6} \text{ m s}^{-1}$ ,
$d_m$	$= 2.0 \cdot 10^{-4} \text{ m}$ ,	$p_1$	$= 100854 \text{ Pa}$ ,
$p_2$	$= 1.00 \cdot 10^5 \text{ Pa}$ ,	$\mu$	$= 1.15 \cdot 10^{-3} \text{ Pa s}$ ,
$\theta_0$	$= 0.35$ ,	$\alpha_L$	$= 0.01 \text{ m}$ ,
$\alpha_T$	$= 0.001 \text{ m}$ ,	$L$	$= 1.0 \text{ m}$ ,
$M$	$= 0.5 \text{ m}$ ,	$t_{max}$	$= 6.12 \cdot 10^5 \text{ s}(=170\text{h})$ .

Table 2.1: The values that are taken for the various constants.

### 2.4.1 Configuration and boundary conditions for a simulation with the one-dimensional model

The domain is a line segment with length  $L$ , which can be the one-dimensional representation of a column with a small diameter and length  $L$ . The domain is subdivided into 50 (line) elements.

There are several possibilities for boundary conditions. The pressure may be equal to a constant at the inflow boundary and at the outflow boundary as well (the pressure driven case). Another possibility is that the flow through the inflow boundary is constant (the flow driven case). These two cases will be simulated with the model. The results will show the influences of these two cases on the calcium carbonate concentration. The boundary at the left-hand side,  $\Gamma_1$ , is the inflow boundary, the boundary at the right-hand side,  $\Gamma_2$ , is the outflow boundary.



Figure 2.2: Configuration of the one-dimensional domain.

Table 2.2 displays the boundary conditions that are chosen for the pressure and the concentration of urea, calcium and ammonium in the one-dimensional configuration, for both the flow driven case and the pressure driven case.

	$\Gamma_1$	$\Gamma_2$
$p$	$\begin{cases} -\frac{k}{\mu} \frac{\partial p}{\partial n} = q_{in} & \text{flow driven case} \\ p = p_1 & \text{pressure driven case} \end{cases}$	$p = p_2$
$C^{urea}$	$C^{urea} = c_{in}$	$\frac{\partial C^{urea}}{\partial n} = 0$
$C^{Ca^{2+}}$	$C^{Ca^{2+}} = c_{in}$	$\frac{\partial C^{Ca^{2+}}}{\partial n} = 0$
$C^{NH_4^+}$	$C^{NH_4^+} = 0$	$\frac{\partial C^{NH_4^+}}{\partial n} = 0$

Table 2.2: Boundary conditions for the pressure and the concentration of urea, calcium and ammonium in the one-dimensional case.

The differential equation for the concentration of calcium is equal to the differential equation for urea. Since also the initial conditions and the boundary conditions are equal, the concentration of urea and calcium are equal. Hence, it is not necessary to calculate them both. Only the urea concentration is calculated.

### 2.4.2 Results from a simulation with the one-dimensional model

This subsection contains results of simulations for a one-dimensional configuration. Figures are shown with the pressure and the velocity at the inflow boundary. It also contains some plots of the urea concentration as a function of space and time and some plots of the calcium carbonate concentration, porosity and intrinsic permeability.

#### Pressure and velocity at the inflow boundary

Figure 2.3 shows the inflow velocity and the pressure at the inflow boundary for both the pressure driven case and the flow driven case. Initially, the inflow velocity is high in the pressure driven case. Due to the precipitation of calcium carbonate, the porosity and the permeability decrease. Since the pressure at the inflow and outflow boundary stays constant, the inflow velocity decreases. In the flow driven case, the flow rate is constant. Since the porosity and the intrinsic permeability decrease due to the precipitation of calcium carbonate, the pressure at the inflow boundary should increase to keep the flow rate constant.

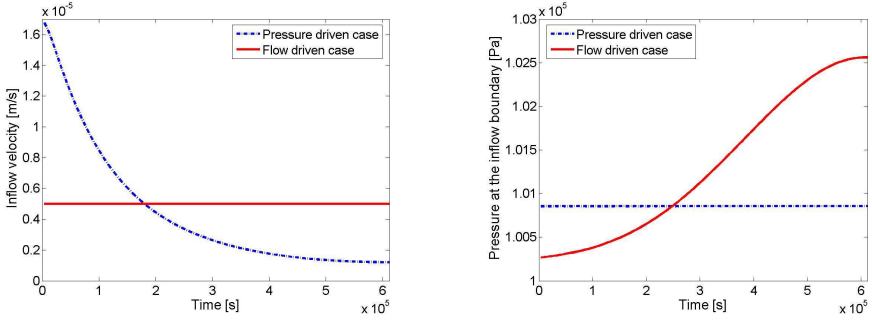


Figure 2.3: Left: the inflow velocity as a function of time for the pressure driven case and the flow driven case, right: the pressure at the inflow boundary as a function of time for the pressure driven case and the flow driven case.

## Results for urea

Figure 2.4 displays the concentration of urea as a function of the position in the column at several times and Figure 2.5 shows the concentration of urea as a function of time at several positions in the column, for both the flow driven case and the pressure case. Figure 2.6 displays the penetration depth of urea and also  $M_{CaCO_3} = \int_{\Omega} C^{CaCO_3} d\Omega$ , the total amount of calcium carbonate as a function of time, both for the flow driven case and the pressure driven case. The penetration depth has been defined as the largest distance from the inflow boundary for which  $C^{urea} \geq \frac{K_{m,urea}}{100}$ . From Figure 2.4 and 2.5 it can be seen that in the flow driven case, the urea concentration is a non-decreasing function of time at all specified positions in the column. In the pressure driven case, the urea concentration at  $x=0.2m$  and  $x=0.5m$  decreases in time for some while. These results correspond to the plot of the penetration depth of urea as a function of time in Figure 2.6. In the flow driven case, the urea penetrates further and further into the column. At the end, the urea even flows out. In the pressure driven case, initially the penetration depth increases very rapidly. Then it decreases for a while and after that it starts increasing again. The urea does not flow out within a time period of  $6.12 \cdot 10^5 s = 170h$ .

These results are explained as follows: Let us start with the flow driven case. In this case the flow rate is constant. Initially the reaction rate of the urea hydrolysis is high. Hence the urea does not get the possibility to penetrate far into the column. The reaction rate decreases in time. Hence, at a later stage, the urea can penetrate further into the column before all urea molecules react. This effect is enhanced by the fact that, when urea reacts in the presence of carbonate, the solid calcium carbonate will be formed. This decreases the porosity. As a result, the pore water velocity,  $v$ , increases, since  $v = \frac{q}{\theta}$ . That also causes urea to penetrate further into the column before it is hydrolysed.

In the pressure driven case, initially, the inflow velocity is high, so the urea can penetrate far into the column. Then, the penetration depth decreases and halfway, it starts increasing again. This behaviour of the penetration depth is the result of several phenomena: The porosity and the permeability decrease due to the formation

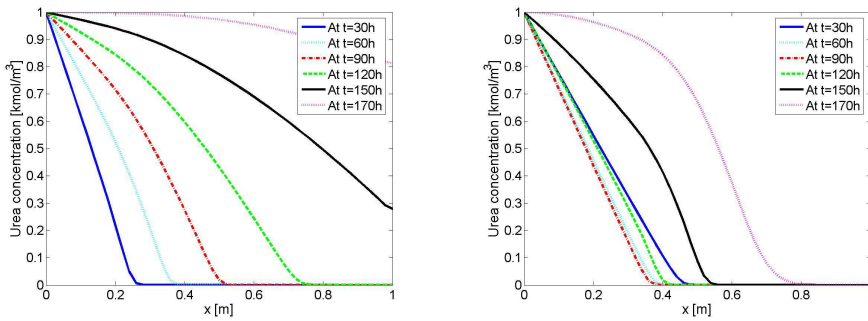


Figure 2.4: The urea concentration as a function of x at several times. Left: flow driven case, right: pressure driven case.

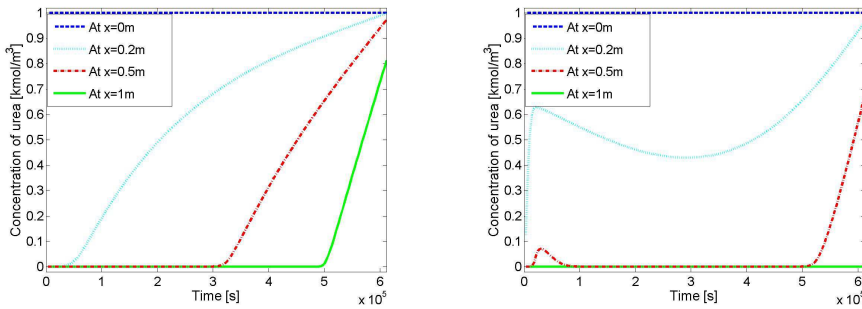


Figure 2.5: The urea concentration as a function of time at several positions in the column. Left: flow driven case, right: pressure driven case.

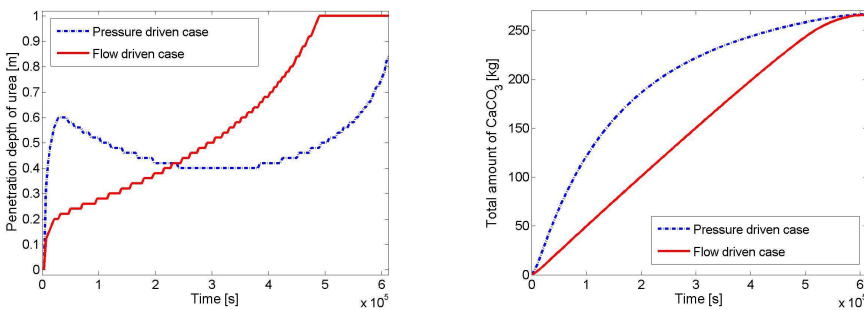


Figure 2.6: Left: the penetration depth of urea as a function of time for the pressure driven case and the flow driven case, right: the total amount of calcium carbonate as a function of time for the pressure driven case and the flow driven case.

of the solid calcium carbonate. As a consequence, the flow rate decreases too, since the pressure stays constant at the inflow boundary and at the outflow boundary, as

can also be seen from Figure 2.3. Another phenomenon is the decreasing reaction rate. As a result, the urea can penetrate further into the column before all urea molecules react.

After 170 hours, the reaction rate is equal to zero. However, the urea concentration in the column is not immediately equal to the inflow concentration everywhere. During the hours before, there was a reaction from bacterial activity and hence the urea concentration is lower than the inflow concentration (except at the inflow boundary). Only after some hours, the content of the pore volume of the column is fully refreshed and the urea concentration is equal to the inflow concentration everywhere.

### Results for calcium carbonate, porosity and permeability

Figure 2.6 also shows the total amount of calcium carbonate in the domain. Except for the last hours, the total amount of calcium carbonate grows linearly in time in the flow driven case. This means that per unit of time the same amount of calcium carbonate is formed. In the model, the reaction rate is linearly decreasing, so this result might look strange at first sight. However, the amount of urea and calcium that flows in per unit of time is constant and the urea and calcium should react or flow out. From Figure 2.6 it can be seen that the urea, and hence also the calcium, only flows out during the last hours. Hence, during the rest of the time all the urea and calcium, that flows in, should react. Since the supply of urea and calcium is constant in time, the amount of calcium carbonate that is formed per unit of time is also constant. During the last hours, urea flows out. That explains why the total amount of calcium carbonate is no longer growing that fast.

In the pressure driven case, the total amount of calcium carbonate is not linear in time so the production rate is not constant. From Figure 2.6 it can be seen that the urea does not flow out, so only the supply of urea (and calcium) influences the curve. In the pressure driven case, during the first hours the inflow velocity is higher than in the flow driven case. As a result, per unit of time more urea and calcium come in and hence more calcium carbonate will be formed. Hence, the slope of the graph is steeper than in the flow driven case. The inflow velocity decreases in time as can be seen from Figure 2.3. Per unit of time less urea and calcium flow in and hence less calcium carbonate can be formed. As a result the slope of the graph becomes less steep. Eventually the same amount of calcium carbonate has been formed.

Figure 2.7 displays the calcium carbonate concentration in the column at several times, both for the pressure driven case and the flow driven case. The relation with the penetration depth of urea is clear. For example, in the first 30 hours, in more than the half of the depth of the column, calcium carbonate has been formed in the pressure driven case. Eventually, the inflow velocity became that low, that the urea molecules could not reach the end of the column. As a result, no calcium carbonate has been formed in the last part of the column. In the flow driven case, only in the first part of the column calcium carbonate has been formed in the first 30 hours. Eventually the urea molecules reached the end of the column. As a result, everywhere in the column some calcium carbonate has been formed.

At  $x = 0$ , the urea concentration is constant during the process. Hence, using

formula (2.22), the analytic solution can be calculated. The analytical solution is  $602.1 \text{ kg/m}^3$ . The numerical solution at this position, in both the pressure driven case and the flow driven case, is equal to  $601.4 \text{ kg/m}^3$ . This is a relative error of only 0.12%. By increasing the number of time steps with a factor 2, the error in this point decreases also with a factor 2, so the error depends linearly on the size of the time step.

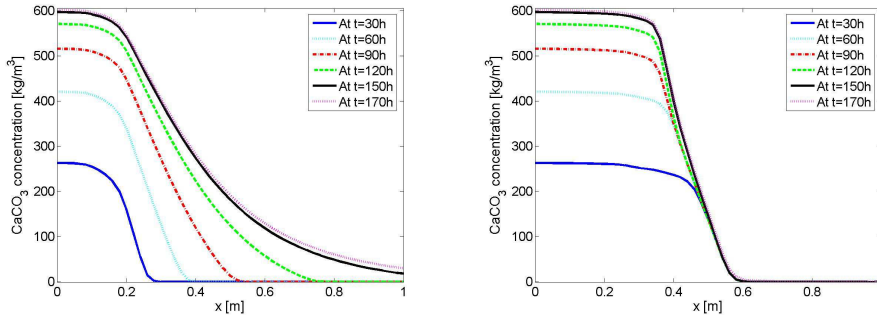


Figure 2.7: The concentration of calcium carbonate as a function of  $x$  at several times. Left: flow driven case, right: pressure driven case.

An increase of the generated calcium carbonate concentration, gives a decrease of both the porosity and intrinsic permeability. This phenomenon is confirmed in Figure 2.8. At  $x=0$ , the porosity equals 0.128, while the initial porosity was 0.35. So at  $x=0$ , the porosity has been decreased with a factor 2.7. At  $x=0$ , the intrinsic permeability was initially  $2.26 \cdot 10^{-11} \text{ m}^2$  and after the treatment  $6.14 \cdot 10^{-13} \text{ m}^2$ . That means a decrease by a factor of 37.

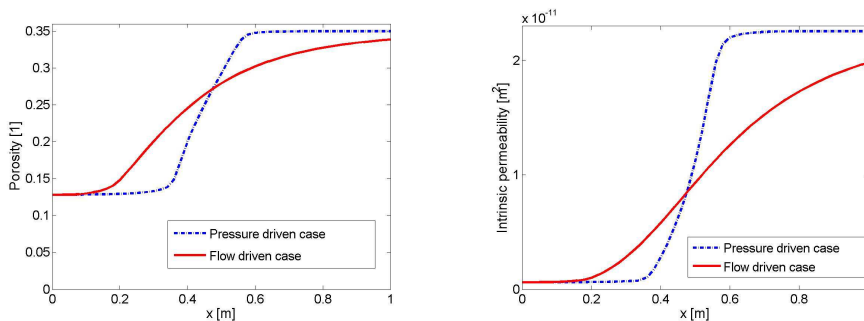


Figure 2.8: Left: the porosity as a function of the position at  $t=t_{max}$ , right: the intrinsic permeability as a function of the position at  $t=t_{max}$ .

In most applications, low-strength cementation (up to 1.5 MPa) will be sufficient, see [76]. This corresponds to a calcium carbonate content of approximately  $250 \text{ kg/m}^3$ , see [87]. In some specific cases, such as preventing liquefaction, only a minor increase in strength (up to 0.15 MPa) is necessary to prevent sand from flowing, see

[76]. This corresponds with a calcium carbonate content of approximately  $80 \text{ kg/m}^3$ , see [97]. BiogROUTed sand with a calcium carbonate concentration of approximately  $400 \text{ kg/m}^3$  has the same strength as low-strength concrete, see [76].

It depends on the application which injection strategy should be chosen. If one wants to reinforce only the first part of the column, but homogeneously, the pressure driven case (with the parameters chosen as in Table 2.1) is a good option, as displays Figure 2.7. If, for example, a calcium carbonate content of  $200 \text{ kg/m}^3$  is asked, the injection can be stopped after 30 hours. If one wants at least a minor increase in strength in the whole column, the flow driven case (with the parameters chosen as in Table 2.1) is a good option (Figure 2.7), although a better injection strategy can be chosen since only a minor increase in strength is sufficient.

### 2.4.3 Configuration and boundary conditions for a simulation with the two-dimensional model

In two dimensions, geometrical effects can be investigated, which was not possible in 1D. Also the influence of density driven flow can be investigated, now. In this subsection, the configuration and boundary conditions are given for five different cases. The first three cases have been constructed to investigate the effect of different permeabilities in one domain. The last two cases have been constructed to investigate the phenomenon density flow and the effect of the reaction on it.

In each case is the domain a rectangle which size  $L \times M$ . The domain is subdivided into 5,000 (triangular) elements. The fluid enters the domain through boundary  $\Gamma_1$  and flows out through boundary  $\Gamma_2$ . All cases are flow driven. The following five cases will be considered:

- Case 1: the lower half of the domain has a low permeability, inflow through the whole boundary at  $x = 0$ , no density flow;
- Case 2: the lower half of the domain has a low permeability, inflow through the upper part of the boundary at  $x = 0$ , no density flow;
- Case 3: the kernel of the domain has a low permeability, inflow through the lower part of the boundary at  $x = 0$ , no density flow;
- Case 4: density flow, without reaction, inflow through the whole boundary at  $x = 0$ ;
- Case 5: density flow, with reaction, inflow through the whole boundary at  $x = 0$ .

In the first two cases, the permeability of the lower half of the domain is initially  $10^{-4}$  times the permeability of the upper half, which has been achieved by choosing the mean particle size of the grains in the lower half to be  $10^{-2}d_m$ . This application accounts for two different adjacent soils. The permeability of the lower half is comparable with the permeability of clay. It is still assumed that there is no sorption. In the first case, the inflow boundary is the whole boundary at  $x = 0$  and the outflow boundary is the whole boundary at  $x = L$ .

In case 2 and 3, the inflow and outflow boundary are only one third of these boundaries. To have the same amount of urea and calcium chloride flowing into the

domain for all cases, the inflow velocity in case 2 and 3 has been chosen to be equal to  $3 \cdot q_{in}$ .

In case 3, there is a rectangle with a low permeability in the middle of the domain. In that rectangle, the mean particle size of the grains also equals  $10^{-2}d_m$ , like in the less permeable zones in case 1 and 2. In the plots with the numerical results the inflow and outflow boundaries are indicated with a thick black line. The low permeable zones are dark.

In case 4, the focus is on the density flow, without reaction. Urea and calcium chloride are injected with several inflow velocities. For the inflow velocities the following values has been chosen:  $q_{inflow}^1 = 1.0 \cdot 10^{-6} \text{m/s}$ ,  $q_{inflow}^2 = 5.0 \cdot 10^{-6} \text{m/s}$  and  $q_{inflow}^3 = 20 \cdot 10^{-6} \text{m/s}$ . In the one dimensional numerical simulations, the inflow velocity equals  $q_{inflow}^2$  in the flow driven case. In the pressure driven case, the inflow velocity varies between  $q_{inflow}^1$  and  $q_{inflow}^3$ . The simulation time has been chosen in such a way that the volume of injected fluid is equal.

In case 5, density flow is simulated in combination with reaction.

Table 2.3 displays the boundary conditions that are chosen. An extra term has been added to the pressure at the outflow boundary to deal with the gravity in the vertical plane.

	$p/q$	$C^{urea}/C^{Ca^{2+}}$	$C^{NH_4^+}$
$\Gamma_1$	$-\mathbf{q} \cdot \mathbf{n} = \begin{cases} q_{in} & \text{case 1, 4 and 5} \\ 3q_{in} & \text{case 2 and 3} \end{cases}$	$C = c_{in}$	$C^{NH_4^+} = 0$
$\Gamma_2$	$p = p_2 + \int_z^M \rho_l g \bar{z} d\bar{z}$	$\frac{\partial C}{\partial n} = 0$	$\frac{\partial C^{NH_4^+}}{\partial n} = 0$
$\Gamma_3$	$-\frac{k}{\mu} (\nabla p + \rho_l g \mathbf{e}_z) \cdot \mathbf{n} = 0$	$\frac{\partial C}{\partial n} = 0$	$\frac{\partial C^{NH_4^+}}{\partial n} = 0$

Table 2.3: Boundary conditions for the pressure and the concentration of urea, calcium and ammonium in the two-dimensional, flow driven case.

#### 2.4.4 Results from a simulation with the two-dimensional model

In this subsection, some two-dimensional results will be shown for the five cases, that are all flow driven. In the first three cases, the focus is on the effect of different permeabilities in one domain. The last two cases have been constructed to investigate the phenomenon density flow and the effect of the reaction on it.

##### The effect of different permeabilities in one domain

The calcium carbonate concentration (contour plot) and the flow (arrows) after the Biogrout process are shown in Figure 2.9 for case 1 and 2 and in Figure 2.10 for case 3.

From the result of case 1, it can be seen that the flow through the lower half of boundary  $\Gamma_1$  tries to reach the upper half of the domain, where the permeability is much higher. As a result, in the upper half of the domain more calcium carbonate

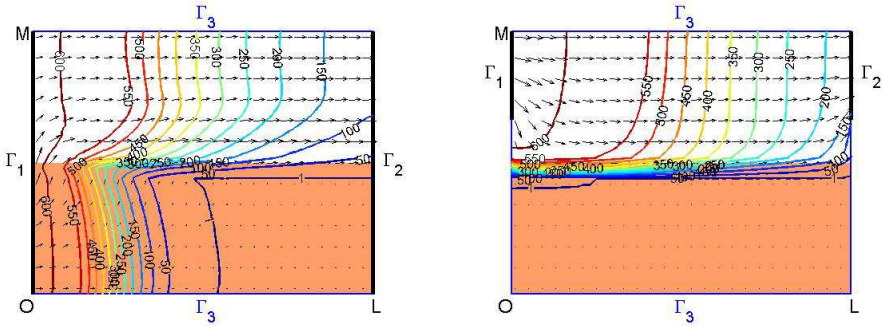


Figure 2.9: The flow (arrows) and a contour plots of the calcium carbonate concentration at  $t=t_{max}$  in a domain, of which the lower half is less permeable than the upper half, for different choices for the inflow and outflow boundaries. Left: case 1, right: case 2.

is formed. In case 2, urea and calcium are only flushed into the permeable layer. From the result of case 2, it can be seen that the flow hardly penetrates into the layer with low permeability. Hence, such a layer can be seen as an (almost) closed boundary. This is very advantageous if only the upper layer should be reinforced.

From Figure 2.10 it can be seen that in case 3 the flow goes through the whole domain, although the inflow and outflow are in the lower part of the domain. Again, in the low permeable zone is hardly any flow, and hence hardly any calcium carbonate is generated there.

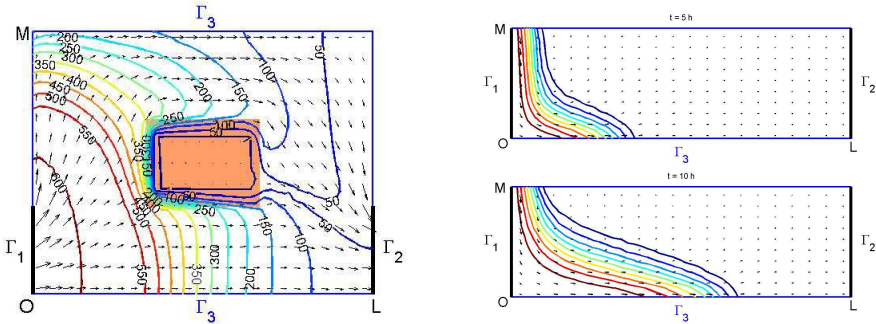


Figure 2.10: Left: The flow (arrows) and a contour plot of the calcium carbonate concentration at  $t=t_{max}$  in a domain with a kernel with a low permeability (case 3). Right: The flow (arrows) and a contour plot of the urea concentration (case 4). The inflow velocity is  $q_{inflow}^1 = 1.0 \cdot 10^{-6} \text{m/s}$ .

### Density flow and the effect of the reaction on it

From Figure 2.10 and 2.11, it can be seen that there is more density driven flow if the velocity in horizontal direction is low, since the relation between the vertical

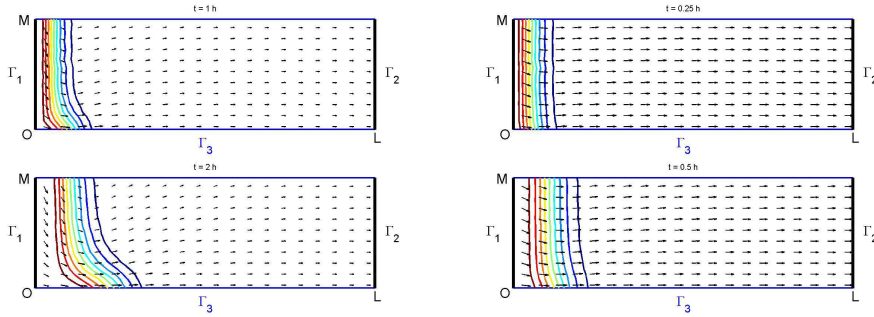


Figure 2.11: The flow (arrows) and a contour plot of the urea concentration (case 4). Left: The inflow velocity is  $q_{inflow}^2 = 5.0 \cdot 10^{-6} \text{m/s}$ . Right: The inflow velocity is  $q_{inflow}^3 = 20 \cdot 10^{-6} \text{m/s}$ .

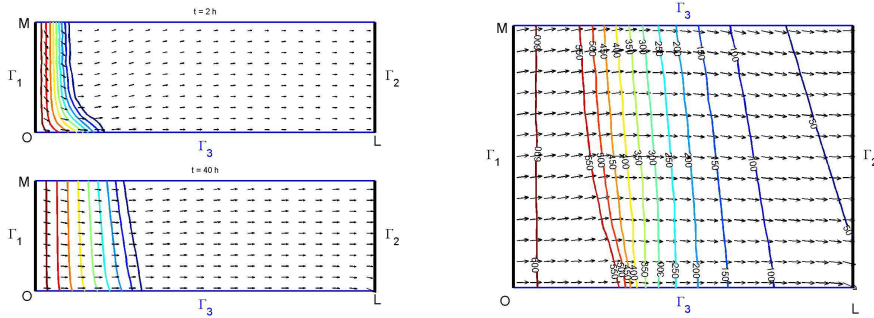


Figure 2.12: Contour plot of the urea concentration after 2 hours and 40 hours (left) and the calcium carbonate concentration after the treatment (right) for the case with density flow (case 5). The arrows display the flow.

(density driven) flow and the horizontal flow is large.

In case 5, the biochemical reaction (2.1) is simulated, too. The inflow velocity equals  $q_{in}$ , again. The left plot in Figure 2.12 displays a contour plot of the urea concentration after 2 hours and after 40 hours. Comparing Figure 2.12 with Figure 2.11, it can be seen that the urea concentration after 2 hours is lower in the case with reaction than in the case without reaction, since urea is hydrolysed due to microbial activity. Comparing the urea concentration after 2 hours and after 40 hours in Figure 2.12, it can be seen that there is more density flow after 2 hours. There are two reasons for this. Initially a solution of 1 molar urea and calcium chloride is injected in water. The density of this solution is  $1102 \text{ kg/m}^3$  (see (2.17)). The difference in density between this solution and water is  $102 \text{ kg/m}^3$ . When urea and calcium chloride react, ammonium is formed. The density of a 2 molar ammonium solution is  $1032 \text{ kg/m}^3$ . The difference between the urea/calcium chloride solution and the ammonium solution is smaller than the difference between the urea/calcium chloride solution and water. Hence, there is less density flow, since it is the difference

in density that causes density flow. The second reason is the increase in pore water velocity due to the decreasing porosity. As could be seen in Figure 2.10 and 2.11, there is less density flow if the horizontal velocity increases. These two phenomena cause a decrease in density flow.

Initially, when there is relatively much density flow, the urea is in the first part of the column. Hence in the first part of the column, the largest effect of density flow can be seen. This is also visible in Figure 2.12.

## 2.5 Conclusions and Discussion

A model has been formulated to describe the Biogrout process. The model gives insight into several aspects of the Biogrout process. The Biogrout process influences several properties of the subsoil. The precipitation of the solid calcium carbonate decreases the porosity and the permeability. According to the model, the precipitation of approximately  $600 \text{ kg/m}^3$  calcium carbonate at an initial porosity of 0.35 causes a decrease in the porosity by only a factor 3, while the permeability decreases by a factor 37. A consequence of a decreasing permeability is that the pressure should increase to keep up the same flow rate, or, if the pressure is constant, that the flow rate decreases.

In the first part of the column, more calcium carbonate precipitated than in the end of the column. The reason is that many urea molecules did already react in the first part of the column and could not reach the end of the column within the simulation time. The penetration depth of urea especially depends on the reaction rate and the inflow velocity. For this configuration and these values for the several constants, the pressure driven case resulted in a rather homogeneous calcium carbonate concentration in the first part of the column, while at the end of the column (almost) nothing precipitated. In the middle of the column, the calcium carbonate concentration decreases very fast. The flow driven case results in a calcium carbonate concentration that slowly decreases while the distance to the inflow boundary increases. In comparison with the pressure driven case, no steep gradients are present.

When injecting a urea and calcium chloride solution with a small inflow velocity, the effect of density flow is larger than in the case that the same volume is injected, but with a high injection velocity.

Initially, the urea and calcium chloride solution is injected into water. Due to the reaction, the density of the fluid decreases. Since the differences in densities are not that large any more, there is less density flow.

At the places where the urea and calcium concentration are constant, the calcium carbonate concentration can be calculated, using an analytic expression. In the model, the urea and calcium concentration were constant at the inflow boundary. The theoretical solution corresponds well with the numerical solution, although the time steps where reasonable large.

The model has been created under several assumptions. These assumptions should be validated using experiments. The first assumption was that the process is governed by the biochemical reaction (2.1). However, in reality this reaction happens in several steps. Some of these steps are equilibrium reactions that depend

on the pH. Other assumptions are that the retardation factors are equal to 1 and that the total volume of the fluid does not change due to the hydrolysis of urea and the precipitation of calcium carbonate. These assumptions should be verified.

It has also been assumed that calcium carbonate precipitates locally and will not be transported. Calcium carbonate can precipitate in several ways. It can attach to sand grains but can also form crystals. When these crystals are large enough, they will stick in the pore throats and it can be assumed that they are not transported. But when these crystals are small, probably they can be transported. It should be verified if this phenomenon is really negligible.

Another assumption is that the distribution of bacteria is homogeneous and that the reaction rate has a linear decay in time. These bacteria have been placed in the subsurface by injecting a solution with bacteria and a fixation fluid. The bacteria are assumed to attach to the solid particles and this effect will be enlarged by the fixation fluid. This fixation fluid causes the flocculation of bacteria and hence they cannot easily flow out anymore but will be filtered by the sand. It is not likely that these processes will result in a homogeneous bacteria distribution. The formula for the reaction rate includes the saturation constant  $K_{m,urea}$ . Experiments should be done to determine the value of this constant. From experiments, it is known that the reaction rate decreases in time, but the reasons are not yet clear. Hence as a starting point, a reaction rate has been assumed, that has a linear decay in time. Probably, this decay is not linear. Further research should be done to find out which circumstances influence the reaction rate and a better formula for the reaction rate should be found.

To calculate the intrinsic permeability the Kozeny-Carman relation has been used. This empirical relation turns out to be a good relation for many cases. It is questionable if this is also true for the Biogrout process, with its changing porosity. Another difficulty is the choice of the mean particle size  $d_m$  in this relation. Perhaps the mean particle size needs to be adapted as a result of calcium carbonate precipitation. If the calcium carbonate mainly attaches to the sand grains, the mean particle size increases. If mainly crystals are formed that are smaller than the sand grains, the mean particle size decreases. Experiments need to be done to find out what actually happens. Furthermore, alternative relationships between the intrinsic permeability and the porosity have been reported. An example concerns the study due to [19], where a fractal pore-space geometry has been assumed. In this study, any relation can be incorporated, but since this issue is not crucial here, the use of the classical Kozeny-Carman relation is maintained.

The last assumption is that the viscosity is constant and not dependent on the various concentrations. This is also a simplification of reality.

So, although the assumptions should be verified, the model is a good tool to get insight into the process.

For engineering design, it is necessary to know the relation between the calcium carbonate and the mechanical characteristics of the soil. For the strength of the soil, it is important where the calcium carbonate precipitates. Calcium carbonate, connecting sand grains, will give a contribution to strength, while loose crystals hardly will. Furthermore, calcium carbonate is a polymorph, which means that

several mineral types exist with similar molecular composition (amorphous calcium carbonate, vaterite and calcite). The crystal properties (size, shape, mineral type) are dependent on, among others, the precipitation conditions [83] and will result in a different contribution to strength. In order to find correlations between calcium carbonate content and strength of Biogrouted sand, several cores have been collected from a field scale Biogrout experiment and have been tested. In [87] correlations between Unconfined Compressive Strength (UCS),  $\text{CaCO}_3$  content and dry density are found from approximately 50 tests. Several other tests have been done to find the strength at different confining pressures. Using these test results, failure criteria (angle of internal friction and cohesion) were determined. These failure criteria can be used to assess the stability of (biologically) cemented soil.

## ACKNOWLEDGEMENTS

Special thanks to Jitse Puijsma (Deltares) and Leon van Paassen (Delft University of Technology) for partly deriving the differential equations.

## Modelling Biogrout: extension to 3D

This chapter has been published as:

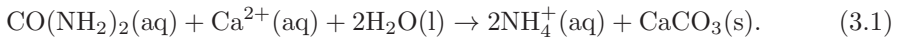
Van Wijngaarden, W.K., Vermolen, F.J., Van Meurs, G.A.M., Vuik, C.: Modelling the New Soil Improvement Method Biogrout: Extension to 3D. In: G. Kreiss et al. (eds.) Numerical Mathematics and Advanced Applications, 893–900 (2010)

## Abstract

Biogrout is a new soil improvement method based on microbial induced carbonate precipitation. Bacteria and reactants are flushed through the soil, resulting in calcium carbonate precipitation and consequent soil reinforcement. A mathematical model was created to describe the process. The model contains the concentrations of the dissolved species that are present in the precipitation reaction. These concentrations can be solved from a convection-dispersion-reaction equation with a variable porosity. Other model equations involve the concentrations of the bacteria and of the solid calcium carbonate, the decreasing porosity (due to precipitation) and the flow. The partial differential equations are solved by the Standard Galerkin Finite Element Method. The subject of this chapter is the extension of the mathematical model to 3D.

### 3.1 Introduction<sup>1</sup>

Biogrout is a new soil reinforcement method based on microbial induced carbonate precipitation [97]. The overall Biogrout reaction equation is given by:



Urea ( $\text{CO}(\text{NH}_2)_2$ ) is hydrolysed and if calcium ions ( $\text{Ca}^{2+}$ ) are present, ammonium ( $\text{NH}_4^+$ ) and calcium carbonate ( $\text{CaCO}_3$ ) are formed.

A model to describe the Biogrout process was proposed in [89] (Chapter 2). Thus far, only simulations for 1D and 2D configurations have been done. In this chapter, a simulation will be carried out for a 3D configuration.

This chapter contains the following sections. Section 3.2 summarizes the model for the Biogrout process that was derived in [89] (Chapter 2). Section 3.3 is devoted to the numerical methods, used to solve the model equations. Section 3.4 contains some computer simulations for a 3D configuration and in Section 3.5 conclusions and discussions can be found.

### 3.2 The Mathematical Model

In this section, the (differential) equations that are needed to describe the Biogrout process are given, together with a short explanation. In [89] (Chapter 2) the derivation can be found. These (differential) equations were derived in respect with the following assumptions:

- Only dissolved species do react;
- The biochemical reaction of the Biogrout process is the only reaction that takes place and this reaction is governed by reaction (3.1);
- The concentration of the bacteria is constant in time and homogeneous;

---

<sup>1</sup>Parts of the original introduction have been skipped in order to prevent too much repetition of the Introduction from Chapter 1.

- Calcium carbonate is not transported but it precipitates on the matrix of the porous medium;
- The precipitation of calcium carbonate has no influence on the total volume of the fluid over the entire domain of computation;
- The flow is incompressible;
- The viscosity is constant.

The biochemical reaction of the Biogrout process is given by equation (3.1). We will start by giving the differential equations for the aqueous species in this equation. The differential equation for the concentration of urea is given by:

$$\theta \frac{\partial C^{urea}}{\partial t} = \nabla \cdot (\theta \mathbf{D} \cdot \nabla C^{urea}) - \vec{q} \cdot \nabla C^{urea} - \theta r_{hp}. \quad (3.2)$$

In this equation,  $\theta$  is the porosity,  $C^{urea}$  is the dissolved concentration of urea,  $\mathbf{D}$  is the dispersion tensor,  $\vec{v}$  is the pore water velocity and  $r_{hp}$  is the reaction rate of the production of calcium carbonate, which is a non-linear function of the urea concentration and the time.

The term at the left-hand side represents the accumulation. The first term at the right-hand side represents the effect of dispersion and diffusion, the second term models advection and the last term stands for the biochemical reaction. The minus-sign comes from the fact that urea is consumed at the same rate as calcium carbonate is formed, see (3.1).

In three dimensions, the coefficients of the dispersion tensor  $\mathbf{D}$  equal  $D_{ij} = (\alpha_L - \alpha_T) \frac{v_i v_j}{|\vec{v}|} + \delta_{ij} \alpha_T \sum_i \frac{v_i^2}{|\vec{v}|}$ , see [100]. The quantity  $\alpha_L$  is the longitudinal dispersivity and  $\alpha_T$  is the transverse dispersivity.

Analogously, we have the following differential equation for the concentrations of calcium and ammonium:

$$\theta \frac{\partial C^{Ca^{2+}}}{\partial t} = \nabla \cdot (\theta \mathbf{D} \cdot \nabla C^{Ca^{2+}}) - \vec{q} \cdot \nabla C^{Ca^{2+}} - \theta r_{hp}, \quad (3.3)$$

$$\theta \frac{\partial C^{NH_4^+}}{\partial t} = \nabla \cdot (\theta \mathbf{D} \cdot \nabla C^{NH_4^+}) - \vec{q} \cdot \nabla C^{NH_4^+} + 2\theta r_{hp}. \quad (3.4)$$

Note the +2 in the biochemical reaction term in the differential equation for ammonium: for each produced mole of calcium carbonate, two moles of ammonium are generated.

For the non-aqueous species in reaction equation (3.1), calcium carbonate, we have the following differential equation:

$$\frac{\partial C^{CaCO_3}}{\partial t} = m_{CaCO_3} \theta r_{hp}. \quad (3.5)$$

In this equation,  $m_{CaCO_3}$  is the molar mass of calcium carbonate and is used to convert number of molecules (moles) into mass (kilograms). The right-hand side of this differential equation only contains the reaction term since it has been assumed that calcium carbonate is not transported.

We have the following relation between the concentration of calcium carbonate and the porosity:

$$\theta(t) = \theta(0) - \frac{C^{CaCO_3}(t) - C^{CaCO_3}(0)}{\rho_{CaCO_3}}, \quad (3.6)$$

where  $\rho_{CaCO_3}$  is the density of calcium carbonate.

The flow is calculated from Darcy's Law, given in [100]:

$$q_x = -\frac{k_x}{\mu} \frac{\partial p}{\partial x}, \quad q_y = -\frac{k_y}{\mu} \frac{\partial p}{\partial y}, \quad q_z = -\frac{k_z}{\mu} \left( \frac{\partial p}{\partial z} + \rho_l g \right). \quad (3.7)$$

In Darcy's Law,  $p$  is the pressure,  $k_i$  is the intrinsic permeability in the various coordinate directions ( $i = x, y, z$ ),  $\mu$  is the viscosity that is assumed to be constant in the Biogrout case,  $\rho_l$  is the density of the solution and  $g$  is the gravitational constant.

The intrinsic permeability  $k$  is determined, using the Kozeny-Carman relation: an empirical relation between the intrinsic permeability and the porosity that is commonly used in ground water flow modelling (see [7]):

$$k = \frac{(d_m)^2}{180} \frac{\theta^3}{(1 - \theta)^2}. \quad (3.8)$$

In this relation,  $d_m$  is the mean particle size of the subsurface medium. If the porosity is small, it might be that the pores are not connected. Hence, the permeability is zero. This phenomenon is not directly incorporated in the Kozeny-Carman relation. Since in our simulations the porosity is not that small, we assume that the Kozeny-Carman relation is a good relation between the permeability and the porosity.

The density of the solution (at 20°C),  $\rho_l$ , will be calculated with the following experimental relation:

$$\rho_l = 1000 + 15.4996C^{urea} + 86.7338C^{Ca^{2+}} + 15.8991C^{NH_4^+}. \quad (3.9)$$

For the pressure, the following differential equation was derived in [89] (Chapter 2) by the use of Darcy's Law (3.7):

$$-\nabla \cdot \left( \frac{k}{\mu} (\nabla p + \rho_l g \mathbf{e}_z) \right) = \frac{m_{CaCO_3}}{\rho_{CaCO_3}} \theta r_{hp}. \quad (3.10)$$

Differential equation (3.2), (3.3), (3.4), (3.5) and (3.10) contain the reaction rate  $r_{hp}$  of the biochemical reaction (3.1). This rate decreases in time as is shown in experiments, see [97]. In [89] (Chapter 2) a linear reduction had been assumed, combined with Monod kinetics, [57]. In this chapter, we will combine Monod kinetics with an exponential reduction, since this is commonly used as a first approximation (see [64]):

$$r_{hp} = v_{max} \frac{C^{urea}}{K_{m,urea} + C^{urea}} e^{-bt}. \quad (3.11)$$

In this equation,  $v_{max}$  is the initial activity,  $K_{m,urea}$  is the saturation constant and  $b$  is some constant, representing the reduction in bacterial activity in the course of

time.

As initial conditions, the concentration of calcium carbonate, urea, calcium and ammonium are equal to zero and the porosity equals  $\theta_0$ .

As a model experiment, a container ( $8\text{m} \times 5.6\text{m} \times 1.5\text{m}$ ) has been taken, having closed boundaries (represented by boundary  $\Gamma_3$ ). In this container injection and extraction wells have been placed (Figure 3.1). The injection wells are represented by boundary  $\Gamma_1$ , whereas the extraction wells are represented by boundary  $\Gamma_2$ . The following flow strategy has been chosen: there are three batches, starting with nine hours of injection and no injection during the rest of the batch. The duration of the batches is respectively 1, 2 and 3 days, see Figure 3.1.

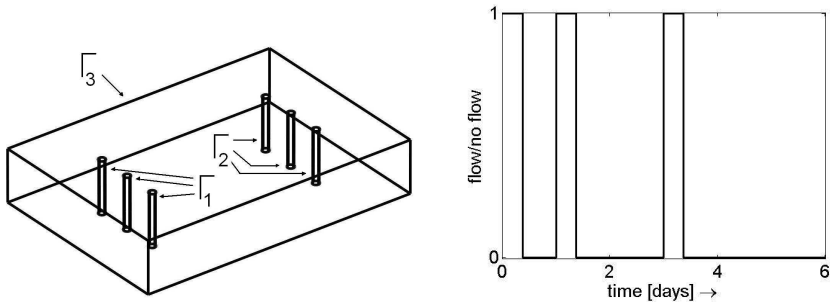


Figure 3.1: Experimental set-up. Left: Configuration, Right: Flow strategy

Table 3.2 displays the boundary conditions that are chosen.

	$p$	$C^{urea}$	$C^{Ca^{2+}}$	$C^{NH_4^+}$
$\Gamma_1$ (injection)	$-\frac{k}{\mu}(\nabla p + \rho_l g \mathbf{e}_z) \cdot \mathbf{n} = q_{in}$	$C = c_{in}$	$C = c_{in}$	$C = 0$
$\Gamma_1$ (rest)	$p = p_2 + \int_z^{1.5} \rho_l g \bar{z} d\bar{z}$	$\frac{\partial C}{\partial n} = 0$	$\frac{\partial C}{\partial n} = 0$	$\frac{\partial C}{\partial n} = 0$
$\Gamma_2$	$p = p_2 + \int_z^{1.5} \rho_l g \bar{z} d\bar{z}$	$\frac{\partial C}{\partial n} = 0$	$\frac{\partial C}{\partial n} = 0$	$\frac{\partial C}{\partial n} = 0$
$\Gamma_3$	$-\frac{k}{\mu}(\nabla p + \rho_l g \mathbf{e}_z) \cdot \mathbf{n} = 0$	$\frac{\partial C}{\partial n} = 0$	$\frac{\partial C}{\partial n} = 0$	$\frac{\partial C}{\partial n} = 0$

Table 3.1: Boundary conditions for the pressure and the concentration of urea, calcium and ammonium

Since we have the same differential equation, initial condition and boundary conditions for both the concentration of urea and calcium chloride, these concentrations are equal. Hence it is sufficient to calculate only the urea concentration.

### 3.3 Numerical Method

The differential equations for the pressure, the velocity and the concentration of the aqueous species are solved by the Standard Galerkin Finite Element Method. The weak formulation is derived by multiplication by a test function  $\eta \in H^1(\Omega)$  and integration over the domain  $\Omega$ . For the time integration, an IMEX-scheme is used: all components are solved implicitly, except for the porosity  $\theta$ , the intrinsic

permeability  $k$  and the density of the solution  $\rho_l$ . Solving the differential equation for the pressure, the reaction rate  $r_{hp}$  is also computed explicitly. While solving the differential equation for the urea concentration, Newton's method is used, because of the non-linearity in the reaction term (3.11). The Newton-Cotes quadrature rules have been used for the approximation of the element matrices and vectors. Tetrahedral elements have been used, in combination with linear basis functions.

Since the differential equation for the concentration of calcium carbonate, (3.5), is an ordinary differential equation (in each grid point), it is not necessary to use the Finite Element Method. For the time integration, an IMEX-scheme is used: solving all components implicitly, except for the porosity.

At each time step, the differential equations for the following components are solved successively: the pressure, the flow and the concentration of urea, calcium, ammonium and calcium carbonate. For more details, see [89].

Finally, the porosity ( $\theta$ ), the intrinsic permeability ( $k$ ) and the density of the fluid ( $\rho_l$ ) are recalculated with (3.6), (3.8) and (3.9), respectively. Also the boundary conditions are updated.

Since the porosity, the permeability and the density of the solution (may) vary, at each time step all the matrices are rebuilt. That means, calculate for each element a  $4 \times 4$  element matrix and add them to the large matrix. This is done for 10 different matrices + the number of Newton-iterations, since in each Newton-iteration a new matrix is built.

## 3.4 Results

In this section, the results of the simulation with the model for a 3D configuration are shown. Matlab has been used to do the numerical simulations. The linear systems are solved by a direct method. The time step  $\Delta t = 1$  h,  $q_{in} = 2.29 \times 10^{-4} \text{ m s}^{-1}$ ,  $v_{max} = 1.621 \times 10^{-2} \text{ mol m}^{-3} \text{ s}^{-1}$  and  $b = 7.15 \times 10^{-6} \text{ s}^{-1}$ . The values of the other constants can be found in [89].

All the three batches start with nine hours of injection with inflow velocity  $q_{in}$ . During injection, the amount of urea in the domain increases, although this phenomenon is diminished by the hydrolysis of urea. During rest, the total amount of urea decreases, due to the hydrolysis of urea. The reaction rate (3.11) decreases in time. As a consequence, the total amount of urea decreases slower during the period of rest as time proceeds.

The urea/calcium chloride solution is heavier than water and is also heavier than the solution of the reaction product ammonium chloride as can be seen from formula (3.9). As a result, in the lower parts of the domain a higher urea and calcium chloride concentration are expected. This will result in a higher calcium carbonate concentration in the lower parts of the domain. Figure 3.2 confirms these expectations and also gives some quantitative details.

At each time step, new matrices are built, since porosity, permeability and density of the solution (may) vary. In this chapter, the relation between the CPU time for the building part and for the solving part has been investigated. Seven different meshes have been taken, with increasing number of elements. With each mesh 10 time steps have been taken, registering the average CPU time per time step and the average CPU time per time step for the building part and the solving part. The

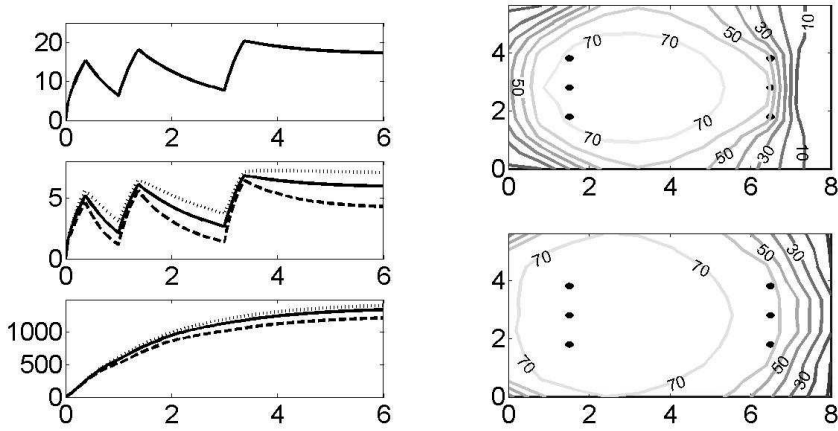


Figure 3.2: Some results of the 3D model experiment. Top left: total amount of urea (kmol) in time (days) in the whole domain; Middle left: amount of urea (kmol) in time (days) in several parts of the domain:  $--$  upper part,  $-$  middle part,  $\cdots$  lower part; Bottom left: the amount of calcium carbonate (kg) in the same parts of the domain:  $--$  upper part,  $-$  middle part,  $\cdots$  lower part. Top right: a contour plot of the calcium carbonate concentration ( $\text{kg}/\text{m}^3$ ) after the three batches at  $z=1.5$  m (top domain),  $x[\text{m}]$  and  $y[\text{m}]$  on the x-axis and y-axis; Bottom right: a contour plot of the calcium carbonate concentration ( $\text{kg}/\text{m}^3$ ) after the three batches at  $z=0$  m (bottom domain),  $x[\text{m}]$  and  $y[\text{m}]$  on the x-axis and y-axis

results can be found in Table 3.4. This table also contains the percentage solving time/total time.

From this table, it can be seen that, if the number of elements increases with a factor 2, so does the CPU time for the building part. This is what is expected: for each element a  $4 \times 4$  element matrix is created and is added to the large matrix. If the number of elements doubles, the amount of work doubles, too.

If the number of elements doubles, the amount of solving work increases with a factor 2.5, 2.6, 3.6, 4.2, 3.8 and 4.3, respectively. So the amount of work increases with more than a factor 2, what can also be expected from the analysis of a band matrix solver. For a mesh with 2500 elements only 30% of the CPU time is spent in the solving part. For a mesh with 160000 elements this is even 91%. If the number of elements increases further, it will be necessary to use an iterative method instead of a direct method.

The discretization error is  $O(\Delta x^2 + \Delta t)$ . If the number of elements is increased with a factor 2,  $\Delta x^2$  is decreased with a factor  $2^{2/3}$ . If the time step is also decreased with a factor  $2^{2/3}$ , then, in the limit, the error should decrease with a factor  $2^{2/3}$  ( $\approx 1.6$ ). The last column of Table 3.4 contains the relative error in the concentration after six hours in an arbitrary point in the domain with respect to the finest mesh. For the coarsest mesh, a time step of  $\Delta t=0.5$  h has been taken and this time step has been decreased while doubling the number of elements. The relative error decreases

number of elements (approximately)	per time step (s)	CPU time		percentage solving part	relative error
		building part (s)	solving part (s)		
2500	0.344	0.242	0.102	30%	24%
5000	0.715	0.459	0.255	36%	15%
10000	1.58	0.921	0.661	42%	10%
20000	4.28	1.88	2.39	56%	6.3%
40000	13.9	3.80	10.1	73%	3.5%
80000	46.8	8.23	38.6	82%	1.1%
160000	182	17.0	165	91%	(0%)

Table 3.2: CPU time per time step, subdivided in the building part and the solving part for seven different meshes, with increasing number of elements and the relative error.

with a factor 1.6, 1.5, 1.6, 1.8 and 3.2, respectively. So in the limit, the error decreases with even more than a factor 1.6.

### 3.5 Conclusions and Discussion

An extension to 3D of the Biogrout model has been made. The results of the numerical simulation with the 3D configuration with three injection lances and three extraction lances look promising. Also the error analysis gives a good result.

For a small number of elements, building matrices takes more CPU time than solving the matrix vector systems. For a large number of elements it is the other way around. In building matrices, the amount of work increases linearly with the number of elements. If the number of elements increases further, it will be necessary to use an iterative method instead of a direct method.

## A mathematical model and analytical solution for the fixation of bacteria in Biogrout

This chapter has been published as:

Van Wijngaarden, W.K., Vermolen, F.J., Van Meurs, G.A.M., Vuik, C.: A mathematical model and analytical solution for the fixation of bacteria in Biogrout. *Transport in Porous Media* **92**, 847–866 (2012)

## Abstract

Biogrout is a new method for soil reinforcement, which is based on microbial induced carbonate precipitation. Bacteria and reactants are flushed through the soil, resulting in calcium carbonate precipitation and consequent soil reinforcement. Bacteria are crucially important in the Biogrout process since they catalyze the reaction. Hence, to control the process, it is essential to know where the bacteria are located. The bacteria are possibly in suspension but can also be adsorbed or fixated on the matrix of the porous structure. In this chapter, a model is derived for the placement of bacteria. The model contains three phases of bacteria: bacteria in suspension, adsorbed bacteria and fixed bacteria. An analytical solution is derived for instantaneous reactions between these three phases. The analytical solution is compared to numerical simulations for finite reaction rates. For the numerical simulations the standard Galerkin Finite Element Method is used.

### 4.1 Introduction<sup>1</sup>

When applying Biogrout, first the bacteria are cultivated. Subsequently, the bacteria are injected into the subsoil and transported by water flow to the location where strengthening is required. The bacterial suspension is directly followed by a fixation fluid, which is a solution with high salinity. As a consequence of the retardation of the bacteria, the fixation fluid will overtake the weakly adsorbed bacteria and strongly fix them to the soil particles [36]. This will result into a rather homogeneous distribution of bacteria. After the placement of the bacteria, the urea and calcium chloride ( $\text{CaCl}_2$ ) solution is supplied [97]. Due to the calcium chloride, this solution has a high salinity and will therefore also act as a fixation fluid. The bacteria provide the hydrolysis of urea and the calcium and carbonate ions precipitate as calcium carbonate. The calcium carbonate crystals form bridges between the sand grains, thereby increasing the strength and stiffness of the soil. The by-product ammonium chloride ( $\text{NH}_4\text{Cl}$ ) needs to be removed. The bacteria and reactants are not injected at the same time to prevent clogging and crystal accumulation around the injection point(s). The procedure, in which the bacteria are first injected and only then followed by the injection of the reactants, also results into a more homogeneous distribution of calcium carbonate.

Since the bacteria provide the hydrolysis of urea, they are crucial in the Biogrout process. The reaction rate increases with an increasing bacterial concentration and urease activity. Further, if no bacterium is present, no carbonate is formed and consequently no calcium carbonate appears. Therefore, it is essential to know where the bacteria are located in the aquifer.

When modelling bacterial transport, it is not sufficient to consider advection and dispersion only. Adsorption and desorption are important phenomena as well, but also the pore size of the matrix, the size of the microorganisms, filtration and elimination ([32,33,55,56]), ionic strength of the ground water ([32,33]), systematic

---

<sup>1</sup>Parts of the original introduction have been skipped in order to prevent too much repetition of the Introduction from Chapter 1.

(chemotaxis) and random (tumbling) motion of bacteria ([99]), residence time ([41]), decay and growth ([33,99]) effect the (rate of) transport of microorganisms.

[38,41,74] provide various models that consider several of these phenomena and compare the model results with experimental results.

In [90] and [91] (Chapter 2 and 3), the study focusses on modelling the transport of the reactants, assuming a homogeneous distribution of bacteria. The present study is devoted to the transport, adsorption and fixation of the injected bacteria. In Section 4.2, a model is derived for the placement of bacteria. Further, initial and boundary conditions are given. In Section 4.3, the analytical solution for a simplified version of the model equations, described in Section 4.2, is presented. In Section 4.3, the Numerical Methods to solve the model equations are described. In Section 4.4, the results are displayed and a comparison is made between the analytical solution and the numerical solutions. In the last section, some conclusions and a discussion can be found.

## 4.2 Mathematical model

### 4.2.1 Derivation of the model equations

First we present the general equation for the transport of bacteria in a fully saturated porous medium, as in for example [74]:

$$\frac{\partial (\theta C^{bac})}{\partial t} + \frac{\partial (\theta C^{ads})}{\partial t} = \nabla \cdot (D_{bac} \theta \nabla C^{bac}) - \nabla \cdot (\mathbf{q} C^{bac}). \quad (4.1)$$

In this equation,  $\theta$  is the porosity,  $C^{bac}$  is the bacterial concentration in suspension,  $C^{ads}$  is the imaginary concentration that would result if the attached bacteria were to be resuspended in a solution volume equivalent to that of the surrounding water. Note that in literature,  $C^{ads}$  is frequently expressed in units of milligrams per kilogram, see for example [100]. Here,  $C^{ads}$  has the same unit as  $C^{bac}$ . Further,  $D_{bac}$  is the dispersion coefficient of bacteria in suspension and  $\mathbf{q}$  is the Darcy velocity, which relates to the pore water flow velocity  $\mathbf{v}$  as

$$\mathbf{q} = \nu \theta. \quad (4.2)$$

The terms at the left-hand side in equation (4.1) are the accumulation terms for the suspended and adsorbed bacteria. The first term at the right-hand side accounts for dispersion and the last term is the advection term. Since bacterial growth and decay are processes with a large time scale we neglect them. Further, we assume bacterial movement to be determined by flow only, which means that their systematic movement is neglected.

In the case of an equilibrium-controlled adsorption,  $C^{ads}$  tends to the equilibrium  $\varphi(C^{bac})$ , where  $\varphi$  is an adsorption isotherm, which depends on the concentration of bacterial cells in suspension ( $C^{bac}$ ) and also possibly depends on properties of the microorganisms, the porous medium and the pH. To be able to calculate  $C^{bac}$  and

$C^{ads}$  separately, equation (4.1) is split into two equations:

$$\frac{\partial (\theta C^{bac})}{\partial t} = \nabla \cdot (D_{bac} \theta \nabla C^{bac}) - \nabla \cdot (\mathbf{q} C^{bac}) - \theta r_{ads} + \theta r_{des}, \quad (4.3)$$

$$\frac{\partial (\theta C^{ads})}{\partial t} = \theta r_{ads} - \theta r_{des}, \quad (4.4)$$

where

$$r_{ads} = k_{ads} (\varphi(C^{bac}) - C^{ads})_+, \quad (4.5)$$

$$r_{des} = k_{des} (C^{ads} - \varphi(C^{bac}))_+. \quad (4.6)$$

The reaction  $r_{ads}$  is the adsorption reaction,  $r_{des}$  is the desorption reaction,  $k_{ads}$  and  $k_{des}$  are respectively the adsorption and desorption rate constant. The notation  $(\cdot)_+$  considers the positive part of an expression and has been defined as  $(\cdot)_+ := \max(0, \cdot)$ . Equations (4.5) and (4.6) account for the difference in desorption and adsorption rate. If there are no bacteria in suspension, no bacteria adsorb onto the matrix of the aquifer, therefore  $\varphi(0) = 0$ . The number of bacteria that adsorb increases with the number of bacteria in suspension, hence  $\varphi'(C^{bac}) > 0$  and  $\varphi(C^{bac}) > 0$ . It is also assumed that  $\varphi''(C^{bac}) < 0$  and  $\lim_{C^{bac} \rightarrow \infty} \varphi'(C^{bac}) = 0$ , which implies that the adsorption rate decreases as adsorption proceeds. This is a logical consequence from the fact that a higher number of adsorbed bacteria gives a lower number of free adsorption sites.

In the Biogrout process, the bacterial suspension is directly followed by a fixation fluid, which is a solution with a high salinity. This fixation fluid will overtake the weakly adsorbed bacteria and strongly fix them onto the solid matrix. In order to model this,  $C^{ads}$  is split up into a temporarily adsorbed part  $\bar{C}^{bac}$  and a permanently adsorbed, or fixed, part  $S^{bac}$ :

$$C^{ads} = \bar{C}^{bac} + S^{bac}. \quad (4.7)$$

In the case of an equilibrium, the concentration of temporarily adsorbed bacteria  $\bar{C}^{bac}$  is given by  $\bar{C}^{bac} = (1 - \beta)\varphi(C^{bac})$  and, since  $S^{bac}$  is the concentration of *permanently* adsorbed bacteria, which can not decrease, the following equilibrium holds:  $S^{bac}(\mathbf{x}, t) = \max_{0 \leq \bar{t} \leq t} \{\beta\varphi(C^{bac}(\mathbf{x}, \bar{t}))\}$ . From this equation, it follows that, for a constant  $C^{bac}$ ,  $S^{bac} = \beta\varphi(C^{bac})$ . The fraction  $\beta$  ranges between 0 and 1, where the value depends on the concentration of the fixation fluid and it may also depend on, for example, properties of the microorganisms, the pH and the porous medium.

Substituting relation (4.7) into equations (4.5), (4.5) and (4.6), gives the following equations for the adsorbed bacteria:

$$\frac{\partial (\theta (\bar{C}^{bac} + S^{bac}))}{\partial t} = \theta r_{ads} - \theta r_{des}, \quad (4.8)$$

$$r_{ads} = k_{ads} (\varphi(C^{bac}) - (\bar{C}^{bac} + S^{bac}))_+, \quad (4.9)$$

$$\begin{aligned} r_{des} &= k_{des} (\bar{C}^{bac} + S^{bac} - \varphi(C^{bac}))_+ \\ &= k_{des} ((\bar{C}^{bac} - (1 - \beta)\varphi(C^{bac})) + (S^{bac} - \beta\varphi(C^{bac})))_+. \end{aligned} \quad (4.10)$$

Next, we show that equation (4.10) needs to be adjusted. According to this equation, both the difference between  $\bar{C}^{bac}$  and its equilibrium and the difference between  $S^{bac}$  and its equilibrium, are driving forces for desorption. Next, consider the situation  $\bar{C}^{bac} + S^{bac} > \varphi(C^{bac})$ ,  $\bar{C}^{bac} < (1 - \beta)\varphi(C^{bac})$  and  $S^{bac} > \beta\varphi(C^{bac})$ , which can happen if  $C^{bac}$  (and hence  $\beta\varphi(C^{bac})$ ) is decreasing and if the adsorption rate  $r_{ads}$  is not so high. Compared to the equilibrium  $\beta\varphi(C^{bac})$ , too many bacteria are adsorbed, and according to equation (4.10) there is a driving force for desorption. Concentration  $S^{bac}$  is the concentration of permanently adsorbed bacteria and these bacteria will not desorb again. This implies that the concentration temporarily adsorbed bacteria  $\bar{C}^{bac}$  will decrease. However, this concentration is already lower than its equilibrium  $(1 - \beta)\varphi(C^{bac})$ . This means that the difference between  $S^{bac}$  and its equilibrium  $\beta\varphi(C^{bac})$  will lead to extra desorption and this is not allowed. Therefore, the difference between  $S^{bac}$  and its equilibrium should only be taken into account if  $S^{bac} < \beta\varphi(C^{bac})$ . In that case, it will diminish desorption. Hence, equation (4.10) is replaced with

$$r_{des} = k_{des} \left( \left( \bar{C}^{bac} - (1 - \beta)\varphi(C^{bac}) \right) + \left( S^{bac} - \beta\varphi(C^{bac}) \right)_- \right)_+, \quad (4.11)$$

where the notation  $(\cdot)_-$  considers the negative part of an expression and is defined by  $(\cdot)_- := \min(0, \cdot)$ .

For the concentration of permanently adsorbed bacteria  $S^{bac}$ , the following equation is used:

$$\frac{\partial (\theta S^{bac})}{\partial t} = \theta r_{fix}, \quad (4.12)$$

where the fixation rate  $r_{fix}$  is given by

$$r_{fix} = k_{fix} \bar{C}^{bac} (\beta\varphi(C^{bac}) - S^{bac})_+. \quad (4.13)$$

The constant  $k_{fix}$  is the fixation rate constant. The driving force for fixation is the difference between the concentration of fixated bacteria  $S^{bac}$  and its equilibrium  $\beta\varphi(C^{bac})$ , which is accounted for by the term  $(\beta\varphi(C^{bac}) - S^{bac})$ . Only the positive part of this expression is taken into account, since  $S^{bac}$  is the concentration of *permanently* adsorbed bacteria, which can not decrease. If there are no adsorbed bacteria, they can not be fixated. If there are many adsorbed bacteria it is likely that fixation proceeds faster than in the case in which there are only a few adsorbed bacteria on the matrix. That is the reason why the fixation rate also contains a multiplication by  $\bar{C}^{bac}$ . Note that the fixation of bacteria only occurs after adsorption.

From equations (4.8) and (4.12), the following differential equation is found for the concentration temporarily adsorbed bacteria:

$$\frac{\partial (\theta \bar{C}^{bac})}{\partial t} = \theta r_{ads} - \theta r_{des} - \theta r_{fix}. \quad (4.14)$$

For the concentration of the fixation fluid  $C^{fix}$ , the following differential equation is used:

$$\frac{\partial (\theta C^{fix})}{\partial t} = \nabla \cdot (D_{fix} \theta \nabla C^{fix}) - \nabla \cdot (\mathbf{q} C^{fix}), \quad (4.15)$$

where  $D_{fix}$  is the dispersion coefficient of the fixation fluid.

To summarize, we solve the following system of equations for the transport of bacteria in a saturated porous medium, in combination with a fixation fluid.

$$\frac{\partial(\theta C^{bac})}{\partial t} = \nabla \cdot (D_{bac}\theta\nabla C^{bac}) - \nabla \cdot (\mathbf{q}C^{bac}) - \theta r_{ads} + \theta r_{des}, \quad (4.16)$$

$$\frac{\partial(\theta \bar{C}^{bac})}{\partial t} = \theta r_{ads} - \theta r_{des} - \theta r_{fix}, \quad (4.17)$$

$$\frac{\partial(\theta S^{bac})}{\partial t} = \theta r_{fix}, \quad (4.18)$$

$$r_{ads} = k_{ads} \left( \varphi(C^{bac}) - (\bar{C}^{bac} + S^{bac}) \right)_+, \quad (4.19)$$

$$r_{des} = k_{des} \left( (\bar{C}^{bac} - (1 - \beta)\varphi(C^{bac}))_+ + (S^{bac} - \beta\varphi(C^{bac}))_- \right)_+, \quad (4.20)$$

$$r_{fix} = k_{fix} \bar{C}^{bac} (\beta\varphi(C^{bac}) - S^{bac})_+, \quad (4.21)$$

$$\frac{\partial(\theta C^{fix})}{\partial t} = \nabla \cdot (D_{fix}\theta\nabla C^{fix}) - \nabla \cdot (\mathbf{q}C^{fix}). \quad (4.22)$$

## 4.2.2 Initial conditions and boundary conditions

For the concentration of suspended, adsorbed and fixed bacteria and for the concentration of the fixation fluid, the following initial conditions are chosen:

$$C^{bac}(x, 0) = \bar{C}^{bac}(x, 0) = S^{bac}(x, 0) = C^{fix}(x, 0) = 0. \quad (4.23)$$

At time  $t = T_0$  the injection of bacteria is stopped and from then on the fixation fluid is injected. This results into the following boundary condition for the concentration of suspended bacteria:

$$C^{bac}(0, t) = \begin{cases} 1 & \text{for } 0 < t < T_0, \\ 0 & \text{for } t > T_0, \end{cases} \quad (4.24)$$

and for the concentration of fixation fluid:

$$C^{fix}(0, t) = \begin{cases} 0 & \text{for } 0 < t < T_0, \\ 1 & \text{for } t > T_0. \end{cases} \quad (4.25)$$

## 4.3 Analytical Solution and Numerical Methods

In this section, the analytical solution for a simplified version of system (4.16)-(4.22) is derived. These simplifications have been made in order to be able to construct an analytical solution. Subsequently, a case study is presented for one particular

adsorption isotherm. The model equations have also been solved numerically. The numerical strategy is described at the end of this section. The following simplifications have been made:

- Restriction to one dimension;
- The pore water velocity  $v$  and the porosity  $\theta$  are constant;
- Dispersion and diffusion are neglected:  $D_{bac} = D_{fix} = 0 \text{ m}^2/\text{h}$ ;
- For  $\beta$  the following has been chosen:  $\beta = \beta_0 C^{fix}$ , in which  $\beta_0$  is a constant;
- The adsorption isotherm only depends on the concentration suspended bacteria:  $\varphi = \varphi(C)$ .

A discussion on these assumptions can be found in Section 4.5.

These simplifications result into the following system of equations:

$$\frac{\partial C^{bac}}{\partial t} = -v \frac{\partial C^{bac}}{\partial x} - r_{ads} + r_{des}, \quad (4.26)$$

$$\frac{\partial \bar{C}^{bac}}{\partial t} = r_{ads} - r_{des} - r_{fix}, \quad (4.27)$$

$$\frac{\partial S^{bac}}{\partial t} = r_{fix}, \quad (4.28)$$

$$r_{ads} = k_{ads} \left( \varphi(C) - \left( \bar{C}^{bac} + S^{bac} \right) \right)_+, \quad (4.29)$$

$$r_{des} = k_{des} \left( \left( \bar{C}^{bac} - (1 - \beta) \varphi(C^{bac}) \right)_+ + \left( S^{bac} - \beta \varphi(C^{bac}) \right)_- \right)_+, \quad (4.30)$$

$$r_{fix} = k_{fix} \bar{C}^{bac} \left( \beta \varphi(C^{bac}) - S^{bac} \right)_+, \quad (4.31)$$

$$\frac{\partial C^{fix}}{\partial t} = -v \frac{\partial C^{fix}}{\partial x}. \quad (4.32)$$

The initial and boundary conditions are given in Section 4.2.2.

### 4.3.1 Analytical solution

In this subsection, we describe the analytical solution for the various components: the fixation fluid and the bacteria.

#### Fixation fluid

Before deriving the analytical solution for the bacteria, first the solution for the fixation fluid is derived. A solution of equation (4.32) is  $C^{fix}(x - vt)$ . Combining this with the initial and boundary condition gives the following solution for the fixation fluid:

$$C^{fix}(x, t) = H(v(t - T_0) - x), \quad (4.33)$$

where  $H : \mathbb{R} \rightarrow \{0, 1\}$  represents a Heaviside function, given by

$$H(y) = \begin{cases} 1 & \text{for } y > 0, \\ 0 & \text{for } y < 0. \end{cases} \quad (4.34)$$

### Bacteria

For the derivation of the analytical solution for the concentration of suspended, adsorbed and fixed bacteria, an extra simplification has been made: the reaction constants are infinitely large:  $k_{ads} \rightarrow \infty$ ,  $k_{des} \rightarrow \infty$  and  $k_{fix} \rightarrow \infty$ . This simplification implies an instantaneous equilibrium. As a result,  $\bar{C}^{bac}$  and  $S^{bac}$  can be found directly as a function of  $C^{bac}$ :

$$\bar{C}^{bac} = (1 - \beta_0 C^{fix}) \varphi(C^{bac}), \quad (4.35)$$

$$S^{bac} = \max_{0 \leq \bar{t} \leq t} \{ \beta_0 C^{fix} \varphi(C^{bac}) \}. \quad (4.36)$$

The total bacterial concentration  $\Psi$  is defined by  $\Psi := C^{bac} + \bar{C}^{bac} + S^{bac}$ . Adding the differential equations for  $C^{bac}$ ,  $\bar{C}^{bac}$  and  $S^{bac}$  (equations (4.26), (4.27) and (4.28)), gives the following differential equation for  $\Psi$ :

$$\frac{\partial \Psi(C^{bac})}{\partial t} = -v \frac{\partial C^{bac}}{\partial x}. \quad (4.37)$$

It is assumed that  $C^{bac}$  is piecewise continuously differentiable in  $t$  and  $x$  and that  $\varphi$  and  $\Psi$  are continuous functions in  $C^{bac}$ .

Along characteristics, we have

$$0 = \frac{d}{dt} C^{bac}(t, x(t)) = C_t^{bac} + C_x^{bac} x'(t) \quad (4.38)$$

and hence

$$x'(t) = \frac{v}{\Psi'(C^{bac})}, \quad (4.39)$$

where  $\Psi'(C^{bac})$  is given by

$$\Psi'(C^{bac}) = \begin{cases} 1 + \varphi'(C^{bac}) & \text{if } C^{fix}(x, t) \varphi(C^{bac}(x, t)) > \\ & \max_{0 \leq \bar{t} < t} \{0, C^{fix}(x, \bar{t}) \varphi(C^{bac}(x, \bar{t}))\}; \\ 1 + (1 - \beta_0 C^{fix}) \cdot \varphi'(C^{bac}) & \text{else.} \end{cases} \quad (4.40)$$

Based on the above relations, we present a sketch of the (x-t)-diagram in Figure 4.1.

The velocity of the characteristics originating for the  $x$ -axis, where  $C = C^{fix} = 0$ , is calculated with equations (4.39) and (4.40):

$$x'(t) = \frac{v}{\Psi'(0)} = \frac{v}{1 + \varphi'(0)}. \quad (4.41)$$

For the characteristics, originating from the  $t$ -axis, we distinguish between  $0 < t < T_0$  and  $t > T_0$ . For  $0 < t < T_0$ , since  $C^{bac} = 1$  at the inflow boundary, the following expression is found for the velocity of the characteristics, originating from the  $t$ -axis:

$$x'(t) = \frac{v}{\Psi'(1)} = \frac{v}{1 + (1 - \beta_0 C^{fix}) \varphi'(1)}. \quad (4.42)$$

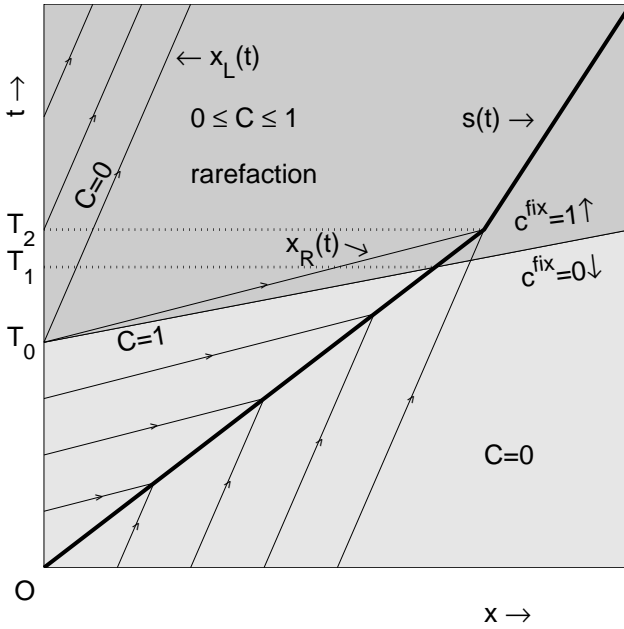


Figure 4.1: Sketch of the (x-t)-diagram.

Note that the velocity of the suspended bacteria changes, when they are overtaken by the fixation fluid. The characteristic of the front of the fixation fluid starts in  $(0, T_0)$ . Below this characteristic, we have  $C^{fix} = 0$  and therefore  $x'(t) = \frac{v}{1+\varphi'(1)}$ . Above this characteristic, we have  $C^{fix} = 1$  and  $x'(t) = \frac{v}{1+(1-\beta_0)\varphi'(1)}$ .

For  $t > T_0$ , since  $C^{bac} = 0$  and  $C^{fix} = 1$  at the inflow boundary, the velocity of the characteristics is given by:

$$x'(t) = \frac{v}{\Psi'(0)} = \frac{v}{1 + (1 - \beta_0)\varphi'(0)}. \quad (4.43)$$

The characteristics from  $(0, T_0)$  have a lower velocity than the characteristics originating from the x-axis. This is a result of the retardation effect due to adsorption and this lower velocity results into a shock. The shock position is denoted by  $s(t)$ . Let  $t = T_1$  be the time at which the front of the fixation fluid reaches the front of the pulse with bacteria. For  $0 < t < T_1$ , the shock speed  $s'(t)$  is determined by the Rankine-Hugoniot condition (where  $[\cdot]$  means the jump over the quantity):

$$s'(t) = \frac{[vC^{bac}]}{[\Psi(C^{bac})]} = \frac{[vC^{bac}]}{[C^{bac} + (1 - \beta_0 C^{fix})\varphi(C^{bac})]} = \frac{v}{1 + \varphi(1)} < v. \quad (4.44)$$

Since  $s(0) = 0$ , for  $0 < t < T_1$  the shock position is given by

$$s(t) = \frac{vt}{1 + \varphi(1)}. \quad (4.45)$$

From the intersection of the shock position with the position of the fixation fluid front,  $T_1$  can be found:  $\frac{vT_1}{1+\varphi(1)} = v(T_1 - T_0)$ . Hence,

$$T_1 = \frac{1 + \varphi(1)}{\varphi(1)} T_0. \quad (4.46)$$

Since  $\varphi(1)$  is positive, we have that  $T_1 > T_0$ .

Let  $t = T_2$  be the time at which the shock speed changes. This change is a consequence of the decrease of  $C(s(t), t)$ . For  $T_1 < t < T_2$ , the shock speed is given by

$$\begin{aligned} s'(t) &= \frac{[vC^{bac}]}{[\Psi(C^{bac})]} \\ &= \frac{[vC^{bac}]}{[C^{bac} + (1 - \beta_0 C^{fix})\varphi(C^{bac}) + \max_{0 \leq \tilde{t} \leq t} \{\beta_0 C^{fix} \varphi(C^{bac})\}]} \\ &= \frac{v}{1 + \varphi(1)}. \end{aligned} \quad (4.47)$$

For  $T_1 < t < T_2$ , the same shock speed has been found as for  $0 < t < T_1$ , as can be seen from equations (4.44) and (4.47). While deriving the model for the placement of bacteria, this turned out to be very important, since a change in the shock speed at  $t = T_1$  turned out to lead to a violation of the conservation of mass requirement. Here, the development of the analytical solution, though for a simplified case, turned out to be very helpful to the actual construction of the model.

For  $0 < t < T_2$  the shock position is given by

$$s(t) = \frac{vt}{1 + \varphi(1)}. \quad (4.48)$$

At  $t = T_0$ , the boundary condition changes. This gives a rarefaction wave, which is illustrated in the  $(x-t)$ -diagram. To this extent, we use the Ansatz  $C^{bac}(t, x) = \tilde{C}(\eta)$ ,  $\eta = \frac{x}{v(t-T_0)}$ . This gives the following derivatives:

$$\left\{ \begin{array}{l} C_t = -\frac{\eta}{t-T_0} \tilde{C}'(\eta), \\ C_x = \frac{1}{v(t-T_0)} \tilde{C}'(\eta), \\ (\Psi(C))_t = -\Psi'(\tilde{C}) \tilde{C}'(\eta) \frac{\eta}{t-T_0}. \end{array} \right. \quad (4.49)$$

Substituting equation (4.49) in relation (4.37) gives

$$\left( -\Psi'(\tilde{C})\eta + 1 \right) \tilde{C}'(\eta) = 0. \quad (4.50)$$

This equation admits two states:

$$\left\{ \begin{array}{l} 1) \quad \tilde{C}'(\eta) = 0 \quad (\text{constant state}), \\ 2) \quad \eta = \frac{1}{\Psi'(\tilde{C})} \quad (\text{variable state}). \end{array} \right. \quad (4.51)$$

The variable state implies that

$$\Psi'(\tilde{C}) = \frac{1}{\eta}. \quad (4.52)$$

Since  $\Psi'(\tilde{C}) > 0$  and  $\Psi$  is a continuous function in  $\tilde{C}$ , this equation can be solved ( $\Psi'(\tilde{C})$  is invertible). The solution is  $C^{bac} = (\Psi')^{-1}\left(\frac{1}{\eta}\right)$ . The constant states are located at

$$\frac{x_L(t)}{v(t-T_0)} = \eta_L = \frac{1}{\Psi'(0)} < \frac{1}{\Psi'(1)} = \eta_R = \frac{x_R(t)}{v(t-T_0)}. \quad (4.53)$$

Time  $T_2$  can be found from the intersection point of  $s(t)$  and  $x_R(t)$ :  $\frac{vT_2}{1+\varphi(1)} = \frac{v(T_2-T_0)}{\Psi'(1)}$ . Solving this equation gives

$$T_2 = \frac{1+\varphi(1)}{1+\varphi(1)-\Psi'(1)}T_0 = \frac{1+\varphi(1)}{\varphi(1)-(1-\beta_0)\varphi'(1)}T_0, \quad (4.54)$$

which has a solution  $T_2 > 0$  iff  $\varphi(1) > (1-\beta_0)\varphi'(1)$ . If  $\varphi(1) \leq (1-\beta_0)\varphi'(1)$ , then  $s(t)$  is given by equation (4.48) for  $t > 0$ . Next,  $s(t)$  is derived for  $t > T_2$  for the case that  $\varphi(1) > (1-\beta_0)\varphi'(1)$ . The shock speed  $s'(t)$  is given by  $s'(t) = \frac{vC^{bac}(t,s(t))}{\Psi(C^{bac}(t,s(t)))}$ .

On the shock position, the solution is given by  $C^{bac}(t,s(t)) = (\Psi')^{-1}\left(\frac{v(t-T_0)}{s(t)}\right)$ . This gives the following differential equation in  $s(t)$ :

$$s'(t) = \frac{v(\Psi')^{-1}\left(\frac{v(t-T_0)}{s(t)}\right)}{\Psi\left((\Psi')^{-1}\left(\frac{v(t-T_0)}{s(t)}\right)\right)}, \quad s(T_2) = \frac{vT_2}{1+\varphi(1)}. \quad (4.55)$$

Solving this differential equation gives the shock position  $s(t)$  for  $t > T_2$  for the case that  $\varphi(1) > (1-\beta_0)\varphi'(1)$ . Summarizing, the following has been found for the shock position  $s(t)$ :

$$s(t) = \begin{cases} \frac{vt}{1+\varphi(1)} & \text{if } \varphi(1) \leq (1-\beta_0)\varphi'(1), \\ & \text{for } t > 0; \\ \frac{vt}{1+\varphi(1)} & \text{if } \varphi(1) > (1-\beta_0)\varphi'(1), \\ & \text{for } 0 < t < T_2; \\ \frac{vT_2}{1+\varphi(1)} + \int_{T_2}^t \frac{v(\Psi')^{-1}\left(\frac{v(\bar{t}-T_0)}{s(\bar{t})}\right)}{\Psi\left((\Psi')^{-1}\left(\frac{v(\bar{t}-T_0)}{s(\bar{t})}\right)\right)} d\bar{t} & \text{if } \varphi(1) > (1-\beta_0)\varphi'(1), \\ & \text{for } t > T_2. \end{cases} \quad (4.56)$$

Next, the solution for the concentration of suspended bacteria is constructed:

$$C^{bac} = \begin{cases} 1 & \text{for } (t,x) \in (0,T_0) \times (0,s(t)) \cup (T_0,T_2) \times \\ & \quad \times (x_R(t),s(t)); \\ 0 & \text{for } (t,x) \in (T_0,\infty) \times (0,x_L(t)) \cup \mathbb{R}^+ \times \\ & \quad \times (s(t),\infty); \\ (\Psi')^{-1}\left(\frac{v(t-T_0)}{x}\right) & \text{for } (t,x) \in (T_0,\infty) \times (x_L(t),\min(x_R(t),s(t))). \end{cases} \quad (4.57)$$

The concentration of adsorbed bacteria  $\bar{C}^{bac}$  and fixated bacteria  $S^{bac}$  is found, using equations (4.35) and (4.36).

The preferred result is an homogeneous distribution of bacteria. To achieve this distribution, according to the present model, the following relation should hold:

$$L \leq s(T_2), \quad (4.58)$$

where  $L$  is the length of the column. Substituting equations (4.48) and (4.54) into relation (4.58) gives the following relation between the length of the column  $L$  and the switch time  $T_0$ .

$$L \leq \frac{vT_0}{\varphi(1) - (1 - \beta_0)\varphi'(1)}. \quad (4.59)$$

The above relation (4.59) implies the following criterion on the switch time  $T_0$ :

$$T_0 \geq \frac{\varphi(1) - (1 - \beta_0)\varphi'(1)}{v} L. \quad (4.60)$$

### 4.3.2 Case study

In this subsection, the solution, derived in the last subsection is applied to the Langmuir isotherm. According to [100], the Langmuir isotherm is given by

$$\varphi(C^{bac}) = \frac{\alpha \bar{C}_{\max} C^{bac}}{1 + \alpha C^{bac}}, \quad (4.61)$$

where the positive constant  $\alpha$  denotes the Langmuir constant and  $\bar{C}_{\max}$  is the maximum adsorption capacity. Substituting equation (4.61) into relations (4.46) and (4.54) gives the following expressions in  $\mathbb{R}^+$  for  $T_1$  and  $T_2$ :

$$T_1 = \frac{1 + \alpha + \alpha \bar{C}_{\max}}{\alpha \bar{C}_{\max}} T_0; \quad (4.62)$$

$$T_2 = \frac{\frac{(1+\alpha)^2}{\alpha \bar{C}_{\max}} + (1 + \alpha)}{\alpha + \beta_0} T_0. \quad (4.63)$$

The following expression for  $s(t)$  is derived:

$$s(t) = \begin{cases} \frac{vt}{1+\varphi(1)} & \text{for } t < T_2; \\ \frac{v(1+\alpha)T_2}{1+\alpha+\alpha\bar{C}_{\max}} + \int_{T_2}^t \frac{v\sqrt{(1-\beta_0)\alpha\bar{C}_{\max}(\bar{t}-T_0)}}{\sqrt{(1-\beta_0)\alpha\bar{C}_{\max}(\bar{t}-T_0)+\alpha\bar{C}_{\max}\sqrt{s(\bar{t})-(\bar{t}-T_0)}}} d\bar{t} & \text{for } t > T_2. \end{cases} \quad (4.64)$$

The constant states are located at

$$x_L = \frac{v(t - T_0)}{1 + (1 - \beta_0)\alpha\bar{C}_{\max}}; \quad (4.65)$$

$$x_R = \frac{v(t - T_0)}{1 + \frac{(1-\beta_0)\alpha\bar{C}_{\max}}{(1+\alpha)^2}}. \quad (4.66)$$

The solution for the concentration of suspended bacteria is given by

$$C^{bac} = \begin{cases} 1 & \text{for } (t, x) \in (0, T_0) \times (0, s(t)) \cup \\ & \cup (T_0, T_2) \times (x_R(t), s(t)); \\ 0 & \text{for } (t, x) \in (T_0, \infty) \times \\ & \times (0, x_L(t)) \cup \mathbb{R}^+ \times (s(t), \infty); \\ \frac{1}{\alpha} \left( \sqrt{\frac{(1-\beta_0)\alpha\bar{C}_{\max} \frac{x}{t-T_0}}{v - \frac{x}{t-T_0}}} - 1 \right) & \text{for } (t, x) \in (T_0, \infty) \times \\ & \times (x_L(t), \min(x_R(t), s(t))). \end{cases} \quad (4.67)$$

Finally, the concentration adsorbed bacteria  $\bar{C}^{bac}$  and fixated bacteria  $S^{bac}$  are given by

$$\bar{C}^{bac} = (1 - \beta_0 C^{fix}) \frac{\alpha \bar{C}_{\max} C^{bac}}{1 + \alpha C^{bac}}, \quad (4.68)$$

$$S^{bac} = \max_{0 \leq \bar{t} \leq t} \left\{ \beta_0 C^{fix} \frac{\alpha \bar{C}_{\max} C^{bac}}{1 + \alpha C^{bac}} \right\}. \quad (4.69)$$

### 4.3.3 Numerical Methods

The differential equations for the concentrations of bacteria and fixation fluid are solved by the standard Galerkin Finite Element Method. First, the weak formulation is derived by multiplication by a test function  $\eta \in L^2(\Omega)$  and integration over the domain  $\Omega$ . As an example, the differential equation for the suspended bacteria, see equation (4.26), is taken. For the adsorption isotherm, the Langmuir isotherm, see equation (4.61), is used. This gives

$$\int_{\Omega} \frac{\partial C^{bac}}{\partial t} \eta d\Omega + \int_{\Omega} v \frac{\partial C^{bac}}{\partial x} \eta d\Omega = \int_{\Omega} (-r_{ads} + r_{des}) \eta d\Omega. \quad (4.70)$$

For the time integration, an implicit scheme is used. That gives the following weak formulations for the urea concentration:

$$\int_{\Omega} \frac{C^{bac,n+1} - C^{bac,n}}{\Delta t} \eta d\Omega + \int_{\Omega} v \frac{\partial C^{bac,n+1}}{\partial x} \eta d\Omega = \int_{\Omega} (-r_{ads}^{n+1} + r_{des}^{n+1}) \eta d\Omega. \quad (4.71)$$

This equation holds for all  $\eta \in L^2(\Omega)$ , which vanish at location of the boundary where  $C^{bac}$  and  $C^{fix}$  are prescribed explicitly, hence at  $x = 0$ .

The Newton-Cotes quadrature rules have been used for the development of the element matrices and vectors. For this 1D case, line elements are used. Furthermore, linear basis functions are applied.

The differential equations for the various concentrations of bacteria are coupled, due to the reaction terms  $r_{ads}$  (equation (4.29)),  $r_{des}$  (equation (4.30)) and  $r_{fix}$  (equation (4.31)). Since these reaction rates are also nonlinear functions of the concentration suspended bacteria (because of the Langmuir isotherm in equation (4.61)), Newton's method is used for the solution of the differential equations containing these reaction rates. By doing so, the three various concentrations of bacteria come together in one matrix-vector system.

This leads to two matrix-vector systems: one for the fixation fluid and one for the three various concentrations of bacteria.

The time span has been divided into equisized discrete time steps. First, the differential equation for the concentration of fixation fluid is solved. Next, the solution to the coupled system of differential equations for the various concentrations of bacteria is computed. Some numerical results can be found in the next section.

## 4.4 Results

In this section, the analytical solution is visualized for some particular times and locations. For one particular time, we show the comparison between the analytical

solution and numerical simulations. The length of the column  $L$  has been chosen in such a way that relation (4.59) holds.

The solution expressed by equations (4.67), (4.68) and (4.69) is visualised in Figure 4.2 and 4.3. These figures display the concentration of suspended, adsorbed and fixated bacteria at several times and locations. For this visualisation the following values have been used:  $\alpha = 1$ ,  $\beta_0 = 0.5$ ,  $\bar{C}_{\max} = 1$ ,  $T_0 = 0.5$  and the length of the column  $L = s(T_2)$ .

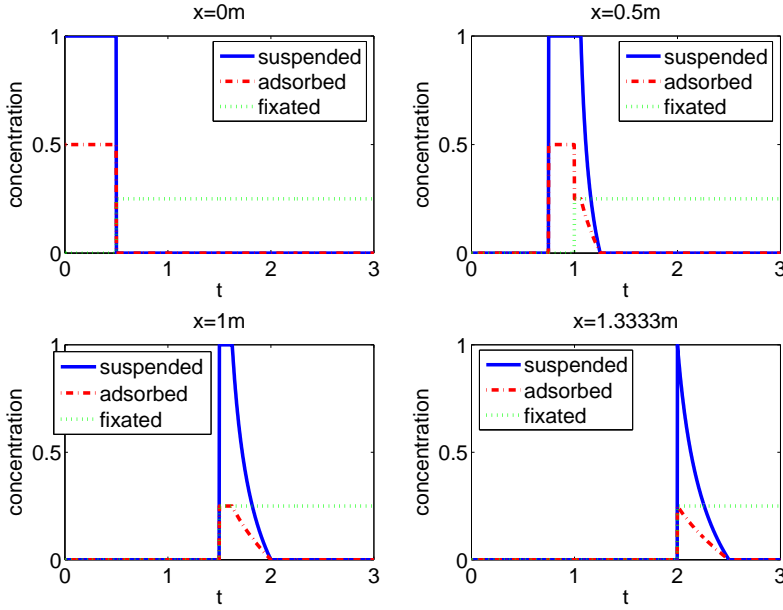


Figure 4.2: The concentration of suspended, adsorbed and fixated bacteria as a function of time at  $x = 0, 0.5, 1$  and  $1.3333\text{m}$ .

The top left graph of Figure 4.2 shows the concentrations at the inlet. The concentration of suspended bacteria  $C^{bac}$  and the concentration fixation fluid  $C^{fix}$  at the inflow boundary are prescribed in boundary conditions (4.24) and (4.25). From equations (4.61), (4.68) and (4.69) the other concentrations ( $\bar{C}^{bac}$  and  $S^{bac}$ ) can be found.

The top right graph of Figure 4.2 shows the concentrations at  $x = 0.5\text{m}$ . The front of the fixation fluid starts moving at  $t = T_0 = 0.5\text{h}$ , at a velocity  $q = 1\text{m/h}$ . At  $t = 1\text{h}$  the front of the fixation fluid reaches the position  $x = 0.5\text{m}$ . At that time and location, both suspended and temporarily adsorbed bacteria are present. A part of the temporarily adsorbed bacteria is fixated by the fixation fluid. That explains the sudden change in the concentration of temporarily adsorbed bacteria  $\bar{C}^{bac}$ . This is also in accordance with equation (4.68). This equation contains the multiplication factor  $(1 - \beta_0 C^{fix})$ . At  $t = 1\text{h}$  the concentration of fixation fluid changes from 0 into 1 at  $x = 0.5\text{m}$  and consequently the multiplication factor changes from 1 into 0.5. As a result,  $\bar{C}^{bac}$  changes from 0.5 into 0.25. At  $t = 1\text{h}$ , the concentration of

fixated bacteria  $S^{bac}$  changes from 0 into 0.25. Since  $C^{bac}$  does not increase in time after  $t = 1\text{h}$ ,  $S^{bac}$  does not change anymore.

At  $x = 1\text{m}$ , the pulse bacteria is fully overtaken by the fixation fluid. Hence, the maximum of  $\bar{C}^{bac}$  is 0.25 in the bottom graphs of Figure 4.2. Whereas the graphs in Figure 4.2 have different maxima for the concentration of temporarily adsorbed bacteria, the maximum of the concentration of fixated bacteria is the same for all the graphs. This has the following reason. When there is no fixation fluid present, the bacteria are not fixated, but as soon as there is fixation fluid present, a part of the bacteria is fixated. According to equation (4.69), the maximum depends on the maximum of  $C^{bac}$ , which is in all cases equal to 1. The bottom right graph of Figure 4.2 shows the concentrations at the outflow boundary.

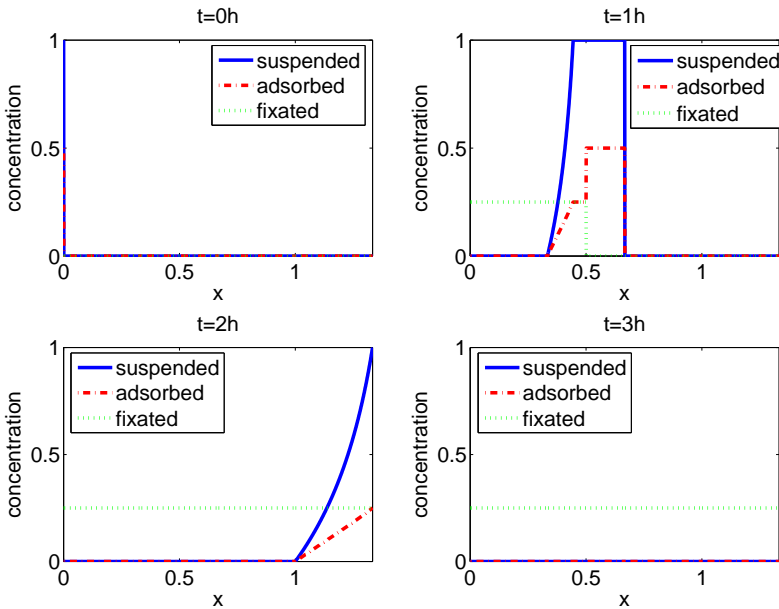


Figure 4.3: The concentration of suspended, adsorbed and fixated bacteria as a function of location at several times.

The top left graph of Figure 4.3 shows the initial situation: all concentrations are equal to 0 as prescribed in (4.23). The top right graph of Figure 4.3 shows the situation in which the pulse bacteria is partly overtaken by the fixation fluid. At  $t = 1\text{h}$  the front of the fixation fluid is located at  $x = 0.5\text{m}$ . The fixation fluid causes a sudden change in the concentration of temporarily adsorbed bacteria as was also observed in Figure 4.2.

At  $t = 2\text{h}$  the front of the bacterial pulse reaches the outflow boundary as is displayed in the bottom left graph of Figure 4.3. The bottom right graph of Figure 4.3 shows the final situation: all non fixated bacteria are flushed out and only the permanently adsorbed bacteria stay in the domain, which will provide the hydrolysis of urea.

As a result of the conservation of bacteria, at each time, the number of bacteria in the domain must be equal to the number of bacteria that flowed in minus the bacteria that flowed out:

$$\int_0^t qc_{in}d\bar{t} - \int_0^t qc_{out}d\bar{t} = \int_{\Omega} (C^{bac} + \bar{C}^{bac} + S^{bac})d\Omega, \quad (4.72)$$

where  $c_{in}$  is the inflow concentration and  $c_{out}$  is the concentration at the outflow boundary. This condition holds, as is required.

Furthermore, the analytical solution is compared to the results of the numerical simulations. This is presented for one particular time:  $t = 1h$ , but note that this could have been done for any other time. The numerical simulations have been done for several values of the reaction constants  $k_{ads}$ ,  $k_{des}$  and  $k_{fix}$ . Figure 4.4 shows the results of this comparison. As a value for the reaction constants we use the following exemplary values:  $K := k_{ads} = k_{des} = k_{fix} = 0.01 s^{-1} (= 36 h^{-1})$ ,  $K := k_{ads} = k_{des} = k_{fix} = 0.1 s^{-1} (= 360 h^{-1})$ ,  $K := k_{ads} = k_{des} = k_{fix} = 1 s^{-1} (= 3,600 h^{-1})$  and  $K := k_{ads} = k_{des} = k_{fix} = 10 s^{-1} (= 36,000 h^{-1})$ . The following time step and element size have been chosen:  $\Delta x = 0.001m$ ,  $\Delta t = 0.001h$ .

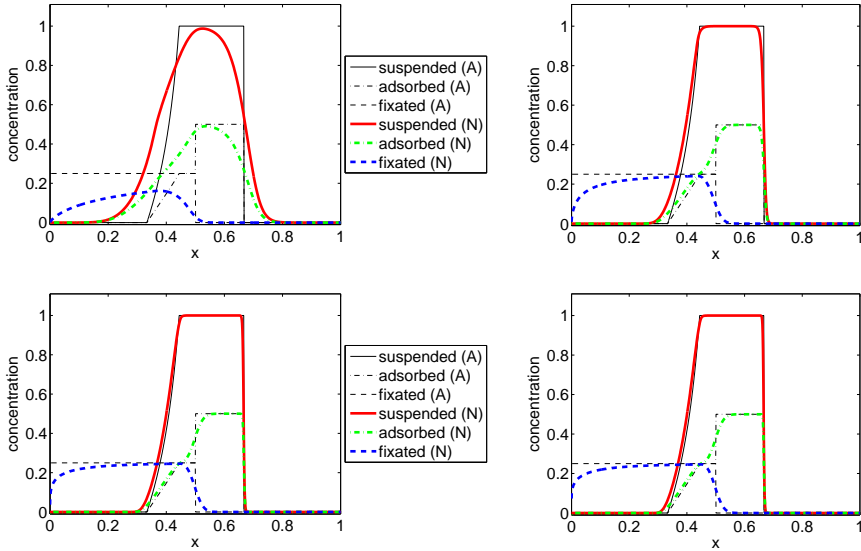


Figure 4.4: Comparison of the analytical solution (A) at  $t=1h$  with the solutions from numerical simulations (N) for several values of the adsorption, desorption and fixation constant ( $K = k_{ads} = k_{des} = k_{fix}$ ). The following values have been assigned to the constants:  $K = 0.01 s^{-1}$  (top left),  $K = 0.1 s^{-1}$  (top right),  $K = 1 s^{-1}$  (bottom left),  $K = 10 s^{-1}$  (bottom right). The graphs of the analytical solutions are marked with an A and the graphs of the numerical solutions are marked with an N.

From Figure 4.4 it can be seen that, upon increasing the reaction constants,

the numerical solution approaches the analytical solution. There is hardly any difference between the graph for  $K = 1 s^{-1}$  and the graph for  $K = 10 s^{-1}$  in Figure 4.4.

Figure 4.5 shows the results of spatial and temporal refinement. The time and place steps have been decreased two times by a factor of 2. It follows that in most cases the numerical solution approaches the analytical solution even more for smaller time and place steps, although it is not necessarily a result of refining. Each step of refining should result into a better approximation of the exact solution and in the limit, the numerical solution will equal the exact solution with given reaction rate constants. Note that in this case the exact solution is not the analytical (instantaneous) solution but the solution to the model with *finite* reaction rates, with  $K = 10 s^{-1}$  as a reaction constant. Therefore, the numerical solution with  $K = 10 s^{-1}$  will not converge to the analytical solution, presented in this chapter for instantaneous reactions, as  $\Delta t$  and  $\Delta x$  tend to zero.

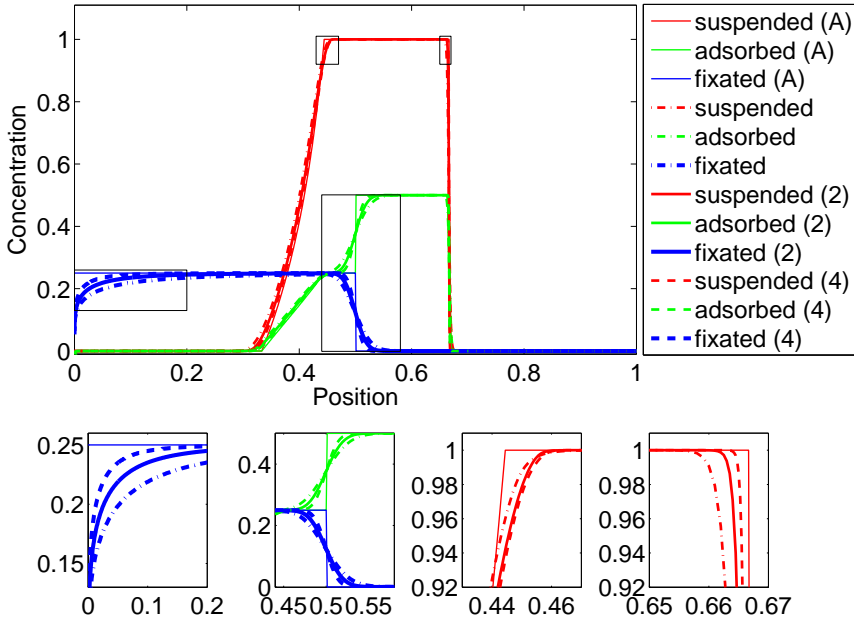


Figure 4.5: Comparison of the analytical solution at  $t=1h$  with the numerical solution for decreasing time and place steps. Some details of the graph in the large subplot are given in the four subplots below. The number between brackets is the refinement factor. Again, the analytical solutions are marked with an *A*. In the numerical solutions, the reaction constant has been chosen to be  $K = 10 s^{-1}$ .

## 4.5 Discussion and Conclusions

A model has been derived for the placement of bacteria. The model contains the most important phenomena of the transport of bacteria: advection, dispersion, adsorption, desorption and fixation. Of course, other phenomena can be added, like decay, growth and systematic motion of bacteria.

The model needs to be simplified in order to be able to construct an analytical solution. The analytical solution is only valid in 1D and can be used in cases in which there are variations in only one direction. Further, the pore water velocity and the porosity have been chosen to be constant. While deriving this model, it turned out that the shock speed needs to be constant until time  $T_2$  to avoid violation of conservation of mass. To avoid unphysical behaviour, the desorption, adsorption and fixation rate should be chosen carefully from a mathematical point of view.

This choice to simplify has been made to avoid a complex model, including a complicated coupling between the differential equation for the concentration of suspended bacteria, the pore water velocity and the porosity. However, since bacteria are fixated, the porosity decreases and that will result into a somewhat larger pore water velocity. The pore water velocity, in turn, influences the concentration of suspended bacteria. The influence of these effects depends on the volume of fixated bacteria. If this volume is not too large, this simplification will only lead to a small error. However, if the pores are almost fully filled with bacteria, this effect really should be taken into account. Although it is difficult (if ever possible) to find an analytical solution for the case that these differential equations are coupled, it is possible to find a numerical solution. [90] and [91] (Chapter 2 and 3) deal with a decreasing porosity (in these papers, due to precipitation) and its effect on the flow, and obtain a numerical solution to the system of coupled differential equations.

In the model, the pore water velocity  $v$  is assumed to be a constant. Due to a decreasing porosity effect, this might differ from reality as is explained in the previous paragraph. In the case study, the pore water velocity has been chosen to be  $v = 1\text{m/h}$ . The solutions can easily be adapted for other values of  $v$ . After replacing all  $x$ -values by  $x/v$ , the results will be the same. The question is whether this is realistic. For example, the velocity might have an influence on the adsorption, desorption and fixation. Real world experiments should be carried out to examine the effect of the velocity on the processes.

In the case study, the reaction constants are equal. The larger the reaction constant, the more this reaction dominates the other reactions. If, for example, the reaction constant of the fixation reaction is large compared to the reaction constant of the adsorption reaction, the bacteria that are being adsorbed almost immediately will be fixated. Until the equilibrium of the fixated bacteria is reached, there will be far more fixated bacteria than adsorbed bacteria. If, on the other hand, the fixation constant is small, there will be more adsorbed bacteria than fixated bacteria. The fixated bacteria will not reach its equilibrium if the pulse of bacteria is too short.

Another simplification is the ignoring of dispersion and diffusion. Due to this, the front of the bacteria and the fixation fluid is very steep. Adding dispersion and diffusion to the model will result into smoother graphs. By solving the model equations numerically, always some numerical diffusion will be introduced. The finer the mesh and the smaller the time steps, the smaller the numerical diffusion. From

Figure 4.5 it can be seen that the numerical solution is smoother than the analytical one (note that this is not only a result of the numerical diffusion but also of the finite reaction kinetics) and that the refinements result into a steeper front.

The ratio of the fixated bacteria  $\beta$  versus the adsorbed bacteria depends on the concentration of the fixation fluid, but it may also depend on the properties of the microorganisms, the pH and the porous medium. Since the fixation fluid has a large influence on the fixation of the bacteria and hence on  $\beta$ , a simple linear relation between  $\beta$  and the concentration of the fixation fluid has been chosen. However, it is likely that this ratio also depends on the flow velocity. The larger the flow velocity, probably the more bacteria are released from fixation and that will lead to a smaller  $\beta$ . Additional research needs to be carried out to find a good expression for this ratio. It is crucial to find a good estimation, since in the model,  $\beta$  prescribes the amount of fixated bacteria, and finally these bacteria provide the production of calcium carbonate, which is the aim of the Biogrout process.

In the case study, the Langmuir isotherm has been chosen as the adsorption isotherm. Real life experiments should point out whether this is a good choice for the transport of bacteria in combination with fixation.

The last simplification, that is made in order to be able to construct an analytical solution, is that the equilibrium between suspended bacteria, adsorbed bacteria and fixated bacteria is instantaneous. Therefore, no kinetics are involved and consequently, the concentration of adsorbed bacteria ( $\bar{C}^{bac}$ ) and the concentration of fixated bacteria ( $S^{bac}$ ) are a direct function of the concentration of suspended bacteria ( $C^{bac}$ ). Especially when the flow velocity is low, the equilibrium reaction is fast with respect to the transport. In that case, an instantaneous equilibrium can be assumed. However, since the bacteria are injected in the soil, the flow velocity will be not very low. In that case, this simplification might be not realistic and a non instantaneous equilibrium should be considered. In Figure 4.4, some results are displayed for an increasing value of the reaction constants. For a small reaction constant, the result clearly differs from the solution for an instantaneous equilibrium. The larger the reaction constants are, the more the numerical solution approaches the analytical solution, and hence, the instantaneous case.

Constructing an analytical solution contributed to the derivation of a physically consistent model. Although some simplifications might be not realistic, the analytical solution gives a good idea of what the distribution of bacteria in the aquifer looks like. The analytical solution can also be used as a benchmark for the numerical solution. For increasing reaction constants, the numerical solution should approximate the analytical solution. This turns out to be the case (see Figure 4.4). Refinement of the place and time step results into smaller numerical errors and in most cases in a better convergence to the analytical solution. In future, the analytical solution will be compared to real life bacterial placement experiments.



## A Mathematical model for Biogrout: Bacterial placement and soil reinforcement.

This chapter has been published as:

Van Wijngaarden, W.K., Vermolen, F.J., Van Meurs, G.A.M., Vuik, C.: A Mathematical model for Biogrout: Bacterial placement and soil reinforcement. *Computational Geosciences* **17-3**, 463–478 (2013)

## Abstract

We present a mathematical model for Biogrout, which is a technique for soil reinforcement that is based on Microbially Induced Carbonate Precipitation. The model deals with the entire process, consisting of fixation of bacteria, as well as of the subsequent soil reinforcement. This chapter deals with the coupling of two earlier models for bacterial placement and reinforcement, where the construction of the model is discussed, as well as numerical results. Further, we present analytical solutions for the constant flow velocity case. The model is based on the assumption that the porous medium is stiff.

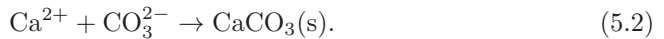
## 5.1 Introduction<sup>1</sup>

The first step in the Biogrout process is the injection of bacteria. The bacteria will adsorb onto the porous matrix. That gives retardation. To fixate the bacteria onto the porous matrix, a fixation fluid is injected. This fixation fluid is a solution with a high salinity, and it will overtake the weakly adsorbed bacteria and strongly fix them onto the solid matrix. In [92] (Chapter 4), a model has been derived to describe the placement of the bacteria.

The second part in the Biogrout process is the injection of reactants. Urea ( $\text{CO}(\text{NH}_2)_2$ ) and calcium chloride ( $\text{CaCl}_2$ ) are injected into the soil. The bacteria catalyse the hydrolysis of urea, and ammonium ( $\text{NH}_4^+$ ) and carbonate ( $\text{CO}_3^{2-}$ ) are formed. In the presence of calcium ions ( $\text{Ca}^{2+}$ ), the carbonate precipitates as calcium carbonate ( $\text{CaCO}_3$ ). In [97], the reaction equations are discussed in more detail. The hydrolysis reaction is given by



The precipitation of calcium carbonate happens in several steps, depending on the pH. The overall reaction equation for the precipitation is given by:



Combining the hydrolysis reaction equation (5.1) and the reaction equation for the precipitation of calcium carbonate (5.2) gives the overall Biogrout reaction equation:



The side-product ammonium ( $\text{NH}_4^+$ ) has to be removed. The solid calcium carbonate forms bridges between the sand grains. These bridges cause an increase in the strength and stiffness of the soil.

A model for the transport and reaction of the reactants and the formation of calcium carbonate has been proposed in [90] and [91] (Chapter 2 and 3). In [90, 91], a homogeneous bacterial activity was assumed, which is probably not realistic. Therefore, in [92] (Chapter 4) a model was derived that describes the placement of the bacteria. Solving the model equations gives the distribution of the bacteria. In

---

<sup>1</sup>Parts of the original introduction have been skipped in order to prevent too much repetition of the Introduction from Chapter 1.

this chapter, these two models are combined to end up with a model that describes the placement of bacteria as well as the transport of the reactants and the formation of calcium carbonate. In Section 5.2, the (partial differential) equations are given for both models and shortly discussed. Further, analytical solutions are presented that are valid under idealized conditions. In Section 5.3, it is described which numerical methods are used to solve the model equations. Some results of the numerical simulations with the combined model are presented in Section 5.4 as well as a comparison with the model in which a homogeneous bacterial activity was assumed. Some discussion and conclusions can be found in Section 5.5.

## 5.2 Mathematical Model

In this section, the model equations are given for the Biogrout process. In Subsection 5.2.1, the (partial differential) equations are given for the placement of the bacteria, whereas the equations for the precipitation of calcium carbonate are presented in Subsection 5.2.2. Finally, some analytical solutions are derived.

### 5.2.1 Model equations for the placement of the bacteria

The first step in the Biogrout process is the injection of bacteria. These bacteria will partly adsorb onto the solid matrix. This adsorption gives retardation. Next, a fluid with high salinity is injected into the subsoil. This solution acts as a fixation fluid to the bacteria. This fluid will overtake the adsorbed bacteria and strongly fixate them onto the matrix of the porous media. When, later on, the suspended bacteria are flushed away, the fixated bacteria stay in place and will play an important role in the precipitation of calcium carbonate, which is the second part in the Biogrout process. For completeness, we give the model equations for the placement of bacteria, as derived in [92] (Chapter 4).

The model for the placement of bacteria contains three phases of bacteria: bacteria in suspension, adsorbed bacteria and fixated bacteria. Concentration  $C^{bac}$  is defined as the bacterial concentration in suspension, concentration  $\bar{C}^{bac}$  is the concentration of adsorbed bacteria and  $S^{bac}$  is the concentration of fixated bacteria. Note that, for convenience, the concentrations  $\bar{C}^{bac}$  and  $S^{bac}$  have the same unit as  $C^{bac}$ , although the adsorbed and fixated bacteria are no longer in suspension, but adsorbed or fixated onto the porous matrix. The following differential equations are derived for the concentrations of the bacteria:

$$\frac{\partial (\theta C^{bac})}{\partial t} = \nabla \cdot (\mathbf{D}_{bac} \theta \nabla C^{bac}) - \nabla \cdot (\mathbf{q} C^{bac}) - \theta r_{ads} + \theta r_{des}, \quad (5.4)$$

$$\frac{\partial (\theta \bar{C}^{bac})}{\partial t} = \theta r_{ads} - \theta r_{des} - \theta r_{fix}, \quad (5.5)$$

$$\frac{\partial (\theta S^{bac})}{\partial t} = \theta r_{fix}, \quad (5.6)$$

In these equations,  $\theta$  is the porosity,  $\mathbf{D}_{bac}$  is the dispersion tensor,  $\mathbf{q}$  is the Darcy flow velocity which relates to the pore water flow velocity  $\mathbf{v}$  as  $\mathbf{q} = \mathbf{v}\theta$ ,  $r_{ads}$  is the adsorption reaction rate,  $r_{des}$  is the desorption reaction rate and  $r_{fix}$  is the

fixation reaction rate. The left-hand side of equations (5.4), (5.5) and (5.6) models accumulation, the first term at the right-hand side of equation (5.4) represents the dispersion and diffusion of the bacteria and the second term is the advection term. Since the adsorbed and fixated bacteria can not be transported, there are no dispersion/diffusion and advection terms in equations (5.5) and (5.6). The other terms in equations (5.4), (5.5) and (5.6) stand for the adsorption, desorption and fixation reactions. These equations show that it is assumed that only adsorbed bacteria are fixated (only equation (5.5) and (5.6) contain a fixation reaction term).

In the case of an equilibrium-controlled adsorption, the concentration of the adsorbed species tend to the adsorption isotherm. In the Biogrout process, there are both temporarily adsorbed and permanently adsorbed (fixed) bacteria. The adsorption isotherm  $\varphi(C^{bac})$  depends on the concentration of bacterial cells in suspension ( $C^{bac}$ ) and may also depend on properties of the microorganisms, the porous medium and the pH. It has been assumed that the equilibrium of the permanently adsorbed bacteria is equal to  $\beta\varphi(C^{bac})$  and that the equilibrium of the temporarily adsorbed bacteria is equal to  $(1 - \beta)\varphi(C^{bac})$ . The fraction  $\beta$  ranges between 0 and 1. Its value depends on the concentration of the fixation fluid  $C^{fix}$ , but may also depend on properties of the microorganisms, the pH and the porous medium.

As a driving force for the adsorption reaction, the difference between the adsorption isotherm and the concentration of the adsorbed (temporarily or permanently) bacteria is used. Adsorption only takes place when the adsorption isotherm is larger than the concentration of the adsorbed and fixated bacteria. That gives the following adsorption reaction rate:

$$r_{ads} = k_{ads} \left( \varphi(C^{bac}) - \left( \bar{C}^{bac} + S^{bac} \right) \right)_+, \quad (5.7)$$

where  $k_{ads}$  is the adsorption reaction rate constant. The notation  $(.)_+$  considers the positive part of an expression and has been defined as  $(.)_+ := \max(0, .)$ .

In the same way, the driving force for the fixation reaction is the difference between concentration  $S$  and its equilibrium  $\beta\varphi(C^{bac})$  and fixation only takes place if  $S^{bac}$  is smaller than its equilibrium. We multiply this driving force by the concentration of adsorbed bacteria  $\bar{C}^{bac}$  to guarantee that bacteria only can be fixated if there are adsorbed bacteria present, hence

$$r_{fix} = k_{fix} \bar{C}^{bac} (\beta\varphi(C^{bac}) - S^{bac})_+. \quad (5.8)$$

In this equation,  $k_{fix}$  is the fixation reaction constant.

As a reaction rate for desorption (the opposite phenomenon of adsorption), the following equation was derived:

$$r_{des} = k_{des} \left( \left( \bar{C}^{bac} - (1 - \beta)\varphi(C^{bac}) \right) + \left( S^{bac} - \beta\varphi(C^{bac}) \right) \right)_-, \quad (5.9)$$

where  $k_{des}$  is the desorption reaction rate. The notation  $(.)_-$  has been defined as  $(.)_- := \min(0, .)$ , which implies that only the negative part of an expression is considered. Again, the driving force is the difference between the concentration of temporarily and permanently adsorbed bacteria (respectively  $\bar{C}^{bac}$  and  $S^{bac}$ ) and their equilibria (respectively, being  $(1 - \beta)\varphi(C^{bac})$  and  $\beta\varphi(C^{bac})$ ). Desorption only

takes place if the difference is positive. Otherwise, it would be *adsorption*. The term  $(S^{bac} - \beta\varphi(C^{bac}))$  is only considered if it is negative for the following reason: Consider the case that  $S^{bac}$  is larger than its equilibrium,  $S^{bac} > \beta\varphi(C^{bac})$  (which can happen, if  $C^{bac}$  is decreasing) and that  $\bar{C}^{bac}$  is smaller than its equilibrium,  $\bar{C}^{bac} < (1 - \beta)\varphi(C^{bac})$ , while the sum of adsorbed bacteria is larger than the adsorption isotherm,  $\bar{C}^{bac} + S^{bac} > (1 - \beta)\varphi(C^{bac}) + \beta\varphi(C^{bac}) = \varphi(C^{bac})$ . The latter implies that there is a driving term for desorption and that the concentration of temporarily adsorbed bacteria  $\bar{C}^{bac}$  will decrease. However, this temporarily adsorbed bacteria concentration is already smaller than its equilibrium, which would give adsorption rather than desorption. Hence, if  $S^{bac}$  is larger than its equilibrium, the difference should not contribute to desorption. That explains why this difference is only taken into account if it is negative.

The ratio  $\beta$  depends on the concentration of fixation fluid  $C^{fix}$ . As a relation between  $\beta$  and the concentration of fixation fluid, the following Monod equation is used:

$$\beta = \beta_0 \frac{C^{fix}}{K_{m,fix} + C^{fix}}, \quad (5.10)$$

for some positive constant  $\beta_0$ .

For this concentration of fixation fluid, the following partial differential equation is derived

$$\frac{\partial(\theta C^{fix})}{\partial t} = \nabla \cdot (\mathbf{D}_{fix} \theta \nabla C^{fix}) - \nabla \cdot (\mathbf{q} C^{fix}), \quad (5.11)$$

where,  $\mathbf{D}_{fix}$  is the dispersion tensor. The left-hand side of this equation models accumulation, the first term at the right-hand side stands for dispersion and diffusion and the last term is the advection term.

For the simulations in this chapter, a Langmuir adsorption isotherm is used, as given in [100]:

$$\varphi(C^{bac}) = \frac{\alpha \bar{C}_{\max} C^{bac}}{1 + \alpha C^{bac}}, \quad (5.12)$$

where the positive constant  $\alpha$  denotes the Langmuir constant and  $\bar{C}_{\max}$  is the maximum adsorption capacity.

A differential equation for the flow is given in the next subsection.

### 5.2.2 Model equations for the precipitation of calcium carbonate

After the placement of bacteria, urea ( $\text{CO}(\text{NH}_2)_2$ ) and calcium chloride ( $\text{CaCl}_2$ ) are injected into the soil. The bacteria provide the hydrolysis of urea according to reaction (5.1). Carbonate ( $\text{CO}_3^{2-}$ ) and ammonium ( $\text{NH}_4^+$ ) are formed. The carbonate precipitates with the calcium ( $\text{Ca}^{2+}$ ) as calcium carbonate ( $\text{CaCO}_3$ ), see precipitation reaction (5.2). The solid calcium carbonate causes a (slight) decrease in porosity and in permeability, which has an influence on the flow and the pressure. The hydrolysis and precipitation reactions influence the density of the solution. In [90, 91], partial differential equations are given for the concentration of urea, calcium chloride, ammonium chloride and calcium carbonate, for the pressure and

the flow, as well as relations for the porosity, permeability and density of the fluid. In this subsection we repeat them and shortly discuss them.

We start with the partial differential equations for the aqueous species:

$$\frac{\partial(\theta C^i)}{\partial t} = \nabla \cdot (\theta \mathbf{D} \cdot \nabla C^i) - \nabla \cdot (\mathbf{q} C^i) + n_i \theta r_{hp}. \quad (5.13)$$

In this equation,  $\theta$  is the porosity,  $C^i$  is the dissolved concentration of species  $i$ ,  $i \in \{\text{urea}, \text{Ca}^{2+}, \text{NH}_4^+\}$  with  $\text{M}$  (=kmol/m<sup>3</sup>) as a unit,  $\mathbf{D}$  is the dispersion tensor,  $\mathbf{q}$  is the Darcy velocity,  $n_i$  is a constant that deals with the stoichiometry in the biochemical reaction equation (5.3) and  $r_{hp}$  is the reaction rate of the production of calcium carbonate, which is a function of the urea concentration and the bacterial concentrations. From the stoichiometry of reaction (5.3), the values of  $n_i$  for the various aqueous species are given by:  $n_{\text{urea}} = -1$ ,  $n_{\text{Ca}^{2+}} = -1$ , and  $n_{\text{NH}_4^+} = 2$ .

The left-hand side of equation (5.13) stands for the accumulation. In the right-hand side, we have terms for dispersion/diffusion, for the advection and for the biochemical reaction (5.3).

For the reaction rate  $r_{hp}$  of equation (5.3), the following relation has been used:

$$r_{hp} = v_{max} \frac{C^{\text{urea}}}{K_{m,\text{urea}} + C^{\text{urea}}} (C^{\text{bac}} + \bar{C}^{\text{bac}} + S^{\text{bac}}). \quad (5.14)$$

Here,  $v_{max}$  is the bacterial conversion rate constant and  $K_{m,\text{urea}} \geq 0$  is the saturation constant.

For the concentration of the solid calcium carbonate  $C^{\text{CaCO}_3}$ , we have the following differential equation:

$$\frac{\partial C^{\text{CaCO}_3}}{\partial t} = m_{\text{CaCO}_3} \theta r_{hp}. \quad (5.15)$$

In this equation,  $m_{\text{CaCO}_3}$  is the molar mass of calcium carbonate, which is used to convert moles into mass. Since it has been assumed that the calcium carbonate is not transported, there are no transport terms in the differential equation. Hence, equation (5.15) only contains an accumulation term and a reaction term.

The solid calcium carbonate that is formed in the pores, causes a decrease in porosity. The difference  $(C^{\text{CaCO}_3}(t) - C^{\text{CaCO}_3}(0))$  gives the amount of calcium carbonate that has been formed per unit of volume. Division by the density of calcium carbonate  $\rho_{\text{CaCO}_3}$  gives the decrease in pore volume per unit of volume. That leads to the following relation between the calcium carbonate concentration and the porosity:

$$\theta(t) = \theta(0) - \frac{C^{\text{CaCO}_3}(t) - C^{\text{CaCO}_3}(0)}{\rho_{\text{CaCO}_3}}. \quad (5.16)$$

For the flow, we use the continuity equation, that was derived in [93] (Chapter 6), which is an adaptation of the differential equation derived in [91] (Chapter 2).

$$\nabla \cdot \mathbf{q} = K \theta r_{hp}. \quad (5.17)$$

The constant  $K$  has been defined as

$$K := \left( \frac{m_{\text{CaCO}_3}}{\rho_{\text{CaCO}_3}} - (1 - V_s) \right). \quad (5.18)$$

In this definition,  $1 - V_s$  is the decrease of liquid volume as a result of the biochemical reaction (5.3). In [93] (Chapter 6), we compared equation (5.17) to another differential equation for the flow:

$$\frac{\partial(\rho_l \theta)}{\partial t} = -\nabla \cdot (\rho_l \mathbf{q}) - m_{CaCO_3} \theta r_{hp}. \quad (5.19)$$

The results were very similar, at least in 1D, but equation (5.17) turned out to be more stable than equation (5.19). We also note that equation (5.17) is consistent with the Oberbeck-Boussinesq approximation as  $r_{hp} \rightarrow 0$ , i.e. in absence of the reaction.

As a relation between the flow and the pressure  $p$ , Darcy's law is used, [100]

$$q_x = -\frac{k_x}{\mu} \frac{\partial p}{\partial x}, \quad (5.20)$$

$$q_y = -\frac{k_y}{\mu} \frac{\partial p}{\partial y}, \quad (5.21)$$

$$q_z = -\frac{k_z}{\mu} \left( \frac{\partial p}{\partial z} + \rho_l g \right). \quad (5.22)$$

In Darcy's law,  $k_i$  is the intrinsic permeability in the various coordinate directions,  $i \in \{x, y, z\}$ ,  $\mu$  is the viscosity of the fluid,  $\rho_l$  is the density of the fluid and  $g$  is the gravitational constant.

The Kozeny-Carman equation is used to determine the intrinsic permeability. This equation is an empirical relation between the intrinsic permeability and the porosity, that is commonly used in ground water flow modelling (see [7]):

$$k = k_x = k_y = k_z = \frac{(d_m)^2}{180} \frac{\theta^3}{(1 - \theta)^2}. \quad (5.23)$$

In this relation,  $d_m$  is the mean particle size of the sand.

For the fluid density, the empirical relation that is given in [91] is used:

$$\rho_l = 1000 + 15.4996C^{urea} + 86.7338C^{Ca^{2+}} + 15.8991C^{NH_4^+}. \quad (5.24)$$

The bacteria hardly influence the density. Hence, they are not taken into account in the density calculation.

Substituting equations (5.20), (5.21) and (5.22) into equation (5.17), using relation (5.23), gives a partial differential equation for the pressure, which can be used to solve for the flow pattern if the boundary conditions are given in terms of pressure, or if density differences influence the flow.

$$\nabla \cdot \mathbf{q} = \nabla \cdot \left( -\frac{k}{\mu} (\nabla p + \rho_l g \mathbf{e}_z) \right) = K \theta r_{hp}. \quad (5.25)$$

Here,  $\mathbf{e}_z$  is the unit vector in vertical direction, taken positive upwards.

### 5.2.3 Boundary Conditions and Initial Conditions

We consider a one dimensional configuration, which corresponds to a column. We take a line with a length of 1 m, with inflow at the left-hand side ( $\Gamma_1$ ) and outflow at the right-hand side ( $\Gamma_2$ ).

The injection strategy exists of 3 phases. During phase 1, from time  $t=T_0=0$  h until time  $t=T_1$ , bacteria are injected. During phase 2, from time  $t=T_1$  until time  $t=T_2$ , a fixation fluid is injected. The third phase is from time  $t=T_2$  until time  $t=T_{end}$ . During this phase, urea and calcium chloride are injected.

Table 5.1 gives the boundary conditions for the one dimensional configuration.

Table 5.1: Boundary conditions for the various concentrations and the flow for the one dimensional configuration.

	$\Gamma_1$	$\Gamma_2$
$C^{bac}$	$(D\theta\nabla C - \mathbf{q}C) \cdot \mathbf{n} = \begin{cases} q_{in}c_{in} & \text{phase 1} \\ 0 & \text{else} \end{cases}$	$\frac{\partial C}{\partial n} = 0$
$C^{fix}$	$(D\theta\nabla C - \mathbf{q}C) \cdot \mathbf{n} = \begin{cases} q_{in}c_{in} & \text{phase 2} \\ 0 & \text{else} \end{cases}$	$\frac{\partial C}{\partial n} = 0$
$C^{urea}$	$(D\theta\nabla C - \mathbf{q}C) \cdot \mathbf{n} = \begin{cases} q_{in}c_{in} & \text{phase 3} \\ 0 & \text{else} \end{cases}$	$\frac{\partial C}{\partial n} = 0$
$C^{Ca^{2+}}$	$(D\theta\nabla C - \mathbf{q}C) \cdot \mathbf{n} = \begin{cases} q_{in}c_{in} & \text{phase 3} \\ 0 & \text{else} \end{cases}$	$\frac{\partial C}{\partial n} = 0$
$C^{NH_4^+}$	$(D\theta\nabla C - \mathbf{q}C) \cdot \mathbf{n} = 0$	$\frac{\partial C}{\partial n} = 0$
$p/q$	$q = q_{in}$	$p = 10^5$

Initially, all concentrations are equal to zero. The initial porosity is equal to some constant  $\theta_0$ . Since the partial differential equations for the concentration of urea and the concentration of calcium ions are the same, as well as the initial and boundary conditions, both concentration-distributions are identical. Therefore, we only consider the concentration of urea. We use the parameter values given in Table 5.2.

### 5.2.4 Analytical solution

In this subsection, an analytical solution is derived for a simplified version of system (5.4)-(5.18). For the analytical solution, we restrict ourselves to one dimension. Furthermore, the reaction constants are infinitely large:  $k_{ads}, k_{des}, k_{fix} \rightarrow \infty$  and dispersion and diffusion are neglected:  $\mathbf{D}_i = 0$  for  $i \in \{\text{bac, fix, urea, Ca}^{2+}, \text{NH}_4^+\}$ . The decrease of the porosity and the change of liquid volume as a result of the reaction are also neglected:  $\theta(x, t) = \theta_0$  and  $K = 0$ . As we consider one dimensional flow without sinks and sources and a constant porosity, the pore water velocity  $v$  is constant.

The analytical solution for the concentration of suspended bacteria  $C^{bac}$ , the concentration of temporarily adsorbed bacteria  $\bar{C}^{bac}$  and the concentration of fixated bacteria  $S^{bac}$  are derived in [92] (Chapter 4). We give the analytical solution for

Table 5.2: The values that are taken for the various parameters.

$\alpha_{bac}$	= 0.001 m,	$\alpha_{fix}$	= 0.001 m,
$\alpha_{urea}$	= 0.001 m,	$\alpha_{Ca^{2+}}$	= 0.001 m,
$\alpha_{NH_4^+}$	= 0.001 m,	$D_{m,bac}$	= $10^{-9}$ m <sup>2</sup> /s,
$D_{m,fix}$	= $10^{-9}$ m <sup>2</sup> /s,	$D_{m,urea}$	= $10^{-9}$ m <sup>2</sup> /s,
$D_{m,Ca^{2+}}$	= $10^{-9}$ m <sup>2</sup> /s,	$D_{m,NH_4^+}$	= $10^{-9}$ m <sup>2</sup> /s,
$\alpha$	= 0.5 [1],	$\bar{C}_{max}$	= 1 [1],
$\beta_0$	= 0.505 [1],	$K_{m,urea}$	= 0.01 kmol/m <sup>3</sup> ,
$K_{m,fix}$	= 0.01 kmol/m <sup>3</sup> ,	$m_{CaCO_3}$	= 100.1 kg/kmol,
$\rho_{CaCO_3}$	= 2710 kg/m <sup>3</sup> ,	$V_s$	= 0.97035 m <sup>3</sup> /kmol,
$d_m$	= 200 $\mu$ m,	$g$	= 9.81 m/s <sup>2</sup> ,
$\theta_0$	= 0.35 [1],	$q_{in}$	= 0.35 m/h,
$v_{max}$	= 0.72 kmol/m <sup>3</sup> /h,	$c_{in}$	= 1 [1] or kmol/m <sup>3</sup> ,
$T_1$	= 0.5 h,	$T_2$	= 1.0 h,
$T_{end}$	= 2.0 h.		

$C^{bac}$ :

$$C^{bac} = \begin{cases} 1 & \text{for } (t, x) \in (0, T_1) \times (0, s(t)) \cup \\ & \cup (T_1, T_3) \times (x_R(t), s(t)); \\ 0 & \text{for } (t, x) \in (T_1, \infty) \times \\ & \times (0, x_L(t)) \cup \mathbb{R}^+ \times (s(t), \infty); \\ \frac{1}{\alpha} \left( \sqrt{\frac{(1-\beta(1))\alpha\bar{C}_{max} \frac{x}{t-T_1}}{v - \frac{x}{t-T_1}}} - 1 \right) & \text{for } (t, x) \in (T_1, \infty) \times \\ & \times (x_L(t), \min(x_R(t), s(t))), \end{cases} \quad (5.26)$$

where the shock speed  $s(t)$  is given by

$$s(t) = \begin{cases} \frac{vt}{1+\varphi(1)} & \text{for } t < T_3; \\ \frac{v(1+\alpha)T_3}{1+\alpha+\alpha\bar{C}_{max}} + \int_{T_3}^t \frac{v\sqrt{(1-\beta(1))\alpha\bar{C}_{max}(\bar{t}-T_1)}}{\sqrt{(1-\beta(1))\alpha\bar{C}_{max}(\bar{t}-T_1)+\alpha\bar{C}_{max}\sqrt{s(\bar{t})-(\bar{t}-T_1)}}} d\bar{t} & \text{for } t > T_3, \end{cases} \quad (5.27)$$

and the location of the endpoints of the constant states are determined by

$$x_L = \frac{v(t-T_1)}{1+(1-\beta(1))\alpha\bar{C}_{max}}; \quad (5.28)$$

$$x_R = \frac{v(t-T_1)}{1+\frac{(1-\beta(1))\alpha\bar{C}_{max}}{(1+\alpha)^2}}. \quad (5.29)$$

Time  $T_3$  is the time at which the shock speed of the bacteria changes, which is calculated from

$$T_3 = \frac{\frac{(1+\alpha)^2}{\alpha\bar{C}_{max}} + (1+\alpha)}{\alpha + \beta(1)} T_1. \quad (5.30)$$

The concentrations of temporarily adsorbed bacteria  $\bar{C}^{bac}$  and fixated bacteria  $S^{bac}$  are determined as a function of the concentration of suspended bacteria  $C^{bac}$ :

$$\bar{C}^{bac} = (1 - \beta(c^{fix})) \frac{\alpha \bar{C}_{\max} C^{bac}}{1 + \alpha C^{bac}}, \quad (5.31)$$

$$S^{bac} = \max_{0 \leq \bar{t} \leq t} \left\{ \beta(c^{fix}) \frac{\alpha \bar{C}_{\max} C^{bac}}{1 + \alpha C^{bac}} \right\}, \quad (5.32)$$

see [92] (Chapter 4) for a derivation.

In [92], the ratio  $\beta$  is given by  $\beta(C^{fix}) = \beta_0 C^{fix}$ . In this chapter we use the more complex but also more physical relation  $\beta(C^{fix}) = \beta_0 \frac{C^{fix}}{K_{m,fix} + C^{fix}}$ , see relation (5.10). Here,  $\beta_0$  has a somewhat larger value, such that the value of  $\beta(1)$  is the same as for the case in [92].

In this chapter, the fixation fluid is only injected for a finite time, while in [92] (Chapter 4), the injection of fixation fluid is never stopped. In this chapter, a solution containing  $\text{Ca}^{2+}$  is being injected after the injection of fixation fluid. The  $\text{Ca}^{2+}$  is needed for the precipitation reaction but also acts as a fixation fluid, due to its high salinity. Hence, the solution in [92] is still valid for this study.

The analytical solution for the concentration of urea is constructed with the method of characteristics. Along characteristics, we have

$$\begin{aligned} \frac{d}{dt} C^{urea}(t, x(t)) &= C_t^{urea} + C_x^{urea} x'(t) = \\ &= -v_{max} \frac{C^{urea}}{K_{m,urea} + C^{urea}} \left( C^{bac} + \bar{C}^{bac} + S^{bac} \right), \end{aligned} \quad (5.33)$$

with

$$x'(t) = v. \quad (5.34)$$

The injection of the urea starts at time  $T_2$ . This time has been chosen in such a way that the urea does not overtake the non fixated bacteria within the domain. We define  $x_{fu}$  as the position of the urea front. If  $x_{fu}, x_L < L$ , it should hold that:

$$x_{fu} = v(t - T_2) < x_L. \quad (5.35)$$

Hence, everywhere in the domain where the urea concentration is non zero, only fixated bacteria are left. The length of the domain  $L$  has been chosen such that finally a constant concentration of fixated bacteria is reached, which is the case if  $L < s(T_3)$ . Therefore, on the locations where the concentration of urea is non negative, it holds that

$$C^{bac} + \bar{C}^{bac} + S^{bac} = S^{bac} = \beta(1) \frac{\alpha \bar{C}_{\max}}{1 + \alpha}, \quad (5.36)$$

which is a constant. This constant is substituted into equation (5.33).

A solution to equation (5.33) is the trivial solution:

$$C^{urea}(x, t) = 0. \quad (5.37)$$

The non trivial solution can be found by application of separation of variables on equation (5.33), to give the following implicit solution:

$$K_{m,urea} \ln \left( \frac{C_0^{urea}}{C^{urea}} \right) + C_0^{urea} - C^{urea} = v_{max} \beta(1) \frac{\alpha \bar{C}_{max}}{1 + \alpha} (t - t_0), \quad (5.38)$$

with  $C_0^{urea}$  the concentration at time  $t_0$ .

Figure 5.1 displays the (x-t)-diagram for the concentration of urea.

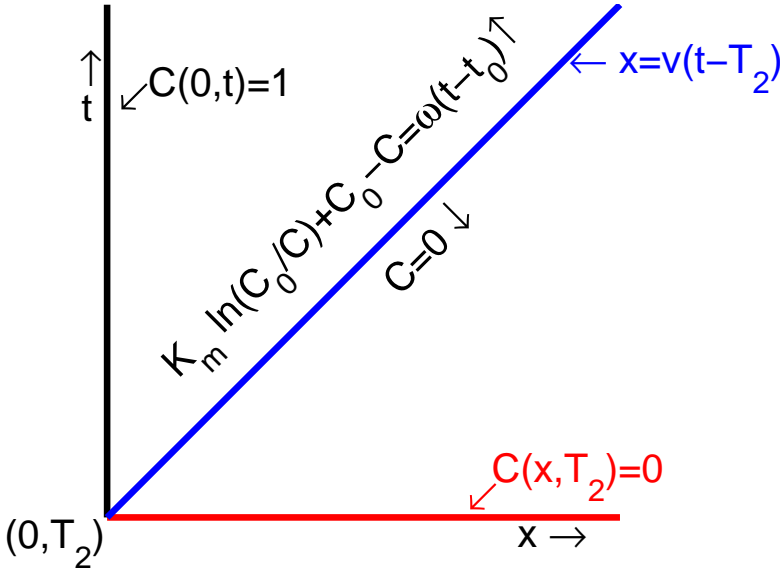


Figure 5.1: The (x-t)-diagram for the concentration of urea. In this diagram we have that  $C = C^{urea}$ ,  $C_0 = C_0^{urea}$  and  $\omega = v_{max} \beta(1) \frac{\alpha \bar{C}_{max}}{1 + \alpha}$ .

The factors that determine the concentration of urea at time  $t$  and location  $x$  for the non trivial case, are the initial concentration and the time difference between time  $t$  and the starting point of the characteristic on the  $t$ -axis  $t_0$ . With equation (5.34) we find that this time difference equals  $t - t_0 = x/v$  and hence

$$\begin{aligned} K_{m,urea} \ln \left( \frac{C_0^{urea}}{C^{urea}} \right) + C_0^{urea} - C^{urea} &= v_{max} \beta(1) \frac{\alpha \bar{C}_{max}}{1 + \alpha} (t - t_0) \\ &= v_{max} \beta(1) \frac{\alpha \bar{C}_{max}}{1 + \alpha} \frac{x}{v}. \end{aligned} \quad (5.39)$$

That implies that the concentration of urea has a fixed value on a fixed position  $x$  for a time  $t > T_2 + x/v$ . Further,  $C^{urea} = 0$  for  $t < T_2 + \frac{x}{v}$ . These identities will be used in the construction of the solution for the calcium carbonate concentration.

The partial differential equation for the concentration of calcium carbonate is given in equation (5.15), which contains reaction rate  $r_{hp}$ . This reaction rate is given in equation (5.14). Substituting relation (5.36) in this rate, gives the following differential equation for the concentration of calcium carbonate:

$$\frac{\partial C^{\text{CaCO}_3}}{\partial t} = m_{\text{CaCO}_3} \theta r_{hp} = m_{\text{CaCO}_3} \theta v_{max} \beta(1) \frac{\alpha \bar{C}_{max}}{1 + \alpha} \frac{C^{urea}}{K_{m,urea} + C^{urea}}. \quad (5.40)$$

Integrating this equation leads to

$$\begin{aligned} C^{\text{CaCO}_3}(x, t) &= \int_0^t \frac{\partial C^{\text{CaCO}_3}}{\partial \bar{t}} d\bar{t} \\ &= m_{\text{CaCO}_3} \theta v_{max} \beta(1) \frac{\alpha \bar{C}_{max}}{1 + \alpha} \int_0^t \frac{C^{urea}}{K_{m,urea} + C^{urea}} d\bar{t}. \end{aligned} \quad (5.41)$$

Since it holds that  $C^{urea} = 0$  for  $0 \leq \bar{t} < T_2 + x/v$  and since  $C^{urea}$  is equal to a constant for  $\bar{t} \geq T_2 + x/v$  on a fixed position  $x$ , equation (5.41) becomes

$$\begin{aligned} C^{\text{CaCO}_3}(x, t) &= \\ &= \begin{cases} 0 & \text{for } t < T_2 + \frac{x}{v}; \\ m_{\text{CaCO}_3} \theta v_{max} \beta(1) \frac{\alpha \bar{C}_{max}}{1 + \alpha} \int_{T_2 + \frac{x}{v}}^t \frac{C^{urea}}{K_{m,urea} + C^{urea}} d\bar{t}; & \text{for } t \geq T_2 + \frac{x}{v}. \end{cases} \\ &= \begin{cases} 0 & \text{for } t < T_2 + \frac{x}{v}; \\ m_{\text{CaCO}_3} \theta v_{max} \beta(1) \frac{\alpha \bar{C}_{max}}{1 + \alpha} \frac{C^{urea}}{K_{m,urea} + C^{urea}} (t - T_2 - \frac{x}{v}); & \text{for } t \geq T_2 + \frac{x}{v}. \end{cases} \\ &= m_{\text{CaCO}_3} \theta v_{max} \beta(1) \frac{\alpha \bar{C}_{max}}{1 + \alpha} \frac{C^{urea}}{K_{m,urea} + C^{urea}} (t - T_2 - \frac{x}{v})_+. \end{aligned} \quad (5.42)$$

In the derivation of these analytical solutions we substituted relation (5.36) into rate (5.14). According to this equation, the reaction rate is related to the concentration of urea via a Monod equation. For completeness, we consider the case that the rate is linear in the urea concentration. Then, we have

$$r_{hp} = v_{max} \beta(1) \frac{\alpha \bar{C}_{max}}{1 + \alpha} C^{urea}. \quad (5.43)$$

Then, the analytical solution for the concentration of urea and calcium carbonate reads as:

$$\begin{aligned} C^{urea}(x, t) &= C_0^{urea}(x - vt) \exp\{-v_{max} \frac{\alpha \bar{C}_{max}}{1 + \alpha} t\}, \\ &= \begin{cases} 0 & \text{for } t < T_2 + x/v; \\ \exp\{-v_{max} \frac{\alpha \bar{C}_{max}}{1 + \alpha} \frac{x}{v}\} & \text{for } t \geq T_2 + x/v, \end{cases} \end{aligned} \quad (5.44)$$

$$\begin{aligned} C^{\text{CaCO}_3}(x, t) &= \begin{cases} 0 & \text{for } t < T_2 + \frac{x}{v}; \\ (t - T_2 - x/v) v_{max} \beta(1) \frac{\alpha \bar{C}_{max}}{1 + \alpha} \\ \cdot \theta \exp\{-v_{max} \frac{\alpha \bar{C}_{max}}{1 + \alpha} \frac{x}{v}\} & \text{for } t \geq T_2 + \frac{x}{v}. \end{cases} \end{aligned} \quad (5.45)$$

## 5.3 Numerical Methods

The differential equations for the pressure, the flow and the concentrations of fixation fluid, bacteria and the aqueous species are solved by the Standard Galerkin Finite Element Method. The weak formulations have been derived by multiplication by a test function  $\eta \in H^1(\Omega)$  and integration over the domain  $\Omega$ . The Newton-Cotes quadrature rules are used for the development of the element matrices and vectors. Furthermore, line elements are used, as well as linear basis functions. For the time integration, the Euler Backward method is used.

The differential equations for the concentrations of bacteria (5.4), (5.5) and (5.6) are coupled, due to the reaction terms  $r_{ads}$  (5.7),  $r_{des}$  (5.9) and  $r_{fix}$  (5.8). Due to the Langmuir isotherm (5.12), the differential equations are nonlinear in the concentration of suspended bacteria  $C^{bac}$ . Hence, Newton's method is used to solve for the differential equations for the concentrations of bacteria. By doing so, the three various concentrations of bacteria come together in one matrix-vector system.

Since the differential equation for the concentration of urea is also nonlinear in the concentration, due to the reaction term, Newton's method is used to calculate the concentration of urea.

The partial differential equation for the concentration of calcium carbonate, equation (5.15), can be considered as an ordinary differential equation in each grid point. To calculate the concentration of calcium carbonate, the following scheme is used:

$$(C^{CaCO_3})^{n+1} = (C^{CaCO_3})^n + \Delta t m^{CaCO_3} \theta^n r_{hp}^{n+1}, \quad (5.46)$$

which uses the porosity  $\theta$  from the previous time step and the reaction rate  $r_{hp}$  (5.14) from the current time step.

As a step size for the time integration is taken  $\Delta t = \frac{1}{640}$ h and as the length of an element is taken  $\Delta x = \frac{1}{640}$ m. For a more detailed description of the numerical methods, see [90–92].

At each time step, the equations are solved sequentially in the following order: First, the flow is calculated. This can be done by solving the differential equation for the pressure (5.25), and from this pressure, the flow is calculated with Darcy's law, (5.20), (5.21) and (5.22). Since the pressure is not involved in the boundary terms for the flow in this case, the flow can be calculated directly from equation (5.17). Subsequently, the partial differential equation for the concentration of the fixation fluid (5.11) is solved. Then, the equations for the concentrations of bacteria (5.4), (5.5) and (5.6) are solved as a coupled system, applying Newton's method. These concentrations partly determine the reaction rate  $r_{hp}$  (5.14) of the biochemical reaction, given by equation (5.3). The partial differential equation for the urea concentration (5.13) is solved, again, using Newton's method and the reaction rate  $r_{hp}$  (5.14) is updated. Usually, the Newton method converges in approximately three iterations. Finally, the concentration of ammonium ( $C^{NH_4^+}$ ) and calcium carbonate ( $C^{CaCO_3}$ ) are calculated sequentially and the porosity ( $\theta$ ), intrinsic permeability ( $k$ ) and fluid density ( $\rho_l$ ) are updated, using equations (5.13), (5.15), (5.16), (5.23) and (5.24), respectively.

## 5.4 Results

In this section, some analytical and numerical results are shown, as well as a comparison of the current model and the model with a homogeneous bacterial activity, that was used in [92] (Chapter 4). The numerical results are in Subsection 5.4.1, the comparison of the two models is in Subsection 5.4.2, the analytical results are in Subsection 5.4.3 and the comparison of the numerical and analytical solutions are in Subsection 5.4.4.

### 5.4.1 Numerical results

We start with the one dimensional configuration. Numerical simulations have been done for two different values of the adsorption, desorption and fixation reaction rate constant. The first value is  $K_{bac} := k_{ads} = k_{des} = k_{fix} = 10h^{-1}$ . The results are displayed in the left graphs of Figure 5.2. As a second value has been chosen  $K_{bac} = k_{ads} = k_{des} = k_{fix} = 1000h^{-1}$ . The results for that value are displayed in the right graphs of Figure 5.2. A small reaction constant means that the process is slow. The larger the reaction constant is, the more the result tends to the equilibrium.

The top graphs of Figure 5.2 show a situation in the first phase, in which bacteria are injected. The graphs show a non zero concentration of suspended bacteria ( $C^{bac}$ ) and adsorbed bacteria ( $\bar{C}^{bac}$ , in the legend called  $C^{bar}$ ). The concentration of adsorbed bacteria in the equilibrium case is a function of the concentration of suspended bacteria as described by the Langmuir isotherm (5.12). The bacteria enter the domain with a steep front, somewhat smoothed by dispersion and diffusion. Retardation of the front takes place, due to the adsorption process. The top right graph of Figure (5.2) shows a situation that is close to equilibrium. The top left graph, where the adsorption process is slow compared to the top right graph, has a very smooth front. Since, in this phase, fixation fluid is not yet being injected, there are no fixated bacteria.

The second row of Figure 5.2 shows a situation in the second phase, where fixation fluid is injected. The concentration of fixated bacteria,  $S^{bac}$  is no longer zero. Since in the right graph, the fixation rate constant is larger than in the left graph, the concentration of fixated bacteria is also higher there. In the left graph, the concentration of adsorbed bacteria is larger than the concentration of suspended bacteria in a part of the domain. The reason is the slow desorption process.

The bottom four graphs of Figure 5.2 display some shots of phase 3, where urea and calcium chloride are injected. Note that the calcium carbonate concentration is scaled, such that the range is comparable to the range of the other graphs. Since the concentration of fixated bacteria in the left graphs is lower than in the right graphs, the concentration of calcium carbonate is lower as well. An exception to this situation is the zone around  $x = 0.6m$  in the bottom graphs. Although the concentration of fixated bacteria is smaller for a smaller  $K_{bac}$ -value, there are still adsorbed and suspended bacteria left in that zone, which also contribute to the hydrolysis of urea and hence to a higher calcium carbonate concentration. The calcium carbonate concentration in the left graphs has its maximum somewhere in the middle of the domain, whereas in the right graph, the maximum is close to the injection point.

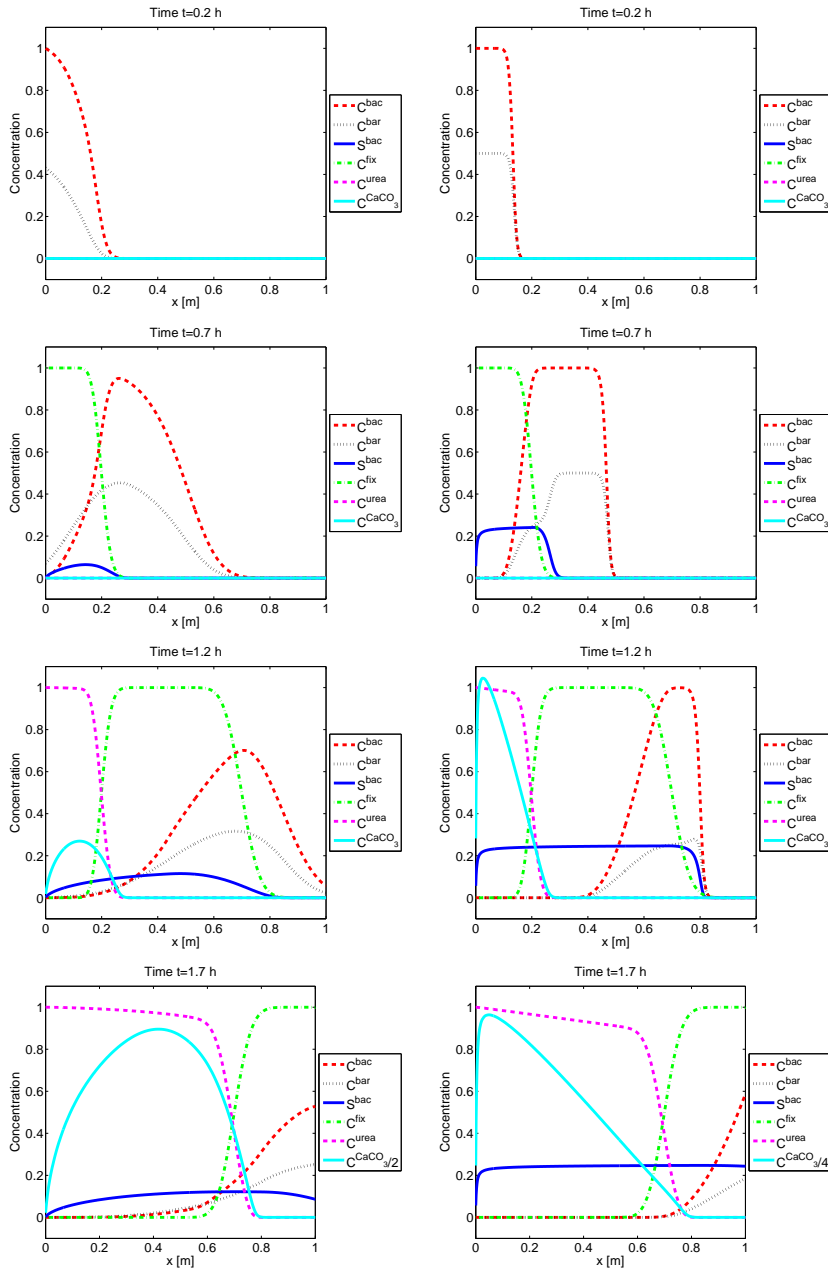


Figure 5.2: Numerical solution for the concentration of suspended, temporarily adsorbed and fixated bacteria and the concentration of fixation fluid, urea and  $CaCO_3$  as a function of location at several times ( $t=0.2h$ ,  $t=0.7h$ ,  $t=1.2h$ ,  $t=1.7h$ ) for  $K_{bac}=10h^{-1}$  (left graphs) and  $K_{bac}=1000h^{-1}$  (right graphs).

Both for the calculation of the concentration of the bacteria and the concentration of urea, Newton iterations are performed. As long as the concentrations are constant, only one iteration is needed for convergence. Else, for the calculation of the urea concentration, approximately 3 iterations are needed for convergence and approximately 3 or 4 iterations are needed for the calculation of the bacteria. Although the number of iterations that is needed for convergence is almost similar, the CPU-time per iteration differs significantly. It takes 9 times as much CPU time per Newton iteration to calculate the (three) concentrations of bacteria as to calculate the urea concentration. The reason is that the matrix that is built for the calculation of the concentrations of the bacteria is 9 times as large as the matrix for the calculation of the urea concentration, since the concentrations of bacteria are solved from one matrix-vector system.

### 5.4.2 Results of the comparison between the current model and the model with a homogeneous distribution of bacteria

In this section, the current model is compared to the previous model, where the previous model assumes a homogeneous distribution of bacteria. As in the previous subsections, this comparison is carried out for two  $K_{bac}$ -values:  $K_{bac}=10\text{h}^{-1}$  and  $K_{bac}=1000\text{h}^{-1}$ . To be able to make a good comparison, the average of the concentration of fixated bacteria in the current model is used as a value for the (constant) concentration of fixated bacteria in the previous model. Some results of this comparison are shown in Figure 5.3. The left graphs display the results for the low  $K_{bac}$ -value:  $K_{bac}=10\text{h}^{-1}$  and the right graphs show the results for the high  $K_{bac}$ -value:  $K_{bac}=1000\text{h}^{-1}$ .

The top graphs show the concentration of fixated bacteria at time  $t=2\text{h}$ . The right plot, which displays the situation for a high  $K_{bac}$ -value, shows two graphs that are almost similar. Only at the inflow boundary, a large difference is visible. That has the following reason. First, a pulse with bacteria is injected, without injection of fixation fluid. There is no fixation fluid in the domain, so there are only non fixated bacteria. Then a pulse with fixation fluid is injected. Bacteria are only fixated at that location where both bacteria and a fixation fluid are present. The latter can only happen where the fixation fluid is overtaking the bacteria, since they are injected after each other. The reason that they are not injected together, is that this would result in clogging in the injection filter, what leads to stoppage of the filter. Hence, the injection point is a critical point, where (almost) no bacteria are fixated.

The middle graphs of Figure 5.3 show the urea concentration at time  $t=2\text{h}$ . For the high  $K_{bac}$ -value, there is visually no difference. But also in the left plot, there is only a small difference between the graphs.

The bottom graphs display the concentration of calcium carbonate. The concentrations from the high  $K_{bac}$ -value are again similar, except near the injection point. The concentrations, calculated with the low  $K_{bac}$ -value, however, show a large difference.

It can be concluded that, if the concentration of fixated bacteria is similar for both models, the calcium carbonate profile is similar as well. A high reaction constant leads to a homogeneous bacterial distribution, at least for the first part of the domain, except for the region around the injection point. A low reaction rate constant, corresponding to slow adsorption, desorption and fixation processes, leads to a non homogeneous bacterial distribution and hence to a different calcium carbonate profile. An instantaneous equilibrium, however, is not a guarantee that the bacterial distribution will be homogeneous. The concentration of fixated bacteria does not depend on the length of the domain. Since only a finite amount of bacteria is injected, the domain can be chosen so large that only around the injection boundary bacteria are fixated and that there are no bacteria in the rest of the domain. This can also be seen from the analytical solution for the instantaneous equilibrium, equations

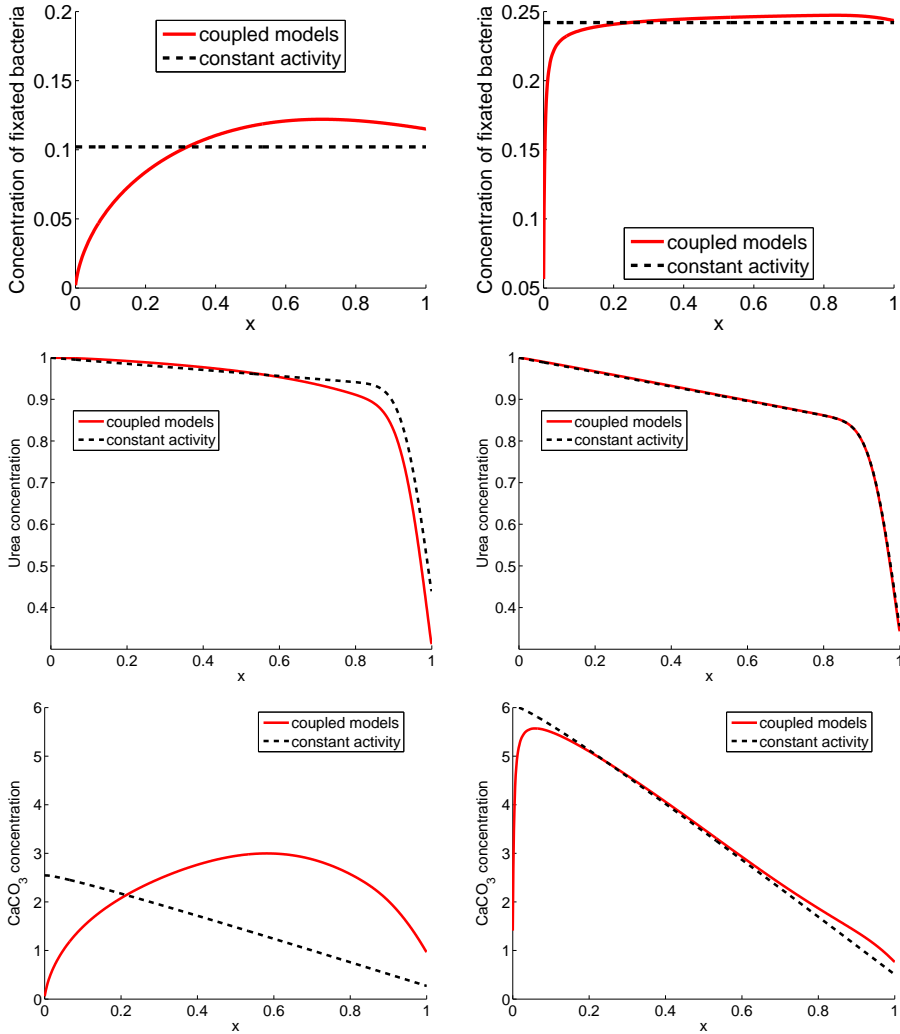


Figure 5.3: Several concentrations as a function of location at time  $t=2\text{h}$ , for  $K_{bac}=10\text{h}^{-1}$  (left graphs) and  $K_{bac}=1000\text{h}^{-1}$  (right graphs). Top graphs: concentration of fixed bacteria, middle graphs: urea concentration and bottom graphs:  $\text{CaCO}_3$  concentration.

(5.26), (5.31) and (5.32). In order to get a homogeneous distribution of bacteria in this case, more bacteria should be injected, possibly via multiple injection points.

### 5.4.3 Analytical results

The analytical solution for the equilibrium case, while dispersion, diffusion, decrease of the porosity and the change of liquid volume are neglected, is shown in Figure 5.4. As a reaction rate has been taken equation (5.14). This figure shows the analytical

solutions at the same times as the numerical solutions are shown (Figure 5.2). The top left graph shows a situation of the first phase where only bacteria are injected. The top right graphs displays a shot of the second phase, in which fixation fluid is injected. Where both bacteria and fixation fluid are present, bacteria are fixated. The bottom graphs show two shots of the last phase in which calcium carbonate is formed.

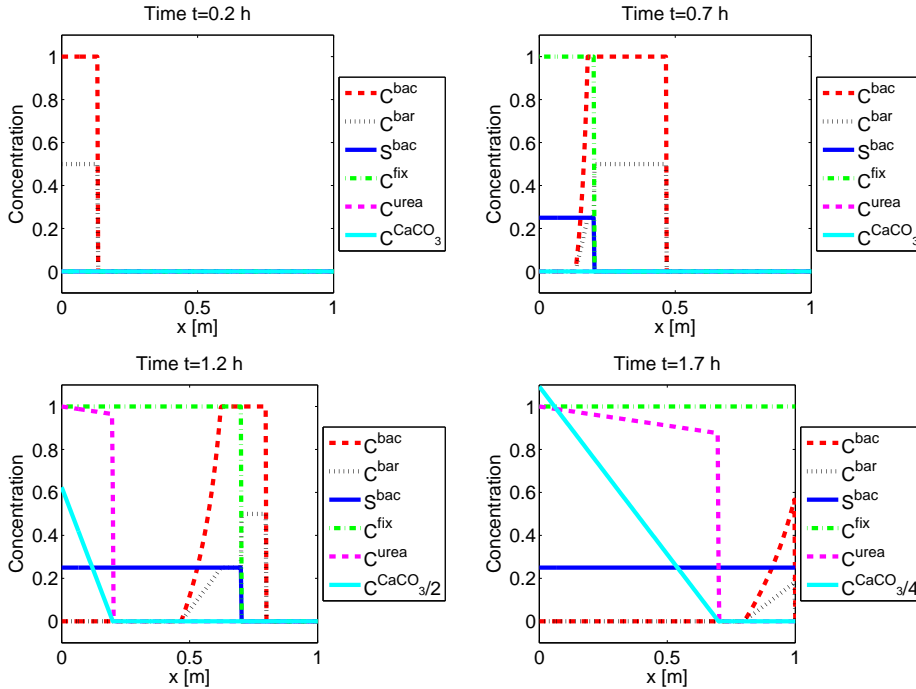


Figure 5.4: The analytical solution for the concentration of suspended, temporarily adsorbed and fixated bacteria and the concentration of fixation fluid, urea and  $CaCO_3$  as a function of location at several times ( $t=0.2h$ ,  $t=0.7h$ ,  $t=1.2h$ ,  $t=1.7h$ ).

#### 5.4.4 Comparison of the numerical solutions to the analytical solutions

In this subsection, we compare the numerical and analytical solution for the concentration of urea and calcium carbonate. The comparison for the concentrations of bacteria for the bacterial injection model has been made in [92] (Chapter 4). In order to make a valid comparison, we redo our numerical simulations for  $\mathbf{D}_{bac} = \mathbf{D}_{fix} = \mathbf{D}_{urea} = \mathbf{D}_{Ca^{2+}} = \mathbf{D}_{NH_4^+} = \mathbf{0}$  and for a constant porosity and flow rate. We do take a finite  $K_{bac}$ -value, however, namely  $K_{bac} = 10h^{-1}$  and  $K_{bac} = 1000h^{-1}$ .

Figure 5.5 shows the numerical and analytical solution of the concentration of urea and calcium carbonate. The figures display the situation at times  $t=1.2\text{h}$  and  $t=1.7\text{h}$ , as in Figures 5.2 and 5.4. The results at time  $t=0.2\text{h}$  and  $t=0.7\text{h}$  are not shown, since the urea and calcium carbonate concentration are zero then. Again, the left graphs show the situation for  $K_{bac} = 10h^{-1}$  and the right graphs for  $K_{bac} = 1000h^{-1}$ .

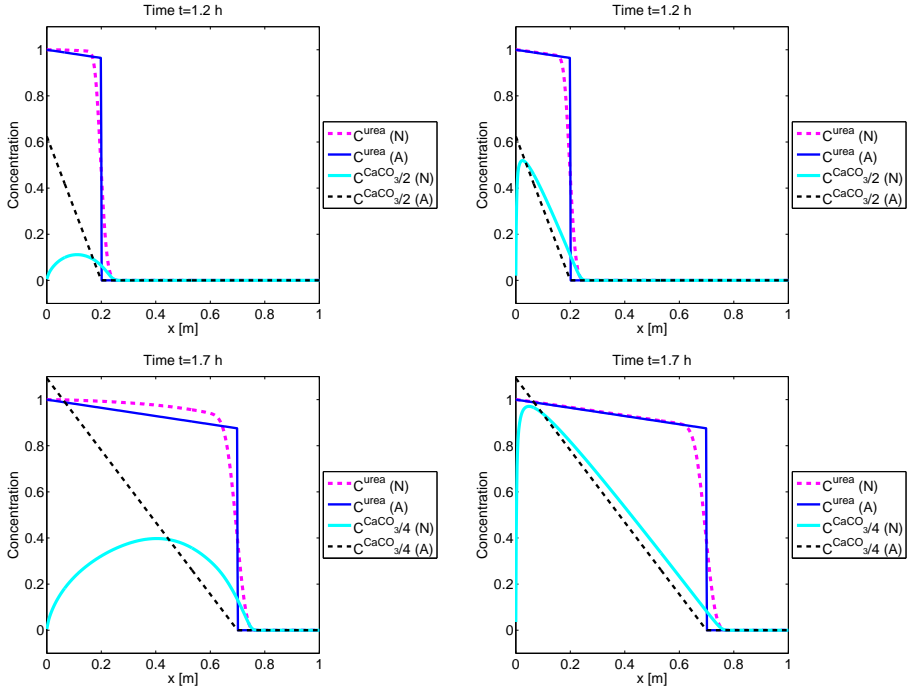


Figure 5.5: The numerical and analytical solution of the urea and calcium carbonate concentration at times  $t=1.2\text{h}$  and  $t=1.7\text{h}$  for  $K_{bac}=10h^{-1}$  (left graphs) and  $K_{bac}=1000h^{-1}$  (right graphs). The numerical solutions are marked with N and the analytical solutions are marked with A. In both the analytical and numerical solutions, dispersion and diffusion are neglected, as well as the effect of the reaction on the porosity and flow rate.

In all the graphs of Figure 5.5, the analytical solution of the urea concentration corresponds well with the numerical solution. The front of the numerical solution is less steep than the front of the analytical solution, due to numerical diffusion. For the low  $K_{bac}$ -value (left graphs) is the numerical urea concentration higher than the analytical urea concentration in the first part of the domain. The reason is that not so much urea is consumed due to the low concentration of fixated bacteria, which is a consequence of the low  $K_{bac}$ -value.

The analytical solution of the calcium carbonate concentration is not similar to the numerical solution for  $K_{bac} = 10h^{-1}$ . The reason is that the analytical solution

has been constructed for an infinite  $K_{bac}$ -value. The numerical solution for the high  $K_{bac}$ -value,  $K_{bac} = 1000h^{-1}$ , is similar to the analytical solution, except close to the inlet. Although the graphs are similar, the difference is not equal to zero. This time, the reason is not the difference in  $K_{bac}$ -value but the numerical diffusion. Due to the numerical diffusion, the numerical solution to the urea concentration has a less steep front and the urea penetrates a little further in the column. Although the concentration is small, reaction (5.3) can happen and calcium carbonate is formed. Hence, the numerical solution to the calcium carbonate concentration is somewhat larger than the analytical solution.

In Figure 5.5, as a reaction rate for reaction (5.3) has been taken rate (5.14). The urea concentration is related to the reaction rate via a Monod equation. This chapter also provides an analytical solution for a reaction rate that is linear in the urea concentration, equation (5.43). For this case, the analytical solutions are given in equations (5.44) and (5.45). Figure 5.6 shows the comparison between the analytical and numerical solution for both reaction rates at time  $t=1.7h$ . In the left graph, the urea concentration is related to the hydrolysis reaction rate via a Monod equation, see equation (5.14). In the right graph, the reaction rate is linear in the urea concentration, see equation (5.43).

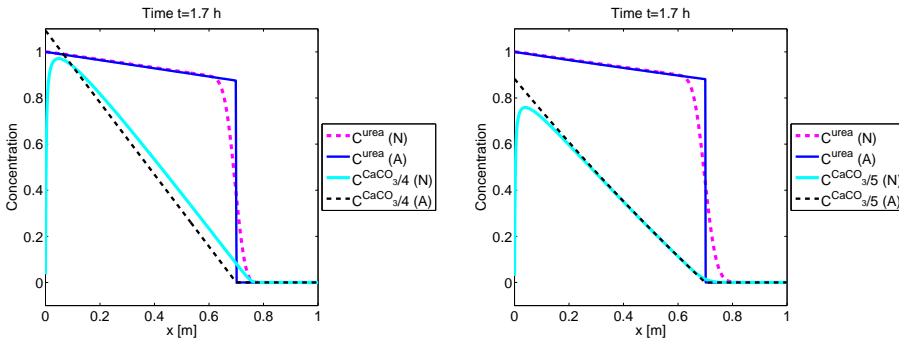


Figure 5.6: The numerical and analytical solution of the urea and calcium carbonate concentration at time  $t=1.7h$  for  $K_{bac}=1000h^{-1}$ . The numerical solutions are marked with N and the analytical solutions are marked with A. Left graph: the urea concentration is related to the hydrolysis reaction rate via a Monod equation (5.14). Right graph: the hydrolysis reaction rate is linear in the urea concentration, see equation (5.43).

The left graph of Figure 5.6 is equal to the bottom right graph of Figure 5.5. In both graphs of Figure 5.6, the numerical solution to the urea concentration corresponds well with the analytical one, as well for rate (5.14) (left graph) as for rate (5.43) (right graph).

In the right graph, which is calculated with rate (5.43), the numerical solution for the calcium carbonate concentration is closer to the analytical solution than in the left graph. Due to numerical diffusion, the numerical urea concentration

approximates zero at a location further away from the inlet than the analytical urea concentration does. Since for a small urea concentration, we have that

$$\begin{aligned} r_{hp} &= v_{max}(C^{bac} + \bar{C}^{bac} + S^{bac}) \frac{C^{urea}}{K_{m,urea} + C^{urea}} \sim \\ &\sim v_{max}(C^{bac} + \bar{C}^{bac} + S^{bac}) \frac{C^{urea}}{K_{m,urea}}, \end{aligned} \quad (5.47)$$

and since  $K_{m,urea} = 0.01$  (see Table 5.2), the rate as determined by equation (5.14) is 100 times larger as the rate as computed by equation (5.43). This implies that the numerical calcium carbonate concentration has a larger increase in the case of use of equation (5.14). Therefore, the difference between the analytical and numerical solution is larger if equation (5.14) is used.

## 5.5 Discussion and Conclusions

In this chapter, the model for the placement of bacteria and the model for the hydrolysis of urea and the precipitation of calcium carbonate are coupled. These two models were introduced and discussed in [91] and [92] (Chapter 2 and 4). We shortly mention some of the discussion points.

It is crucial to find a good relation for ratio  $\beta$ . This ratio determines the amount of fixated bacteria. These bacteria eventually provide the production of calcium carbonate, which is the aim of Biogrout. Laboratory experiments need to be carried out to find such a relation. From these experiments should also follow whether the Langmuir isotherm is a good choice for an adsorption isotherm, as well as the values of the various constants in this isotherm. Furthermore, experiments need to be done to find the right values for the adsorption, desorption and fixation reaction constants. Another important effect that should be investigated is the possible wash-out of bacteria as a result of a high pore water velocity. This wash-out violates the present model assumption that fixated bacteria will always stay stucked to the sand grains.

The precipitation model is based on the biochemical reaction equation (5.3). In reality, this reaction happens in several steps. Some of these steps are equilibrium reactions that depend on the pH. The differential equation for the calcium carbonate concentration does not contain a transport term as it has been assumed that calcium carbonate precipitates locally and will not be transported. Calcium carbonate can precipitate in several ways. It can attach to sand grains but can also form crystals. Especially when these crystals are small, they can be transported before they will stick in the pore throats. The retardation of urea, calcium, ammonium and fixation fluid is neglected for the moment. Especially when the particles are charged there can be retardation.

In this chapter, the two models are coupled. It is possible that the parameters in both models will influence each other. For example, the bacteria can be encapsulated by the calcium carbonate. Then, the urea can no longer reach these bacteria and therefore, these bacteria can not contribute to the hydrolysis of urea any more.

In the biochemical reaction rate  $r_{hp}$  (5.14), the concentration of bacteria is used, multiplied by the maximal bacterial activity  $v_{max}$ . What actually provides the hydrolysis of urea are some enzymes in the bacteria. These enzymes can be released from the bacteria and flow with the water. Consequently, the activity of the bacteria decreases. It would be better to use the activity of the bacteria in the reaction rate (5.14). From experiments it is known that the reaction rate decreases [97]. For a good estimation of the hydrolysis reaction rate, it is necessary to know what the reasons are and how they influence the rate.

We succeeded in coupling the model for the placement of bacteria with the precipitation model. From the numerical simulations with the coupled model, it can be concluded that, when the adsorption, desorption and fixation processes are fast and hence the  $K_{bac}$ -value is large, the calcium carbonate concentration has its maximum close to the injection point. When the  $K_{bac}$ -value is small, less calcium carbonate is formed and its maximum lies further away from the injection point.

Furthermore, a Newton iteration to calculate the concentrations of bacteria costs nine times as much CPU-time as a Newton iteration to calculate the concentration of urea.

A high reaction constant leads to a homogeneous bacterial distribution, at least for the first part of the domain, except for the region around the injection point. Furthermore, the calcium carbonate content that is calculated from the coupled model is similar to the calcium carbonate that is calculated from the model where a homogeneous bacterial distribution is assumed. A low reaction rate constant, corresponding to slow adsorption, desorption and fixation processes, leads to a non homogeneous bacterial distribution and hence to a different calcium carbonate profile. High reaction rates, however, do not guarantee that the bacterial distribution will be homogeneous. This can also be seen from the analytical solution for the instantaneous equilibrium, equations (25), (31) and (32). The reason is that the concentration of fixated bacteria does not depend on the length of the domain. Since only a finite amount of bacteria is injected, the domain can be chosen so large that only close to the inlet bacteria are fixated and that there are no bacteria in the rest of the domain.

An analytical solution has been constructed for the coupled model for the case that dispersion, diffusion, decrease of the porosity and the change of liquid volume are neglected and the concentrations of suspended, adsorbed and fixated bacteria are in equilibrium. Although these phenomena are neglected, the analytical solution of the calcium carbonate concentration is similar to the numerical solution with a high  $K_{bac}$ -value, see Figures 5.2 and 5.4. Hence, in real life applications that can be modelled through a 1D model, the analytical solution can be used as a first estimate for engineering purposes. If the sorption and fixation processes are close to equilibrium, the analytical solution might be as good as the numerical solution, since the numerical solution also includes some error as a result of the error in the estimation of the various parameters.

We further think that the models can be extended with the following features:

- The model for the placement of bacteria contains the most important phenomena of the transport of bacteria: advection, dispersion, adsorption, desorption and fixation. Other phenomena, like decay, growth and systematic motion of

bacteria can be included.

- The fixation of bacteria will cause a decrease in porosity and permeability. This has not yet been added to the model.
- As a function for the ratio  $\beta$ , a Monod equation is used. In this chapter, the ratio is only a function of the fixation fluid, whereas it may also depend on the properties of the microorganisms, the pH and the porous medium.
- The (saturated) flow equation can be extended to unsaturated flow to be able to model also the unsaturated zones.

# 6

## **Various flow equations to model the new soil improvement method Biogrout**

This chapter has been published as:

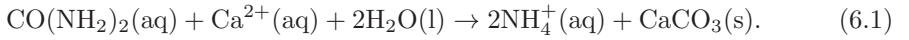
Van Wijngaarden, W.K., Vermolen, F.J., Van Meurs, G.A.M., Vuik, C.: Various flow equations to model the new soil improvement method Biogrout. *Numerical Mathematics and Advanced Applications* 2011, 633–641, (2013)

## Abstract

We consider a mathematical model for Biogrout, which is a novel soil reinforcement technique based on Microbially Induced Carbonated Precipitation. We focus on an adaptation of the flow equation such that mass is conserved instead of volume. The adaptation is validated by a mass balance. Some numerical simulations are presented and used for the discussion on the various adjustments of the flow equation.

## 6.1 Introduction<sup>1</sup>

To describe the Biogrout process, a mathematical model was constructed in [91] (Chapter 2), including equations for concentrations, flow and porosity. These equations are presented in Section 6.2. The model is based on the overall Biogrout reaction equation:



Urea ( $\text{CO}(\text{NH}_2)_2$ ) is hydrolysed and if calcium ions ( $\text{Ca}^{2+}$ ) are present, ammonium ( $\text{NH}_4^+$ ) and calcium carbonate ( $\text{CaCO}_3$ ) are formed.

The partial differential equation for the flow, as displayed in Section 6.2, is based on the assumption that the volume of the fluid is conserved. This is verified by a mass balance calculation, which can also be found in Section 6.2. It appears that the volume of the fluid is not conserved. Two other partial differential equations are derived, which are based on the conservation of mass.

In Section 6.3, the numerical methods that are used to solve the system of equations are presented, as well as the simulations that have been done. In Section 6.4, the results of the application of the various partial differential equations for the flow are compared. In Section 6.5, some discussion and conclusions can be found.

## 6.2 The Mathematical Model

In this section, the model equations for the Biogrout process are presented and shortly discussed. The derivation can be found in [91] (Chapter 2).

The concentrations of the aqueous species are modelled through the following advection-dispersion-reaction equation:

$$\frac{\partial(\theta C^i)}{\partial t} = \nabla \cdot (\theta \mathbf{D} \cdot \nabla C^i) - \nabla \cdot (\mathbf{q} C^i) + n_i \theta r. \quad (6.2)$$

In this equation,  $\theta$  is the porosity,  $C^i$  is the dissolved concentration of species  $i$  with  $\text{M} (= \text{kmol}/\text{m}^3)$  as a unit,  $\mathbf{D}$  is the dispersion tensor,  $\vec{v}$  is the pore water velocity,  $n_i$  is a constant that deals with the stoichiometry in the biochemical reaction equation (6.1) and  $r$  is the reaction rate of the production of calcium carbonate, which is a non-linear function of the urea concentration. Since the relevant aqueous species in the Biogrout process are urea, calcium and ammonium, we have

---

<sup>1</sup>Parts of the original introduction have been skipped in order to prevent too much repetition of the Introduction from Chapter 1.

$i \in \{\text{urea}, \text{Ca}^{2+}, \text{NH}_4^+\}$ . From the stoichiometry of reaction (6.1), the values of  $n_i$  for the various aqueous species are given by:  $n_{\text{urea}} = -1$ ,  $n_{\text{Ca}^{2+}} = -1$ , and  $n_{\text{NH}_4^+} = 2$ .

The left-hand side of equation (6.2) represents the accumulation. The first term at the right-hand side stands for the effect of dispersion and diffusion, the second term represents advection and the last term models the biochemical reaction.

For the reaction rate  $r_{hp}$  of equation (6.1), a Monod equation has been used:

$$r_{hp} = v_{max} \frac{C^{\text{urea}}}{K_m + C^{\text{urea}}}. \quad (6.3)$$

Here,  $v_{max}$  is the reaction rate constant and  $K_m$  is the saturation constant.

Since it has been assumed that the non-aqueous calcium carbonate is not transported, there are no transport terms in the corresponding differential equation. The concentration of calcium carbonate  $C^{\text{CaCO}_3}$  can be calculated from the following differential equation:

$$\frac{\partial C^{\text{CaCO}_3}}{\partial t} = m_{\text{CaCO}_3} \theta r_{hp}. \quad (6.4)$$

In this equation,  $m_{\text{CaCO}_3}$  is the molar mass of calcium carbonate, which is used to convert moles into mass.

Due to the precipitation of calcium carbonate, the porosity decreases. The following relation exists between the porosity and the calcium carbonate concentration:

$$\theta(t) = \theta(0) - \frac{C^{\text{CaCO}_3}(t) - C^{\text{CaCO}_3}(0)}{\rho_{\text{CaCO}_3}}. \quad (6.5)$$

Here  $\rho_{\text{CaCO}_3}$  denotes the density of calcium carbonate.

It has been assumed that reaction (6.1) has no influence on the total volume of the fluid over the entire domain of computation and that the fluid is incompressible. This implies that the total volume of the fluid is conserved. Hence based on this hypothesis, the following partial differential equation was derived for the Darcy flow velocity  $\mathbf{q}$ :

$$\nabla \cdot \mathbf{q} = \frac{m_{\text{CaCO}_3}}{\rho_{\text{CaCO}_3}} \theta r_{hp}. \quad (6.6)$$

Since the porosity decreases, due to the calcium carbonate precipitation, there is less space available for the fluid. This lack of space explains the non-zero right-hand side of equation (6.6). The last differential equation completes the set of equations that is necessary to simulate the Biogrout process.

Differential equation (6.6) is based on the assumption that the total volume of the fluid is conserved. With a mass balance calculation it is verified, whether this assumption is true.

As a relation for the density of the solution, we use

$$\rho_l = 1000 + 15.4996C^{\text{urea}} + 86.7338C^{\text{Ca}^{2+}} + 15.8991C^{\text{NH}_4^+}, \quad (6.7)$$

as derived in [91]. Table 6.1 contains the molar mass of urea, calcium chloride ( $\text{CaCl}_2$ ), ammonium chloride ( $\text{NH}_4\text{Cl}$ ) and water ( $\text{H}_2\text{O}$ ).

$m_{urea}$	=	60.0551 kg/kmol	$m_{CaCl_2}$	=	110.9840 kg/kmol
$m_{NH_4Cl}$	=	53.4913 kg/kmol	$m_{CaCO_3}$	=	100.0869 kg/kmol
$m_{H_2O}$	=	18.0152 kg/kmol			

Table 6.1: Molar mass of urea, calcium chloride, ammonium chloride and water.

We consider 1 m<sup>3</sup> of a 1M urea/calcium chloride solution. All the urea and calcium chloride are converted to calcium carbonate and ammonium chloride, which means that 1 kmol urea, 1 kmol calcium chloride and 2 kmol water disappear from the solution and 2 kmol ammonium chloride and 1 kmol calcium carbonate are formed. The calcium carbonate precipitates out of the solution. The ammonium chloride stays in the solution.

Table 6.2 displays the mass and mole balances of the reaction.

	Initial state		Conversion		Final state	
	kmol	kg	kmol	kg	kmol	kg
urea	1	60.0551	-1	-60.0551	0	0
CaCl <sub>2</sub>	1	110.9840	-1	-110.9840	0	0
NH <sub>4</sub> Cl	0	0	+2	+106.9826	2	106.9826
CaCO <sub>3</sub>	0	0	+1	+100.0869	(1)	(100.0869)
H <sub>2</sub> O	51.6894	931.1943	-2	-36.0304	49.6894	895.1645

Table 6.2: The mass and mole balances of the reaction.

We define  $V_s$  as the volume after conversion. The density of the solution equals  $\rho_l = 1000 + 15.8991 \cdot \frac{2}{V_s}$  and the mass of the liquid equals  $1000V_s + 15.8991 \cdot 2$ . From the mass balance in Table 6.2, it follows that this must be equal to 1002.1471 kg. Therefore,  $V_s = 0.97035$  m<sup>3</sup>, which is not equal to 1 m<sup>3</sup>.

From this mass balance calculation, it follows that the hydrolysis of urea and the precipitation of calcium carbonate do influence the volume of the fluid and that the assumption of conservation of fluid volume is not valid. Hence, the differential equation for the flow, based on this assumption, should be adapted.

Therefore, two alternative partial differential equations are introduced. The first one is almost similar to the previously used differential equation (6.6), but corrects for the shrinking liquid volume. In the previous paragraphs, we calculated that for each converted kmol urea and calcium chloride, the total liquid volume shrinks with  $1 - V_s = 0.02965$  m<sup>3</sup>. Therefore, an extra term is added to equation (6.6) to correct for this phenomenon. The following alternative partial differential equation for the flow is derived:

$$\nabla \cdot \mathbf{q} = \left( \frac{m_{CaCO_3}}{\rho_{CaCO_3}} - (1 - V_s) \right) \theta r_{hp}. \quad (6.8)$$

As a second alternative partial differential equation for the flow, the following equation was derived from a more physical point of view:

$$\frac{\partial(\rho_l \theta)}{\partial t} = -\nabla \cdot (\rho_l \mathbf{q}) - m_{CaCO_3} \theta r_{hp}. \quad (6.9)$$

The left-hand side represents the accumulation of mass in the pores. The first term at the right-hand side models mass flow and the last term stands for the mass that disappears from the fluid, as a result of precipitation.

## 6.3 Strategy and Numerical Methods

The aim of this research is to find out whether an alternative differential equation for the flow will result into a different calcium carbonate content, between realistic bounds for the process variables that can be chosen freely. In order to do so, these process variables are varied. As an experimental set-up, we take a one dimensional configuration, which corresponds to a column experiment. The inflow is at the left-hand side and the outflow at the right-hand side.

The process variables that can be chosen are: the inflow velocity  $q_{in}$ , the inflow concentration of urea and calcium chloride  $c_{in}$  and the maximal bacterial activity  $v_{max}$ . The latter can be chosen during the cultivation or by diluting a suspension with a high activity. The (initial) porosity  $\theta_0$  is given, but varies initially locally. In laboratory experiments one can more or less adapt the porosity by filling the experimental set-up with sand.

Several computer simulations have been done to examine whether the various differential equations for the flow lead to different calcium carbonate contents. These computations have been done as follows: Certain values have been assigned to the four process variables. These values are the bold values that can be found in Table 6.3, which forms the basis combination. Then, four sets of simulations are done. In each set, only one variable from this basis combination is adjusted. The values are given in Table 6.3, again. The results from this comparison can be found in Section 6.4.

Process variable	Value					
$q_{in}$ [m/h]	0	0.001	<b>0.01</b>	0.1	1	
$\theta_0$ [1]		0.1	<b>0.3</b>	0.5		
$v_{max}$ [kmol/m <sup>3</sup> /h]		0.0036	<b>0.036</b>	0.36		
$c_{in}$ [kg/m <sup>3</sup> ]		0.5	<b>1</b>	2	3	4

Table 6.3: The process variables that can be varied. In each simulation set, only one variable is varied, while the **bold values** are assigned to the other variables.

Initially, all concentrations are zero. Only for the case  $q_{in}=0$ , we need to take an alternative initial condition for the concentration of urea and calcium chloride, otherwise nothing will happen. As an initial condition for the urea and calcium chloride concentration, we take:

$$C^i(t, 0) = \begin{cases} 1 & \text{for } 0 \leq x \leq 0.90; \\ 0 & \text{for } 0.90 < x \leq 1, \end{cases} \quad (6.10)$$

with  $i \in \{\text{urea}, \text{Ca}^{2+}\}$ . The initial porosity is given in Table 6.3.

As a boundary condition for the flow at the inflow boundary we take the Dirichlet boundary condition  $q(0, t) = q_{in}$ . The values of  $q_{in}$  can be found in Table 6.3. For the

concentration of urea and calcium chloride, we take the following Robin boundary condition at the inflow boundary:  $(D\theta\nabla c - \mathbf{q}c) \cdot \mathbf{n} = q_{in}c_{in}$ , which implies that the amount of urea and calcium chloride that enters the domain per unit of time and surface equals  $q_{in}c_{in}$ . Again, the values of  $c_{in}$  are given in Table 6.3. Since no ammonium chloride is injected, we take  $(D\theta\nabla c - \mathbf{q}c) \cdot \mathbf{n} = 0$  as a boundary condition for the concentration of ammonium chloride at the inflow boundary. At the outflow boundary we choose the homogeneous Neumann condition  $D\theta\nabla c = 0$  for the concentration of all aqueous species, which corresponds to an advective flux. The simulated time is 100 h, unless stated otherwise.

We use the Standard Galerkin Finite Element Method to solve the model equations. For more information on the numerical methods we refer to [90] and [91] (Chapter 2 and 3), where this has been reported in more detail, also for the higher-dimensional cases.

## 6.4 Results

In this section some results (Figure 6.1) are shown from the comparison between the two alternative partial differential equations for the flow, (6.8) and (6.9), and the previously used differential equation (6.6). The left graphs represent the Darcy flow velocity and the right ones the calcium carbonate concentration.

The top graphs of Figure 6.1 show the Darcy flow velocity and the calcium carbonate concentration as a function of location at time  $t=100$  h. The values that have been assigned to the process variables are the bold values in Table 6.3. As can be seen, the flow that is calculated from the old differential equation differs only by 3% from the flow that is calculated from the alternatives. Hence, this adaptation only has a minor effect on the calcium carbonate concentration. The results from the variation of  $\theta_0$ ,  $v_{max}$ ,  $c_{in}$  and  $q_{in}$  are similar: the calculated flows show a small difference, the calcium carbonate content is very similar.

The variation of  $\theta_0$ ,  $v_{max}$  and (non-zero)  $q_{in}$  results into a maximal difference in calcium carbonate content of at most  $2 \text{ kg/m}^3$ , which corresponds to a relative difference in the order of 5%.

The difference in calcium carbonate content increases for an increasing  $c_{in}$ . For  $c_{in}=4\text{M}$ , the maximal difference in calcium carbonate concentration is  $5 \text{ kg/m}^3$  for the first alternative differential equation and  $3 \text{ kg/m}^3$  for the second one. This difference is still in the order of the measurement error. However, since the solubility of urea in water is 18M and the solubility of calcium chloride in water is 7M, one might wonder whether higher urea/calcium chloride concentrations will result into larger differences in calcium carbonate. However, since a concentration of 4M is already toxic for bacteria, high concentrations will never be used in the Biogrout process. The middle graphs of Figure 6.1 show the flow and the calcium carbonate content for  $c_{in} = 4\text{M}$ .

The bottom graphs of Figure 6.1 show the Darcy flow velocity and the calcium carbonate concentration at time  $t = 25 \text{ h}$  for the zero inflow velocity case. In this case the simulated time is 25 h, since at time  $t=100$  h all the urea and calcium chloride have reacted, so there is no driving force for a flow any more. Note that the difference in Darcy flow velocity is more pronounced in the bottom left graph than in the other graphs. The initial conditions for the urea and calcium chloride

concentration, as given in equation (6.10), have been chosen in such a way, that the difference in calcium carbonate content is really large. This difference is  $20 \text{ kg/m}^3$  for the first alternative differential equation and  $19 \text{ kg/m}^3$  for the second one. The graphs are very similar, however. Both graphs have a constant calcium carbonate content for the first 0.9 m, followed by a steep front. The difference in the location of this steep front is in the order of only 1 cm. Due to the very steep front, this difference in location results into a large difference in calcium carbonate content. The step front in calcium carbonate content results from the steep front in urea and calcium chloride that has been chosen as an initial condition. In practice, the gradient will be much smaller due to dispersion and diffusion.

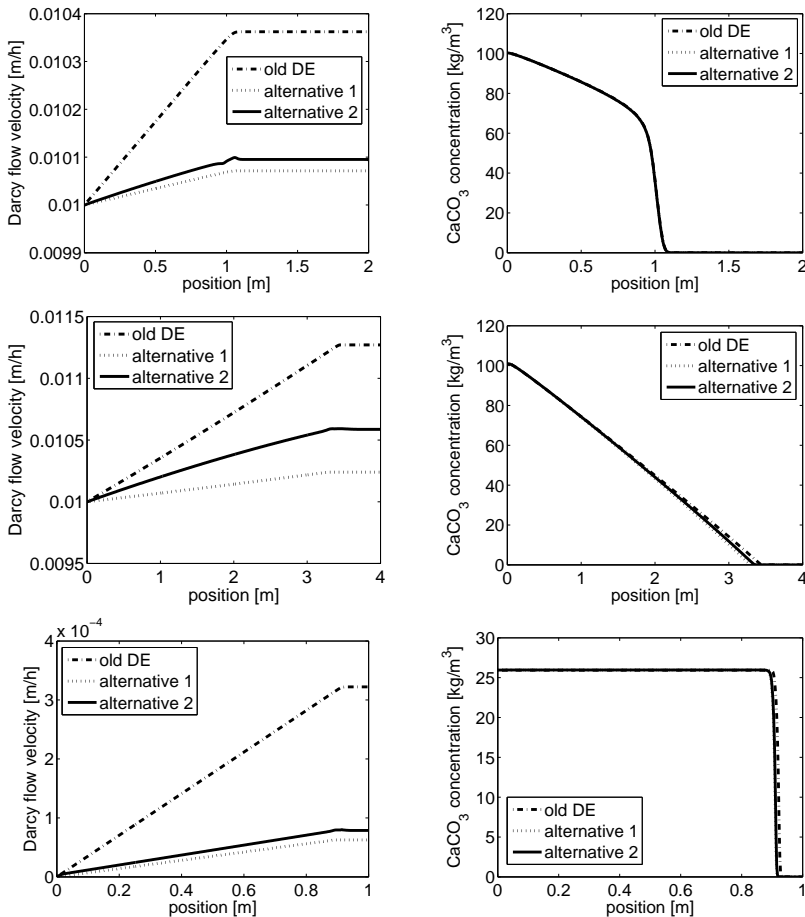


Figure 6.1: The Darcy flow velocity (left graphs) and the calcium carbonate concentration (right graphs) as a function of location, for the bold values from Table 6.3 at time  $t=100 \text{ h}$  (top graphs), for inflow velocity  $c_{in}=4M$  at time  $t=100 \text{ h}$  (middle graphs) and for  $q_{in}=0 \text{ m/h}$  at time  $t=25 \text{ h}$  (bottom graphs).

## 6.5 Discussion and Conclusions

From the results in Section 6.4, we conclude that the three different partial differential equations for the flow lead to different flow patterns. However, the graphs of the corresponding calcium carbonate content are very similar. In most cases the maximal difference between the calcium carbonate content is at most  $2 \text{ kg/m}^3$ , which corresponds to a relative error in the order of 5%.

From the variation of the inflow concentration of urea and calcium chloride  $c_{in}$ , it is concluded that a larger value of  $c_{in}$  leads to a higher maximal difference in calcium carbonate content. But since the inflow concentration that is used is limited, due to its toxicity for the bacteria, the error stays small for realistic values of  $c_{in}$ .

The results of the zero inflow velocity case show that steep gradients in the urea and calcium chloride concentration lead to steep gradients in the calcium carbonate content. A small difference in flow then leads to a small difference in the position of the front (in the order of 1 cm) and to a high difference in calcium carbonate content in that small region. However, since the calcium carbonate fronts are really close and such steep gradients in urea and calcium chloride are not likely to occur, this case does not lead to any important differences in calcium carbonate content.

Therefore, we conclude that the choice of the differential equation for the flow hardly influences the calcium carbonate content for realistic values of the process variables. Since the process variables in [90] and [91] (Chapter 2 and 3) are within the ranges specified in Table 6.3, the results in both articles are still valid.

Although the results are very similar, we will no longer use the previous differential equation for the flow. Instead, we will use one of the alternative differential equations, since they do not violate the requirement of conservation of mass. We choose the first alternative differential equation (6.8) to use from now on, since the first alternative is simpler and more stable than the second one.

We realize that the alternative differential equations, derived in Section 6.2 are based, among others, on the empirical relation between the density and the various concentrations (6.7).

**A robust method to tackle pressure boundary conditions in Porous Media Flow: Application to Biogrout**

This chapter has been published as:

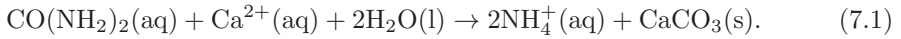
Van Wijngaarden, W.K., Vermolen, F.J., Van Meurs, G.A.M., Vuik, C.: A robust method to tackle pressure boundary conditions in Porous Media Flow: Application to Biogrout *Computational Geosciences*, **18-2**, 103–115, (2013)

## Abstract

Biogrout is a soil improvement method, in which micro-organisms are used to produce the solid calcium carbonate, which strengthens the soil by connecting soil particles. Micro-organisms in the soil are supplied with some nutrients, which they convert into calcium carbonate. These nutrients and the side product of the reaction are dissolved in water. Because of these chemicals, the fluid is denser than water. Moreover, the density changes as a result of the varying composition. This changing density has a significant impact on the flow. Since the composition and hence, the density is not known beforehand, a careful choice of the (pressure) boundary conditions, especially on the outflow boundary, is needed. In this chapter, several methods to approximate the pressure on the outflow boundary are compared. The method that we propose also works for an unstructured mesh, which gives a large freedom in the mesh generation.

## 7.1 Introduction<sup>1</sup>

Biogrout is a soil improvement method, in which micro-organisms are used to produce calcium carbonate ( $\text{CaCO}_3$ ). The overall reaction equation is given by:



The urea ( $\text{CO}(\text{NH}_2)_2$ ) and calcium ( $\text{Ca}^{2+}$ ) are dissolved in water, as well as the side product ammonium ( $\text{NH}_4^+$ ). Because of these chemicals, the fluid is denser than pure water. In [91] (Chapter 2), the following relation between the density of the solution  $\rho_l$  (at 20°C) and these concentrations is used:

$$\rho_l = 1000 + 15.4996C^{urea} + 86.7338C^{Ca^{2+}} + 15.8991C^{NH_4^+}. \quad (7.2)$$

In this relation,  $C^{urea}$  is the concentration of urea,  $C^{Ca^{2+}}$  is the concentration of calcium chloride and  $C^{NH_4^+}$  is the concentration of ammonium chloride, each with  $M(=\text{kmol}/\text{m}^3)$  as a unit. This relation has been found, using [95]. From the tables of the individual species, a linear relation between the various concentrations and the density has been found for a single species dissolved in water. However, in the Biogrout case several species are present in the fluid. We assume that the contributions of the various species can be added in the case that more than one species are dissolved. Experimental validation showed that this relation gives a good description of reality, [88]. In this chapter, equation (7.2) is used in the simulations.

Due to biochemical reaction (7.1), the solution has a varying composition and hence, also the density changes. This changing density has an effect on the water pressure. Flow boundary conditions are often given in terms of pressure, especially on the outflow boundaries, where usually a fixed head is applied to prevent desaturation of the soil. Unsaturated soil can occur when a fixed flow rate is prescribed. A fixed head gives a hydrostatic pressure boundary condition. At the injection, the composition of the solution is usually known, but at the extraction, the density is

---

<sup>1</sup>Parts of the original introduction have been skipped in order to prevent too much repetition of the Introduction from Chapter 1.

not known beforehand. Therefore, a careful choice of the boundary condition is necessary.

In this chapter, several methods to calculate the pressure on the extraction boundary are presented and compared. The last method, which is most robust, works for any finite-element mesh, even including unstructured grids. This gives a large freedom in the mesh generation.

## 7.2 Mathematical model

In this section we give the model equations with the initial and boundary conditions for the model.

### 7.2.1 Model equations

In this subsection the model equations for the Biogrout process are presented. For a derivation and a more thorough discussion, we refer to [91] (Chapter 1).

To model the concentration of the aqueous species (urea, calcium chloride and ammonium chloride) we use an advection-dispersion-reaction equation:

$$\frac{\partial(\theta C^i)}{\partial t} = \nabla \cdot (\theta \mathbf{D}^i \cdot \nabla C^i) - \nabla \cdot (\mathbf{q} C^i) + n_i \theta r_{hp}. \quad (7.3)$$

In this equation,  $\theta$  is the porosity,  $\mathbf{D}$  is the dispersion tensor,  $\mathbf{q}$  is the Darcy velocity,  $n_i$  is a constant that deals with the stoichiometry in the biochemical reaction equation (7.1) and  $r_{hp}$  is the reaction rate of the production of calcium carbonate. From the stoichiometry of reaction (7.1), the values of  $n_i$  for the various aqueous species are given by:  $n_{\text{urea}} = -1$ ,  $n_{\text{Ca}^{2+}} = -1$ , and  $n_{\text{NH}_4^+} = 2$ .

The left-hand side of equation (7.3) models the accumulation. In the right-hand side, we have terms for dispersion/diffusion, for advection and for the biochemical reaction (7.1).

In this chapter, we use the following relation for the reaction rate  $r_{hp}$  in equation (7.1):

$$r_{hp} = v_{max} \frac{C^{\text{urea}}}{K_{m,\text{urea}} + C^{\text{urea}}}. \quad (7.4)$$

Here,  $v_{max}$  is the bacterial conversion rate constant for a (given) specific bacterial density and  $K_{m,\text{urea}} \geq 0$  is the saturation constant. In this chapter, we use a bacterial conversion rate that is constant over the whole domain, thereby neglecting any variations of temperature, bacterial density or pH over the time and space. The concentration of bacteria can also be simulated, using the model proposed in [92] (Chapter 4). This model describes the placement of bacteria: bacteria are injected in the soil. After the injection of the bacteria, a pulse with fixation fluid is injected. This fixation fluid has less retardation than the bacterial pulse and will overtake the bacterial pulse, fixating the bacteria in the subsoil. Since the focus of this chapter is on the pressure boundary condition, we use this simplified reaction rate, which implies a homogeneous distribution of bacteria.

It is assumed that calcium carbonate is not transported. Hence, there is only an accumulation term from the reaction term in the differential equation for the calcium carbonate concentration:

$$\frac{\partial C^{\text{CaCO}_3}}{\partial t} = m_{\text{CaCO}_3} \theta r_{hp}. \quad (7.5)$$

In this equation,  $C^{\text{CaCO}_3}$  is the concentration of calcium carbonate with  $\text{kg}/\text{m}^3$  as a unit and  $m_{\text{CaCO}_3}$  is the molar mass of calcium carbonate, which is used to convert moles into mass.

The solid calcium carbonate that is formed in the pores causes a decrease in porosity. The difference  $(C^{\text{CaCO}_3}(t, \mathbf{x}) - C^{\text{CaCO}_3}(0, \mathbf{x}))$  gives the amount of calcium carbonate that has been formed per unit of volume in time period  $t$ . Division by the density of calcium carbonate  $\rho_{\text{CaCO}_3}$  gives the decrease in pore volume per unit of volume. That leads to the following relation between the calcium carbonate concentration and the porosity:

$$\theta(t, \mathbf{x}) = \theta(0, \mathbf{x}) - \frac{C^{\text{CaCO}_3}(t, \mathbf{x}) - C^{\text{CaCO}_3}(0, \mathbf{x})}{\rho_{\text{CaCO}_3}}. \quad (7.6)$$

For the flow, we use the continuity equation, that was derived in [93] (Chapter 6). This differential equations is an adaptation of the differential equation derived in [91] (Chapter 2), since the differential equation in [91] does not conserve mass. It is based on the assumption that reaction (7.1) does not influence the total amount of liquid volume, which turned out to be untrue. The adapted differential equation is given by:

$$\nabla \cdot \mathbf{q} = K \theta r_{hp}. \quad (7.7)$$

The constant  $K$  represents the amount of volume that is produced per kmol formed calcium carbonate by reaction (7.1) and it has been defined as

$$K := \left( \frac{m_{\text{CaCO}_3}}{\rho_{\text{CaCO}_3}} - (1 - V_s) \right). \quad (7.8)$$

This constant deals with two phenomena. When reaction (7.1) takes place, various species disappear from the solution and therefore the liquid volume decreases. On the other hand, due to the same reaction, the solid calcium carbonate is formed, which causes a decrease in pore space. The decrease in pore space per kmol formed calcium carbonate is  $\frac{m_{\text{CaCO}_3}}{\rho_{\text{CaCO}_3}}$  and the decrease in liquid volume per kmol formed calcium carbonate is  $1 - V_s$ . These two phenomena only partly cancel each other.

As a relation between the flow and the pressure  $p$ , Darcy's law is used [100],

$$q_x = - \frac{k_x}{\mu} \frac{\partial p}{\partial x}, \quad (7.9)$$

$$q_y = - \frac{k_y}{\mu} \frac{\partial p}{\partial y}, \quad (7.10)$$

$$q_z = - \frac{k_z}{\mu} \left( \frac{\partial p}{\partial z} + \rho_l g \right). \quad (7.11)$$

In Darcy's law,  $k_i$  is the intrinsic permeability in the various coordinate directions,  $i \in \{x, y, z\}$ ,  $\mu$  is the viscosity of the fluid,  $\rho_l$  is the density of the fluid and  $g$  is the gravitational constant.

The Kozeny-Carman equation is used to determine the intrinsic permeability. This equation is an empirical relation between the intrinsic permeability and the porosity, that is commonly used in ground water flow modelling (see [7]):

$$k = k_x = k_y = k_z = \frac{(d_m)^2}{180} \frac{\theta^3}{(1 - \theta)^2}. \quad (7.12)$$

In this relation,  $d_m$  is the mean particle size of the soil.

Substituting equations (7.9), (7.10) and (7.11) into equation (7.7), using relation (7.12), gives a partial differential equation for the pressure. This partial differential equation is solved to compute the flow pattern if the boundary conditions are given in terms of pressure, or if density differences influence the flow:

$$\nabla \cdot \mathbf{q} = \nabla \cdot \left( -\frac{k}{\mu} (\nabla p + \rho_l g \mathbf{e}_z) \right) = K \theta r_{hp}. \quad (7.13)$$

Here,  $\mathbf{e}_z$  is the unit vector in vertical direction, taken positive upwards.

### 7.2.2 Experimental set-up and initial and boundary conditions

As a model experiment we take the 100m<sup>3</sup> experiment as reported in [86]. The configuration is shown in Figure 7.1. A concrete box (8m × 5.6m × 2.5m) is filled with sand and fully saturated. Three injection wells (left) and three extraction wells (right) are used to flush the liquids through the sand body. The distance between injection and extraction is 5m. The other boundaries are closed.

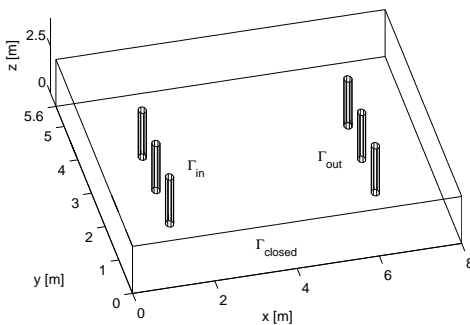


Figure 7.1: Set-up of the experiment. Injection lances are denoted by  $\Gamma_{in}$  and the extraction lances by  $\Gamma_{out}$ . The other boundaries ( $\Gamma_{closed}$ ) are closed.

Initially, the concentration of calcium carbonate, urea, calcium and ammonium are equal to zero and the porosity equals some constant  $\theta_0$ .

	<i>Boundary</i>	<i>Boundary Condition</i>
$C^{urea}$	$\Gamma_{in}$	$(D\theta\nabla C - \mathbf{q}C) \cdot \mathbf{n} = q_{in}c_{in}$
	$\Gamma_{out}$	$(D\theta\nabla C) \cdot \mathbf{n} = 0$
	$\Gamma_{closed}$	$(D\theta\nabla C - \mathbf{q}C) \cdot \mathbf{n} = 0$
$C^{Ca^{2+}}$	$\Gamma_{in}$	$(D\theta\nabla C - \mathbf{q}C) \cdot \mathbf{n} = q_{in}c_{in}$
	$\Gamma_{out}$	$(D\theta\nabla C) \cdot \mathbf{n} = 0$
	$\Gamma_{closed}$	$(D\theta\nabla C - \mathbf{q}C) \cdot \mathbf{n} = 0$
$C^{NH_4^+}$	$\Gamma_{in}$	$(D\theta\nabla C - \mathbf{q}C) \cdot \mathbf{n} = 0$
	$\Gamma_{out}$	$(D\theta\nabla C) \cdot \mathbf{n} = 0$
	$\Gamma_{closed}$	$(D\theta\nabla C - \mathbf{q}C) \cdot \mathbf{n} = 0$
$\mathbf{q}/p$	$\Gamma_{in}$	$-\mathbf{q} \cdot \mathbf{n} = q_{in}$
	$\Gamma_{out}$	$p(x, y, z) = p_{atm} + \int_z^{2.5} \rho_l(x, y, \bar{z})g d\bar{z}$
	$\Gamma_{closed}$	$\mathbf{q} \cdot \mathbf{n} = 0$

Table 7.1: Boundary conditions for the various concentrations and the flow.

Table 7.1 displays the boundary conditions for the various concentrations and the flow. On the inflow boundary, we prescribe the inflow velocity and the flux. On the closed boundary, there is no flow perpendicular to the boundary and hence the flux over the boundary equals zero. On the outflow boundary, we prescribe the pressure and for the concentrations an advective flux is assumed. Due to the gravitational force, it is required that each part of the outflow boundaries is part of a *vertical* plane. In the extraction wells, at a certain depth (equal to the top of the sand body), a pump has been installed, which keeps the water level in the well at a fixed position. Note that the container is covered with a watertight foil, which is loaded with another layer of sand. This makes it possible to create an overpressure around the injection wells, which results into flow from injection to extraction. Since the resistance to flow in the extraction wells is very low, we assume a hydrostatic pressure on its boundaries, see for example [7]. That leads to the following differential equation on the surface of the extraction boundaries:

$$\frac{\partial p}{\partial z} = -\rho_l g, \quad (7.14)$$

with at the height of the pump (at  $z=2.5\text{m}$ )

$$p(2.5) = p_{atm}, \quad (7.15)$$

in which  $p_{atm}$  is the atmospheric pressure. Integration of equation (7.14), combined with boundary condition (7.15), gives the following equation for the pressure for all points  $z$  on the surface of the extraction boundaries, for which holds  $0 \leq z \leq 2.5\text{m}$  :

$$p(x, y, z) = p_{atm} + \int_z^{2.5} \rho_l(x, y, \bar{z})g d\bar{z}, \quad (7.16)$$

see also Table 7.1.

To compute the pressure given by equation (7.16), all the nodes of the mesh should be positioned on vertical lines. On these lines, the  $x$ - and  $y$ -coordinates are constant, while the  $z$ -coordinate is variable. Over these lines, the integral in equation (7.16) is computed, which gives the pressure at all nodes on these lines.

The requirement that all the nodes are on certain vertical lines puts a severe requirement on the mesh generation. Another possibility, which also allows unstructured meshes, is solving differential equation (7.14) with a finite element method. In that case, the partial differential equation is solved on a (2D) manifold as a boundary condition for a 3D domain. Some examples from literature in which differential equations are solved on manifolds are [12], [43], [54] and [69].

## 7.3 Numerical Methods

In this section, it is explained which numerical methods are used to solve the partial differential equations in the 3D domain, equations (7.3) to (7.13), as well as the equations for the pressure boundary condition, equation (7.14) and alternatively equation (7.16).

Equations (7.3), (7.9), (7.10), (7.11) and (7.13) are solved using the Standard Galerkin Finite Element Method. These equations are multiplied by a test function  $\eta$  and integrated over the domain  $\Omega$  to derive the weak formulation. For the time integration of equation (7.3), an implicit scheme is used. Since the reaction rate  $r_{hp}$  is non-linear in the urea concentration, Newton's method is used to calculate the urea concentration. Since in each node the differential equation for the calcium carbonate concentration (7.5) is an ordinary differential equation, the finite element method is not used to solve equation (7.5). An implicit time integration method is used to solve this equation. For more details about the numerical methods to solve these equations, we refer to [90] and [91] (Chapter 2 and 3), where this has been reported in more detail.

In this chapter, the pressure on the outflow boundary is calculated in three different ways. The first two methods involve a calculation, based on equation (7.16). In the first method (method 1), the integral in equation (7.16) is approximated using the Lower Riemann Sum, see [1]. This is a first order method. Let  $n$  be the number of nodes on one of the vertical lines. The nodes on this line are ordered in the following way:  $0 = z_0 < z_1 < \dots < z_{n-1} < z_n = 2.5$ . Then, equation (7.16) is approximated by:

$$p(x, y, z_j) \approx p_{atm} + \sum_{i=j}^{n-1} g \rho_l(x, y, z_{i+1})(z_{i+1} - z_i). \quad (7.17)$$

This sum is calculated for each node on each vertical line.

In the second method (method 2), the second order trapezoid rule is used to approximate (7.16), see [1]. Using the same notation as for the Lower Riemann Sum, we get the following approximation:

$$p(x, y, z_j) \approx p_{atm} + \sum_{i=j}^{n-1} g \frac{\rho_l(x, y, z_i) + \rho_l(x, y, z_{i+1})}{2} (z_{i+1} - z_i). \quad (7.18)$$

This sum is calculated for each node on each vertical line.

As a third method (method 3), the pressure on the boundary is calculated, by solving equation (7.14) subject to boundary condition (7.15). For this calculation the Standard Galerkin Finite Element Method is used. To derive the weak formulation, equation (7.14) is multiplied by a test function  $\eta$  and integrated over the surface of the outflow boundary  $\Gamma_{out}$ :

$$\int_{\Gamma_{out}} \frac{\partial p}{\partial z} \eta dS = - \int_{\Gamma_{out}} \rho_l g \eta dS. \quad (7.19)$$

The pressure  $p$  is approximated by

$$p \approx \sum_{j=1}^N p_j \varphi_j, \quad (7.20)$$

in which  $\varphi_j$  is a linear basis function and where  $p_j$  denote the pressure approximations on nodes on the boundary. The  $z$ -derivatives of the basis functions are determined after a mapping to the  $(x-z)$ -plane. The integral over the outflow boundary is approximated by the sum of the integrals over the elements. The Newton-Cotes quadrature rules have been used to develop the element matrices and vectors. Triangular boundary elements have been used. Differential equation (7.14) with boundary condition (7.15), can be considered as an initial value problem. Using the Standard Galerkin Finite Element Method and choosing  $\eta = \varphi_i$  for  $i \in \{1, \dots, N\}$  as a test function will lead to stability problems. Inspired by the SUPG method, see [80], we choose as a test function:  $\eta = \varphi_i - \frac{h\xi}{2} \frac{\partial \varphi_i}{\partial z}$ , for  $i \in \{1, \dots, N\}$ . In this equation,  $h$  is some representative distance in the element and  $\xi$  is some constant. In case of application on a surface, we choose for  $h$ :

$$h := \sqrt{\frac{2A}{n_{el}}}, \quad (7.21)$$

in which  $A$  is the total surface of the domain and  $n_{el}$  is the number of elements on the surface. As a value for  $\xi$  we take  $\xi = 10^{-5}$ . As differential equation (7.14) is similar to a stationary advection equation, the SUPG method will introduce some artificial diffusion, which stabilizes the system. If the SUPG method is not used, then the discretization matrix might have an eigenvalue that is equal to zero.

In this paragraph, we do some analysis to investigate the influence of the value of  $\xi$  on the differences in eigenvalues of the system with SUPG stabilization and the system without SUPG stabilization, applied on a surface. Let  $H$  be the matrix that is used to solve the system without SUPG stabilization and  $\hat{H}(h\xi)$  the matrix for the system with SUPG. Both matrices are  $n \times n$  matrices. The entries of matrix  $\hat{H}(h\xi)$  are given by  $\hat{H}_{ij}(h\xi) = H_{ij} + h\xi \Delta H_{ij}$  and hence,  $\hat{H}(\varepsilon) = H + \varepsilon \Delta H$ , with  $\varepsilon = h\xi$ . The  $\varepsilon \Delta H$  part in the matrix accounts for the SUPG stabilization. Further, let  $(\lambda, \mathbf{v})$  be an eigenpair of  $H$  ( $H\mathbf{v} = \lambda\mathbf{v}$ ) and let  $(\lambda(\varepsilon), \mathbf{v}(\varepsilon))$  be an eigenpair of  $\hat{H}(\varepsilon)$  ( $\hat{H}(\varepsilon)\mathbf{v}(\varepsilon) = \lambda(\varepsilon)\mathbf{v}(\varepsilon)$ ) and suppose that  $\mathbf{w}^{\mathbf{H}}$  is a left eigenvector of  $H$  ( $\mathbf{w}^{\mathbf{H}}H = \lambda\mathbf{w}^{\mathbf{H}}$ ). Then

$$(H + \varepsilon \Delta H)\mathbf{v}(\varepsilon) = \lambda(\varepsilon)\mathbf{v}(\varepsilon). \quad (7.22)$$

To estimate  $\lambda(\varepsilon)$ , equation (7.22) is differentiated with respect to  $\varepsilon$ , which gives

$$\Delta H \mathbf{v}(\varepsilon) + (H + \varepsilon \Delta H) \frac{d\mathbf{v}(\varepsilon)}{d\varepsilon} = \frac{d\lambda(\varepsilon)}{d\varepsilon} \mathbf{v}(\varepsilon) + \lambda(\varepsilon) \frac{d\mathbf{v}(\varepsilon)}{d\varepsilon}. \quad (7.23)$$

Set  $\varepsilon = 0$ , then we get ( $\mathbf{v}(0) = \mathbf{v}$ ,  $\lambda(0) = \lambda$ )

$$\Delta H \mathbf{v} + H \frac{d\mathbf{v}(0)}{d\varepsilon} = \frac{d\lambda(0)}{d\varepsilon} \mathbf{v} + \lambda \frac{d\mathbf{v}(0)}{d\varepsilon}. \quad (7.24)$$

Left-multiplication by  $\mathbf{w}^H$  gives

$$\mathbf{w}^H \Delta H \mathbf{v} + \mathbf{w}^H H \frac{d\mathbf{v}(0)}{d\varepsilon} = \frac{d\lambda(0)}{d\varepsilon} \mathbf{w}^H \mathbf{v} + \lambda \mathbf{w}^H \frac{d\mathbf{v}(0)}{d\varepsilon}. \quad (7.25)$$

Hence, since  $\mathbf{w}^H H = \lambda \mathbf{w}^H$ :

$$\mathbf{w}^H \Delta H \mathbf{v} = \frac{d\lambda(0)}{d\varepsilon} \mathbf{w}^H \mathbf{v}. \quad (7.26)$$

Since  $\mathbf{w}^H \mathbf{v} \neq 0$ , we get

$$\left| \frac{d\lambda(0)}{d\varepsilon} \right| = \frac{|\mathbf{w}^H \Delta H \mathbf{v}|}{|\mathbf{w}^H \mathbf{v}|} \leq \frac{\|\mathbf{w}^H\|_2 \|\Delta H\|_2 \|\mathbf{v}\|_2}{|\mathbf{w}^H \mathbf{v}|} = \frac{\|\Delta H\|_2}{|\mathbf{w}^H \mathbf{v}|}. \quad (7.27)$$

The last step is motivated by choosing  $\|\mathbf{w}^H\|_2 = \|\mathbf{v}\|_2 = 1$ . Furthermore,

$$\begin{aligned} \|\Delta H\|_2 \leq \|\Delta H\|_F &:= \left[ \sum_i \sum_j |\Delta H_{ij}|^2 \right]^{1/2} \leq \left[ \max_{i,j} cn |\Delta H_{ij}|^2 \right]^{1/2} = \\ &= \frac{C}{h} \max_{i,j} |\Delta H_{ij}|, \end{aligned} \quad (7.28)$$

where  $cn$  is motivated by the sparsity of the matrix  $\Delta H$ . Moreover, it has been used that  $n = L^2/h^2$  with  $L$  the length of the domain and  $C$  has been defined as  $C := L\sqrt{c}$ . Hence, we have

$$\left| \frac{d\lambda(0)}{d\varepsilon} \right| \leq \frac{C \max_{i,j} |\Delta H_{ij}|}{h |\mathbf{w}^H \mathbf{v}|}. \quad (7.29)$$

This can be rewritten as

$$\lim_{\varepsilon \rightarrow 0} \frac{|\lambda(\varepsilon) - \lambda(0)|}{|\varepsilon|} \leq \frac{C \max_{i,j} |\Delta H_{ij}|}{h |\mathbf{w}^H \mathbf{v}|}. \quad (7.30)$$

Herewith, we get for  $\varepsilon \rightarrow 0$

$$|\lambda(\varepsilon) - \lambda| \leq \frac{C \max_{i,j} |\Delta H_{ij}|}{h |\mathbf{w}^H \mathbf{v}|} \varepsilon. \quad (7.31)$$

Substitution of  $\varepsilon = h\xi$  gives

$$|\lambda(h\xi) - \lambda| \leq \frac{C \max_{i,j} |\Delta H_{ij}|}{h |\mathbf{w}^H \mathbf{v}|} h\xi = \frac{C \max_{i,j} |\Delta H_{ij}|}{|\mathbf{w}^H \mathbf{v}|} \xi. \quad (7.32)$$

Hence, we proved:

**Proposition 1** *Let  $H\mathbf{v} = \lambda\mathbf{v}$ ,  $H \in \mathbb{R}^{n \times n}$ , and let  $\mathbf{w}^H H = \lambda\mathbf{w}^H$ , let  $\hat{H}_{ij}(h\xi) = H_{ij} + h\xi\Delta H_{ij}$  where the number of non-zero entries is  $c \cdot n$ , let  $C$  be defined as  $C := L\sqrt{c}$ , then*

$$|\lambda(h\xi) - \lambda| \leq \frac{C \max_{i,j} |\Delta H_{ij}|}{|\mathbf{w}^H \mathbf{v}|} \xi = \mathcal{O}(\xi), \quad (7.33)$$

where

$$\hat{H}(h\xi)\mathbf{v}(h\xi) = \lambda(h\xi)\mathbf{v}(h\xi).$$

The above analysis heavily relies on page 323 in [35]. If  $\mathbf{w}^H \Delta H \mathbf{v} \neq 0$  then from this proposition and equation (7.27) we can conclude that, by applying SUPG stabilization in case of an unstable system, the zero eigenvalue is mapped onto a non-zero one, where its magnitude is bounded by a value of order  $\xi$ .

At each time step, the model equations are solved in the following order. First, the porosity, permeability, fluid density and flow boundary conditions are updated. Then, the flow is calculated. Finally, the boundary conditions for the concentrations are updated and the concentrations of urea, ammonium and calcium carbonate are calculated.

## 7.4 Results

Before the results of the 100m<sup>3</sup> experiment are presented, we start with a simple 2D configuration to compare the three methods to calculate the pressure on the outflow boundary, that were proposed in the last section. This is done in Subsection 7.4.1. Subsequently, in Subsection 7.4.2, we take the configuration from Figure 7.1 with some known density function and calculate the pressure on the outflow boundary. Finally, in Subsection 7.4.3, the model results, which incorporate the numerical solution of the complete set of partial differential equations, of the 100m<sup>3</sup> experiment are shown.

### 7.4.1 Comparison of the three methods to calculate the pressure boundary condition

As a domain, we take a rectangle with a width of 2m and a height of 2.5m. In this domain, we compare the three pressure calculation methods. This is done for two different relations for the density. The comparison is done for six structured meshes, with an increasing number of elements and for some unstructured meshes, with approximately the same number of elements as for the structured meshes.

As a density, the two following (arbitrarily chosen) relations between density and depth are used:

$$\rho_1 = 1000 + 200z, \quad (7.34)$$

$$\rho_2 = 1000 + 200z^3. \quad (7.35)$$

These relations of course do not hold at the same time. Substituting both relations into equation (7.16), gives the following two analytical solutions for the pressure:

$$\begin{aligned} p_1(x, y, z) &= p_{atm} + \int_z^{2.5} \rho_1(x, y, \bar{z}) g d\bar{z} \\ &= p_{atm} + g(1000(2.5 - z) + 100(2.5^2 - z^2)), \end{aligned} \quad (7.36)$$

$$\begin{aligned} p_2(x, y, z) &= p_{atm} + \int_z^{2.5} \rho_2(x, y, \bar{z}) g d\bar{z} \\ &= p_{atm} + g(1000(2.5 - z) + 50(2.5^4 - z^4)). \end{aligned} \quad (7.37)$$

The first method, which uses the Lower Riemann Sum as an integration technique, has a first order error, but is exact for a constant density function. The second method, based on the Trapezium method, has a second order error and is exact for constant and linear density functions. The third method also has a first order error, due to the SUPG method. But since the value of  $\xi$  has been chosen very small, a better convergence is possible. When we describe the error to be of the order  $O(h^\alpha)$ , with  $h$  some measure for the mesh size, we expect that for a regular mesh in the limit,  $\alpha = 1$  for the first and third method and  $\alpha = 2$  for the second method. We calculate the value of  $\alpha$  from the following equation:

$$\frac{e_1}{e_2} = \frac{h_1^\alpha}{h_2^\alpha} = r^\alpha, \quad (7.38)$$

in which  $e_i$  is the error for mesh  $i$ ,  $i \in \{1, 2\}$ ,  $h_i$  is the mesh size of mesh  $i$  and  $r$  is the ratio between  $h_1$  and  $h_2$  ( $r = h_1/h_2$ ). As a measure for  $h_i$ , we use equation (7.21).

In Tables 7.2 to 7.6 we display the results of the comparison of the three pressure calculation methods with the analytical solution on both a structured mesh and an unstructured mesh for an increasing number of elements and for the two relations between the density and the depth. In Table 7.3, the three methods are compared regarding computing time. In the left plot of Figure 7.2, mesh  $a$ , an unstructured mesh with 38 elements, is shown. This mesh is made with the mesh generator in the COMSOL Multiphysics software. Mesh  $b$  is formed from mesh  $a$  by dividing all the elements of this mesh into four equisized elements. Mesh  $b$  is shown in the right plot of Figure 7.2. In the same way, the other unstructured meshes, mesh  $c$  up to mesh  $f$ , are formed by dividing all the elements of the coarser mesh into four smaller, equisized elements. Mesh  $f2$  is not formed from a coarser mesh, but directly generated with the COMSOL Multiphysics software. It has approximately the same number of elements as mesh  $f$  and is unstructured. Mesh  $c$  up to mesh  $f2$  are not shown in this chapter.

The displayed error in Table 7.2 to 7.6 is the mean of the (absolute value of the) error that is made in each node:

$$E = \frac{1}{n} \sum_{j=1}^n |p_j - p_j^E|. \quad (7.39)$$

In this equation for the error,  $n$  is the number of nodes,  $p_j$  is the numerical solution for the pressure in point  $j$  and  $p_j^E$  is the exact solution for the pressure in point  $j$ . The  $\alpha$ -factor is determined from the (unrounded) errors of two subsequent meshes.

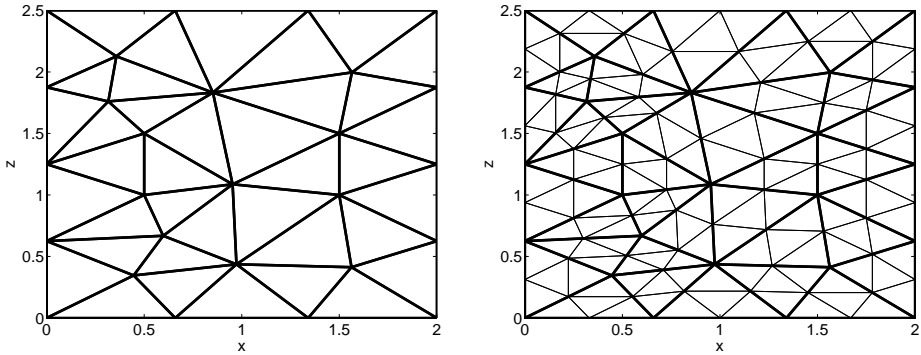


Figure 7.2: Two examples of unstructured meshes. Left: mesh  $a$ , the number of elements is 38. Right: mesh  $b$ , this mesh is formed from mesh  $a$  by dividing each elements into four smaller, equisized elements.

number of elements	method 1		method 2		method 3	
	error	$\alpha$	error	$\alpha$	error	$\alpha$
40	613	1.00	0		302	1.93
160	307	1.00	0		79	1.89
640	153	1.00	0		21	1.89
2560	77	1.00	0		5.8	1.95
10240	38	1.00	0		1.5	1.97
40960	19		0		0.38	

Table 7.2: Comparison of the three pressure calculation methods with the analytical solution on a *structured* mesh for a *linear* relation between the depth and the density. The  $\alpha$ -factor is determined from the (unrounded) errors of two subsequent meshes, using equation (7.38).

number of elements	computing time for method 1 (s)	computing time for method 2 (s)	computing time for method 3 (s)
40	0.0005	0.0005	0.0006
160	0.0008	0.0008	0.0013
640	0.0021	0.0018	0.0036
2560	0.0035	0.0037	0.0193
10240	0.0113	0.0115	0.1335
40960	0.0471	0.0478	1.7352

Table 7.3: The computing time (average of 10 simulations) for the various methods. Simulations are done on a *structured* mesh for a *linear* relation between the depth and the density.

number of elements	method 1		method 2		method 3	
	error	$\alpha$	error	$\alpha$	error	$\alpha$
40	4880	0.879	485	1.963	1798	1.63
160	2654	0.942	125	1.982	580	1.78
640	1382	0.971	32	1.991	169	1.87
2560	705	0.986	7.9	1.996	46	1.94
10240	356	0.993	2.0	1.998	12	1.96
40960	179		0.50		3.1	

Table 7.4: Comparison of the three pressure calculation methods with the analytical solution on a *structured* mesh for a *non linear* relation between the depth and the density. The  $\alpha$ -factor is determined from the (unrounded) errors of two subsequent meshes, using equation (7.38).

	number of elements	method 1		method 2		method 3	
		error	$\alpha$	error	$\alpha$	error	$\alpha$
mesh <i>a</i>	38	1628	-0.05	872	-0.53	296	1.94
mesh <i>b</i>	152	1690	-0.08	1259	-0.30	77	1.39
mesh <i>c</i>	608	1780	-0.05	1547	-0.15	29	2.66
mesh <i>d</i>	2432	1843	-0.03	1721	-0.08	4.6	1.81
mesh <i>e</i>	9728	1879	-0.01	1816	-0.04	1.3	1.73
mesh <i>f</i>	38912	1898		1866		0.40	
mesh <i>f2</i>	40860	1929		1850		0.39	

Table 7.5: Comparison of the three pressure calculation methods with the analytical solution on an *unstructured* mesh for a *linear* relation between the depth and the density. The  $\alpha$ -factor is determined from the (unrounded) errors of two subsequent meshes, using equation (7.38).

	number of elements	method 1		method 2		method 3	
		error	$\alpha$	error	$\alpha$	error	$\alpha$
mesh <i>a</i>	38	9118	-0.05	7147	-0.28	2188	1.23
mesh <i>b</i>	152	9413	-0.08	8704	-0.16	934	1.86
mesh <i>c</i>	608	9974	-0.06	9737	-0.08	258	2.01
mesh <i>d</i>	2432	10394	-0.03	10313	-0.04	64	1.91
mesh <i>e</i>	9728	10645	-0.02	11614	-0.02	17	2.09
mesh <i>f</i>	38912	10781		10768		4.4	
mesh <i>f2</i>	40860	11037		10884		2.3	

Table 7.6: Comparison of the three pressure calculation methods with the analytical solution on an *unstructured* mesh for a *non linear* relation between the depth and the density. The  $\alpha$ -factor is determined from the (unrounded) errors of two subsequent meshes, using equation (7.38).

From Tables 7.2 to 7.4 we conclude that the convergence of methods 1 and 2 is as expected. For method 1,  $\alpha$  converges to 1 and for method 2  $\alpha$  converges to 2. For method 3, we expected a first order convergence but the convergence is even one order better than expected since  $\alpha$  converges to 2. However, although the method behaves like a second order method for a small value of  $\xi$ , the method is first order. The error looks like  $E(h) = \xi h + Kh^2$ . If  $\xi$  is very small, then  $\xi h > Kh^2$  only if  $h$  is very small. This gives  $\xi > Kh \iff h < \xi/K$ . This implies that if  $h = \mathcal{O}(\xi)$ , then the results will actually look first-order. However, as long as  $h \gg \xi/K$ , which is used in general in practical purposes, then  $E(h)$  behaves like  $\mathcal{O}(h^2)$ , which is observed in our experiments.

For a linear relation between density and depth, method 2 is exact and hence, the error is equal to zero. Method 1 results in the largest error. The mean error using method 3 falls within the range of the errors from methods 1 and 2.

The computing time for method 1 and method 2 is almost similar. The computing time for method 2 is slightly larger since it has an extra addition compared to method 1, see equations (7.17) and (7.18). The largest part of the computing time is used for finding the various vertical lines on which the nodes lie and sorting the nodes on this lines. The computing time for method 3 is comparable with method 1 and 2 for the coarse meshes but increases more rapidly for an increasing number of elements.

In an unstructured mesh, the nodes usually do not lie on vertical lines. Hence method 1 and 2 do not work properly. As can be seen from Table 7.5 and 7.6 there is no convergence using these methods and the error even increases somewhat for an increasing number of elements. Method 3, however, also works on an unstructured mesh. The error decreases with a decreasing element size and also here we see a second order convergence, which is one order better than expected, although the convergence is not as regular as on the structured meshes.

In Table 7.7, we show some results of the effect of the variation of  $\xi$  on the error of method 3. We take a mesh of 8 elements as shown in Figure 7.3 and refine this mesh. As can be seen from Table 7.7, method 3 is first order for a high value of  $\xi$ . For values of  $\xi$  around  $\xi = 10^{-2}$ , the method behaves second order. In this chapter, we chose  $\xi = 10^{-5}$ . Its value can be even smaller, but for the several meshes we tried, problems arise around  $\xi = 10^{-15}$ . Hence,  $\xi = 10^{-5}$  is a 'safe' value, which gives a second order method.

## 7.4.2 Calculation of the pressure on the outflow boundary of the 100m<sup>3</sup> experiment

Before simulating the 100m<sup>3</sup> experiment, we first approximate the pressure on the outflow boundaries for a known density and compare this numerical solution with the analytical solution. We use the same relations between fluid density and depth as in the previous subsection:  $\rho_1$  (7.34) and  $\rho_2$  (7.35). We approximate the pressure, using four different meshes: mesh 1, mesh 2, mesh 3 and mesh 3b. Mesh 1 is an irregular mesh. Mesh 2 is formed from mesh 1 by dividing each outflow boundary element into four smaller, equisized elements. Mesh 3 is formed in the same way from mesh 2. Mesh 3b is another irregular mesh, with approximately the same number of outflow boundary elements as mesh 3. The three extraction lances are

number of elements	$\xi = 10^{-1}$		$\xi = 10^{-2}$		$\xi = 10^{-5}$	
	error	$\alpha$	error	$\alpha$	error	$\alpha$
8	555	1.82	323	1.47	287	1.52
32	157	1.76	117	1.92	100	2.01
128	46	1.47	30	1.83	25	2.02
512	17	1.14	8.7	1.90	6.2	1.90
2048	7.6	1.00	2.3	1.87	1.7	2.02
8192	3.8		0.64		0.41	
	$\xi = 10^{-10}$		$\xi = 10^{-15}$		$\xi = 10^{-20}$	
	error	$\alpha$	error	$\alpha$	error	$\alpha$
8	287	1.52	287	0.05	287	-9.25
32	100	2.01	278	0.05	174874	-1.62
128	25	2.02	269	2.5	536618	0.45
512	6.1	2.02	47	-0.40	392351	0.93
2048	1.5	2.01	61	-0.21	206335	0.57
8192	0.38		71		138858	

Table 7.7: Results of the variation of  $\xi$ . Errors for an application on a *structured* mesh and a *linear* relation between the depth and the density. The  $\alpha$ -factor is determined from the (unrounded) errors of two subsequent meshes, using equation (7.38).

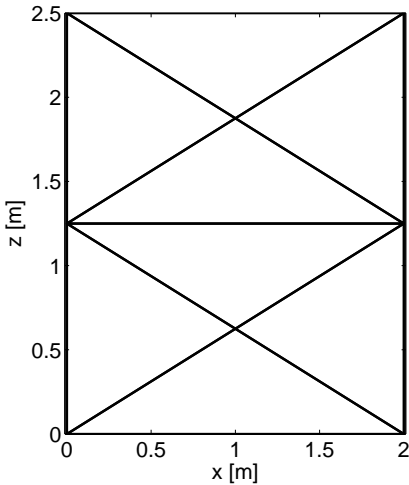


Figure 7.3: The mesh that is used to examine the effect of the value of  $\xi$ .

modelled through a prism with a regular octagon as a base. Partial differential equation (7.14) is solved on the total surface of the extraction boundaries in one matrix-vector solve, using method 3. In Figure 7.4, mesh 1 (top figures) and mesh 3b (bottom) are shown. The results of the comparison of the numerical solution with the analytical solution is shown in Table 7.8. As before, the error is computed from equation (7.39).

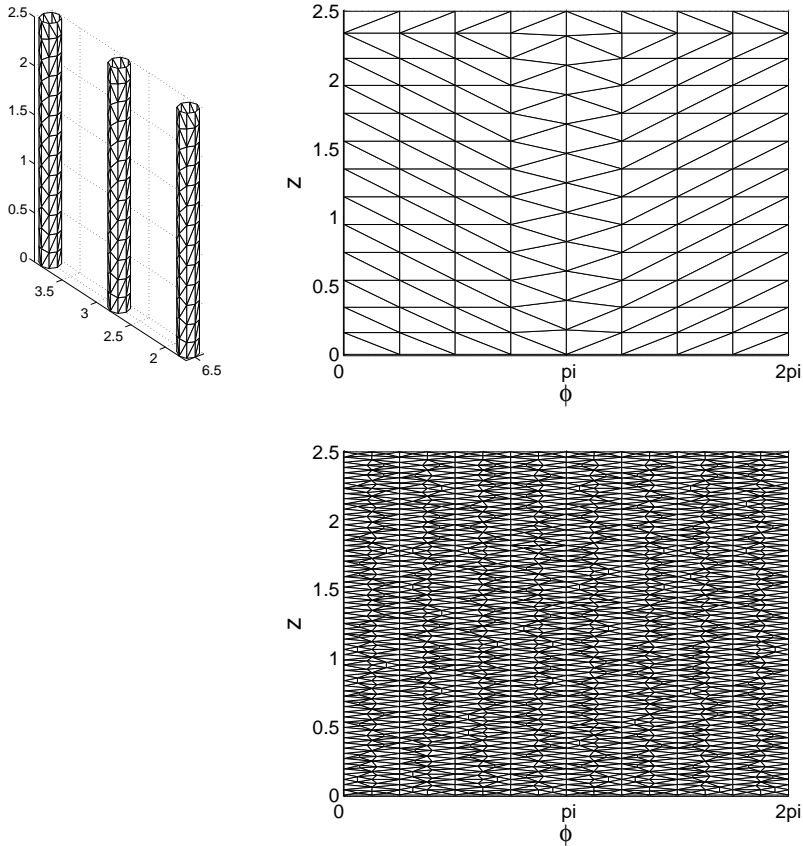


Figure 7.4: Mesh on the extraction lances. The top left plot shows the mesh on the extraction lances for mesh 1. The number of elements on the extraction lances is 618. The top right plot shows the same mesh on one of the extraction lances, but now as a function of the angle. Mesh 2 is formed from mesh 1 by subdividing the outflow boundary elements into four (equisized) elements. Mesh 3 is formed in the same way from mesh 2. In the bottom plot mesh 3b is shown. This is an irregular mesh that has approximately the same number of outflow boundary elements as mesh 3. The number of elements on the extraction lances is 618 for mesh 1, 2472 for mesh 2, 9888 for mesh 3 and 9600 for mesh 3b.

mesh	number of elements on the outflow boundaries	density	error	density	error
mesh 1	618	$\rho_1$	73	$\rho_2$	675
mesh 2	2472	$\rho_1$	17	$\rho_2$	124
mesh 3	9888	$\rho_1$	4.5	$\rho_2$	40
mesh 3b	9600	$\rho_1$	5.9	$\rho_2$	41

Table 7.8: Comparison of the numerical solution with the analytical solution for the pressure on the outflow boundary for three meshes and two relations for the density.

In Table 7.8, we see that the error decreases for an increasing number of elements, as was expected. The convergence is good, as can be seen from Figure 7.5. In this figure, the error is plotted against the number of elements. The errors for density  $\rho_1$  are marked with a + -sign and the errors for density  $\rho_2$  are marked with a diamond-sign. Also the trend line for an  $O(h^2)$ -convergence is given. It is clear that method 3 gives a quadratic convergence approximately.

In Table 7.8, we also compare mesh 3 and mesh 3b. Mesh 3b is a "real" irregular mesh, while mesh 3 is formed from another mesh by splitting the elements. Both meshes have approximately the same number of elements and it turns out that the error is also comparable, as was desired. The size of the boundary elements in mesh 1 is comparable with the mesh size of mesh c, the 2D mesh with 608 elements. In the same way, mesh 2 and mesh 3 are comparable with mesh d (2432 elements) and mesh e (9728 elements). For that reason, one expects that the errors are of the same order of magnitude. This turns out to be the case, although the errors in this subsection are somewhat larger. The reason might be that the geometry is more complex and that the elements are located on three different lances instead of on one rectangular 2D domain.

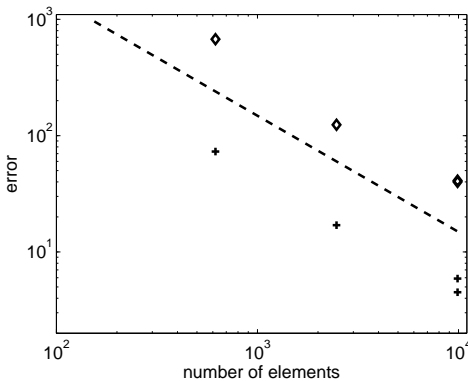


Figure 7.5: The error of the density calculation on the outflow boundary plotted against the number of elements. The errors for density  $\rho_1$  are marked with a + -sign and the errors for density  $\rho_2$  are marked with a diamond-sign. Also the trend line for an  $O(h^2)$ -convergence is given.

---

$\theta_0 = 0.41,$ $\mu = 1.15 \times 10^{-3} \text{ Pa s},$ $\rho_{CaCO_3} = 2,710 \text{ kg/m}^3,$ $v_{max} = 4.3681 \times 10^{-6} \text{ kmol/m}^3/\text{s},$ $g = 9.81 \text{ m/s}^2,$ $d_m = 124 \times 10^{-6} \text{ m}$ $Q_{in} = 5\text{m}^3/(8 \times 3600\text{s})$ $q_{in} = 3.78 \times 10^{-5} \text{ m/s}.$	$m_{CaCO_3} = 100.1 \text{ kg/kmol},$ $\mathbf{D} = 0.05[\text{m}] \text{ diag}([q_x^2 \ q_y^2 \ q_z^2]^T / \ \mathbf{q}\ ),$ $p_{atm} = 10^5 \text{ Pa},$ $K = 0.00728 \text{ m}^3/\text{kmol},$ $K_{m,urea} = 0.01 \text{ kmol/m}^3,$ $c_{in} = 1.00 \text{ kmol/m}^3$ $A_{in} = 4.59 \text{ m}^2$
--	--

---

Table 7.9: The values that have been assigned to the various model parameters.

For mesh 1, we could also have used method 1 or method 2 to calculate the pressure on the boundaries since all the nodes lie on certain vertical lines. In mesh 2 and 3, the nodes also lie on some vertical lines. However, some of these lines do not have a node on the top edge on which the pressure is given. But after calculation of the pressure at the intersection of these lines and the top edges (which is very easy in case of a constant pressure at the top), method 1 and 2 can be used. With mesh 3b it is not possible to use method 1 or 2 to calculate the pressure on the outflow boundary and this mesh clearly needs the application of method 3, where a small SUPG stabilization has been applied.

### 7.4.3 Application: a 100m<sup>3</sup> experiment

For the 100m<sup>3</sup> experiment, we take the configuration (Figure 7.1), the boundary conditions (Table 7.1) and the initial conditions from Subsection 7.2.2. In this chapter, the focus is on the calculation of the pressure on the boundary and not on the validation of the model. Hence, we only model the first part of the experiment. We lower the flow rate, such that the density effect becomes more visible and we extend the injection time to 80 hours to allow the urea/calcium chloride pulse to reach the extraction wells. As a time step we use  $\Delta t = 0.5h$ . The number of elements is approximately 23,000. The values that have been chosen for the various model parameters are shown in Table 7.9. Since the differential equation, the initial condition and boundary conditions are the same for urea and calcium chloride, the urea concentration is equal to the calcium chloride concentration.

In Figure 7.6, we consider the pressure on the outflow boundary of the middle extraction well as a function of time. We focus on the (vertical) edge of the prism closest to the injection. The pressure on this edge is compared to the hydrostatic pressure of water with a density of  $\rho_{water} = 1000\text{kg/m}^3$  and the difference between these two pressures is shown. This is done at several times.

During the first hours, the extraction wells are surrounded by fresh water since it takes some time before the urea/calcium chloride solution reaches the outlet. After some time some urea and calcium chloride will reach the extraction. Due to density

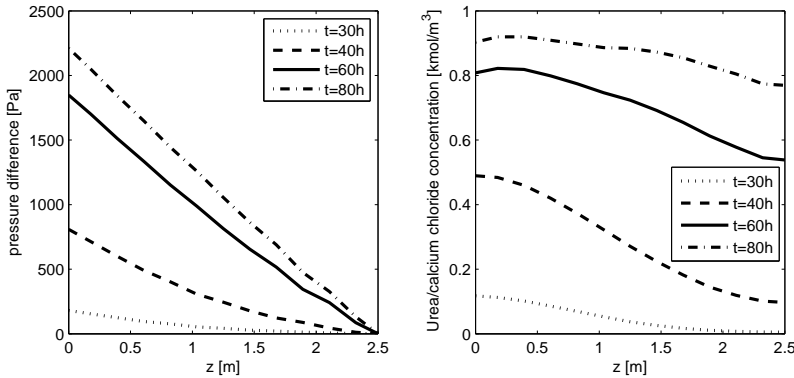


Figure 7.6: Left: The difference between the pressure at the middle extraction well and the hydrostatic pressure of water. Right: The concentration of urea and calcium chloride at the middle extraction well.

flow, this will happen first at the bottom of the extraction, which is illustrated by the curves for time  $t = 30h$  and  $t = 40h$  in the right plot of Figure 7.6. As a result, only in the lower part of the extraction well the pressure (difference) increases, which results into the quadratic-like shape of the pressure difference curves in the left plot of Figure 7.6 at  $t = 30h$  and  $t = 40h$ . Subsequently, the urea/calcium chloride concentration increases and also in higher regions the urea and calcium chloride reach the outflow, as shows the right plot of Figure 7.6. Consequently also the pressure further increases. Eventually, the urea/calcium chloride concentration is more or less constant over the depth. Due to this, finally the pressure distribution becomes linear again, while during the first time only an increase in the deeper parts was observed.

The pressure increase at the outflow at a depth of 2.5 m is approximately  $2.2 \times 10^3$  Pa. We do some simple calculations to get a feeling about the magnitude of this pressure difference. The hydrostatic pressure of water at this depth is  $1.25 \times 10^5$  Pa. This means that the pressure increase is 1.8% of the hydrostatic water pressure. This is not so very much, but flow is caused by pressure gradients rather than by the pressure itself. Given the inflow flow rate  $Q_{in}$  from Table 7.9, the cross section of  $5.6 \times 2.5 \text{ m}^2$ , the permeability  $k$  and viscosity  $\mu$  from this simulation and a distance of 5 m between injection and extraction, it can be calculated that a pressure difference of  $4.7 \times 10^3 \text{ Pa}$  between injection and extraction is needed to generate this flow rate. (Since injection and extraction lances are used, rather than injection and extraction sheets, the difference between the highest and lowest pressure in a horizontal cross section will be somewhat larger.) Compared to the pressure difference of  $4.7 \times 10^3 \text{ Pa}$ , the pressure increase of  $2.2 \times 10^3 \text{ Pa}$  due to the higher density is 47%. Hence, although the absolute pressure does not change so much, the pressure increase due to higher densities is significant compared to the other pressure differences, which henceforth gives a significant diversion of the flow.

Figure 7.7 shows a contour plot of the calcium carbonate concentration in the top and bottom of the domain at time  $t = 80h$ . The highest concentrations are around

the injection wells (the three blue circles left). Since there is urea and calcium chloride present during the whole simulated time the concentration is higher than around the extraction wells (the three blue circles right), which are only after some time reached by urea and calcium chloride. Due to density flow, the urea/calcium chloride concentration is also higher in the lower regions of the domain than in the higher ones. As a result, on the bottom, more calcium carbonate has been formed than in the top of the domain.

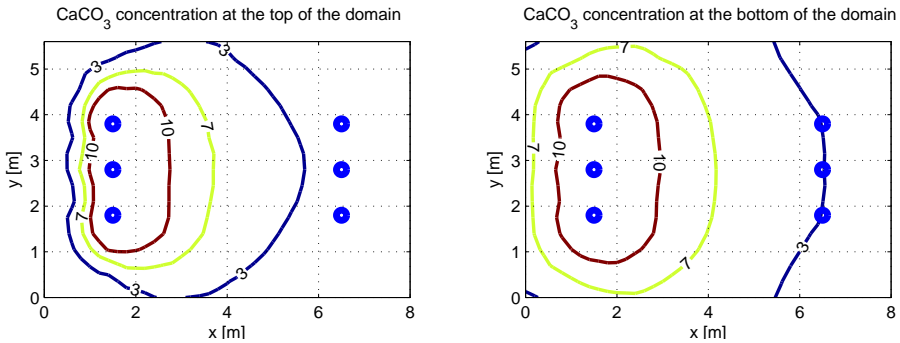


Figure 7.7: The calcium carbonate content in the top (left) and bottom (right) part of the domain at time  $t = 80h$ .

## 7.5 Discussion and Conclusions

This chapter shows three different methods to calculate the pressure on the boundary. In the first method, the lower Riemann sum is used to calculate the pressure and in the second method, the trapezoid rule is used. Both methods require that all the nodes lie on certain vertical lines. In the third method, the SUPG Finite Element method is used to calculate the pressure from the solution of a boundary value problem. The large advantage is that this also works for unstructured meshes. Contrary to the first two methods, it is not required that the nodes lie on certain vertical lines.

In Subsection 7.4.1, the three methods are compared on a (2D) rectangle for two different relations between density and height on a structured and an unstructured mesh. Method 1 is a first order method, while method 2 is a second order method. That agrees with the results. Although method 3 is a first order method, we approximate second order convergence for a small value of  $\xi$ . We approximate first order convergence for a larger value of  $\xi$ . The value of  $\xi$  can be chosen smaller than the value that is used in this chapter, which is  $\xi = 10^{-5}$ . A very small value, however, deletes the Streamline Upwind part of the SUPG method and brings the method back to the Standard Galerkin method (with its instabilities). On a structured mesh, the first method gives the largest error, while the second method gives

the smallest error. For unstructured meshes, only method 3 can be used to get satisfactory results.

In Subsection 7.4.2, the pressure is calculated on the outflow boundaries of the configuration in Figure 7.1. This is done for the same relations between density and height as in Subsection 7.4.1. Method 3 is used to calculate the density on the outflow boundaries and this numerical solution is compared with the analytical solution. This is done on four different meshes. The results show that method 3 is a proper method to calculate the pressure on the boundary.

In Subsection 7.4.3, the first part of the 100m<sup>3</sup> experiment as reported in [86] is simulated. Method 3 is used as a method to calculate the pressure on the outflow boundary at every time step. This results in a stable simulation and the results for the pressure are in agreement with the expectations.

The computing time for the various methods is comparable for coarse meshes but for an increasing number of elements, method 1 and 2 are faster than method 3. Since in method 3 a 2D calculation is performed to calculate the pressure on the boundary, the computing time will be small compared to the computing time for the 3D calculations on the full domain. For example, the computing time for the pressure on the outflow boundaries in the simulation of Subsection 7.4.3 is more than 800 times as small as for the 3D calculations in one time step on the full domain. Hence, the contribution to the overall CPU time is not significant, and thereby the overall CPU-time is about the same for all the three methods.

We can conclude that method 3 provides a good and robust scheme to calculate the pressure on the outflow boundary. It can be applied on a manifold that represents the boundary of some domain. It works for both unstructured and structured meshes. We note that the SUPG stabilization is needed to make the method robust. For the differences in eigenvalues of the system with SUPG stabilization and the system without SUPG stabilization we proved that  $|\lambda(h\xi) - \lambda| = \mathcal{O}(\xi)$ . In our observations, by applying the SUPG stabilization method, the zero eigenvalue is mapped onto a non-zero one, where its value scales with  $\xi$ . The value of  $\xi$  can be chosen very small, which for a reasonable mesh size gives the same convergence as the system without SUPG, but the value should be larger than the round off error of the computer with respect to the 8 bytes storage of floating numbers in Matlab.

Differential equation (7.14), which is solved to find the pressure on the boundary, only contains a  $z$ -derivative. The pressure in a certain point only depends on the density of the fluid straight above it. In this chapter, equation (7.14) is solved on the boundary (elements) only. This approach only works if the faces of the boundary are vertical, such that the fluid that determines the pressure in an arbitrary point at the boundary is on the boundary itself. If this is not the case, considering the (2D) boundary elements only is not sufficient. Instead, one should consider the 3D region above the boundary, since the density in this region determines the pressure on the boundary. Subsequently, one should solve differential equation (7.14) on this 3D subdomain to approximate the pressure on the boundary.



**Simulation of front instabilities in density driven flow, using a reactive transport model for Biogrout combined with a randomly distributed permeability field**

This chapter has been submitted to *Transport in Porous Media* as:

Van Wijngaarden, W.K., Van Paassen, L.A., Vermolen, F.J., Van Meurs, G.A.M., Vuik, C.: Simulation of front instabilities in density driven flow, using a reactive transport model for Biogrout combined with a randomly distributed permeability field.

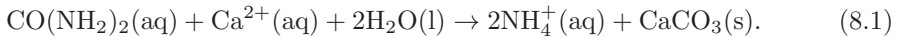
## Abstract

Biogrout is a method to strengthen granular soil, which is based on Microbial-Induced Carbonate Precipitation (MICP). To model the Biogrout process, a reactive transport model is used. Since high flow rates are undesirable for the Biogrout process, the model equations can be solved with a Standard Galerkin Finite Element Method. The Biogrout process involves the injection of dense fluids in the subsurface. In this paper we present our reactive transport model for Biogrout and use it to simulate an experiment in which a pulse of a dense fluid is injected in a porous medium filled with water. In the experiment front instabilities were observed in the form of fingers. The numerical simulations showed that the fingering phenomenon was less pronounced than in the experiment. By reducing the dispersion length and implementing a randomly distributed permeability field, the fingering phenomenon could be induced. Furthermore, the results of a case study to a Biogrout application is reported.

## 8.1 Introduction<sup>1</sup>

The current research is done within the framework of Biogrout. It is investigated what the effects of buoyancy driven flow and the associated fingering phenomenon can be on Biogrout.

The overall reaction equation for Biogrout is:



The substrates and by-product of this reaction are dissolved in water, which increases the fluid density. For example, a 1 molar calcium chloride/urea solution has a density of  $1.1 \times 10^3 \text{ kg/m}^3$ . If all the calcium chloride and urea of a 1 molar solution react, one ends up with a 2 molar ammonium chloride solution, which has a density of  $1.03 \times 10^3 \text{ kg/m}^3$ . In a fresh ground water environment, the dense fluid will move more easily downwards than upwards as a result of density differences. The forces of gravity and buoyancy can generate front instabilities in the form of fingers where a dense fluid is on top of a less dense fluid. In order to get the micro-organisms and their substrates at the desired location and extract the by-product, it is important to examine the effect of fingering on the flow and transport. This will help to decide which concentrations and what flow rate should be used and where the injection and extraction wells should be positioned.

To examine the effect of buoyancy driven flow and the associated fingering phenomenon an experiment has been performed, in which a pulse of saline fluid is injected in a porous media flow cell, generating a two-dimensional flow field. The flow cell is filled with glass beads and saturated with water. The saline pulse is followed by a pulse of water. The experimental results are compared with the outcome of numerical simulations. Besides, a Biogrout case study is performed and reported.

A lot of research on fingering has already been done, both on viscous fingering (Saffman-Taylor instabilities) and instabilities caused by density differences, see for

---

<sup>1</sup>Parts of the original introduction have been skipped in order to prevent too much repetition of the Introduction from Chapter 8.1.

example [26,29,42,78]. There are several approaches. One is the sharp interface approach in which the fluids are assumed to be immiscible, [15,25]. Another approach is the miscible fluid approach. If chemical reactions play a role (like in the Biogrout case), the miscible fluid approach should be taken, since the concentration can have a whole range of values and does not only have to be binary at the vicinity of a sharp interface, see for example [21,40,58,70,94].

The set-up of the experiment and the case study are given in the Sections 8.2 and 8.3. The reactive transport model for Biogrout, derived in [91] and [93] (Chapter 2 and 6), is presented in Section 8.4. Section 8.5 contains the numerical methods that are used to solve the model equations and Section 8.6 reports the results, including the effect of using a random porosity/permeability field to induce the fingering. In Section 8.7 some conclusions and discussion can be found.

## 8.2 Materials and Methods

To evaluate the effect of a buoyancy driven flow on the distribution of injected solutes, a two-dimensional porous media flow cell experiment is performed. The flow cell, constructed from a PVC frame with plexiglass front and back plates is 95 cm wide, 45 cm high and 3 cm thick. The space is filled with glass beads, with a grain size ranging up to 200  $\mu\text{m}$ . A picture of some glass beads is shown in Figure 8.1. Beside glass beads, also some crystals can be seen. These crystals result from the Biogrout experiment that is performed after the buoyancy-driven-flow-experiment, that is reported here. One injection well, a hollow steel tube, is installed at the center of the flow cell and two extraction wells are installed at mid height about 12 cm from the side of the flow cell as shown in Figure 8.2.

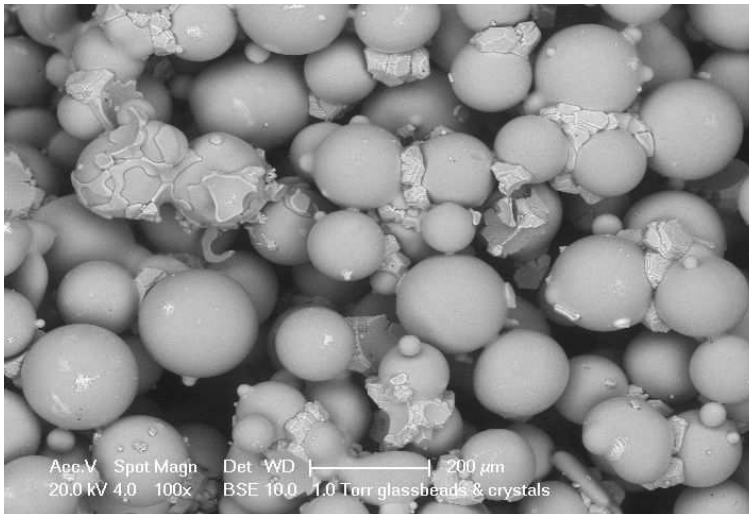


Figure 8.1: A picture of some glass beads (spheres) that are used in the buoyancy-driven-flow experiment.

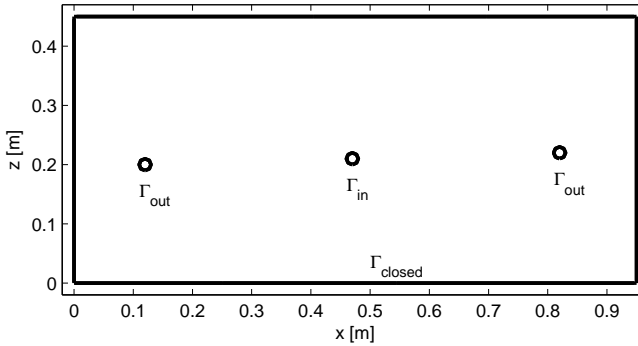


Figure 8.2: Set-up of the experiment. Injection well is denoted by  $\Gamma_{in}$  and the extraction wells by  $\Gamma_{out}$ . The other boundaries ( $\Gamma_{closed}$ ) are closed.

A solution of 0.5 M sodium chloride (NaCl) is prepared to which a bit of red food dye powder (Allura Red, E129) is added. The porous media flow cell is first filled with water and flushed for several hours. The flow rate at the injection and extraction wells is kept constant, where the injection flow rate is equal to the total extraction flow rate of about 300 mL/h. At a certain moment the sodium chloride solution is injected for a period of 30 minutes after which tap water is injected again. The flow of the red sodium chloride solution is monitored using a Canon G7 compact camera at 10 minutes time-lapse intervals.

### 8.3 Case study set-up

Since the scale of the experiment is quite small compared to practical applications, we also do a case study of an application of Biogrout, i.e. to create a cemented zone underneath a levee in order to prevent piping, [8, 9]. Piping is an important failure mechanism of levees in the Netherlands, [75]. Piping starts with heave and cracking of the soft soil top layer at the land side of the levee. The cracks in the top soft soil layer allow for seepage via the permeable sand layer underneath the clay levee. If the water level difference between river and land side is large enough, sand grains may be transported along with the water flow. This will create a pipe underneath the levee, which becomes wider and wider as the process proceeds. Finally, this will lead to failure of the levee and to breakthrough.

One way of decreasing the risk of failure of the levee due to piping is to broaden the levee. This will decrease the pressure gradients in the sandy layer, which is the driving force for the process. This, however, is expensive and not always possible,

for example because of existing buildings close to the levee.

In those cases, BiogROUT can be used to decrease the risk of failure due to piping. As it fixates the sand grains, it will prevent the creation of pipes, or block the propagation of pipes. While the BiogROUTed sand will only have a minor decrease of permeability, the seepage water will flow through the fixated sand body. Hence, the water will not seek another way and herewith the risk of pipe formation is reduced.

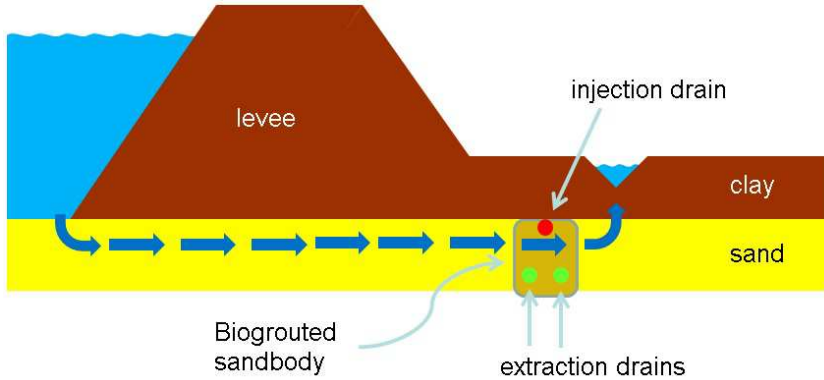


Figure 8.3: The configuration for the case study (cross-section). The levee is shown as well as the desired location of the BiogROUTed sand body. The location of the injection and extraction drains are indicated. The blue arrows display the seepage for a high water situation.

Figure 8.3 shows the cross-section of the configuration for the case study. It shows the levee and the desired location of the BiogROUTed sand body. The blue arrows indicate the seepage. The BiogROUTed sand and the top clay layer should be connected to prevent the formation of pipes in between. Therefore the injection drain is located close to the top clay layer. The extraction drains are two meters below the injection, since the dense fluid will tend to move downwards and since we assume that a BiogROUTed sandbody of 2 meters depth provides a sufficient barrier for the pipes. The distance between the extraction drains is two meters. This case study can be modelled through a 2D simulation, because of the symmetry. For our domain of computation  $\Omega$  we choose a depth of six meters and a width of four meters. We assume that these dimensions are large enough so that the numerical results are not affected by the location of the boundaries.

In the numerical simulation, the seepage is not taken into account. Therefore, we obtain a symmetrical situation. Because of this symmetry, we only calculate the part left to the injection drain and mirror the results. We take the mathematical model as described in Section 8.4.2 and the configuration as in Figure 8.3. We position the origin of the coordinate system above the red circle in this figure, i.e. on the symmetry axis, at the bottom of the clay layer. Then the coordinates of the centers of the extraction wells are  $(\pm 1, -2.2)$ . The radius of the extraction drains is 0.1 m. The injection is placed under the clay layer of the dike. As a simplification, we use a part of the symmetry axis as the inflow boundary, namely the line segment between  $z = -0.3$  m and  $z = -0.1$  m. Hence, a line segment is used as the injection

boundary rather than a semicircle.

As a flow rate, we choose  $Q_{in} = 0.5 \text{ m}^3$  per day per running meter of the drain (for the whole domain). For comparison: this is twice as much as the flow rate in the porous media flow cell experiment. To prevent that the dense fluid will sink away, we choose a larger extraction flow rate, that is  $Q_{out} = 2 \text{ m}^3$  per day per running meter of the drain for both the extraction drains. Since there are two extraction drains, the total extraction flow rate is eight times as large as the injection flow rate. The injection Darcy velocity  $q_{in}$  is calculated from the injection flow rate via  $q_{in} = Q_{in}/A_{in}$ , in which  $A_{in}$  is the surface of the injection. In the same way, we have that the extraction Darcy velocity  $q_{out}$  equals  $q_{out} = Q_{out}/A_{out}$ . The Biogrout liquids are injected for twelve hours, followed by the injection of water to rinse the soil. As the inflow concentration of urea and calcium we choose  $c_{in} = 0.5 \text{ kmol/m}^3$ . Afterwards, water is injected which implies that  $c_{in}$  is given by  $c_{in} = 0 \text{ kmol/m}^3$  for  $t > 12\text{h}$ . Since ammonium chloride is a reaction product, the injected concentration is equal to 0.

## 8.4 Mathematical Model

In this section, we describe the model equations that are used to simulate the experiment. The initial conditions and boundary conditions are given as well. This is done for the experiment as well as for the case study.

### 8.4.1 Model equations, initial and boundary conditions for the simulation of the experiment

In this subsection, we describe the mathematical model as well as the initial and boundary conditions that are used to simulate the experiment. This model is based on the reactive transport model for Biogrout as reported in [91] (Chapter 2) and slightly adapted for this experiment.

We assume that the flow is incompressible and therefore divergence free. Hence, in the domain  $\Omega$  we have for time  $t \geq 0$ :

$$\nabla \cdot \mathbf{q} = 0. \quad (8.2)$$

Here,  $\mathbf{q}$  [m/s] is the Darcy flow velocity .

For the relation between the Darcy flow velocity and the pressure, we use Darcy's law [100]:

$$\mathbf{q} = -\frac{k}{\mu}(\nabla p + \rho_l g \mathbf{e}_z), \quad (8.3)$$

in which  $k$  [m<sup>2</sup>] is the intrinsic permeability,  $\mu$  [Pa·s] is the dynamic viscosity of the fluid,  $p$  [Pa] is the pressure,  $\rho_l$  [kg/m<sup>3</sup>] is the density of the fluid and  $g$  [m/s<sup>2</sup>] is the gravitational constant.

The pore water velocity relates to the Darcy flow velocity via

$$\mathbf{v} = \frac{\mathbf{q}}{\theta}, \quad (8.4)$$

in which  $\theta$  [1] is the porosity.

Substituting equation (8.3) into equation (8.2) gives a partial differential equation for the pressure:

$$\nabla \cdot \left( \frac{k}{\mu} (\nabla p + \rho_l g \mathbf{e}_z) \right) = 0, \text{ in } \Omega. \quad (8.5)$$

This is the Oberbeck-Boussinesq approximation, see for example [26]. The Oberbeck-Boussinesq approximation consists in neglecting all density dependencies, except for the crucial buoyancy term  $\rho_l g$  in equations (8.3) and (8.5).

We model the intrinsic permeability as a function of the porosity via the Kozeny-Carman relation, [7]:

$$k = \frac{(d_m)^2}{180} \frac{\theta^3}{(1 - \theta)^2}. \quad (8.6)$$

In this equation,  $d_m$  [m] is the mean particle size. We assume that the porosity is log-normally distributed  $\theta \sim \log \mathcal{N}(\tilde{\mu}, \sigma^2)$ , see [47, 60].

Sodium chloride is dissolved in water. The resulting concentrations of sodium ( $\text{Na}^+$ ) and chloride ( $\text{Cl}^-$ ) are equal, because their relation in sodium chloride is 1:1. Since the concentrations of sodium and chloride are in the range of  $[0, 0.5]$ , all sodium and chloride ions will dissolve. Hence, it is not necessary to use a crystal precipitation model like [46]. We used the experimental outcomes of [95] to find a relation between the density of the fluid and the concentration of sodium (and chloride). In Figure 8.4 we plotted the fluid density against the concentrations of sodium and chloride and constructed a linear fit. The (average) slope of this graph is 41 kg/kmol. For a zero concentration, the density equals 1000 kg/m<sup>3</sup>. That gives the following relation for the density as a function of the sodium (and chloride) concentration:

$$\rho_l = 1000 + 41C^{\text{Na}^+}, \quad (8.7)$$

in which  $C^{\text{Na}^+}$  [kmol/m<sup>3</sup>] is the concentration of sodium (which is equal to the chloride concentration).

The concentration of sodium is modelled by an advection–dispersion-equation:

$$\frac{\partial(\theta C^{\text{Na}^+})}{\partial t} = \nabla \cdot (\theta \mathbf{D} \cdot \nabla C^{\text{Na}^+}) - \nabla \cdot (\mathbf{q} C^{\text{Na}^+}), \text{ in } \Omega. \quad (8.8)$$

In this equation,  $\mathbf{D}$  [m<sup>2</sup>/s] is the dispersion tensor, which coefficients equal  $D_{ij} = (\alpha_L - \alpha_T) \frac{v_i v_j}{|\mathbf{v}|} + \delta_{ij} \alpha_T \sum_i \frac{v_i^2}{|\mathbf{v}|} + \delta_{ij} D_m$ , see [100]. The constant  $\alpha_L$  [m] is the longitudinal dispersivity,  $\alpha_T$  [m] is the transverse dispersivity and  $D_m$  [m<sup>2</sup>/s] is the molecular diffusion coefficient. In this study, we choose smaller values for  $\alpha_L$  and  $\alpha_T$  than given in [34], because the amount of dispersion is relatively small as indicated by the presence of the fingers and the sharp fronts in the experiment. A large value for the entries in the dispersion tensor would never show the observed fingering behaviour. If dispersion would be more important, then the dependence of the dispersion lengths on the statistical distribution of the permeability can be incorporated. For more details and mathematical relations, we refer to [72, 73].

We assume that the dispersion tensors for sodium and chloride are equal. Furthermore, it is assumed that the porous medium is not charged. Together with similar initial and boundary conditions, we have that the sodium concentration and

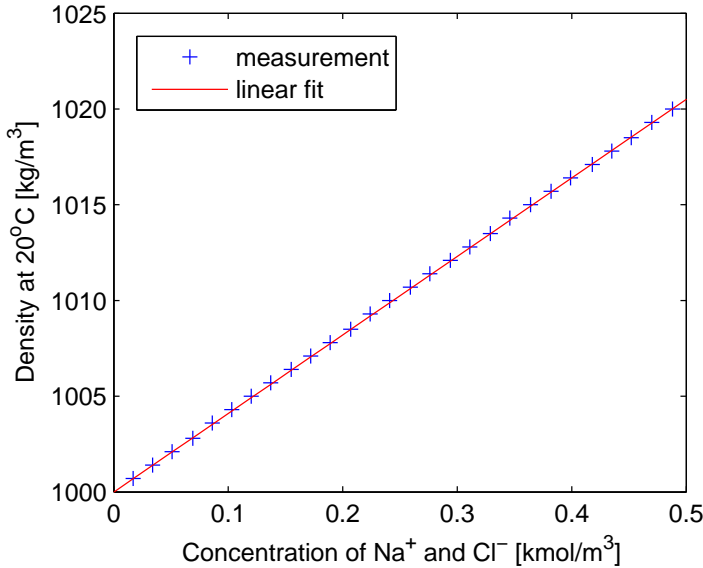


Figure 8.4: The density of the sodium and chloride solution plotted against the concentration. Experimental values and a linear fit:  $\rho_l = 1000 + 41C^{\text{Na}^+}$ .

the chloride concentration are equal. Hence, we consider only one concentration, the sodium concentration. In this paper we choose the longitudinal dispersivity equal to the transverse dispersivity,  $\alpha_L = \alpha_T$ . Usually, the transverse dispersivity is somewhat smaller than the longitudinal dispersivity as reported in [34]. We want the fronts as sharp as possible for the given mesh. A smaller dispersion length may lead to numerical instability, which is a result of the restriction on the mesh Péclet number in case of central differences, see [80]. Hence, we choose equal dispersivities for this research.

The experiment is modelled in 2D with the configuration as shown in Figure 8.2. The region is denoted by  $\Omega$ , which is bounded by  $\Gamma_{\text{closed}}$  and by the holes  $\Gamma_{\text{in}}$  and  $\Gamma_{\text{out}}$ . The interfaces with  $\Omega$  and the injection- and extraction wells are denoted by  $\Gamma_{\text{in}}$  and  $\Gamma_{\text{out}}$ , respectively. The diameter of the injection and extraction wells is 0.02m. The length of the domain is  $L_x = 0.95\text{m}$  and the height is  $L_z = 0.45\text{m}$ .

Initially, the pores are filled with tap water and hence, we have that  $C^{\text{Na}^+}(t = 0, \mathbf{x}) = 0$  in  $\Omega$ . In Table 8.1, the boundary conditions are given. Since the pressure should be prescribed somewhere to get a unique solution for the pressure, we choose to prescribe the pressure at the inflow. At the outflow boundaries we prescribe the flow rate  $q_{\text{out}}$ . The resulting injection flow rate will be twice as large as the extraction flow rate. Of course, there is no flow over the closed boundary. At the inflow boundary we prescribe the mass flux. We assume an advective flux at the outflow boundary and there is no flux over the closed boundary.

We use a mesh with more than three hundred thousand elements. We assign a value for the porosity to each element of this mesh. The values come from a

	$C^{\text{Na}^+}$	$\mathbf{q}$
$\Gamma_{in}$	$(\theta D\nabla C - \mathbf{q}C) \cdot \mathbf{n} = 2q_{out}c_{in}$	$p = p_{atm} + \rho_l(x, z)g(L_z - z)$
$\Gamma_{out}$	$(\theta D\nabla C) \cdot \mathbf{n} = 0$	$\mathbf{q} \cdot \mathbf{n} = q_{out}$
$\Gamma_{closed}$	$(\theta D\nabla C - \mathbf{q}C) \cdot \mathbf{n} = 0$	$\mathbf{q} \cdot \mathbf{n} = 0$

Table 8.1: Boundary conditions for the concentration and the flow.

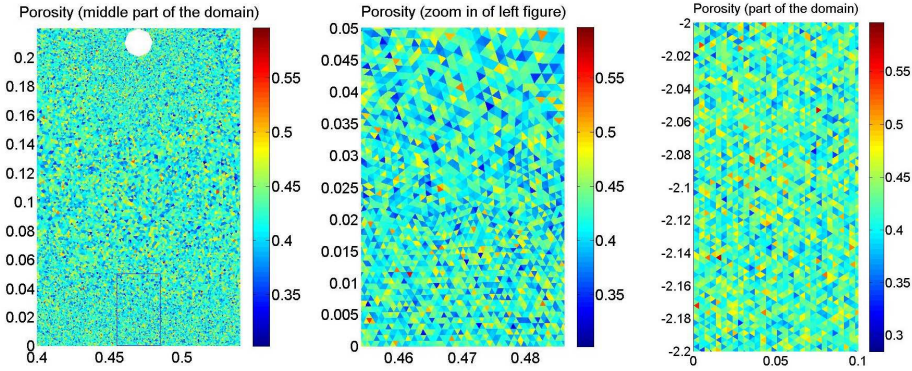


Figure 8.5: Porosity in a region where fingers appear during the simulations. Left: simulated porosity for the experiment. Middle: zoom in of left figure. Right: simulated porosity for the case study. The porosity is shown for a  $\log\mathcal{N}(0.42, 0.001)$  distribution.

log-normal distribution:  $\theta \sim \log\mathcal{N}(\tilde{\mu}, \sigma^2)$ . The mean  $M$  of this distribution equals  $M = e^{\tilde{\mu} + \sigma^2/2}$  and the variance  $V$  equals  $V = (e^{\sigma^2} - 1)e^{2\tilde{\mu} + \sigma^2}$ . From the mean  $M$  and the variance  $V$ , one can calculate the  $\tilde{\mu}$  and  $\sigma^2$  via  $\tilde{\mu} = \log\left(\frac{M^2}{V + M^2}\right)$  and  $\sigma^2 = \log\left(\frac{V + M^2}{M^2}\right)$ . For each simulation, we use the same sampling from the standard normal distribution for reasons of reproducibility. Subsequently, the resulting sample for each element is multiplied by the standard deviation of the normal distribution,  $\sigma$ , and then shifted by the mean of this distribution,  $\tilde{\mu}$ . Finally, the exponential value is computed, which finally results into  $\exp(\tilde{\mu} + \sigma\mathcal{N}(0, 1))$ . The variation in porosity is shown in the left two figures of Figure 8.5 for a  $\log\mathcal{N}(0.42, 0.001)$  distribution.

We calculate the intrinsic permeability  $k$  with the Kozeny-Carman relation (8.6). Since the permeability is a function of the porosity  $\theta$  and the porosity varies from element to element, the permeability varies as well. The scale of variation for the chosen mesh is 1.1 mm, which is the square root of the total surface divided by the number of elements.

The values that have been assigned to the various constants are given in Table 8.2. The value of  $q_{out}$  has been chosen in such a way that the red area at time  $t=0.5$  h in the simulation has the same magnitude as in the experiment. As a result, the pore water velocities at the inflow boundary are equal for all the simulations of the experiment.

$d_m$	$= 200 \mu\text{m}$	$\mu$	$= 10^{-3} \text{ Pa s}$
$D_m$	$= 10^{-9} \text{ m}^2/\text{s}$	$c_{in}$	$= \begin{cases} 0.5 \text{ kmol}/\text{m}^3 & 0 \leq t \leq 0.5 \text{ h} \\ 0 & \text{else} \end{cases}$
$q_{out}$	$= \text{M}/18000 \text{ m/s}$	$g$	$= 9.81 \text{ m/s}^2$
$\alpha_L$	$= 0.001 \text{ m}$	$\alpha_T$	$= 0.001 \text{ m}$
$p_{atm}$	$= 10^5 \text{ Pa}$		

Table 8.2: The values that are taken for the various constants.

### 8.4.2 Model equations, initial and boundary conditions for the case study

In this case study, we try to create a cemented zone underneath a levee in order to prevent piping. Under the clay layer of the levee, the Biogrout substrates are injected for twelve hours, followed by water injection to rinse the soil. Extraction drains are placed a few meters below the injection drain. In order to do this case study, we use the model for Biogrout as derived in [91] and [93] (Chapter 2 and 6). This model is based on the biochemical reaction equation (8.1).

The concentrations of urea, calcium ions and ammonium ions are modelled with the advection-dispersion-reaction equation:

$$\frac{\partial(\theta C^i)}{\partial t} = \nabla \cdot (\theta \mathbf{D} \nabla C^i) - \nabla \cdot (\mathbf{q} C^i) + m_i \theta r_{hp}. \quad (8.9)$$

In this equation,  $C^i$  is the concentration of species  $i$ ,  $i \in \{\text{urea}, \text{Ca}^{2+}, \text{NH}_4^+\}$ ,  $\mathbf{D}$  is again the dispersion tensor with coefficients as in Section 8.4.1,  $r_{hp}$  is the rate of the overall Biogrout reaction (8.1) and  $m_i$  is a constant that follows from the stoichiometry of the reaction. As urea and calcium are consumed in the same ratio, their values of  $m_i$  are equal and negative:  $m_{\text{urea}} = m_{\text{Ca}^{2+}} = -1$ . For the produced ammonium we have  $m_{\text{NH}_4^+} = 2$ . The reaction rate  $r_{hp}$  is modelled with the following relation:

$$r_{hp} = v_{max} S^{bac} \frac{C^{urea}}{K_{m,urea} + C^{urea}}, \quad (8.10)$$

in which  $v_{max}$  in  $\text{kmol}/\text{m}^3/\text{s}$  is the maximal microbial activity constant,  $K_{m,urea}$  [ $\text{kmol}/\text{m}^3$ ] is the saturation constant of urea and calcium chloride and  $S^{bac}$  [1] is the ratio of micro-organisms (with respect to the injected concentration) that is fixated in the placement procedure prior to the injection of the cementation fluids.

Since it is assumed that calcium carbonate is not transported, there is only a reaction term in the differential equation for the time derivative of its concentration:

$$\frac{\partial C^{\text{CaCO}_3}}{\partial t} = m_{\text{CaCO}_3} \theta r_{hp}. \quad (8.11)$$

In this equation,  $C^{\text{CaCO}_3}$  [ $\text{kg}/\text{m}^3$ ] is the concentration of calcium carbonate in mass per total volume rather than per liquid volume and  $m_{\text{CaCO}_3}$  in  $\text{kg}/\text{kmol}$  is the molar mass of calcium carbonate which is used to convert from kilomoles into kilograms.

As illustrated in Figure 8.1, the calcium carbonate crystals are formed in the pores. This causes a decrease in porosity, where the increase of volume of calcium

carbonate is equal to the decrease of pore space. Hence the following differential equation holds:

$$\frac{\partial \theta}{\partial t} = -\frac{1}{\rho_{CaCO_3}} \frac{\partial C^{CaCO_3}}{\partial t}, \quad (8.12)$$

in which  $\rho_{CaCO_3}$  [kg/m<sup>3</sup>] is the density of calcium carbonate. From the above differential equation the following relation between the porosity and the calcium carbonate content is derived:

$$\theta(\mathbf{x}, t) = \theta(\mathbf{x}, 0) - \frac{C^{CaCO_3}(\mathbf{x}, t) - C^{CaCO_3}(\mathbf{x}, 0)}{\rho_{CaCO_3}}. \quad (8.13)$$

Note that the above relation is an averaged approach compared to the upscaling approaches by [10] and [82].

For the flow, we also use the Oberbeck-Boussinesq approximation, see equations (8.2)-(8.5). However, since the liquid volume decreases due to the reaction and since a solid (calcium carbonate) is formed in the pore space, the right-hand side of equation (8.2) (and hence equation (8.5)) is not equal to zero. Instead, we have:

$$\nabla \cdot \mathbf{q} = K\theta r_{hp}. \quad (8.14)$$

The constant  $K$  [m<sup>3</sup>/kmol] has been defined as

$$K := \left( \frac{m_{CaCO_3}}{\rho_{CaCO_3}} - (1 - V_s) \right). \quad (8.15)$$

As a result of the production of the solid calcium carbonate in the pores, there is less space available for the fluid. The decrease in pore space per unit of time is  $m_{CaCO_3}/\rho_{CaCO_3}\theta r_{hp}$ . This process is partly cancelled since the hydrolysis and precipitation reactions cause a decrease in liquid volume. The decrease of liquid volume per kmol reacted urea/calcium chloride equals  $1 - V_s$ . For more details, we refer to [93] (Chapter 6). In absence of the reaction ( $r_{hp} = 0$ ), this is again the Oberbeck-Boussinesq approximation. Substitution of Darcy's law (8.3) gives the following partial differential equation for the pressure:

$$\nabla \cdot \left( -\frac{k}{\mu} (\nabla p + \rho_l g \mathbf{e}_z) \right) = K\theta r_{hp}. \quad (8.16)$$

Again, we use the Kozeny-Carman relation (8.6) to model the intrinsic permeability as a function of the porosity. The porosity is again lognormally distributed, with mean  $M = 0.42$  and variance  $V = 0.001$ . In the right plot of Figure 8.5 a part of the porosity distribution in the domain of computation is shown. In this case study, urea, calcium chloride and ammonium chloride are dissolved, rather than sodium chloride. Hence, the liquid density depends on these species. As a relation between the liquid density  $\rho_l$  [kg/m<sup>3</sup>], and the urea concentration ( $C^{urea}$  [kmol/m<sup>3</sup>]), the concentration of calcium ions ( $C^{Ca^{2+}}$  [kmol/m<sup>3</sup>]) and the ammonium concentration ( $C^{NH_4^+}$  [kmol/m<sup>3</sup>]) we have:

$$\rho_l = 1000 + 15.4996C^{urea} + 86.7338C^{Ca^{2+}} + 15.8991C^{NH_4^+}. \quad (8.17)$$

The values that have been assigned to the various parameters are partly given in Table 8.2. The used parameters that are not given in that table and the parameters that have another value as in the simulation of the experiment, are given in Table 8.3.

$m_{\text{CaCO}_3} = 100.1 \text{ kg/kmol}$	$1 - V_S = 0.02965 \text{ m}^3/\text{kmol}$
$\rho_{\text{CaCO}_3} = 2710 \text{ kg/m}^3$	$v_{\text{max}} = 4.26 \times 10^{-5} \text{ kmol-urea/m}^3/\text{s}$
$K_{m,\text{urea}} = 0.01 \text{ kmol/m}^3$	$S^{\text{bac}} = 0.25$
$A_{\text{in}} = 0.2 \text{ m}$	$Q_{\text{in}} = 0.25 \text{ m}^3/\text{day/meter drain}$
$A_{\text{out}} = 0.628 \text{ m}$	$Q_{\text{out}} = 1.00 \text{ m}^3/\text{day/meter drain}$
$q_{\text{in}} = Q_{\text{in}}/A_{\text{in}}$	$q_{\text{out}} = Q_{\text{out}}/A_{\text{out}}$
$\alpha_L = 0.002 \text{ m}$	$c_{\text{in}} = \begin{cases} 0.5 \text{ kmol/m}^3 & 0 \leq t \leq 12 \text{ h} \\ 0 & \text{else} \end{cases}$
$\alpha_T = 0.002 \text{ m}$	

Table 8.3: The values that are taken for the various constants in the case study.

We use a mesh with almost two million elements. Since the porosity varies from element to element, the scale of variation (defined by the square root of the total surface divided by the number of elements) is 2.5 mm.

The boundary conditions for the flow and concentration in this case study are shown in Table 8.4. We have a no flux condition on the top boundary and the symmetry boundary. At the injection boundary, we prescribe the flow rate and the mass flux. At the extraction boundary, we also prescribe the flow rate and since the concentration is unknown beforehand, we assume an advective flux. At the bottom, right (and left) boundary, we assume hydrostatic pressure. We assume an advective flux in case of outflow over these boundaries and a zero mass flux in case of inflow, although we aimed at choosing the boundaries sufficiently far away such that the concentration at the boundary is (approximately) equal to zero. As an initial condition for the aqueous concentrations, we take  $C^{\text{urea}} = C^{\text{Ca}^{2+}} = C^{\text{NH}_4^+} = 0 \text{ kmol/m}^3$ , for all points in the domain of computation at time  $t=0 \text{ h}$ . Initially, there is no calcium carbonate present in the domain:  $C^{\text{CaCO}_3} = 0 \text{ kg/m}^3$ , for all points in the domain of computation at time  $t=0 \text{ h}$ . The partial differential equations for the concentrations of urea and calcium are equal (assuming that the dispersion coefficients are equal as well). Since the initial and boundary conditions are also similar, these concentrations are equal. We will only show some results for the urea concentration.

## 8.5 Numerical Methods

In this section, we explain which numerical methods are used to solve the partial differential equations.

The partial differential equations are solved using the Standard Galerkin Finite Element Method, with triangular elements and linear functions of local basis.

Since high flow rates are not desirable in the Biogrout process, the advection is not dominant and an upwind/stabilization method is not necessary. Since an upwind

Boundary	Concentration	Flow
symmetry boundary	$(\mathbf{q}C - D\theta\nabla C) \cdot \mathbf{n} = 0$	$\mathbf{q} \cdot \mathbf{n} = 0$
top boundary (‘closed’ clay layer)	$(\mathbf{q}C - D\theta\nabla C) \cdot \mathbf{n} = 0$	$\mathbf{q} \cdot \mathbf{n} = 0$
injection boundary	urea and calcium: $(\mathbf{q}C - D\theta\nabla C) \cdot \mathbf{n} = -q_{in}c_{in}$	$\mathbf{q} \cdot \mathbf{n} = -q_{in}$
	ammonium: $(\mathbf{q}C - D\theta\nabla C) \cdot \mathbf{n} = 0$	$\mathbf{q} \cdot \mathbf{n} = -q_{in}$
extraction boundaries	$(D\theta\nabla C) \cdot \mathbf{n} = 0$	$\mathbf{q} \cdot \mathbf{n} = q_{out}$
right and bottom boundary (open)	if $\mathbf{q} \cdot \mathbf{n} > 0$ : $(D\theta\nabla C) \cdot \mathbf{n} = 0$ else: $(\mathbf{q}C - D\theta\nabla C) \cdot \mathbf{n} = 0$	$p = 2 \cdot 10^5 +$ $-\rho_l g(z - \min(z))$

Table 8.4: The boundary conditions for the case study.

method decrease the order of convergence, in our case the Standard Galerkin method is a better choice.

The partial differential equations are multiplied by a test function  $\eta$  and integrated over the domain  $\Omega$  to derive the weak formulation. For the time integration an implicit Euler scheme is used.

The Newton-Cotes quadrature rules are used for the calculation of the element matrices and vectors. From these element matrices and vectors, the large matrices and vector are built in MATLAB (R2013b\_64). The MATLAB standard direct solver is used to solve the subsequent systems. As a time step we choose  $\Delta t = 36s$ .

Most equations are coupled. We solve them decoupledly and check the mass balances. It appears that the relative deviation is only in the order of tenths of a percent over the entire simulation.

In order to simulate the experiment, the various partial differential equations are solved and updates are done in the following order (in pseudo code):

1.  $\rho_l^{n+1}$  :  $\rho_l^{n+1} = \rho(C^{Na^+,n})$ , according to equation (8.7);
2.  $p^{n+1}$  :  $\nabla \cdot \left( \frac{k}{\mu} (\nabla p^{n+1} + \rho_l^{n+1} g \mathbf{e}_z) \right) = 0$ , partial differential equation (8.5);
3.  $\mathbf{q}^{n+1}$ :  $\mathbf{q}^{n+1} = -\frac{k}{\mu} (\nabla p^{n+1} + \rho_l^{n+1} g \mathbf{e}_z)$ , partial differential equation (8.3);
4.  $C^{Na^+,n+1}$  :  $\left( \theta C^{Na^+,n+1} - \theta C^{Na^+,n} \right) / \Delta t = \nabla \cdot (\theta \mathbf{D}^{n+1} \nabla C^{Na^+,n+1}) +$   
 $-\nabla \cdot (\mathbf{q}^{n+1} C^{Na^+,n+1})$ , partial differential equation (8.8).

The following list presents in pseudo code the order in which the equations are solved and the updates are done for the Biogrout case study:

1.  $\rho_l^{n+1}$  :  $\rho_l^{n+1} = \rho(C^{urea,n}, C^{Ca^{2+},n}, C^{NH_4^+,n})$ , from equation (8.17);
2.  $\theta^{n+1}$  :  $\theta^{n+1} = \theta(\theta_0, C^{CaCO_3,n})$ , from equation (8.13);
3.  $k^{n+1}$  :  $k^{n+1} = k(\theta^{n+1})$ , from equation (8.6);

4.  $p^{n+1} : \nabla \cdot \left( \frac{k^{n+1}}{\mu} (\nabla p^{n+1} + \rho_l^{n+1} g \mathbf{e}_z) \right) = K \theta^{n+1} r_{hp}^n$ , from partial differential equation (8.16);
5.  $\mathbf{q}^{n+1} : \mathbf{q}^{n+1} = -\frac{k^{n+1}}{\mu} (\nabla p^{n+1} + \rho_l^{n+1} g \mathbf{e}_z)$ , from partial differential equation (8.14);
6.  $C^{urea,n+1} : (\theta^{n+1} C^{urea,n+1} - \theta^n C^{urea,n}) / \Delta t = \nabla \cdot (\theta^{n+1} \mathbf{D}^{n+1} \nabla C^{urea,n+1}) - \nabla \cdot (\mathbf{q}^{n+1} C^{urea,n+1}) - \theta r_{hp}^{n+1}$ , from partial differential equation (8.9). Due to the reaction term, this partial differential equation is non linear in the urea concentration. Newton's method is used to deal with that;
7.  $C^{NH_4^+,n+1} : (\theta^{n+1} C^{NH_4^+,n+1} - \theta^n C^{NH_4^+,n+1}) / \Delta t = \nabla \cdot (\theta^{n+1} \mathbf{D}^{n+1} \nabla C^{NH_4^+,n+1}) - \nabla \cdot (\mathbf{q}^{n+1} C^{NH_4^+,n+1}) - \theta r_{hp}^{n+1}$ , from partial differential equation (8.9). The values for  $r_{hp}^{n+1}$  follow from the last Newton iteration in the previous step;
8.  $C^{CaCO_3,n+1} : (C^{CaCO_3,n+1} - C^{CaCO_3,n}) / \Delta t = m_{CaCO_3} \theta^{n+1} r_{hp}^{n+1}$ , from partial differential equation (8.11).

We also investigated the effect of inner iterations on the results. This was done by recalculating the density at each time step. If the difference between the previously calculated density was larger than some tolerance, the equations were solved with the updated density until the difference was smaller than some tolerance. Figure 8.6 shows some results for the scheme for Biogrout, proposed above. The left plot of Figure 8.6 shows the convergence behaviour on a cross section for a two-dimensional Biogrout test case. In each refinement step, the time step size is divided by two and the mesh size is divided by  $\sqrt{2}$ , since the expected order of convergence is  $\mathcal{O}(h^2 + \Delta t)$ , with  $h$  a measure for the mesh size and  $\Delta t$  the size of the time step. Figure 8.6 shows a nice convergence behaviour. In the right plot of this figure, the scheme without inner iterations is compared to the scheme with inner iterations. This is done for the coarsest and the finest simulation. It appears that the scheme with inner iterations only leads to small differences compared to the scheme that was proposed here. When using small time steps, there were no noticeable changes. Similar results were obtained for the other scheme, while investigating the effect of inner iterations on the results.

## 8.6 Results

### 8.6.1 Results of the experiment and a simulation with a homogeneous porous medium

This section reports some results of the two-dimensional porous media flow cell experiment that has been performed. The experimental results are compared to the results of a simulation using a constant porosity and permeability. The left column of Figure 8.7 shows some results of the flow cell experiment. The red fluid is the dense fluid. The colour of the zones, where only water is present, ranges from white

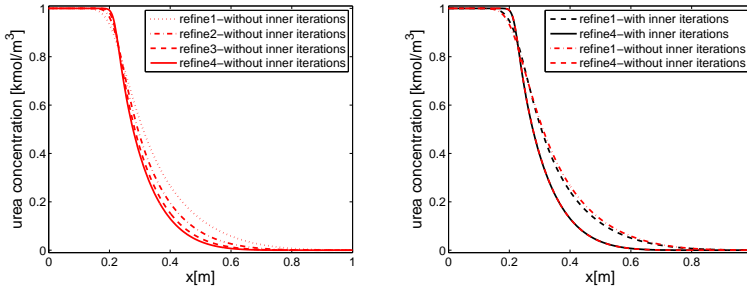


Figure 8.6: Left: the convergence of the Biogrout scheme without inner iterations. Right: the scheme without inner iterations compared to the scheme with inner iterations.

to yellow, depending on the day light and the artificial light. The colours in between this background colour and the red colour correspond to a concentration between 0 and the injected concentration which is  $0.5 \text{ kmol/m}^3$ , but the exact relation is not known. At  $t=0.5\text{h}$ , the injection of the dense fluid stops and the injection of water starts. This gives the red ring in the pictures for  $t=1\text{h}$ ,  $t=2\text{h}$ ,  $t=3\text{h}$ ,  $t=4\text{h}$  and  $t=5\text{h}$ . From  $t=2\text{h}$ , fingers appear on roughly two locations: on the bottom of the ring; and on the top of the ring where the heavy fluid is above the less dense fluid. In either case, fingers appear on positions where a dense fluid is on top of a less dense fluid. Note that the fingers on the bottom of the ring are larger.

The right column of Figure 8.7 shows some results of a simulation of this experiment, using a porosity of  $\theta=0.42$  and a permeability of  $k = 5.0 \times 10^{-11} \text{ m}^2$ . As can be seen in the simulation, no fingers appear. Apparently, the numerical noise is not sufficient to trigger the fingering. Hence, in the next section, we will vary the porosity and permeability to trigger the fingering.

### 8.6.2 Numerical results for an inhomogeneous porosity

In this section we use an inhomogeneous porosity within our simulations. We assign a value for the porosity to every element of the mesh. The values come from a log-normal distribution:  $\theta \sim \log\mathcal{N}(\tilde{\mu}, \sigma^2)$ . We vary the mean porosity  $M$  and the variance  $V$  of this distribution and do several simulations. As the mean  $M$  we choose:  $M = 0.36$ ,  $M = 0.42$  and  $M = 0.49$ . For the variance we choose:  $V = 0.0001$ ,  $V = 0.001$  and  $V = 0.005$ . This results in nine different combinations. From the mean  $M$  and the variance  $V$ , one can calculate the  $\tilde{\mu}$  and  $\sigma^2$  via  $\tilde{\mu} = \log\left(\frac{M^2}{V+M^2}\right)$  and  $\sigma^2 = \log\left(\frac{V+M^2}{M^2}\right)$ . The permeability that corresponds to a mean porosity of  $M = 0.36$  equals  $k = 2.5 \times 10^{-11} \text{ m}^2$ , according the Kozeny-Carman relation (8.6). The corresponding permeabilities of the means  $M = 0.42$  and  $M = 0.49$  are  $k = 5.0 \times 10^{-11} \text{ m}^2$  and  $k = 10 \times 10^{-11} \text{ m}^2$ , respectively.

In the right column of Figure 8.8 some results are shown for one of the simulations. In this simulation, the mean porosity is  $M = 0.42$  and the variance is  $V = 0.001$ .

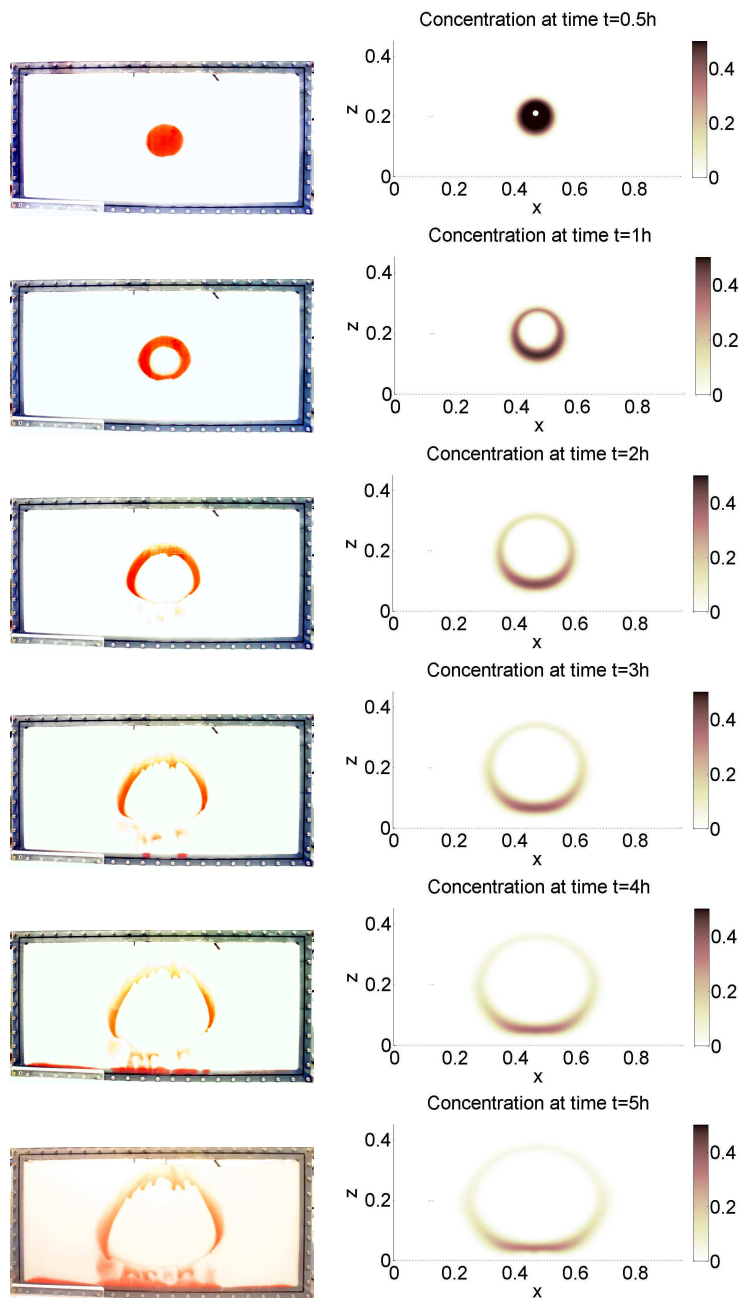


Figure 8.7: Some pictures of the experiment (left) and the numerical simulation with a homogeneous porous medium (right) at several times (from top to bottom:  $t=0.5h$ ,  $t=1h$ ,  $t=2h$ ,  $t=3h$ ,  $t=4h$  and  $t=5h$ ). In the simulation, the porosity  $\theta$  equals  $\theta=0.42$  and the intrinsic permeability  $k$  is  $k = 5.0 \times 10^{-11} \text{ m}^2$ .

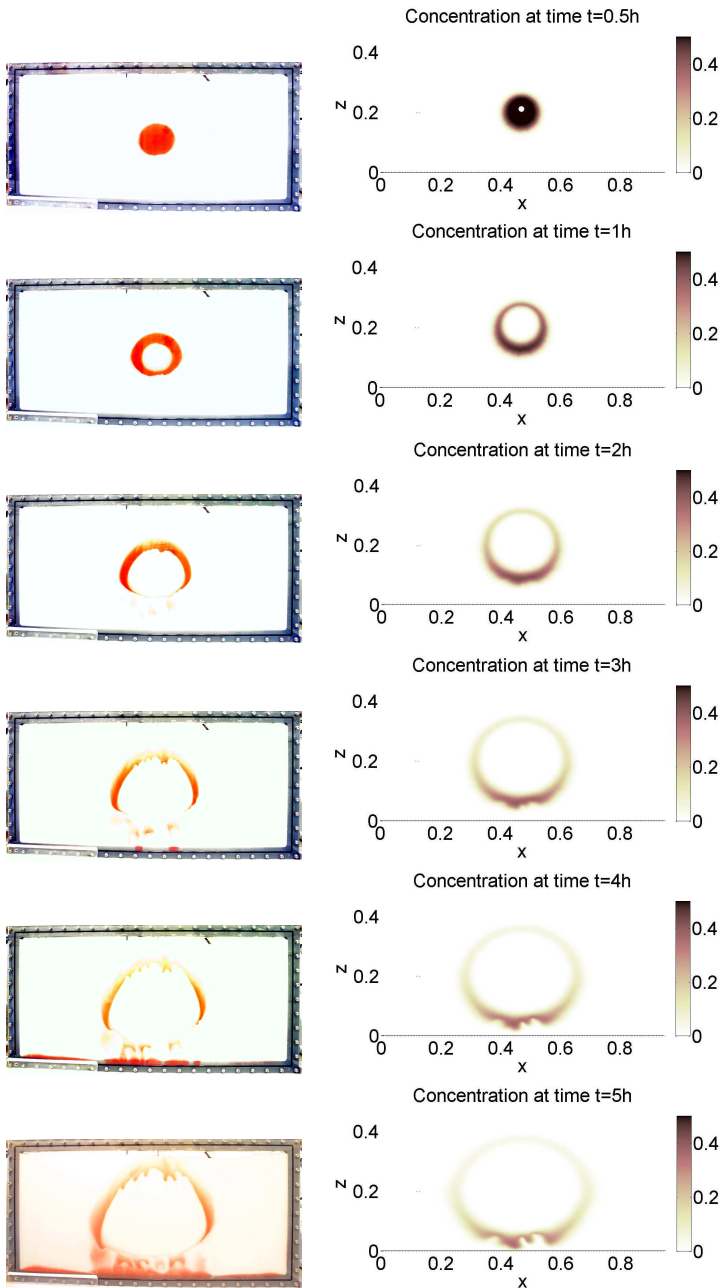


Figure 8.8: Some pictures of the experiment (left) and the numerical simulation (right) at several times (from top to bottom:  $t=0.5\text{h}$ ,  $t=1\text{h}$ ,  $t=2\text{h}$ ,  $t=3\text{h}$ ,  $t=4\text{h}$  and  $t=5\text{h}$ ). In the numerical simulation, the medium is inhomogeneous with a mean porosity of  $\theta=0.42$  and a variance of  $0.001$ . This mean porosity corresponds to an intrinsic permeability of  $k = 5.0 \times 10^{-11} \text{ m}^2$ .

In the numerical simulation with the homogeneous medium, of which the results are shown in Figure 8.7, no fingers appear. In contrast to this simulation, we now see the same phenomenon as in the experiment in Figure 8.8. Moreover, fingers start to appear at approximately the same time as in the experiment.

There are also some differences between modelling and the experiment. In the simulation, the fingers only appear on the bottom side of the ring, whereas in the experiment, also some small fingers appear at the bottom side of the top of the ring. Furthermore, the speed of the fingers in the experiment is larger than in the numerical simulation. From the results of the experiment, it can be seen that the layer close to the lowest boundary is more permeable than elsewhere. At time  $t=4h$ , the red fluid reaches the bottom and in one hour (at time  $t=5h$ ) it has already reached the left and right boundary. Apparently, there is some space between the frame and the plexiglass.

Figure 8.9 shows the effect of the value of the variance. Since the random number generator is reset before every simulation, the values of the porosity are constructed from the same set of random numbers, as explained in Section 8.4. Hence, the fingers appear at the same location. The magnitude, however, depends on the value of the variance. A larger variance results in longer fingers.

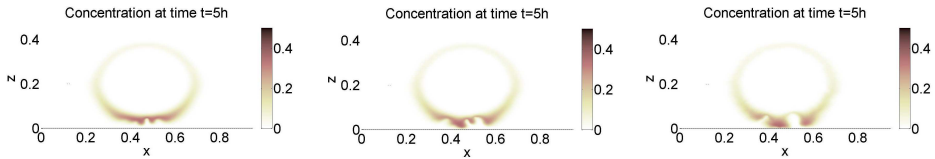


Figure 8.9: The concentration given at time  $t = 5h$ . The mean porosity is  $M = 0.42$ . The variance is  $V = 0.0001$  (left),  $V = 0.001$  (middle) and  $V = 0.005$  (right).

Figure 8.10 displays the effect of the variation of the mean  $M$ . Clearly, the value of the mean has a large effect on the fingering phenomenon. For a small mean, hardly any fingers arise. A larger mean results into more fingers and clearly the bottom is reached earlier. The effect of the mean value of the porosity on the density effect is explained below. Remember that the pore water velocity at the inlet is kept constant in the simulations.

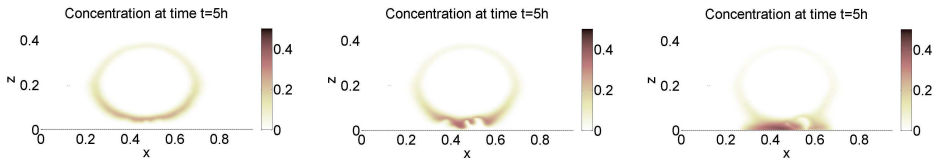


Figure 8.10: The concentration given at time  $t = 5h$ . The variance is  $V = 0.001$ . The mean porosity is  $M = 0.36$  (left),  $M = 0.42$  (middle) and  $M = 0.49$  (right).

The pore water velocity is determined by combining equations (8.3), (8.4) and (8.6):

$$v_x = -\frac{(d_m)^2}{180\mu} \frac{\theta^2}{(1-\theta)^2} \frac{\partial p}{\partial x}, \tag{8.18}$$

$$v_z = -\frac{(d_m)^2}{180\mu} \frac{\theta^2}{(1-\theta)^2} \frac{\partial p}{\partial z} - \frac{(d_m)^2}{180\mu} \frac{\theta^2}{(1-\theta)^2} \rho_l g. \tag{8.19}$$

In case of a higher porosity, the term  $\frac{\theta^2}{(1-\theta)^2}$  is also larger. Now remember that the pore water velocity at the inlet is constant. Hence, the increase in the porosity term in the first term at the right hand side of equations (8.18) and (8.19) is compensated by smaller pressure gradients in these terms. Now, let the ratio between the buoyancy term and the pressure gradient term in the right-hand side of equation (8.19) be a measure for the effect of the density differences. This ratio equals:  $\rho_l g / \frac{\partial p}{\partial z}$ . A higher porosity results in smaller pressure gradients and therefore the value of this ratio increases which indicates a larger effect of density differences.

To quantify the effect of the porosity on the downward movement of the dense fluid, the lowest location of the front is plotted as a function of time in Figure 8.11. For every time step, this location is determined by finding the smallest z-value for which the concentration exceeds some threshold. As a threshold, we choose  $C^{threshold} = 0.05 \text{ kmol/m}^3$ . Figure 8.11 displays some results for various values of the mean and the variance. This figure confirms the observations in Figure 8.10: if the mean is larger, the dense fluid moves faster downwards. Furthermore, a larger variance results in larger fingers, as we concluded from Figure 8.9. As a result, the dense fluid is earlier at the bottom of the domain. In our simulations, the variation of the mean has a larger effect on the fingering than the variation of the variance.

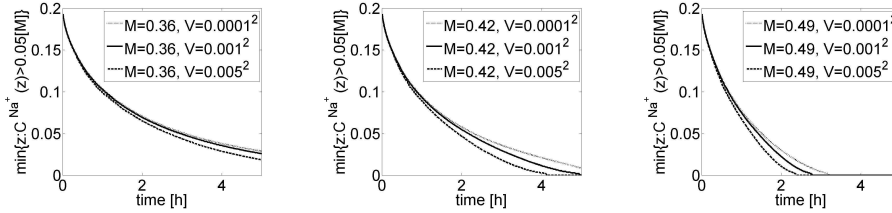


Figure 8.11: The lowest position of the dense fluid as a function of time for various values of the mean and the variance. The mean porosity is  $M = 0.36$  (left),  $M = 0.42$  (middle) and  $M = 0.49$  (right).

### 8.6.3 Variation in substrate concentration

In this section, we vary the inflow concentration of the dense fluid to investigate its effect. In the previous section,  $c_{in} = 0.5 \text{ kmol/m}^3$  has been used as an inflow concentration, like in the experiment. In this section we choose  $c_{in} = 1 \text{ kmol/m}^3$  and  $c_{in} = 2 \text{ kmol/m}^3$ . As a mean porosity we set  $M = 0.42$  and for the variance  $V = 0.001$  is chosen. Figure 8.12 shows the concentration at consecutive times for the various inflow concentrations. For these inflow concentrations, the flow is considerably affected by the density differences. A higher inflow concentration results into a heavier fluid. Thereby the gravity component is larger and hence the dense fluid reaches the bottom earlier. Since the gravity component becomes more significant for a higher inflow concentration, the pressure term is relatively less important, and this results into a buoyancy-dominated flow. Since the bottom is earlier reached, there is less time for the formation of fingers. At the other hand, the density differences are larger, which is in favour of the formation of the fingers.

### 8.6.4 Case study simulations

In this section we present the results of the case study simulations. We use the configuration, initial and boundary conditions as proposed in Section 8.4.2, combined with the heterogeneous porosity distribution. The aim is to construct a calcium carbonate wall as a barrier for the pipes. In order to prevent waste of materials, it is desirable that the urea (and calcium) are consumed rather than extracted. Besides that, it is necessary to remove the ammonium because of its impact on the environment.

#### Development of the various concentrations

Figure 8.13 shows how the concentrations of urea, calcium carbonate and ammonium develop in the domain of computation. The concentration profiles are shown at several times. After 12 hours, the injection of the Biogrout substrates (in the top of the domain) was stopped and the water injection started. This causes a region around the injection well with zero urea concentration, which is visible in the plot of the urea (and calcium) concentration at time  $t=13\text{h}$ . The urea is forced downwards by injection/extraction and by the density differences. At time  $t=13\text{h}$ , the large urea plume just started splitting in two large fingers. We see the same for the produced ammonium. In the right plot of Figure 8.5, the initial porosity distribution is shown for this particular region.

At time  $t=22\text{h}$ , in the same region small fingers arise, but also at the deepest location of the urea and ammonium front. At time  $t=25\text{h}$ , these small fingers are increased.

At time  $t=45\text{h}$ , the urea and calcium are consumed and the calcium carbonate wall has his final shape. A barrier for the pipes has been formed. The plot of the ammonium concentration for this time shows that more and more fingers arise. Due to density differences, these fingers tend to flow down. At the other hand, the extraction (indicated by the white circles) pulls them upwards.

### Extraction of ammonium

In the left column of Figure 8.14 is shown how the ammonium concentration evolves further in time. The heterogeneous porosity causes the ammonium plume to split into two parts (time  $t=22$  h) and later on in multiple fingers that are being extracted (times  $t=60$  h and  $t=100$  h). On the symmetry axis  $x=0$ , the horizontal fluid velocity caused by the extraction drains is equal to zero, since the effect of the one extraction well is cancelled by the other. Closer to the extraction drain, the horizontal velocity in the direction of the drain increases. The splitting of the ammonium plume brings the ammonium closer to the extraction wells. After all the urea is consumed, the ammonium concentration decreases as a result of the extraction. Hence, the density difference with the surrounding water decreases, which makes it easier to extract the ammonium. After 100 hours, only 4 mol ammonium is left in the domain and 121 mol ammonium was extracted.

### Comparison with a homogeneous porosity distribution

We repeated the same simulation for a homogeneous porosity. The ammonium concentration at several times is shown for this simulation in the right column of Figure 8.14. In this case, only one plume is observed and no fingers appear. The ammonium plume moves downwards between the extraction wells. Although the flow rate of the extraction wells is eight times as large as the injection flow rate, only a part of the ammonium is extracted. After 100 hours, only 50 mol is extracted, while 75 mol ammonium is still in the soil. In these simulations, the formation of fingers is advantageous for the removal of ammonium.

Figure 8.15 shows the distribution of the calcium carbonate for the simulation with the heterogeneous porosity distribution and the one with the homogeneous porosity. The aim is to create a calcium carbonate wall below the clay layer of at least two meters length to decrease the risk on piping. The top two meters of the calcium carbonate wall are similar for both simulations. Below these two meters, the distribution of calcium carbonate is rather different. The fingers in the urea and ammonium plume in the simulation with the heterogeneous porosity are also visible in the calcium carbonate profile. Of course, this is not surprising, since calcium carbonate can only be formed where urea is present. In the simulation with the heterogeneous porosity, 6.22 kg calcium carbonate was formed in the soil. In the simulation with the homogeneous porosity, the amount of extracted urea was a little lower and the amount of produced calcium carbonate was therefore a little higher: 6.25 kg.

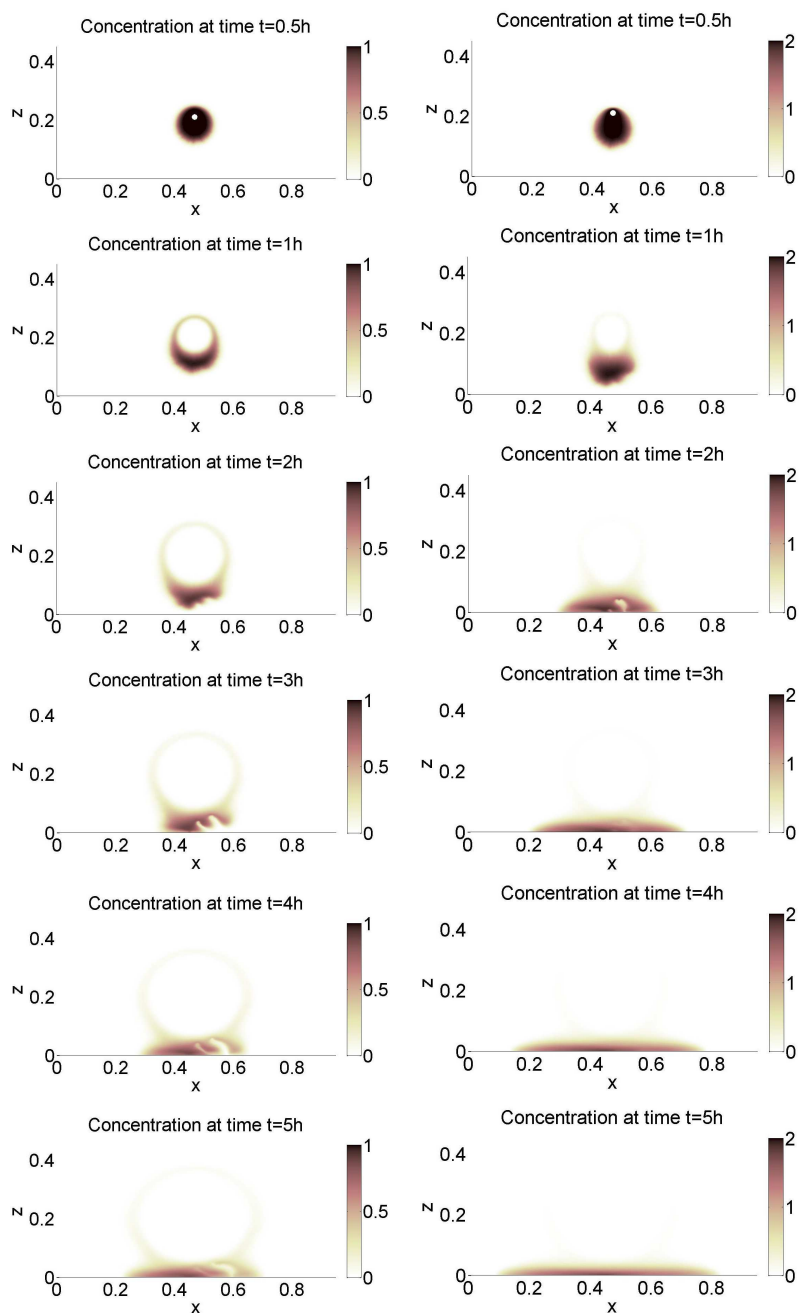


Figure 8.12: The concentration for an inflow concentration of  $c_{in} = 1 \text{ kmol/m}^3$  (left column) and  $c_{in} = 2 \text{ kmol/m}^3$  (right column) at several times (from top to bottom:  $t = 0.5\text{h}$ ,  $t = 1\text{h}$ ,  $t = 2\text{h}$ ,  $t = 3\text{h}$ ,  $t = 4\text{h}$  and  $t = 5\text{h}$ ). The mean porosity is  $M = 0.42$  and the variance is  $V = 0.001$ .

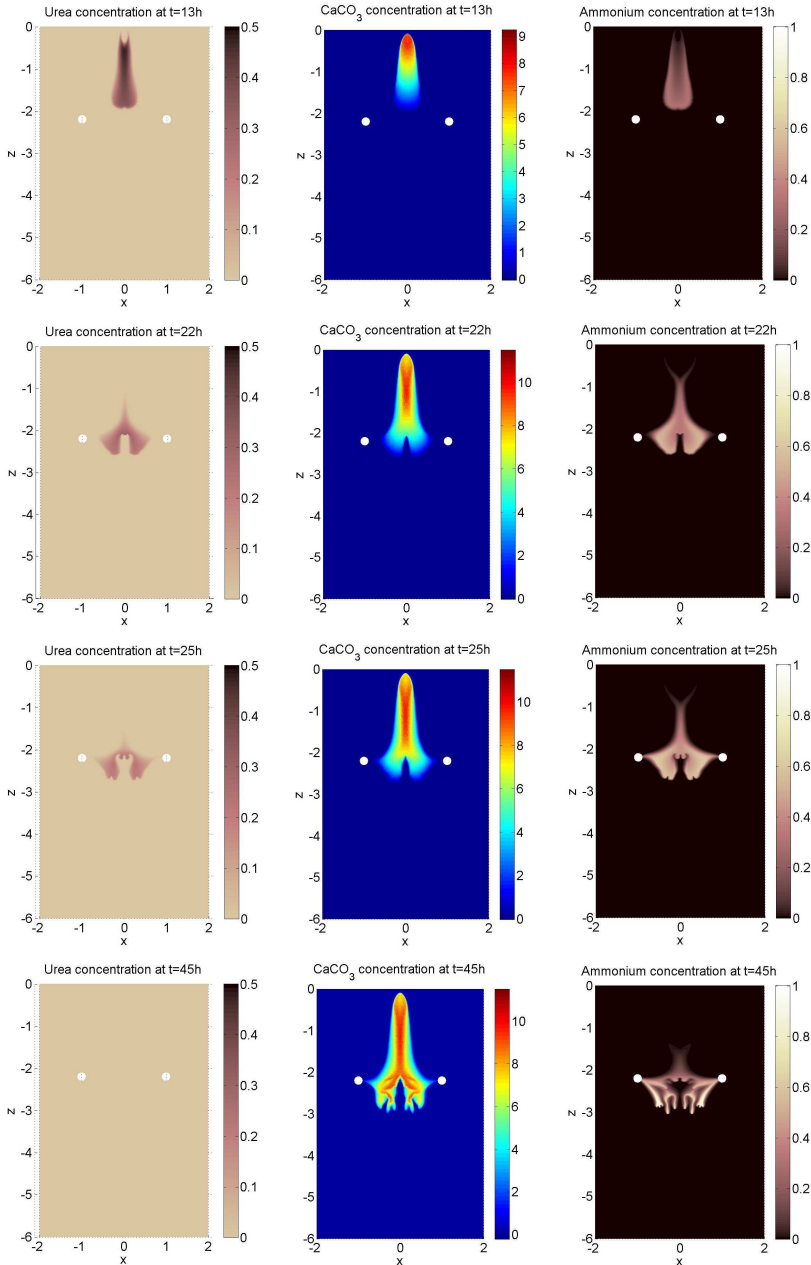


Figure 8.13: Results of the case study simulation with the heterogeneous porosity distribution for time  $t = 13\text{h}$ ,  $t = 22\text{h}$ ,  $t = 25\text{h}$  and  $t = 45\text{h}$ . Presented are the urea concentration (left column), the calcium carbonate concentration (middle column) and the ammonium concentration (right column).

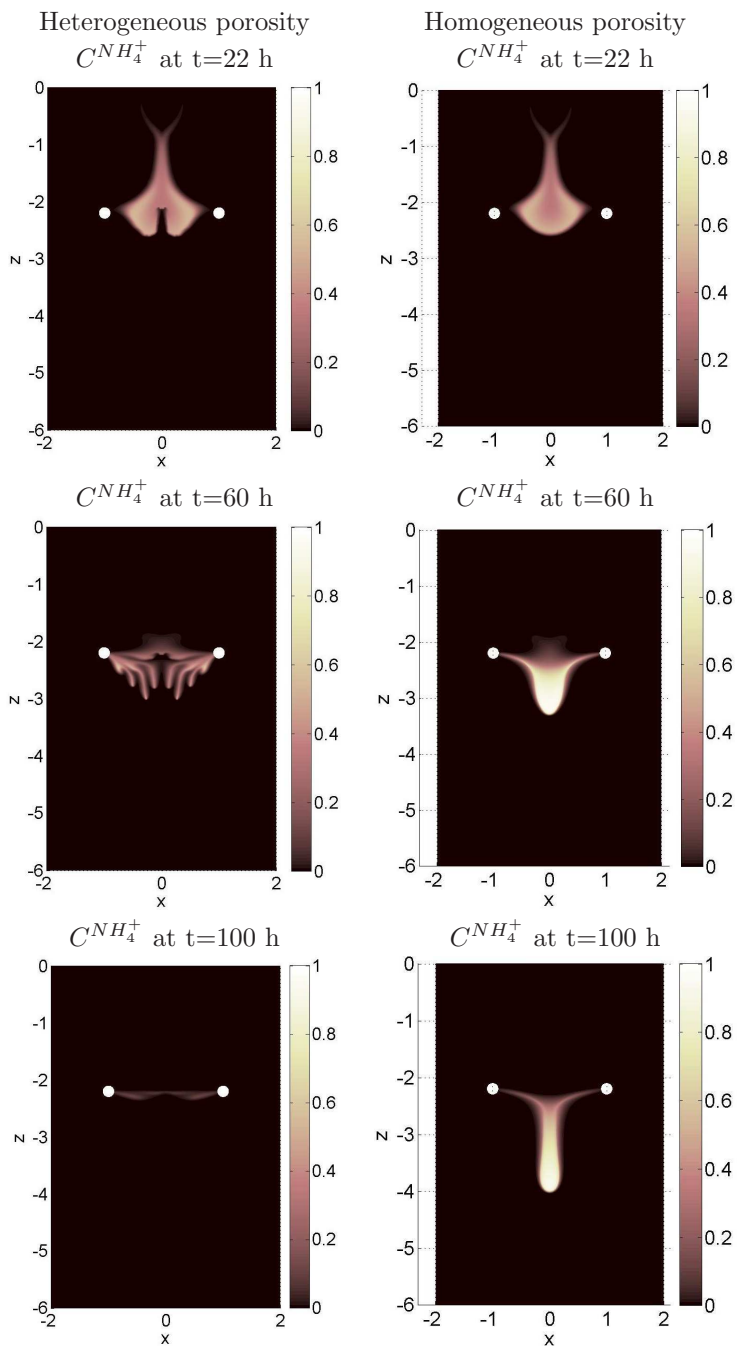


Figure 8.14: Ammonium concentration at several times in the case study. The left column shows the results with the heterogeneous porosity distribution and the right column displays the results for a homogeneous porosity.

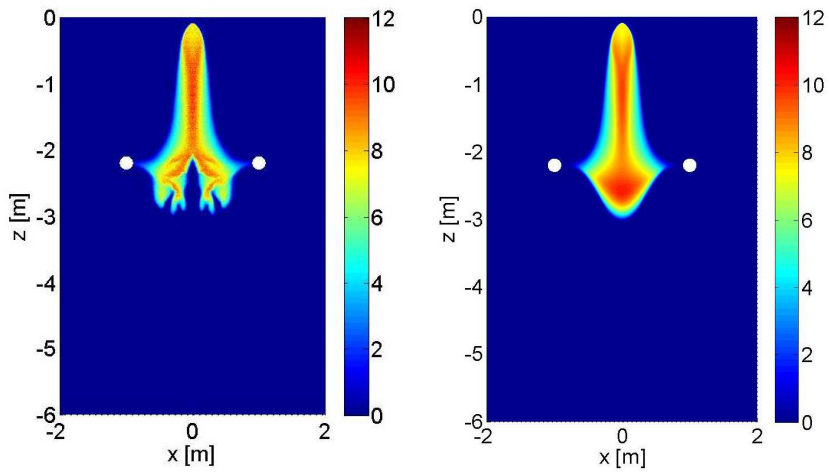


Figure 8.15: Final calcium carbonate concentration for the simulation with the heterogeneous porosity distribution (left) and the homogeneous porosity (right).

## 8.7 Discussion and Conclusions

In the experiment, fingers arise as expected where the dense fluid is on top of the less dense fluid. This happens particularly at the bottom side of the ring. But also at the bottom side of the top of the ring small fingers come into being, which flow downwards, in opposite direction to the flow that is generated by injection and extraction. In the simulation, no fingers appeared in case of a homogeneous medium. When using a variable porosity according to a log-normal distribution fingers developed in the numerical simulation. Fingers started to appear at approximately the same time as in the experiment. Several simulations were performed for various values of the mean porosity and variance. These simulations showed that a large variation in porosity (and hence permeability) results in larger fingers than a small variation, but this effect is not very large. The variation of the mean porosity has a much larger effect on the fingers as can be seen in Figure 8.10. The reason is explained in Subsection 8.6.2.

In comparison with the experiment, the numerical simulations seem to underestimate the fingering phenomenon. Fingers only appear at the bottom side of the ring, while in the experiment also some small fingers appear at the inside of the top of the ring. Furthermore, the flow velocity of the fingers in the experiment is larger than in the numerical simulations.

The numerical simulation, in which the inflow concentration was varied, showed that the concentration has a large effect on the flow as can be seen in Figure 8.12. Compared to the experiment and simulation with an inflow concentration of  $c_{in}=0.5$  kmol/m<sup>3</sup>, the dense fluid moves downwards more rapidly for a higher value for the inflow concentration.

The case study simulations showed that the fingering phenomenon has not necessarily a negative effect on the extraction of the ammonium. By the formation of fingers, the front is dispersed, which brings the dense fluid closer to the extraction drains, with the result that it was easier to extract most of the ammonium. On the other hand, while comparing the experimental results with the numerical simulations, it was concluded that the numerical simulations were underestimating the velocity of the fingers. If the velocity of the fingers would be higher than simulated in the case study, it is likely that more fingers escape from the vicinity of the extraction drains and that more ammonium is left in the soil.

Since the finite-element method is known to suffer from possible numerical mass-conservation errors, we checked mass-conservation for the time- and mesh resolution that we used. We found numerically that the relative violation of the mass-balance was as small as a few tenths of a percent over the entire simulation.

We showed the results of simulations for only one particular drawing from the lognormal distribution. To get an idea of the bandwidth, the simulations should be repeated for a large number of (different) drawings from the same log-normal distribution. Further, the sensitivity of the parameters in the log-normal distribution should be investigated to be able to make a good prediction of the fluid transport.

The scale of porosity and permeability variation in the simulation of the experiment is 1.1 mm (Sections 8.6.2 and 8.6.3) and 2.5 mm for the case study simulation

(Section 8.6.4). The question is what this scale of variation is in practice.

In this article, the transverse dispersivity was chosen equal to the longitudinal dispersivity in order to get the front as sharp as possible for the given mesh. By using a finer mesh, it can be investigated what the effect is of a smaller transverse dispersivity.

In reality, a horizontal seepage flow is occurring from surface water toward drainage ditch. In the case study, the seepage flow is not taken into account during the injection of the Biogrout fluids. However, this flow influences the transport of the fluids and should really be taken into account, while designing an injection and extraction strategy for a real case.

Buoyancy driven flow and associated fingers significantly affect the rate of salt extraction, which is required when applying Biogrout in practice. To reduce the density effect, one can use lower concentrations. However, this leads to a larger injected volume in order to reach a certain target amount of calcium carbonate. Also the reaction rate should be adapted when using lower concentrations in order to prevent that all the calcium carbonate will precipitate close to the injection wells. Another option to mitigate fingering would be to increase the flow rate. This decreases the retention time, such that the dense fluid has less time to form fingers. A drawback of a lower retention time is that the reaction rate should be larger to get the same calcium carbonate production. Furthermore, high injection rates cause large pressure drops close to the injection well which can fracture the soil in its surroundings affecting the distribution of injected fluids. Finally, it is also possible to reduce the effect of density by gradually increasing the inflow concentration. In that case there is no sharp front and it is less likely that fingers come into being.

In laboratory and scale up experiments of Biogrout, typically a concentration of 1 kmol/m<sup>3</sup> is used as an injection concentration for urea and calcium chloride, [36,86]. The density of this fluid is  $1.1 \times 10^3$  kg/m<sup>3</sup>, which is even denser than the 2 kmol/m<sup>3</sup> sodium chloride solution that was used in the simulation described in Subsection 8.6.3, i.e.  $1.08 \times 10^3$  kg/m<sup>3</sup>. If all the urea and calcium chloride reacts, one ends up with a 2 kmol/m<sup>3</sup> ammonium chloride solution, which has a density of  $1.03 \times 10^3$  kg/m<sup>3</sup>. This density lies in between the density of the 0.5 kmol/m<sup>3</sup> and the 1 kmol/m<sup>3</sup> sodium chloride solution. According to our simulations all these dense fluids easily sink away in the subsoil. By the formation of fingers, the dense fluid sinks even faster.

This paper clearly shows that it is important to take buoyancy driven flow into account while simulating the Biogrout process. It is possible to simulate the fingering phenomenon by varying the porosity and the permeability and using a sufficiently fine mesh. In the simulations in this article, the formation of fingers is advantageous for the application of Biogrout, since the ammonium is extracted more easily.



## **A reactive transport model for Biogrout compared to experimental data**

This chapter has been submitted to *Transport in Porous Media* as:

Van Wijngaarden, W.K., Van Paassen, L.A., Vermolen, F.J., Van Meurs, G.A.M.,  
Vuik, C.: A reactive transport model for Biogrout compared to experimental data.

## Abstract

Biogrout is a method for reinforcement of granular soil. In the Biogrout process, calcium carbonate is produced. This solid connects the grains and thereby the strength of the soil is increased. The calcium carbonate is formed with the use of micro-organisms. Experiments and numerical simulations have been performed to demonstrate the process under various conditions. In this paper it has been examined if a reactive transport model can be used to describe a Biogrout experiment that was performed in a column with a length of five meters. Four different models for the course of the reaction rate are considered. The concentration of micro-organisms and the reaction rate are fine-tuned in order to find a description of the experiment that is a best fit for the particular model. This is done by minimizing the error between the experimental and numerical results for the concentration of calcium carbonate and the byproduct of the reaction.

## 9.1 Introduction<sup>1</sup>

The Biogrout process is based on microbial induced carbonate precipitation (MICP), [5, 14, 22] and is a bio-mediated soil improvement method [23, 24, 39]. The proposed variant of Biogrout is urea-based. For a review on urea-based MICP, see [63]. The Biogrout process aims at producing calcium carbonate ( $\text{CaCO}_3$ ), by the hydrolysis of urea ( $\text{CO}(\text{NH}_2)_2$ ). In the presence of calcium ( $\text{Ca}^{2+}$ ), calcium carbonate is formed. Ammonium ( $\text{NH}_4^+$ ) is the byproduct of this reaction. The overall Biogrout reaction equation is:



The solid calcium carbonate forms connections between the grains by which the strength of the soil increases. However, the formation of a solid in the pores decreases the porosity and also leads to a decrease in permeability. This influences the flow and transport. Furthermore, due to the reaction, the fluid concentrations changes, which leads to a change in the fluid density. Combining these phenomena leads to a coupled reactive transport model. Some articles about modelling reactive flow and transport in porous media are [2, 16, 65–68, 81, 82, 98], of which [2, 65, 81] also consider a variable porosity. In [81], the level set function is used for the boundary of the crystals and a homogenization procedure is applied to obtain the upscaled equations. In [65], the differential equation for the porosity is comparable to the one used in this article. In [66, 67], the Newton method is used to deal with the non-linear equations and the convergence of this method is studied.

In this paper it is examined whether the reactive transport model for Biogrout, proposed in [91] (Chapter 2), is able to describe a Biogrout experiment that was performed. This Biogrout experiment has been described in [97] and [83]. A five meters long PVC tube was placed vertically and filled with sand. Ten sample points were made in the column. The flow direction during the experiment was downwards. First, micro-organisms were injected, followed by a pulse of a saline fluid to fixate

---

<sup>1</sup>Parts of the original introduction have been skipped in order to prevent too much repetition of the Introduction from Chapter 1.

the micro-organisms. Then, the column was filled with a urea and calcium chloride solution. After the injection of this solution, the flow was stopped, but the reaction could proceed. During the experiment, samples were taken from the sample points. At the end of the experiment, the calcium carbonate content in the tube was measured at several locations on samples of 1-4 g. The ammonium concentrations that were measured in the sample points and the final calcium carbonate content are used to fine-tune the concentration of fixated micro-organisms and the reaction rate.

In Section 9.2, this Biogrout experiment is described in more detail. The mathematical model is given in Section 9.3 including the initial conditions and boundary conditions that are used to simulate the experiment. In Section 9.4 it is discussed which numerical methods are used for these simulations. The results of both the experiment and the simulations are given in Section 9.5 and a discussion along with some conclusions can be found in Section 9.6.

## 9.2 Materials and Methods

In this section, the Biogrout experiment that was performed is described. More details are given in [97] and [83].

### 9.2.1 Column preparation

A five meters long PVC tube with an internal diameter of 66 mm was placed vertically and filled with a sand from a quarry in Itterbeck, Germany (Smals IKW, SZI 0032, also referred to as Itterbeck fine). This sand was uniform, fine to medium grained:  $d_{10} = 110 \mu\text{m}$  (10% of the grains have a diameter of this size or lower);  $d_{50} = 165 \mu\text{m}$ ;  $d_{90} = 275 \mu\text{m}$ ;  $d_{60}/d_{10} = 1.64$ ; (BSI 1999)). It is mainly siliceous (97%). The packing of the sand was conducted under water to avoid the inclusion of air pockets. The mean particle size of the sand grains was  $165 \mu\text{m}$  and the porosity was 0.378. Each end of the column was fitted with filter material. Ten pore fluid sampling ports were placed in the column, namely at 0.25 m from the top of the column, at 0.5 m and thereafter at intervals of 0.5 m till 4.5 m. The flow direction during the experiment was downwards. A pump was installed at the bottom of the column to regulate the outflow rate. The top of the column was connected to the supply with the urea/calcium solution and hence, no air could enter the column. During the experiment, samples were taken from the sampling ports.

### 9.2.2 Experiment

First, 6.34 l of a liquid containing micro-organisms were injected at a flow rate of 0.35 l/h. The micro-organism used was *Sporosarcina pasteurii*. It contains the enzyme *urease* which can hydrolyse urea. The production of ionic species from non-ionic substrates generates an increase in overall conductivity of the solution. The urease activity of the micro-organisms is determined by measuring this increase in conductivity before injection. This activity was 0.23 mS/min. As determined in [96], this corresponds to  $4.26 \times 10^{-5} \text{ kmol-urea/m}^3/\text{s}$ . In order to immobilize the micro-organisms in the column for use in subsequent cementation, the injection of micro-

organisms was followed by 5.99 l of 0.050 kmol/m<sup>3</sup> calcium chloride solution, as proposed in [36]. The flow rate was again 0.35 l/h. The next phase is the cementation phase, which also consists of two parts. First 8.72 l of a 1.1 kmol/m<sup>3</sup> urea and calcium chloride solution were injected with a flow rate of 0.35 l/h. Subsequently, the flow is stopped and the column is left for 102 h to react. Finally, the column is flushed with tap water, dismantled and the calcium carbonate content is determined at several locations. The injection scheme and the values of the various parameters (input for the simulations) are summarized in Tables 9.1 and 9.2.

Phase	Description	Duration (h)	Flow rate (l/h)
Placement	Bacterial injection	18.1	0.35
	Fixation fluid injection (0.050 kmol Ca <sup>2+</sup> /m <sup>3</sup> )	17.1	0.35
Cementation	Reaction fluid injection (1.1 kmol urea and Ca <sup>2+</sup> per m <sup>3</sup> )	24.9	0.35
	No flow - reaction	102	0
Rinse	Water flush	23.7	0.35

Table 9.1: The injection scheme for the experiment.

$L$	= 5 m	length of the column
$d_{int}$	= $6.6 \times 10^{-2}$ m	internal diameter of the column
$\theta_0$	= 0.378	initial porosity
$d_m$	= $165 \times 10^{-6}$ m	mean particle size of sand
$Q_{in}$	= 0.35 l/h	flow rate
$q_{in}$	= $2.84 \times 10^{-5}$ m/s	inflow velocity
$v_{max}$	= $4.26 \times 10^{-5}$ kmol urea/m <sup>3</sup> /s	maximal bacterial activity
$c_{in}$	= 1.1 kmol/m <sup>3</sup>	inflow concentration of urea and calcium chloride

Table 9.2: The values of various parameters, that are input for the simulations (part I).

## 9.3 Mathematical Model

In this section the model equations and the initial and boundary conditions that are used to simulate the Biogrout experiment are given. They are discussed in more detail in [91] and [93] (Chapter 2 and 6).

### 9.3.1 Model Equations

Important parameters in the Biogrout model are the concentrations of the species in chemical reaction (9.1). The advection-dispersion-reaction-equation is used to

model the concentration of the aqueous species:

$$\frac{\partial(\theta C^i)}{\partial t} = \nabla \cdot (\theta \mathbf{D} \nabla C^i) - \nabla \cdot (\mathbf{q} C^i) + m_i \theta r_{hp}. \quad (9.2)$$

In this equation,  $C^i$  [kmol/m<sup>3</sup>] is the concentration of species  $i$ ,  $i \in \{urea, Ca^{2+}, NH_4^+\}$ ,  $\theta$  [1] is the porosity,  $\mathbf{D}$  [m<sup>2</sup>/s] is the dispersion tensor,  $\mathbf{q}$  [m/s] is the Darcy flow velocity,  $r_{hp}$  [kmol/m<sup>3</sup>/s] is the rate of both the hydrolysis and the precipitation reaction which are equal during the major part of the reaction period [83] and  $m_i$  is a constant that follows from the stoichiometry of the reaction. As urea and calcium are consumed in the same ratio, their values of  $m_i$  are equal and negative:  $m_{urea} = m_{Ca^{2+}} = -1$ . For the produced ammonium the value is  $m_{NH_4^+} = 2$ . The coefficients of the dispersion tensor  $\mathbf{D}$  are given by  $D_{ij} = (\alpha_L - \alpha_T) \frac{v_i v_j}{|\bar{v}|} + \delta_{ij} (\alpha_T \sum_i \frac{v_i^2}{|\bar{v}|} + D_m)$ , with  $v_i = q_i/\theta$  [m/s] the pore water velocity and  $D_m$  [m<sup>2</sup>/s] the diffusion coefficient, see [100]. The quantity  $\alpha_L$  [m] is the longitudinal dispersivity and  $\alpha_T$  [m] is the transverse dispersivity. The term at the left hand side of (9.2) is the accumulation term, the first term at the right hand side stands for dispersion and diffusion, the second term for advection and the last term for the reaction. Urea and calcium are consumed in the same ratio. Choosing an equal dispersion tensor for urea and calcium gives two identical differential equations. Since the initial and boundary conditions are also identical, these concentrations are equal.

Calcium carbonate is a non-aqueous species and it has been assumed that it is not transported. Hence, its partial differential equation does not contain an advection and dispersion/diffusion term. Its concentration  $C^{CaCO_3}$  [kg/m<sup>3</sup>] is given in mass per total volume rather than per pore volume, as is done for the aqueous species. The molar mass of calcium carbonate  $m_{CaCO_3}$  [kg/kmol] is used to convert from kilomoles into kilograms. This gives the following differential equation for the calcium carbonate concentration:

$$\frac{\partial C^{CaCO_3}}{\partial t} = m_{CaCO_3} \theta r_{hp}. \quad (9.3)$$

The solid calcium carbonate is formed in the pores. This process decreases the porosity. The density of calcium carbonate,  $\rho_{CaCO_3}$  [kg/m<sup>3</sup>], is used to calculate the volume that a certain amount of calcium carbonate occupies. Hence, the following differential equation for the porosity results:

$$\frac{\partial \theta}{\partial t} = - \frac{1}{\rho_{CaCO_3}} \frac{\partial C^{CaCO_3}}{\partial t}. \quad (9.4)$$

Solving this differential equation gives the following relation between the calcium carbonate concentration and the porosity:

$$\theta(\mathbf{x}, t) = \theta(\mathbf{x}, 0) - \frac{C^{CaCO_3}(\mathbf{x}, t) - C^{CaCO_3}(\mathbf{x}, 0)}{\rho_{CaCO_3}}. \quad (9.5)$$

Substituting equation (9.3) into equation (9.4), gives the following differential equation for the porosity:

$$\frac{\partial \theta}{\partial t} = - \frac{m_{CaCO_3}}{\rho_{CaCO_3}} \theta r_{hp}. \quad (9.6)$$

This equation is similar to the differential equation for the porosity that is used in [65], where a model for concrete carbonation is considered. Both differential equations for the porosity contain a precipitation reaction rate and a multiplication with the porosity  $\theta$ , indicating that the precipitation reaction does not take place in the solid, but in the pore space or on the boundary of the solid. There are also some differences, but they do not lead to any substantial deviations in the calculated results. The equation for the porosity in [65] contains some extra terms to prevent the porosity from exceeding one or becoming negative. Besides this feature, dissolution is also taken into account and the value of the precipitation rate depends on the difference between the concentration of the chemicals in solution and its equilibrium. As discussed in Section 1, in (the urea-based) BiogROUT the (net) dissolution is negligible. Since the reaction rate in this article is non-negative, the porosity is non-increasing and due to its initial value between zero and one, the porosity will never exceed one in the current modelling. If the porosity becomes very small, the permeability will drastically decrease according to the Kozeny-Carman relation. In a pressure driven case (with the pressure prescribed on boundaries rather than the flow), there will hardly be any flow to the clogged zone nor will there hardly be any supply of nutrients and the porosity will not decrease further. If the flow is prescribed on a boundary and the fluid is pressed through the clogged porous media, this will result in extremely high pressures. High pressures will lead to cracks and preferential flow through the cracks. One could use a poro-elastic model where one evaluates the local stresses to predict the initiation of cracks. The appearance of cracks could give a sudden increase of the porosity and permeability. This issue is not dealt with in the current modelling.

For the flow, the continuity equation that was derived in [93] (Chapter 6) is used. This equation is an adaptation of the differential equation derived in [91] (Chapter 2).

$$\nabla \cdot \mathbf{q} = K\theta r_{hp}. \quad (9.7)$$

The constant  $K$  [ $\text{m}^3/\text{kmol}$ ] deals with volume changes due to the reaction and has been defined as

$$K := V_{\text{decrease\_of\_pore\_space}} - V_{\text{decrease\_of\_liquid\_volume}}. \quad (9.8)$$

Next, the above formula will be explained. The constant  $K$  deals with two processes:

1. As a result of the production of the solid calcium carbonate in the pores, there is less space available for the fluid. This space reduction per kmol produced calcium carbonate equals the molar volume of calcium carbonate:  $V_{\text{decrease\_of\_pore\_space}} = m_{\text{CaCO}_3} / \rho_{\text{CaCO}_3}$   $\text{m}^3/\text{kmol}$ . Recall that  $m_{\text{CaCO}_3}$  is the molar mass of calcium carbonate and that  $\rho_{\text{CaCO}_3}$  is the density of calcium carbonate. Hence, the decrease in pore space per unit of time and volume is  $V_{\text{decrease\_of\_pore\_space}}\theta r_{hp} = m_{\text{CaCO}_3} / \rho_{\text{CaCO}_3}\theta r_{hp}$ .
2. The hydrolysis and precipitation reactions cause a decrease in liquid volume. This decrease is partly caused by the water uptake in reaction (9.1). Furthermore urea and calcium do not occupy the same amount of volume as the produced ammonium. In [92], it has been derived that  $V_{\text{decrease\_of\_liquid\_volume}} =$

0.030 m<sup>3</sup>/kmol. Therefore, the decrease in liquid volume per unit of time and volume is  $V_{decrease\_of\_liquid\_volume}\theta r_{hp}$ .

Note that equation (9.7) is consistent with the Oberbeck-Boussinesq approximation as  $r_{hp} \rightarrow 0$ , i.e. in absence of the reaction.

Adding equations (9.6) and (9.7) gives

$$\frac{\partial \theta}{\partial t} + \nabla \cdot \mathbf{q} = \left( K - \frac{m_{CaCO_3}}{\rho_{CaCO_3}} \right) \theta r_{hp}. \quad (9.9)$$

Substitution of the definition of constant  $K$  (9.8) into equation (9.9) gives the following balance equation:

$$\frac{\partial \theta}{\partial t} + \nabla \cdot \mathbf{q} = -V_{decrease\_of\_liquid\_volume}\theta r_{hp}. \quad (9.10)$$

The right-hand side of this equation is the decrease in liquid volume per unit of time and volume.

For a relation between the pressure and the flow, Darcy's law is used, see [100]:

$$\mathbf{q} = -\frac{k}{\mu}(\nabla p + \rho_l g \mathbf{e}_z). \quad (9.11)$$

In Darcy's law,  $p$  [Pa] is the pressure,  $k$  [m<sup>2</sup>] is the intrinsic permeability,  $\mu$  [Pa·s] is the viscosity of the fluid,  $\rho_l$  [kg/m<sup>3</sup>] is the density of the fluid,  $g$  [m/s<sup>2</sup>] is the gravitational constant and  $\mathbf{e}_z$  is a unit vector in vertical direction.

The Kozeny-Carman equation is used to determine the intrinsic permeability. This equation is an empirical relation between the intrinsic permeability and the porosity that is commonly used in ground water flow modelling (see [7]):

$$k = \frac{(d_m)^2}{180} \frac{\theta^3}{(1 - \theta)^2}. \quad (9.12)$$

In this relation,  $d_m$  [m] is the mean particle size of the sand. Since the permeability is an increasing function of the porosity (for  $0 < \theta < 1$ ), a decrease in porosity will lead to a decrease in permeability.

The density of the fluid depends on the concentrations. The following relation, as derived in [91] (Chapter 2), is used:

$$\rho_l = 1000 + 15.4996C^{urea} + 86.7338C^{Ca^{2+}} + 15.8991C^{NH_4^+}. \quad (9.13)$$

By substitution of Darcy's law in equation (9.7), one gets the following differential equation for the pressure.

$$\nabla \cdot \left( -\frac{k}{\mu}(\nabla p + \rho_l g \mathbf{e}_z) \right) = K\theta r_{hp}. \quad (9.14)$$

### 9.3.2 Reaction rate

To complete the model, the rate  $r_{hp}$  of the biochemical reaction (9.1) is needed. In this section, it is explained how this reaction rate is composed.

### Micro-organisms

First of all, before the reaction can take place, the micro-organisms should be present. It has been assumed that the rate is proportional to the number of micro-organisms per unit of volume. According to [36], the fixation procedure that was used in this experiment leads to a rather homogeneous distribution of micro-organisms. Hence, for the moment a homogeneous distribution of micro-organisms is used. The quantity  $C^{bac}$  [1] is defined as the normalized concentration of micro-organisms that is injected. It has  $v_{max}$  as its initial activity. The quantity  $S^{bac}$  [1] is defined as the ratio between the concentration of fixated bacteria and the (normalized) injected concentration of micro-organisms (the latter is, by definition, equal to one). This give the following rate:

$$r_{hp} = v_{max}S^{bac}. \quad (9.15)$$

### Presence of urea

Secondly, before the reaction can take place, urea and calcium should be present. This relation is modelled with Monod kinetics [57]:

$$r_{hp} = \frac{C^{urea}}{K_{m,urea} + C^{urea}} v_{max} S^{bac}. \quad (9.16)$$

In this equation,  $K_{m,urea}$  [kmol/m<sup>3</sup>] is the half-saturation constant.

### Time effect

The rate may also depend on time. There are several processes that make it likely that the rate decreases. The micro-organisms need oxygen, which is only scarcely available in the soil. The micro-organisms are encapsulated by the calcium carbonate they produce and hence they can be reached by the urea less easily. On the other hand, if the micro-organisms are not encapsulated, they can be flushed out of the sand. Four different models for the production rate of calcium carbonate (in kmol/m<sup>3</sup>/s) are proposed. It was assumed that the decay starts at the beginning of the cementation phase.

1. The reaction rate is constant over time:

$$r_{hp}^{cons} = \frac{C^{urea}}{K_{m,urea} + C^{urea}} v_{max} S^{bac}. \quad (9.17)$$

This is the simplest model. It neglects growth, death and flush-out of micro-organisms, as well as other processes that may influence the rate.

2. The decay of the active population of micro-organisms is proportional to the active population [68], with decay constant  $b$  [s<sup>-1</sup>]:

$$\frac{\partial S^{bac,active}}{\partial t} = -bS^{bac,active}, \text{ for } t > t_{cem}.$$

This results into an exponential decay, with the following solution for the active population:

$$S^{bac,active} = S^{bac} e^{-b(t-t_{cem})_+},$$

with  $S^{bac}$  as the initial active population, present in the soil. The notation  $(\cdot)_+$  only uses the value of the quantity between brackets if it is positive and uses zero otherwise. This gives the following reaction rate:

$$r_{hp}^{exp1} = \frac{C^{urea}}{K_{m,urea} + C^{urea}} v_{max} S^{bac} e^{-b(t-t_{cem})_+}. \quad (9.18)$$

An exponential decay was also proposed in [83].

3. As a third model for the time effect, a simple engineering approach is proposed, which is a linearisation of the exponential decay model, proposed above. It states that the rate is maximal at time  $t = t_{cem}$  and is zero from time  $t = t_{max}$ . In between, the rate decreases linearly. That gives the following rate:

$$r_{hp}^{lin} = \frac{C^{urea}}{K_{m,urea} + C^{urea}} v_{max} S^{bac} \left( 1 - \frac{(t - t_{cem})_+}{t_{max}} \right)_+. \quad (9.19)$$

4. The last model for the time effect is a variation on the exponential decay model proposed above and it has two different decay constants. It has  $b_1$  [s<sup>-1</sup>] as the exponential decay constant during the flow part of the cementation phase and  $b_2$  [s<sup>-1</sup>] as the exponential decay constant during no flow:

$$r_{hp}^{exp2} = \begin{cases} \frac{C^{urea}}{K_{m,urea} + C^{urea}} v_{max} S^{bac} e^{-b_1(t-t_{cem})} & \text{for } t_{cem} \leq t \leq t_{noflow}; \\ \frac{C^{urea}}{K_{m,urea} + C^{urea}} v_{max} S^{bac} \times \\ \quad \times e^{-b_1(t_{noflow}-t_{cem})} e^{-b_2(t-t_{noflow})} & \text{for } t > t_{noflow}. \end{cases} \quad (9.20)$$

Here,  $t_{noflow}$  [s] is the time in the cementation phase at which the flow is stopped. This model is continuous at  $t = t_{noflow}$  but provides another decay constant when the flow is switched off. This is feasible, since there is no flush out of micro-organisms if there is no flow. Also other processes that influence the rate might depend on the flow.

All these rates will be used in order to find the best description of the experiment.

### 9.3.3 Parameter values

Not all the values of the model parameters are given in Table 9.2. In Table 9.3, the values of the other model parameters that we need to have in order to do simulations are given.

### 9.3.4 Initial and boundary equations

As the diameter of the column is quite small compared to the length, the variation in radial direction has been neglected and hence a 1D simulations is performed.

Initially, there is no urea, calcium, ammonium or calcium carbonate present in the column. Hence, the initial concentrations are equal to zero. The initial porosity is equal to  $\theta_0$ .

For urea, calcium and ammonium a mass flux is prescribed at the inlet. Since ammonium is a reaction product, it is not being injected, so the inward mass flux

Universal constants	
$g = 9.81 \text{ m/s}^2$	
Chemical properties	
$m_{CaCO_3} = 100.1 \text{ kg/kmol}$	
$\rho_{CaCO_3} = 2710 \text{ kg/m}^3$	
Hydrodynamic parameters	Reference
$\alpha_L = 0.001 \text{ m}$	
$D_m = 10^{-9} \text{ m}^2/\text{s}$	[20]
$\mu = 1.15 \cdot 10^{-3} \text{ Pa} \cdot \text{s}$	[95]
$p_{ref} = 1.5 \cdot 10^5 \text{ Pa}$	chosen
Reaction parameters	Reference
$K_{m,urea} = 0.01 \text{ kmol/m}^3$	[83]
$1-V_s = 0.02965 \text{ m}^3/\text{kmol}$	[93]

Table 9.3: The values of various parameters, that are input for the simulations (part II).

equals zero. To prescribe the mass flux for urea and calcium, the inflow rate should be known. There is a pump at the bottom of the column that regulates the outflow, so the outflow rate is known. In the simulations, the inflow rate equals this outflow rate. In practice, there might be a small deviation, since at each sample time approximately 1% of the pore volume is withdrawn and the reaction might also have an influence. In the determination of the inflow rate, this small change is neglected. At the outflow boundary, an advective flux is assumed for the concentrations of the aqueous species. Equations (9.7) and (9.14) describe the effect of the reaction on the flow. These equations imply that the flow is not necessarily uniform. Hence, on the outflow boundary, the pressure is prescribed rather than the outflow rate. This is also necessary to obtain a unique solution. The boundary conditions are summarized in Table 9.4.

	inlet	outlet
Urea and $\text{CaCl}_2$	$(\mathbf{D}\theta\nabla C - \mathbf{q}C) \cdot \mathbf{n} = q_{in}c_{in}$	$(\mathbf{D}\theta\nabla C) \cdot \mathbf{n} = 0$
$\text{NH}_4\text{Cl}$	$(\mathbf{D}\theta\nabla C - \mathbf{q}C) \cdot \mathbf{n} = 0$	$(\mathbf{D}\theta\nabla C) \cdot \mathbf{n} = 0$
flow	$\mathbf{q} \cdot \mathbf{n} = -q_{in}$	$p = p_{ref}$

Table 9.4: The boundary conditions for the simulations.

## 9.4 Numerical Methods

In this section, the numerical methods that are used to solve the system of (partial) differential equations are given.

The differential equations for the pressure (9.14), the flow (9.11) and the concentrations (9.2) are solved using the Standard Galerkin Finite Element Method. These equations are multiplied by a test function  $\eta$  and integrated over the domain  $\Omega$  to derive the weak formulation. For the time integration an implicit scheme is used (Euler Backward).

The Newton-Cotes quadrature rules [80] are used for the development of the element matrices and vectors. Line elements are used in this 1D experiment in combination with linear basis functions.

Since the differential equation for calcium carbonate (9.3) is an ordinary differential equation in each grid point, the (implicit) Backward Euler method is used to solve it.

The calculations are done with MATLAB. As a mesh size,  $\Delta x=0.002$  m is used. This gives a mesh with 2500 elements. The time span is divided in several equal time steps, with length  $\Delta t = 36$  s. At each time step, first the density, porosity and intrinsic permeability are updated, using equation (9.13), (9.5) and (9.12). Then, the pressure and the flow are calculated, solving equations (9.7) and (9.14). Subsequently, the concentrations are updated by solving equations (9.2) and (9.3). Due to reaction term in the partial differential equation for urea, this equation is non linear. Newton's method [1,66,67] is used to deal with that. As a stopping criterion

$$\frac{\|(\mathbf{c}^{n+1,k+1} - \mathbf{c}^{n+1,k})\|_2}{\|\mathbf{c}^{n+1,k}\|_2} < 10^{-10}$$

is used, with vectors  $\mathbf{c}^{n+1,k+1}$  and  $\mathbf{c}^{n+1,k}$  the latest results of the iterative process. In our case, Newton's method converges within a few iterations. The following list presents in pseudo code the order in which the equations are solved and the updates are done. The superscript  $n$  and  $n + 1$  denote the approximation at time  $t^n$  and  $t^{n+1}$ .

1.  $\rho_l^{n+1} : \rho_l^{n+1} = \rho(C^{\text{urea},n}, C^{\text{Ca}^{2+},n}, C^{\text{NH}_4^+,n})$ , from equation (9.13);
2.  $\theta^{n+1} : \theta^{n+1} = \theta(\theta_0, C^{\text{CaCO}_3,n})$ , from equation (9.5);
3.  $k^{n+1} : k^{n+1} = k(\theta^{n+1})$ , from equation (9.12);
4.  $p^{n+1} : \nabla \cdot \left( \frac{k^{n+1}}{\mu} (\nabla p^{n+1} + \rho_l^{n+1} g \mathbf{e}_z) \right) = K \theta^{n+1} r_{hp}^n$ , from partial differential equation (9.14);
5.  $\mathbf{q}^{n+1} : \mathbf{q}^{n+1} = -\frac{k^{n+1}}{\mu} (\nabla p^{n+1} + \rho_l^{n+1} g \mathbf{e}_z)$ , from partial differential equation (9.7);
6.  $C^{\text{urea},n+1} : (\theta^{n+1} C^{\text{urea},n+1} - \theta^n C^{\text{urea},n}) / \Delta t = \nabla \cdot (\theta^{n+1} \mathbf{D}^{n+1} \nabla C^{\text{urea},n+1}) - \nabla \cdot (\mathbf{q}^{n+1} C^{\text{urea},n+1}) - \theta r_{hp}^{n+1}$ , from partial differential equation (9.2). Due to the reaction term, this partial differential equation is non linear in the urea concentration and Newton's method is used;
7.  $C^{\text{NH}_4^+,n+1} : (\theta^{n+1} C^{\text{NH}_4^+,n+1} - \theta^n C^{\text{NH}_4^+,n+1}) / \Delta t = \nabla \cdot (\theta^{n+1} \mathbf{D}^{n+1} \nabla C^{\text{NH}_4^+,n+1}) - \nabla \cdot (\mathbf{q}^{n+1} C^{\text{NH}_4^+,n+1}) - \theta r_{hp}^{n+1}$ , from partial differential equation (9.2). The values for  $r_{hp}^{n+1}$  follow from the last Newton iteration in the previous step.
8.  $C^{\text{CaCO}_3,n+1} : (C^{\text{CaCO}_3,n+1} - C^{\text{CaCO}_3,n}) / \Delta t = m_{\text{CaCO}_3} \theta^{n+1} r_{hp}^{n+1}$ , from partial differential equation (9.3).

To solve the (coupled) model equations, a splitting is performed. This splitting introduces an error of  $\mathcal{O}(\Delta t)$ . Since the backward Euler time integration scheme also results into an  $\mathcal{O}(\Delta t)$  error, the splitting does not worsen the order of convergence. The mass balance is regularly checked and deviations are only in the order of a few tenths of a percent.

For each measurement of the ammonium concentration in the experiment, the value is compared with the outcome of the numerical simulation. The total error for ammonium is calculated by summing up the squares of the differences and taking the square root of this sum. Finally, the result is normalized by dividing it by the number of measurements  $n_{am}$  and the theoretical maximum of the ammonium concentration, which is  $2.2 \text{ kmol/m}^3$  (if the small decrease in liquid volume due to the reaction is not taken into account):

$$E_{am} = \frac{1}{2.2n_{am}} \sqrt{\sum_i \sum_j (y_{ij} - f(x_i, t_j))^2}, \quad (9.21)$$

where  $y_{ij}$  are the values of the ammonium measurements at location  $x_i$  and time  $t_j$  and  $f(x_i, t_j)$  is the corresponding numerical value at the same time and location. In the same way the error for calcium carbonate is defined (for which we only have experimental data at the end of the experiment):

$$E_{cc} = \frac{1}{105.1n_{cc}} \sqrt{\sum_i (y_i - g(x_i))^2}, \quad (9.22)$$

with  $n_{cc}$  the number of calcium carbonate measurements,  $y_i$  the values of the calcium carbonate measurements at the end of the experiment at location  $x_i$  and  $g(x_i)$  is the corresponding numerical value at the same time and location. The maximal calcium carbonate concentration measured was  $105.1 \text{ kg/m}^3$ .

The total error is calculated by summing both errors:

$$E_{tot} = E_{am} + E_{cc}. \quad (9.23)$$

The Matlab built-in minimization algorithm *fminsearch* is used to find the unknowns (concentration of fixated micro-organisms and decay constant(s)) in the rate functions that minimize the total error (9.23). This is done for the four different rate functions that are considered.

With the error definition (9.21) and (9.22), steep fronts may lead to considerable errors, while the error in location of the front might be very small. Since the aim of the paper is to examine if this reactive transport model can be used to model a Bigrou experiment, rather than finding the best solution, this simple error calculation is sufficient.

## 9.5 Results

In this section the results of the experiment and the numerical results for the various models for the activity decrease are reported.

### 9.5.1 Experimental Results

The results of the experiment have been reported in detail in [97] and [83]. Here, only the evolution of the ammonium concentration in the various sampling ports is shown (Figure 9.1) as well as the final calcium carbonate concentration (Figure 9.3). As in [97] and [83] the time is reset such that the cementation phase starts at time  $t=0$ h.

#### Ammonium

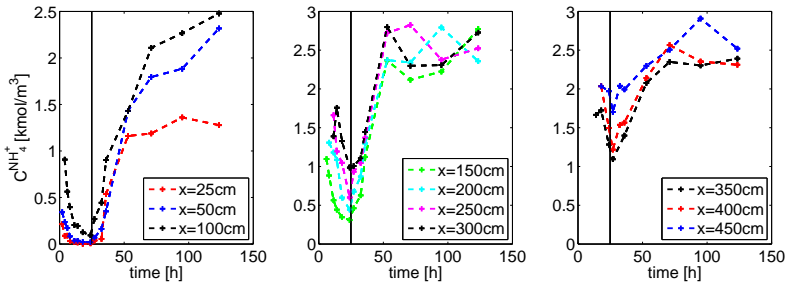


Figure 9.1: The course of the ammonium concentration [kmol/m<sup>3</sup>] in the sample ports.

Figure 9.1 shows the ammonium concentration in time for various sample ports. The vertical line at time  $t=24.9$  h divides the graph in the flow part (left) and the no flow part (right) of the cementation phase.

There is no ammonium present in the column at the beginning of the cementation phase. Hence, the initial ammonium concentration equals zero. Initially, the reaction rate is quite high, causing a sharp increase in the ammonium concentration. Once the reactive front has passed a sample port, the ammonium concentration rapidly decreases. Since the supply is constant, it seems that the activity is decreasing.

Figure 9.2 shows the ammonium concentrations as a function of the position in the column. The left figure shows the ammonium profile at several times during the flow phase. Samples were only taken, when the concentration in the sample port was expected to be larger than zero, i.e. when the front is passing/has passed. This implies that a zero concentration is expected on the sample port locations where no data are shown. The ammonium penetrates further into the column as time proceeds. Furthermore, the concentration increases with the position in the column. This increase was expected, since ammonium is produced by the micro-organisms and a longer retention time results into a higher concentration. From the slope of the various graphs, it can be concluded that the production rate, which is a measure for the microbial activity, decreases in time. The right plot of Figure 9.2 shows the ammonium profile at several times after  $t=24.9$  h, when the flow was stopped. Since there is still urea and calcium present in the column, the reaction continues. The ammonium concentration increases until it reaches a maximum at which all urea has been consumed. Based on the injected concentration of urea and the reaction

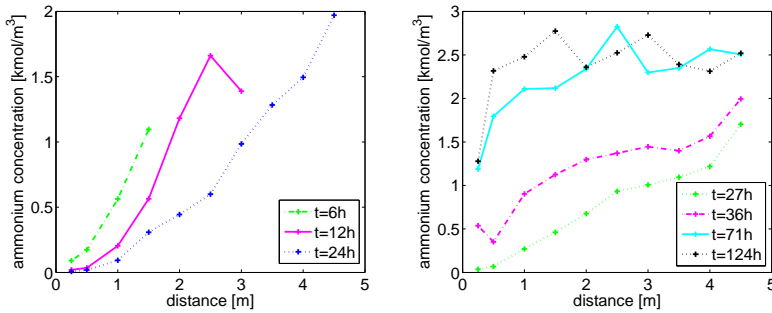


Figure 9.2: The ammonium concentration in the column at several times. Left: during flow, right: during no flow.

stoichiometry, the theoretical maximum ammonium concentration is  $2.274 \text{ kmol/m}^3$ , taking the consumption of water in the hydrolysis reaction into account. However, the measured concentrations at the end of the cementation phase are significantly larger than this theoretical maximum, showing a structural difference of 8% with an average of  $2.459 \text{ kmol/m}^3$  and a standard deviation 10% or  $0.237 \text{ kmol/m}^3$ . In the first sample port, the maximum is not reached within the time of the experiment.

### Calcium carbonate

The results for the final calcium carbonate concentration are shown in Figure 9.3. Since the largest heterogeneity was expected in the first part of the column, additional samples were taken from this part. The first meter shows indeed a large spread in results. The results in the rest of the column only show a little deviation from the trend. In [83], several mechanisms which can explain the observed heterogeneities are suggested: Possibly, the micro-organisms were not distributed as homogeneously as expected. Perhaps, the initial column material contained some inhomogeneities. Furthermore, locally clogged areas (by micro-organisms or crystals) can cause preferential flow paths and stagnant zones.

The calcium carbonate content is decreasing with the length of the column. This was expected, since the substrates are injected at  $x = 0 \text{ m}$  and the reaction time (the time needed for full conversion of the injected concentration) is comparable to the retention time. Consequently, the first part of the column has received more substrates resulting in a higher calcium carbonate concentration than in the last part. If the reaction rate would be very large, the substrates are converted before the end of the column is reached and in that case there would not be any calcium carbonate at the end of the column. Too high reaction rates could also cause clogging at the inlet. A high flow rate or a lower reaction rate would result in a more homogeneous distribution. However, high flow rates could possibly wash out micro-organisms, whereas low reaction rates will increase the reaction time.

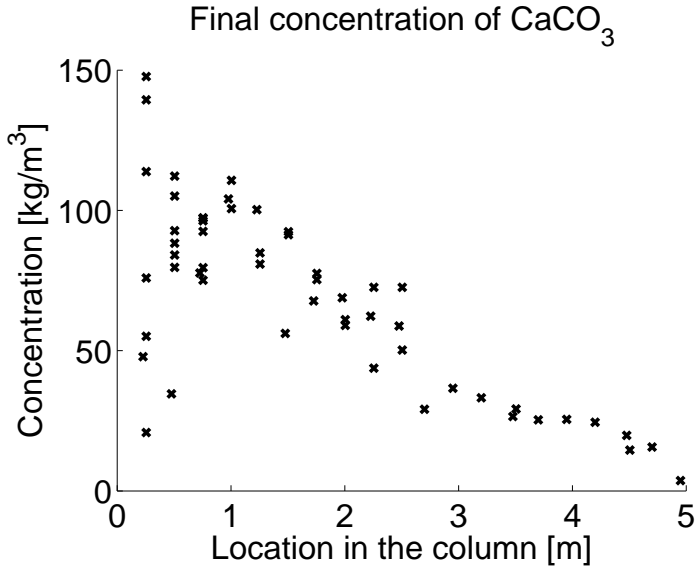


Figure 9.3: The concentration of calcium carbonate [ $\text{kg/m}^3$ ] in the column at the end of the experiment.

### Nitrogen concentration

Considering that both the nitrogen (N) atoms in urea are converted to ammonium, at first sight, one could expect that the total nitrogen concentration in the cementation solution should not change, but since in the reaction also water is consumed, this concentration slightly increases. Since the injected concentration of urea equals  $1.1 \text{ kmol/m}^3$  the total nitrogen concentration would increase from  $2.2 \text{ kmol/m}^3$  to  $2.274 \text{ kmol/m}^3$  when all urea is converted to ammonium. Assuming that the concentrations of urea and calcium are equal during the reaction in the sand column (which is justified since urea is injected at the same concentration as calcium and both react with the same rate), the total nitrogen concentration can be calculated by adding the calcium concentration, multiplied by two, to the ammonium concentration. Figure 9.4 shows the results of the calculations and the theoretical bandwidth. The figure shows that in many cases the deviation is considerable, potentially indicating significant measurement inaccuracies. The same discrepancy as mentioned earlier is observed, namely that at the final stage of the reaction the ammonium concentrations show structurally higher values than expected. Secondly some outliers in the measurements were identified at which the total nitrogen concentration is significantly lower than expected. These outliers should not be taken into account when comparing the different model simulations with the experimental results.

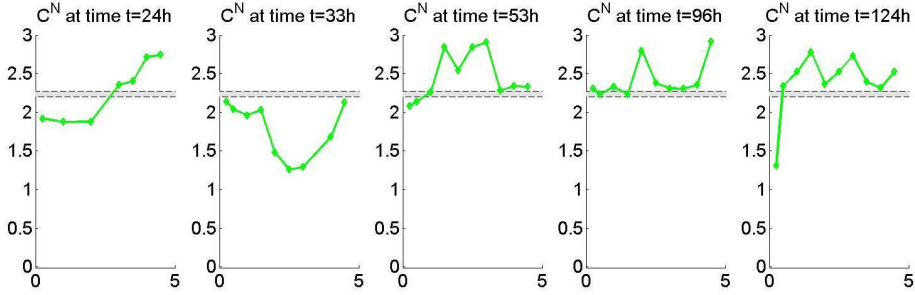


Figure 9.4: Concentration of nitrogen ( $C^N$  [kmol/m<sup>3</sup>]) in the column (distance in [m]) at several times (green line) and the theoretical bandwidth for this concentration (two dotted horizontal lines).

## 9.5.2 Numerical Results

In this subsection the numerical results are reported and compared with the experimental results.

### Minimizing errors

In Section 9.3.2, four different models were proposed for the reaction rate. In all cases, a value has to be assigned to one or more parameters. Table 9.5 shows which values minimize the error as defined in (9.21), (9.22) and (9.23) for these four cases.

Model	Parameter values	Error in NH <sub>4</sub> <sup>+</sup>	Error in CaCO <sub>3</sub>
Model with one unknown parameter			
Constant activity	$S^{bac}=0.418$	0.021	0.021
Models with two unknown parameters			
Exponential decrease	$S^{bac}=0.707$ $b=1.12 \cdot 10^{-5} \text{ s}^{-1}$	0.012	0.020
Linear decrease	$S^{bac}=0.537$ $t_{max}=2.24 \cdot 10^5 \text{ s}$	0.015	0.020
Model with three unknown parameters			
Exponential decrease 2	$S^{bac}=0.902$ $b_1=1.64 \cdot 10^{-5} \text{ s}^{-1}$ $b_2=8.28 \cdot 10^{-6} \text{ s}^{-1}$	0.012	0.019

Table 9.5: The values for which the error between the experimental and numerical results is minimal for the four models describing the course of the reaction rate.

Biochemical rates (9.17) up to (9.20) are plotted as a function of time for the parameter values from Table 9.5. The graphs are shown in Figure 9.5. The rates also depend on the urea concentration, which is a function of location and time. Since the focus here is on the course of the rates in time, the urea term ( $\frac{C^{urea}}{K_{m,urea}+C^{urea}}$ ) in all rate functions is replaced by 1.

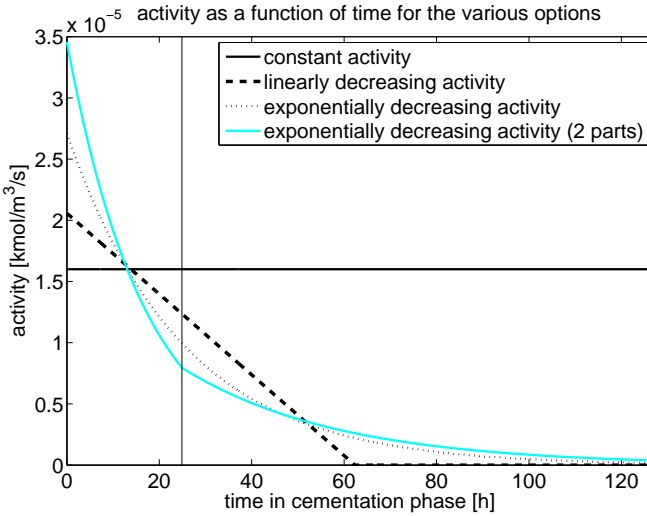


Figure 9.5: The activity of the micro-organisms in the column as a function of time for the four models that describe the course of the reaction rate. The urea term in the rate functions is neglected here.

In the constant activity model, one parameter has to be estimated. Compared to the other models, it leads to the largest errors, both for the ammonium concentration and the calcium carbonate concentration.

Both for the exponential decrease model with one decay constant and the linear decrease model, two parameters need to be estimated. These two decay models perform similarly with respect to the error in the calcium carbonate content, however the exponential decay model leads to a smaller error in ammonium concentration.

For the last proposed decay model, three parameters needed to be estimated. It is also an exponential decay model, but now with two decay constants, one for the period during flow and one for the period without flow. Although an extra parameter was involved, it led to an only slightly smaller error in calcium carbonate content, compared to the simpler exponential decay model.

It can be concluded that the models, which consider decay, should be preferred over the constant activity model. As it could be expected, involving more parameters led to smaller errors. The exponential decay model with one decay constant performed a little better than the linear decrease model and therefore it should be preferred since it is based on physics rather than on a linearisation. In this experiment, it was not really worth while to introduce an extra decay constant for the period without flow. Other experiments are needed to conclude whether this is the case in general.

### Ammonium concentration

Figure 9.6 displays the experimental and numerical results for the ammonium concentration. After the first appearance, the ammonium concentration decreases dur-

ing the flow part of the cementation phase, indicating a decreasing reaction rate. For both the exponential decay models, this decrease is captured quite well, where the first part of the column performs a little less well. There, the experiment shows a drastic decrease in activity. The constant activity model is not able to handle a decreasing activity as it is based on a constant activity. The small decrease in ammonium concentration is the result of the decreasing porosity. The latter causes a decrease in residence time which results in a lower amount of reaction product. The linear decrease model gives better results than the constant activity model, but performs worse than the two exponential decay models.

After 24.9 hours, the flow was stopped and the substrates were left to react. The constant activity model gives the poorest results. It predicts that the maximum ammonium concentration is reached quite fast. In all sample ports it is reached earlier than it really does in the experiment. The other three models perform better than the constant activity model and they are comparable to each other. In some parts of the column one model describes the experiment the best and in other parts another model. None of the models gives a good description of the final concentration at the sample port at  $x = 0.25$  m.

### Calcium carbonate concentration

In this subsection the experimental results are compared to the numerical results for the calcium carbonate concentration. Again, this comparison is done for the four different models for the activity decrease. The results are shown in Figure 9.7. The numerical results are quite good for all models and they hardly differ from each other. There is a large spreading in the experimental results for the calcium carbonate content in the first part of the column. Possible reasons for this scatter are discussed in Section 9.5.1.

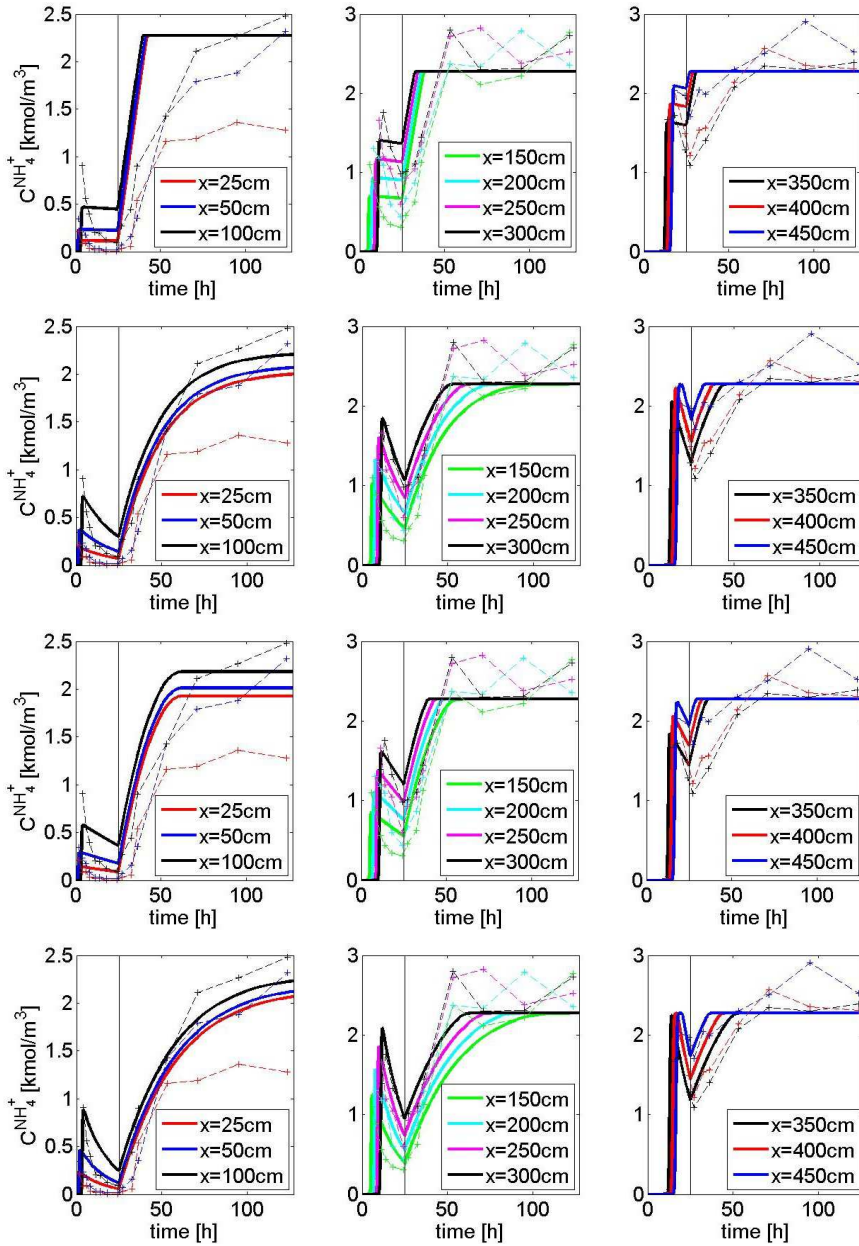


Figure 9.6: The ammonium concentration [kmol/m<sup>3</sup>] in the various sample ports as a function of time. Both the experimental and numerical values are shown. First row: constant activity model, second row: exponential activity decrease model, third row: linear activity decrease model, last row: exponential activity decrease model with two decay constants.

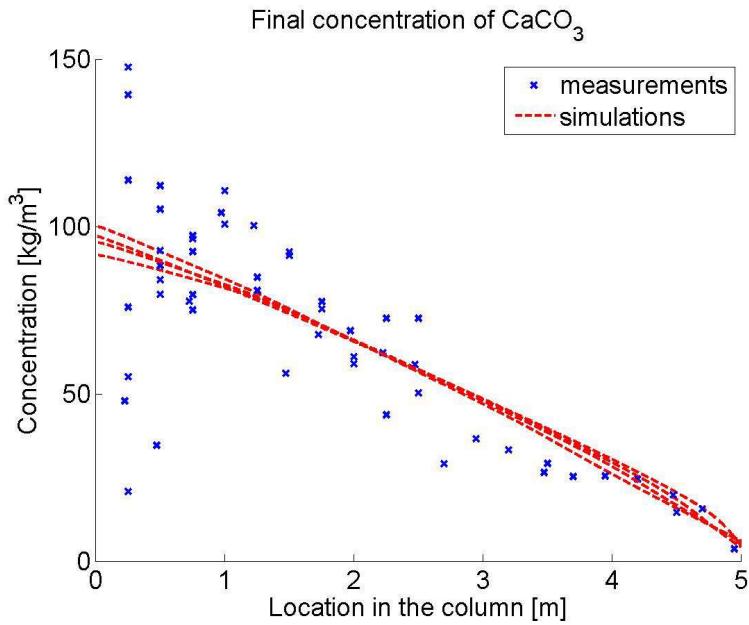


Figure 9.7: The calcium carbonate concentration in the column at the end of the experiment. Both the experimental values and the numerical values for the four models are shown.

## 9.6 Conclusions and Discussion

In this paper, a reactive transport model which was developed to simulate the Biogrout process was compared to the results of a sand column experiment. This experiment is presented in [97] and [83]. The measured ammonium concentrations during the Biogrout experiment and the final calcium carbonate concentrations are shown in this paper as well.

From the ammonium measurements it followed that the reaction rate is decreasing in time. For that reason, various models were proposed, in which the activity decreases in time. A model with a constant activity was also considered. These models were compared to a Biogrout experiment.

The amount of the final calcium carbonate content appeared to decrease with the distance to the injection, although the experimental results are quite scattered, especially close to the injection. Close to the inlet, the average amount of calcium carbonate is approximately  $100 \text{ kg/m}^3$ . This implies a porosity reduction from 0.378 to 0.341. According to the Kozeny-Carman relation (9.12), the permeability decreases with a factor 1.5. Close to the outlet, the calcium carbonate content is almost zero. On that location, the porosity and permeability were hardly influenced.

In a 1D experiment, the decreases in porosity and permeability are not very important, since there is only 'one way' to travel from the inlet to the outlet. In two or three dimensions, these reductions become more important, since the liquid will flow around a cemented zone, where the resistance is relatively high. Furthermore, the porosity reduction in general can be larger than in this experiment. Therefore it is important that the porosity and permeability reduction are considered.

The mathematical model, proposed in this article, is quite detailed with respect to the flow equation in order to have conservation of mass. In [93] it has been shown that small deviations in the flow equations have a minor effect on the final calcium carbonate content.

Analysis of the experimental data highlighted several inaccuracies in the measurements. First, the final ammonium concentrations obtained after completion of the reaction showed significantly higher values (8%) than expected according to the theoretical stoichiometry. Second, assuming that the concentration of urea and calcium ions are equal throughout the experiment, the total nitrogen concentration was calculated from the ammonium concentrations and measured calcium concentrations. Analysis of this total nitrogen concentration identified several outliers with significantly lower values than expected. These outliers were not taken into account when comparing the various kinetic models. Finally, the volume of each liquid sample is approximately 5 ml. In the calculations for both the experiment and the simulations this volume is neglected. However, especially in the no flow part, this volume might influence the experimental results.

Considering the calcium carbonate concentration, all the models led to a similar description of the average final calcium carbonate concentration. This is partly because the experiment contains a no flow part. In case of no flow, the value of the reaction rate does not influence the final distribution, as long as it is high enough to get full conversion in the course of the experiment. Changing the experimental conditions, such as the flow period and flow rate or initial activity and concentrations,

would increase the differences between the various simulations. In the first part of the column the calcium carbonate measurements showed large variations. Several mechanisms, explaining the observed heterogeneities have been suggested in [83], including a heterogeneous distribution of bacteria, locally clogged areas (by bacteria or crystals) causing preferential flow paths and stagnant zones and the kinetics of the precipitation reaction. The prediction of this local variability requires a far more advanced model, taking these processes into account. However, measurement of the parameters which are required to describe these processes at pore scale and the upscaling of these processes to continuum scale are hard to achieve and will introduce a significant amount of uncertainty. It is therefore questionable whether such a complex model will result in a better performance. In order to predict radial variations, a 1D simulation is not adequate. However, since this paper assumes a homogeneous distribution of micro-organisms, it is expected that a full 3D modelling approach for simulating this experiment will not lead to radial variation, except for a possible fingering effect as a result of buoyancy driven flow. The latter could have occurred since a dense fluid is injected on top of a less dense fluid.

Ammonium, the side product of the reaction, was measured at several times and locations during the experiment. Hence, these results are more appropriate to compare the various model scenarios. The constant reaction rate model does not perform very well since it is not able to model a decreasing reaction rate, which is observed in the experiment. The other models are able to capture a decreasing reaction rate and they perform quite good. Only in the first meter of the column they predict too high concentrations. The two exponential decay models can be preferred above the linear decay model since decay processes are often described using exponential models and since the two exponential models gave the smallest total error. It was excluded that the differences between the numerical and experimental results were caused by numerical errors by redoing a calculation for a finer mesh, combined with a smaller time step. The numerical results were overlapping, indicating that the numerical errors are very small.

According to the ammonium measurements, the microbial activity decreases drastically in the first meter of the column during flow. Trying to get a better fit for this part of the column during flow, results in a rapidly declining reaction rate. Consequently, the simulated calcium carbonate concentrations are much lower than the experimental concentrations. It seems that in the first part of the column the reaction rate decreases during flow but subsequently increases after the flow has been switched off. Since the time dependent activity models that are used assume a continuous, monotonously decreasing rate, they are not able to handle this discontinuity in reaction rate.

On the other hand, the measured ammonium concentrations in the first part of the column seem to be too low. If the concentrations of ammonium at  $x = 25$  cm and  $x = 50$  cm are used to calculate the final calcium carbonate concentration in the first 25 cm or 50 cm, values are found that are lower than the average measured calcium carbonate concentrations. These calculations are done as follows. The concentrations of (produced) ammonium at  $x = 25$  cm are used as a measure for the activity in the first 25 cm between that time and the next sample. This gives an

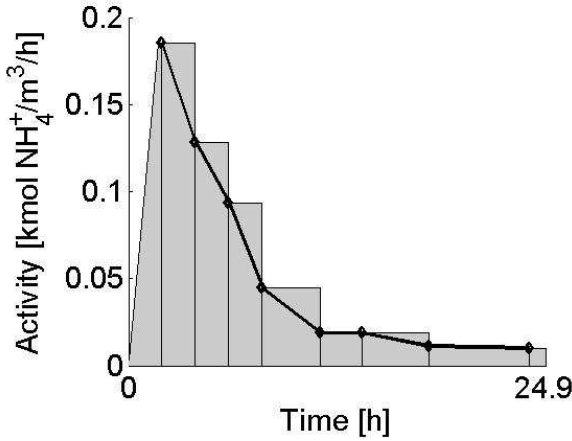


Figure 9.8: The activity of the micro-organisms in the first part of the column, calculated from the produced ammonium concentration.

upperbound since the activity decreases between the samples. This is illustrated in Figure 9.8. From these activities, the amount of produced calcium carbonate during flow is calculated. This value is added to the amount of calcium carbonate that is produced during no flow. The latter is easily calculated by subtracting the ammonium concentration at the beginning of no flow from the final ammonium concentration and converting it into calcium carbonate. These calculations give an upperbound for the calcium carbonate content of  $41 \text{ kg/m}^3$  for the first 25 cm and  $58 \text{ kg/m}^3$  for the first 50 cm. From the measured calcium carbonate concentrations a value of  $86 \text{ kg/m}^3$  was expected in both cases. This value is much higher than the one calculated from the ammonium concentrations, which either could indicate an error or a large spread in radial direction in the ammonium measurements. The radial heterogeneity is confirmed by the variation in the final calcium carbonate concentration.

It can be concluded that, in order to properly simulate the Biogrout process, a time dependent decay of the reaction rate should be included. The exponential decay models performed the best. From this experiment it can not yet be concluded whether an extra decay constant for the period without flow is really necessary. Although the models performed quite well, the concentration of micro-organisms and the decay rate were fine-tuned on the measurements to achieve a good fit. In order to improve the performance of these numerical simulations, more advanced models are required. These models should incorporate the placement of micro-organisms (including the way of cultivation of micro-organisms, sand type, pH, flow, concentrations, etc.) and other processes, like process-induced preferential flow and the kinetics of the precipitation reaction [83].



## General conclusions and Outlook

A model has been developed for the urea-based Biogrout method. The model includes Darcy flow with fluid density differences, the transport and reaction of micro-organisms, fixation fluid, urea, calcium and ammonium and finally the production of calcium carbonate. The changing fluid density and the decreasing porosity and permeability are also incorporated in the model. Several simulations were performed in one, two and three spatial dimensions. An analytical solution has been derived for a specific (simplified) case. Furthermore, some simulations were compared to experimental results.

To prevent numerical instabilities, the Euler Backward method is used for the numerical time integration. Since high flow rates should be avoided to prevent the flush-out of the micro-organisms, the system is not advection dominated and the Standard Galerkin Finite Element Method can be used to solve the model equations.

A hydrostatic pressure is often used as a boundary condition. In case of an evolving fluid density, this pressure can be calculated by solving an additional differential equation on the boundary.

Since a model is always a simplification of reality, a balance between simplicity and complexity should be sought. A major issue is that very complicated models often require the use of many parameters that are hard or even impossible to obtain. On the other hand, the model should contain the important phenomena in order to be reliable. We propose the following list of phenomena and assumptions that are possibly relevant to incorporate into future modelling studies for Biogrout:

- Calcium carbonate precipitation; in the current model it is assumed that calcium carbonate precipitates locally and that calcium carbonate is not transported. However, it is likely that small crystals can be transported before they will stick in the pore throats.
- Governing biochemical reaction equation; the combined hydrolysis precipitation reaction is assumed to govern the process. Injection into an acid environment can have an effect on the equilibria and hence on the amount of precipitated calcium carbonate. Also the pressure and the temperature may influence the governing biochemical reaction equation. Furthermore, the precipitation of calcium carbonate takes place by the formation of new crystals

(for which supersaturation of the solution is needed) and the growth of these crystals [83]. This may take some time and in the meanwhile the species are transported. This can be the reason, besides the flush-out of micro-organisms, that around injection wells the calcium carbonate concentration is quite low like in [85, 86]. The current model, however, predicts the highest calcium carbonate concentrations around the injection.

- Retardation; the retardation of urea, calcium and ammonium is not taken into account. Nevertheless, there can be some retardation, especially when particles are charged.
- Kozeny-Carman relation for the permeability; it should be tested if this relation is suitable for the Biogrout process, where the porosity and mean particle size evolve over time and space.
- Decay of reaction rate; the reaction rate decreases in time, which can be caused by encapsulation, flush out and death of micro-organisms. It is useful for the model if a proper relation is available.
- Effect of micro-organisms on the porosity; the injection of micro-organisms will effect the porosity and may even lead to clogging of the porous medium. This is not yet included in the model.
- Effect of flow velocity on the detachment of the micro-organisms;
- Biofilm growth; this is especially relevant if micro-organisms are used that are present in the soil.

The current model is applicable under saturated conditions. It would be interesting to extend the model with unsaturated flow in order to be able to model the unsaturated zones.

Next to urea hydrolysis, there are other microbial processes, which lead to the precipitation of calcium carbonate, [84]. In the study in [84], a process is proposed in which a gas is produced as a by-product of the calcium carbonate production. In that case a multiphase flow model is needed.

The model for the placement of micro-organisms has not yet been compared to experiments. This is indispensable for the reliability of the model. The hydrolysis-precipitation model is compared to a density driven flow experiment in Chapter 8 and to a Biogrout experiment in Chapter 9. The variation of the initial porosity in space is favourable to induce the formation of the fingers. After finding a best fit for a couple of parameters, the hydrolysis-precipitation model could describe the Biogrout experiment quite well. The comparison to more experiments, including experiments with density driven flow, is necessary for validation and in order to get a reliable predictive model for the application of Biogrout.

For the simulations, the Standard Galerkin FEM is used for discretisation in space. In order to model density driven flow including the fingering phenomenon, one should be able to model sharp fronts which imply a small dispersion length. In the current modelling, this leads to the need of small elements, due to the mesh-Péclet condition [80], which forces the dispersion length to be larger than half the element size. Adaptive mesh refinement at the location of the fronts can be applied to reduce the computational work. A SUPG method can be applied to avoid unphysical oscillations.

## LIST OF SYMBOLS

**Concentrations and retardation factor**

- $C^{urea}$  = concentration of dissolved urea molecules, [kmol/m<sup>3</sup>];  
 $C^{Ca^{2+}}$  = concentration of dissolved calcium ions, [kmol/m<sup>3</sup>];  
 $C^{NH_4^+}$  = concentration of dissolved ammonium ions, [kmol/m<sup>3</sup>];  
 $C^{fix}$  = concentration of fixation fluid, [kmol/m<sup>3</sup>];  
 $C^{Na^+}$  = concentration of dissolved sodium ions, [kmol/m<sup>3</sup>];  
 $C^{CaCO_3}$  = concentration of calcium carbonate molecules, [kg/m<sup>3</sup>];  
 $\bar{C}^k$  = sorbed concentration of species  $k$ ,  
 $k \in \{\text{urea}, Ca^{2+}, NH_4^+\}$ , [kmol/kg];  
 $C_s^k$  = concentration of species  $k$  in the source or sink,  
 $k \in \{\text{urea}, Ca^{2+}, NH_4^+\}$ , [kmol/m<sup>3</sup>];  
 $C^{bac}$  = injected concentration of micro-organisms  
(normalized), [1];  
 $\bar{C}^{bac}$  = ratio of the micro-organisms that is adsorbed (with  
respect to the injected concentration), [1];  
 $S^{bac}$  = ratio of the micro-organisms that is fixated (with respect  
to the injected concentration), [1];  
 $\Psi$  = total concentration of micro-organisms  
( $\Psi = C^{bac} + \bar{C}^{bac} + S^{bac}$ ), [1];  
 $R^k$  = retardation factor of species  $k$ ,  $k \in \{\text{urea}, Ca^{2+}, NH_4^+\}$ ,  
[1];  
 $c_{in}$  = inflow concentration, [kmol/m<sup>3</sup>];

**Properties of the porous medium**

$\rho_b$	=	bulk dry density of the subsurface medium, [kg/m <sup>3</sup> ];
$\theta$	=	porosity, [1];
$\theta_0$	=	initial porosity, [1];
$k$	=	intrinsic permeability, [m <sup>2</sup> ];
$d_m$	=	mean particle size of the subsurface medium, [m];

**Reaction rate related symbols**

$r_{hp}$	=	reaction rate of the hydrolysis and precipitation processes, [kmol/m <sup>3</sup> /s];
$v_{max}$	=	maximal reaction rate, [kmol/m <sup>3</sup> /s];
$t_{max}$	=	life time of the bacteria, [s];
$K_{m,urea}$	=	saturation constant of urea, [kmol/m <sup>3</sup> ];
$K_{m,fix}$	=	saturation constant of the fixation fluid, [kmol/m <sup>3</sup> ];
$r_{ads}$	=	adsorption reaction rate, [1/h];
$r_{des}$	=	desorption reaction rate, [1/h];
$r_{fix}$	=	fixation adsorption rate, [1/h];
$k_{ads}$	=	adsorption rate constant, [1/h];
$k_{des}$	=	desorption rate constant, [1/h];
$k_{fix}$	=	fixation rate constant, [1/h];
$\varphi$	=	adsorption isotherm, [1];
$\beta$	=	factor that describes which part of the adsorbed micro-organisms are fixated, [1];
$\beta_0$	=	constant that describes which part of the adsorbed micro-organisms are fixated, [m <sup>3</sup> /kmol] or [1];
$\alpha$	=	Langmuir constant, [1];
$\overline{C}^{max}$	=	Maximum adsorption capacity, [1];

**Flow related symbols**

$p$	=	pressure, [Pa];
$\mathbf{q}$	=	Darcy flow velocity vector, [m/s];
$\mathbf{v}$	=	pore water velocity vector, [m/s];
$Q_{in}$	=	injected flow rate, [m <sup>3</sup> /s];
$q_{in}$	=	inflow velocity, [m/s];
$q_s^k$	=	volumetric flow rate per unit volume of aquifer of species $k$ , $k \in \{\text{urea}, \text{Ca}^{2+}, \text{NH}_4^+\}$ , [1/s];
$K$	=	constant in the differential equation for the flow, [m <sup>3</sup> /kmol];
$1 - V_s$	=	liquid volume that disappears per number of converted particles, [m <sup>3</sup> /kmol];
$\rho_l$	=	density of the fluid, [kg/m <sup>3</sup> ];
$\mu$	=	dynamic viscosity of the fluid, [Pa·s];

**Dispersion and diffusion related symbols**

$\mathbf{D}$	=	hydrodynamic dispersion coefficient tensor, [m <sup>2</sup> /s];
$D_m$	=	Molecular diffusion coefficient, [m <sup>2</sup> /s];
$\alpha_L$	=	longitudinal dispersivity, [m];
$\alpha_T$	=	transverse dispersivity, [m];

**Miscellaneous**

$t$	=	time, [s];
$x, y, z$	=	Cartesian coordinates, [m];
$g$	=	gravitational constant, [m/s <sup>2</sup> ];
$m_{CaCO_3}$	=	molecular mass of calcium carbonate, [kg/kmol];
$\rho_{CaCO_3}$	=	density of calcium carbonate, [kg/m <sup>3</sup> ];
$\mathbf{n}$	=	outward normal vector, [m];

**Chemical components**

$CaCl_2$	=	calcium chloride;
$CaCO_3$	=	calcium carbonate;
$Ca^{2+}$	=	calcium ions;
$CO(NH_2)_2$	=	urea;
$CO_3^{2-}$	=	carbonate ions;
$H_2O$	=	water;
$NaCl$	=	sodium chloride;
$NH_4Cl$	=	ammonium chloride;
$NH_4^+$	=	ammonium ions.



## Bibliography

- [1] R.A. Adams. *Calculus: a complete course*. Addison Wesley Longman, Toronto, 2003.
- [2] A Agosti, L Formaggia, and A Scotti. Analysis of a model for precipitation and dissolution coupled with a Darcy flux. *Journal of Mathematical Analysis and Applications*, 431(2):752–781, 2015.
- [3] H.L. Atkins and C.-W. Shu. Quadrature-free implementation of Discontinuous Galerkin method for hyperbolic equations. *AIAA Journal*, 36(5):2440–2463, 1998.
- [4] K.L. Bachmeier, A.E. Williams, J.R. Warmington, and S.S. Bang. Urease activity in microbiologically-induced calcite precipitation. *Journal of Biotechnology*, 93(2):171–181, 2002.
- [5] S.S. Bang, J.K. Galinat, and V. Ramakrishnan. Calcite precipitation induced by polyurethane-immobilized *Bacillus pasteurii*. *Enzyme and microbial technology*, 28(4):404–409, 2001.
- [6] T.H. Barkouki, B.C. Martinez, B.M. Mortensen, T.S. Weathers, J.D. De Jong, T.R. Ginn, N.F. Spycher, R.W. Smith, and Y. Fujita. Forward and inverse bio-geochemical modeling of microbially induced calcite precipitation in half-meter column experiments. *Transport in Porous Media*, 90(1):23–39, 2011.
- [7] J. Bear. *Dynamics of Fluids in Porous Media*. Dover Publications, New York, 1972.
- [8] M. Blauw, M.P. Harkes, V.M. van Beek, A.R. Koelewijn, W.K. van Wijngaarden, and G.A. van den Ham. Bio-technological strengthening of flood embankments. including the applicability based on experiments,

- and concepts close to industrial application. Technical report, Flood-ProBE, co-funded by the European Community Seventh Framework Programme for European Research and Technological Development (2009-2013), [http://www.floodprobe.eu/partner/assets/documents/Deliverable4.1\\_final\\_jan2013.pdf](http://www.floodprobe.eu/partner/assets/documents/Deliverable4.1_final_jan2013.pdf), 2013.
- [9] M. Blauw, M.P. Harkes, V.M. van Beek, and G.A. van den Ham. Biogrout, an innovative method for preventing internal erosion. In *Comprehensive Flood Risk Management: Research for Policy and Practice*. CRC Press, 2012.
- [10] Carina Bringedal, Inga Berre, Iuliu Sorin Pop, and Florin Adrian Radu. A model for non-isothermal flow and mineral precipitation and dissolution in a thin strip. *Journal of Computational and Applied Mathematics*, 289:346 – 355, 2015. Sixth International Conference on Advanced Computational Methods in Engineering (ACOMEN 2014).
- [11] J. Bruining, D. Marchesin, and C.J. Van Duijn. Steam injection into water-saturated porous rock. *Computational & Applied Mathematics*, 22:359 – 395, 00 2003.
- [12] C.J. Budd and A. Iserles. Geometric integration: numerical solution of differential equations on manifolds. *Philosophical Transactions of the Royal Society of London. Series A: Mathematical, Physical and Engineering Sciences*, 357(1754):945–956, 1999.
- [13] M.A. Celia, J.S. Kindred, and I. Herrera. Contaminant transport and biodegradation; a numerical model for reactive transport in porous media. *Water Resources Research*, 25(6):1141–1148, 1989.
- [14] L. Cheng, M. Shahin, and R. Cord-Ruwisch. Bio-cementation of sandy soil using microbial-induced carbonate precipitation (MICP) for marine environments. *Géotechnique*, 64(2):1010–1013, 2014.
- [15] C. Chevalier, M. Ben Amar, D. Bonn, and A. Lindner. Inertial effects on Saffman-Taylor viscous fingering. *J. Fluid Mech.*, 552:83–97, 2006.
- [16] A. Chilakapati, S. Yabusaki, J. Szecsody, and W. MacEvoy. Groundwater flow, multicomponent transport and biogeochemistry: development and application of a coupled process model. *Journal of Contaminant Hydrology*, 43(34):303 – 325, 2000.
- [17] B. Cockburn. An introduction to the discontinuous Galerkin method for convection-dominated problems. In *Advanced numerical approximation of nonlinear hyperbolic equations*, pages 151–268. Springer, 1998.
- [18] B. Cockburn and C.-W. Shu. The local discontinuous Galerkin method for time-dependent convection-diffusion systems. *SIAM Journal on Numerical Analysis*, 35(6):2440–2463, 1998.
- [19] A. Costa. Permeability-porosity relationship: A reexamination of the Kozeny-Carman equation based on a fractal pore-space geometry assumption. *Geophysical research letters*, 33(2), 2006.

- [20] E.L. Cussler. *Diffusion: mass transfer in fluid systems*. New York: Cambridge University Press, 2nd edition, 1997.
- [21] A. de Wit. Miscible density fingering of chemical fronts in porous media: Nonlinear simulations. *Physics of Fluids*, 16(1), 2004.
- [22] J.T. DeJong, M.B. Fritzes, and K. Nusslein. Microbially induced cementation to control sand response to undrained shear. *Journal of Geotechnical and Geoenvironmental Engineering*, 132(11):1381–1392, 2006.
- [23] J.T. DeJong, B.M. Mortensen, B.C. Martinez, and D.C. Nelson. Bio-mediated soil improvement. *Ecological Engineering*, 36(2):197–210, 2010.
- [24] J.T. DeJong, K. Soga, E. Kavazanjian, S. Burns, L.A. Van Paassen, A. Al Qabany, A. Aydilek, S.S. Bang, M. Burbank, L.F. Caslake, C.Y. Chen, X. Cheng, J. Chu, S. Ciurli, A. Esnault-Filet, S. Fauriel, N. Hamdan, T. Hata, Y. Inagaki, S. Jefferis, M. Kuo, L. Laloui, J. Larrahondo, D.A.C. Manning, B. Martinez, B.M. Montoya, D.C. Nelson, A. Palomino, P. Renforth, J.C. Santamarina, E.A. Seagren, B. Tanyu, M. Tsesarsky, and T. Weaver. Biogeochemical processes and geotechnical applications: progress, opportunities and challenges. *Géotechnique*, 63(4):287–301, 2013.
- [25] D.A. DiCarlo. Stability of gravity-driven multiphase flow in porous media: 40 years of advancements. *Water Resources Research*, 49:4531–4544, 2013.
- [26] H.-J.G. Diersch and O. Kolditz. Variable-density flow and transport in porous media: approaches and challenges. *Advances in Water Resources*, 25(812):899 – 944, 2002.
- [27] A. Ebigbo, A. Phillips, R. Gerlach, R. Helmig, A. B. Cunningham, H. Class, and L.H. Spangler. Darcy-scale modeling of microbially induced carbonate mineral precipitation in sand columns. *Water Resources Research*, 48(7), 2012.
- [28] R. Ewing and H. Wang. A summary of numerical methods for time-dependent advection-dominated partial differential equations. *Journal of Computational and Applied Mathematics*, 128(1):423–445, 2001.
- [29] R. Farajzadeh, B. Meulenbroek, D. Daniel, A. Riaz, and J. Bruining. An empirical theory for gravitationally unstable flow in porous media. *Computational Geosciences*, 17(3):515–527, 2013.
- [30] S. Fauriel and L. Laloui. A bio-hydro-mechanical model for propagation of Biogrout in soils. In *Geo-Frontiers 2011*, pages 4041–4048, 2011.
- [31] S. Fauriel and L. Laloui. A bio-chemo-hydro-mechanical model for microbially induced calcite precipitation in soils. *Computers and Geotechnics*, 46:104–120, 2012.
- [32] D.E. Fontes, A.L. Mills, G.M. Hornberger, and J.S. Herman. Physical and chemical factors influencing transport of microorganisms through porous media. *Applied and Environmental Microbiology*, 57(9):2473–2481, 1991.

- [33] J.W.A. Foppen and J.F. Schijven. Evaluation of data from the literature on the transport and survival of *Escherichia coli* and thermotolerant coliforms in aquifers under saturated conditions. *Water Research*, 40(3):401–426, 2006.
- [34] L.W. Gelhar, C. Welty, and K.R. Rehfeldt. A critical review of data on field-scale dispersion in aquifers. *Water Resources Research*, 28(7):1955–1974, 1992.
- [35] G.H. Golub and Ch.F. Van Loan. *Matrix computations*. Johns Hopkins University Press, Third Edition, Baltimore, Maryland, 1996.
- [36] M.P. Harkes, L.A. van Paassen, J.L. Booster, V.S. Whiffin, and M.C.M. van Loosdrecht. Fixation and distribution of bacterial activity in sand to induce carbonate precipitation for ground reinforcement. *Ecological Engineering*, 36(2):112–117, 2010.
- [37] J.C. Heinrich, P.S. Huyakorn, O.C. Zienkiewicz, and A.R. Mitchell. An upwind finite element scheme for two-dimensional convective transport equation. *International Journal for Numerical Methods in Engineering*, 11(1):131–143, 1977.
- [38] G.M. Hornberger, A.L. Mills, and J.S. Herman. Bacterial transport in porous media: Evaluation of a model using laboratory observations. *Water Resources Research*, 28(3):915–923, 1992.
- [39] V. Ivanov and J. Chu. Applications of microorganisms to geotechnical engineering for bioclogging and biocementation of soil in situ. *Reviews in Environmental Science and Bio/Technology*, 7(2):139–153, 2008.
- [40] K. Johannsen, S. Oswald, R. Held, and W. Kinzelbach. Numerical simulation of three-dimensional saltwater-freshwater fingering instabilities observed in a porous medium. *Advances in Water Resources*, 29(11):1690 – 1704, 2006.
- [41] W.P. Johnson, K.A. Blue, B.E. Logan, and R.G. Arnold. Modeling bacterial detachment during transport through porous media as a residence-time-dependent process. *Water Resources Research*, 31(11):2649–2658, 1995.
- [42] Roozbeh Khosrokhavar, Gerritx Elsinga, Rouhi Farajzadeh, and Hans Bruining. Visualization and investigation of natural convection flow of  $\{CO_2\}$  in aqueous and oleic systems. *Journal of Petroleum Science and Engineering*, 122:230 – 239, 2014.
- [43] R. Kimmel and J.A. Sethian. Computing geodesic paths on manifolds. *Proceedings of the National Academy of Sciences*, 95(15):8431–8435, 1998.
- [44] P. Knabner, B.A. Iglar, K.U. Totsche, and P. DuChateau. Unbiased identification of nonlinear sorption characteristics by soil column breakthrough experiments. *Computational Geosciences*, 9(4):203–217, 2005.
- [45] P. Knabner and F. Otto. Solute transport in porous media with equilibrium and nonequilibrium multiple-site adsorption: uniqueness of weak solutions. *Nonlinear Analysis: Theory, Methods & Applications*, 42(3):381–403, 2000.

- [46] P. Knabner, C.J. van Duijn, and S. Hengst. An analysis of crystal dissolution fronts in flows through porous media. part 1: Compatible boundary conditions. *Advances in Water Resources*, 18(3):171 – 185, 1995.
- [47] K. Kosugi. Lognormal distribution model for unsaturated soil hydraulic properties. *Water Resources Research*, 32(9):2697–2703, 1996.
- [48] L. Krivodonova. Limiters for high-order discontinuous Galerkin methods. *Journal of Computational Physics*, 226(1):879–896, 2007.
- [49] K. Kumar, I.S. Pop, and F.A. Radu. Convergence analysis of mixed numerical schemes for reactive flow in a porous medium. *SIAM Journal on Numerical Analysis*, 51(4):2283–2308, 2013.
- [50] K. Kumar, I.S. Pop, and F.A. Radu. Convergence analysis for a conformal discretization of a model for precipitation and dissolution in porous media. *Numerische Mathematik*, 127(4):715–749, 2014.
- [51] G.J. Le Beau and T.E. Tezduyar. *Finite element computation of compressible flows with the SUPG formulation*. Army High Performance Computing Research Center, 1991.
- [52] P.C. Lichtner, C.I. Steefel, and E.H. Oelkers. Reactive transport in porous media. *Reviews in Mineralogy*, 34:83–125, 1996.
- [53] R. Löhner, K. Morgan, and O.C. Zienkiewicz. The solution of non-linear hyperbolic equation systems by the finite element method. *International Journal for Numerical Methods in Fluids*, 4(11):1043–1063, 1984.
- [54] A. Madzvamuse, R.D.K. Thomas, Ph.K. Maini, and A.J. Wathen. A numerical approach to the study of spatial pattern formation in the ligaments of arcoid bivalves. *Bulletin of mathematical biology*, 64(3):501–530, 2002.
- [55] G. Matthess and A. Pekdeger. Concepts of a survival and transport model of pathogenic bacteria and viruses in groundwater. *Science of the Total Environment*, 21:149–159, 1981.
- [56] G. Matthess, A. Pekdeger, and J. Schroeter. Persistence and transport of bacteria and viruses in groundwater - a conceptual evaluation. *Journal of Contaminant Hydrology*, 2(2):171–188, 1988.
- [57] J. Monod. The growth of bacterial cultures. *Annual Reviews in Microbiology*, 3(1):371–394, 1949.
- [58] J.L. Musuuza, S. Attinger, and F.A. Radu. An extended stability criterion for density-driven flows in homogeneous porous media. *Advances in Water Resources*, 32(6):796 – 808, 2009.
- [59] M. Nemati and G. Voordouw. Modification of porous media permeability, using calcium carbonate produced enzymatically in situ. *Enzyme and microbial technology*, 33(5):635–642, 2003.

- [60] J.R. Nimmo. Porosity and pore size distribution. In *Encyclopedia of Soils in the Environment*, volume 3, pages 295–303. Elsevier, London, 2004.
- [61] J.M. Nordbotten. Personal communication with Jan M. Nordbotten, associate professor at Department of Mathematics, University of Bergen, 2009.
- [62] D.L. Parkhurst. Users guide to PHREEQC – a computer program for speciation, reaction-path, advective-transport, and inverse geochemical calculations. Technical report, U.S. GEOLOGICAL SURVEY, 1995.
- [63] A.J. Phillips, R. Gerlach, E. Lauchnor, A.C. Mitchell, A.B. Cunningham, and L. Spangler. Engineered applications of ureolytic biomineralization: a review. *Biofouling: The Journal of Bioadhesion and Biofilm Research*, 29(6):715–733, 2013.
- [64] K.M. Pruitt and D.N. Kamau. Mathematical models of bacterial growth, inhibition and death under combined stress conditions. *Journal of Industrial Microbiology*, 12(3-5):221–231, 1993.
- [65] F.A. Radu, A. Muntean, I.S. Pop, N. Suciu, and O. Kolditz. A mixed finite element discretization scheme for a concrete carbonation model with concentration-dependent porosity. *Journal of Computational and Applied Mathematics*, 246:74 – 85, 2013. Fifth International Conference on Advanced Computational Methods in ENgineering (ACOMEN 2011).
- [66] F.A. Radu and I.S. Pop. Newton method for reactive solute transport with equilibrium sorption in porous media. *Journal of Computational and Applied Mathematics*, 234(7):2118 – 2127, 2010.
- [67] F.A. Radu and I.S. Pop. Mixed finite element discretization and Newton iteration for a reactive contaminant transport model with nonequilibrium sorption: convergence analysis and error estimates. *Computational Geosciences*, 15(3):431–450, 2011.
- [68] J. Samper and G. Zhang. Coupled microbial and geochemical reactive transport models in porous media: Formulation and application to synthetic and in situ experiments. *Journal of Iberian Geology*, 32(2), 2006.
- [69] T. Sekimura, A. Madzvamuse, A.J. Wathen, and Ph.K. Maini. A model for colour pattern formation in the butterfly wing of *Papilio dardanus*. *Proceedings of the Royal Society of London. Series B: Biological Sciences*, 267(1446):851–859, 2000.
- [70] C.T. Simmons, Th.R. Fenstemaker, and J.M. Sharp Jr. Variable-density groundwater flow and solute transport in heterogeneous porous media: approaches, resolutions and future challenges. *Journal of Contaminant Hydrology*, 52(14):245 – 275, 2001.
- [71] S. Stocks-Fischer, J.K. Galinat, and S.S. Bang. Microbiological precipitation of  $\text{CaCO}_3$ . *Soil Biology and Biochemistry*, 31(11):1563–1571, 1999.

- [72] L. Talon, J. Martin, N. Rakotomalala, D. Salin, and Y. C. Yortsos. Lattice bkg simulations of macrodispersion in heterogeneous porous media. *Water Resources Research*, 39(5):n/a–n/a, 2003. 1135.
- [73] Laurent Talon, Jrme Martin, Nicole Rakotomalala, and Dominique Salin. Stabilizing viscosity contrast effect on miscible displacement in heterogeneous porous media, using lattice bhatnagargrosskrook simulations. *Physics of Fluids*, 16(12):4408–4411, 2004.
- [74] Y. Tan, J.T. Gannon, P. Baveye, and M. Alexander. Transport of bacteria in an aquifer sand: Experiments and model simulations. *Water resources research*, 30(12):3243–3252, 1994.
- [75] V. van Beek, H. de Bruijn, J. Knoeff, A. Bezuijen, and U. Förster. Levee failure due to piping: A full-scale experiment. In *Scour and Erosion*, pages 283–292, 2010.
- [76] M. Van der Ruyt and W. van der Zon. Biological in situ reinforcement of sand in near-shore areas. *Proceedings of the ICE-Geotechnical Engineering*, 162(1):81–83, 2009.
- [77] W.R.L. van der Star, W.K. van Wijngaarden, L.A. van Paassen, L.R. van Baalen, and G. van Zwieten. Stabilization of gravel deposits using microorganisms. In *Proceedings of the 15th European Conference on Soil Mechanics and Geotechnical Engineering*, pages 85–90, 2011.
- [78] C.J. van Duijn, G.J.M. Pieters, and P.A.C. Raats. Steady flows in unsaturated soils are stable. *Transport in Porous Media*, 57:215244, 2004.
- [79] C.J. van Duijn and I.S. Pop. Shock waves and two phase porous media flows. *NAW*, 3, 2013.
- [80] J. van Kan, A. Segal, and F. Vermolen. *Numerical methods in scientific computing*. VSSD, Delft, 2005.
- [81] T.L. van Noorden. Crystal precipitation and dissolution in a porous medium: Effective equations and numerical experiments. *Multiscale Modeling & Simulation*, 7(3):1220–1236, 2009.
- [82] T.L. van Noorden, I.S. Pop, A. Ebigbo, and R. Helmig. An upscaled model for biofilm growth in a thin strip. *Water Resources Research*, 46(6), 2010.
- [83] L.A. van Paassen. *Biogrout, ground improvement by microbial induced carbonate precipitation*. PhD thesis, Delft University of Technology, 2009.
- [84] L.A. van Paassen, C.M. Daza, M. Staal, D.Y. Sorokin, W. van der Zon, and M.C.M. van Loosdrecht. Potential soil reinforcement by biological denitrification. *Ecological Engineering*, 36(2):168–175, 2010.
- [85] L.A. van Paassen, R. Ghose, Th.J.M. van der Linden, W.R.L. van der Star, and M.C.M. van Loosdrecht. Quantifying biomediated ground improvement by ureolysis: large-scale biogrout experiment. *Journal of geotechnical and geoenvironmental engineering*, 136(12):1721–1728, 2010.

- [86] L.A. van Paassen, M.P. Harkes, G.A. Van Zwieten, W.H. Van der Zon, W.R.L. Van der Star, and M.C.M. Van Loosdrecht. Scale up of BioGrout: a biological ground reinforcement method. In *Proceedings of the 17th international conference on soil mechanics and geotechnical engineering*, pages 2328–2333, 2009.
- [87] L.A. van Paassen, M. Pieron, A. Mulder, T.J.M. Van der Linden, M.C.M. Van Loosdrecht, and D.J.M. Ngan-Tillard. Strength and deformation of biologically cemented sandstone. In *Proceedings of the ISRM Regional conference EUROCK*, pages 405–410, 2009.
- [88] W.K. Van Wijngaarden. Modelling BIOGROUT - extension to two dimensions and a first glance in three dimensions. Master's thesis, Delft University of Technology, 2008.
- [89] W.K. van Wijngaarden, F.J. Vermolen, G.A.M. van Meurs, and C. Vuik. Modelling Biogrout: a new ground improvement method based on microbial induced carbonate precipitation. Technical report, DIAM 09-09, Delft University of Technology, the Netherlands, 2009.
- [90] W.K. van Wijngaarden, F.J. Vermolen, G.A.M. van Meurs, and C. Vuik. Modelling the new soil improvement method Biogrout: extension to 3D. In *Numerical Mathematics and Advanced Applications 2009*, pages 893–900. Springer, 2010.
- [91] W.K. van Wijngaarden, F.J. Vermolen, G.A.M. van Meurs, and C. Vuik. Modelling biogrout: a new ground improvement method based on microbial-induced carbonate precipitation. *Transport in porous media*, 87(2):397–420, 2011.
- [92] W.K. van Wijngaarden, F.J. Vermolen, G.A.M. van Meurs, and C. Vuik. A mathematical model and analytical solution for the fixation of bacteria in biogrout. *Transport in porous media*, 92(3):847–866, 2012.
- [93] W.K. van Wijngaarden, F.J. Vermolen, G.A.M. van Meurs, and C. Vuik. Various flow equations to model the new soil improvement method Biogrout. In *Numerical Mathematics and Advanced Applications 2011*, pages 633–641. Springer, 2013.
- [94] C.I. Voss and W.R. Souza. Variable density flow and solute transport simulation of regional aquifers containing a narrow freshwater-saltwater transition zone. *Water Resources Research*, 23(10):1851–1866, 1987.
- [95] R.C. Weast. *Handbook of Chemistry and Physics*. CRC Press, Boca Raton, Florida, 60th edition, 1980.
- [96] V.S. Whiffin. *Microbial CaCO<sub>3</sub> Precipitation for the production of Biocement*. PhD thesis, Murdoch University, Perth, Australia, 2004.
- [97] V.S. Whiffin, L.A. van Paassen, and M.P. Harkes. Microbial carbonate precipitation as a soil improvement technique. *Geomicrobiology Journal*, 24(5):417–423, 2007.

- [98] Ch. Yang, J. Samper, and J. Molinero. Inverse microbial and geochemical reactive transport models in porous media. *Physics and Chemistry of the Earth, Parts A/B/C*, 33(1416):1026 – 1034, 2008.
- [99] M. Yavuz Corapcioglu and A. Haridas. Transport and fate of microorganisms in porous media: A theoretical investigation. *Journal of Hydrology*, 72(1):149–169, 1984.
- [100] C. Zheng and G.D. Bennett. *Applied Contaminant Transport Modeling*. Van Nostrand Reinhold, New York, 1995.
- [101] O.C. Zienkiewicz, R.L. Taylor, and R.L. Taylor. *The finite element method for solid and structural mechanics*. Butterworth-Heinemann, Oxford, sixth edition, 2005.



## Curriculum vitae

- 2008-2015: PhD researcher in Numerical Analysis at Deltares, Delft, The Netherlands, supported by the Dutch Technology Foundation STW, subject: *Mathematical Modelling and Simulation of Biogrout*, advisers: Prof.dr.ir. C. Vuik and dr.ir. F.J. Vermolen, Department of Applied Mathematical Analysis, Faculty of Electrical Engineering, Mathematics and Computer Science
- 2006-2008: M.Sc. in Applied Mathematics, Delft University of Technology
- 2003-2006: B.Sc. in Applied Mathematics, Delft University of Technology
- 1997-2003: VWO at Christelijke Scholengemeenschap Prins Maurits in Middelharnis
- Born on May 26, 1985 in Cromstrijen, The Netherlands



## List of publications

### Journal papers

- W.K. van Wijngaarden, F.J. Vermolen, G.A.M. van Meurs and C. Vuik: Modelling biogrout: a new ground improvement method based on microbial-induced carbonate precipitation. *Transport in Porous Media*, 87(2):397–420, 2011.
- W.K. van Wijngaarden, F.J. Vermolen, G.A.M. van Meurs and C. Vuik: A mathematical model and analytical solution for the fixation of bacteria in Biogrout. *Transport in Porous Media*, 92(3):847–866, 2012.
- W.K. van Wijngaarden, F.J. Vermolen, G.A.M. van Meurs and C. Vuik: A mathematical model for Biogrout: Bacterial placement and soil reinforcement. *Computational Geosciences*, 17(3):463–478, 2013.
- W.K. van Wijngaarden, F.J. Vermolen, G.A.M. van Meurs and C. Vuik: A robust method to tackle pressure boundary conditions in Porous Media Flow: Application to Biogrout *Computational Geosciences*, **18-2**, 103–115, 2013.
- W.K. van Wijngaarden, L.A. van Paassen, F.J. Vermolen, G.A.M. van Meurs and C. Vuik: Simulation of front instabilities in density driven flow, using a reactive transport model for Biogrout combined with a randomly distributed permeability field. *Submitted to Transport in Porous Media*.
- W.K. van Wijngaarden, L.A. van Paassen, F.J. Vermolen, G.A.M. van Meurs and C. Vuik: A reactive transport model for Biogrout compared to experimental data. *Submitted to Transport in Porous Media*.

## Refereed proceedings of international conferences

- W.K. van Wijngaarden, F.J. Vermolen, G.A.M. van Meurs and C. Vuik. Modelling the new soil improvement method Biogrout: extension to 3D. In *Numerical Mathematics and Advanced Applications 2009*, pages 893–900. Springer, 2010.
- W.R.L. van der Star, W.K. Van Wijngaarden, L.A. Van Paassen, L.R. Van Baalen, and G. Van Zwieten. Stabilization of gravel deposits using microorganisms. In *Proceedings of the 15th European Conference on Soil Mechanics and Geotechnical Engineering*, pages 85–90, 2011.
- W.K. van Wijngaarden, F.J. Vermolen, G.A.M. van Meurs and C. Vuik. Various flow equations to model the new soil improvement method Biogrout. In *Numerical Mathematics and Advanced Applications 2011*, pages 633–641. Springer, 2013.

## Presentations at international conferences

- Modeling Biogrout. *European Numerical Mathematics and Advanced Applications (ENUMATH)*, Uppsala, Sweden, 2009.
- Fixation of bacteria in Biogrout. *European Numerical Mathematics and Advanced Applications (ENUMATH)*, Leicester, UK, 2011.
- Mathematical Modelling of Biogrout. *Modeling and Simulation of Transport Phenomena (MoST)*, Treis-Karden, Germany, 2014.

## Other presentations

- Mathematical modelling of Biogrout. *Meeting with a research group from Bergen, Norway*, Delft, The Netherlands, 2013.
- Modelling Biogrout. *Burgersdag 2015*, Delft, The Netherlands, 2015.

## Poster presentation

- Modeling Biogrout: a new ground improvement method (Awarded with the second price). *The Thirty-fifth Woudschoten Conference, Werkgemeenschap Scientific Computing*, Zeist, The Netherlands, 2010.